Inflammatory signaling pathways involving the CD40L-CD40-TRAF6 cascade in hypertension and diabetes – insights from animal and human studies

Dissertation
Zur Erlangung des Grades
Doktor der Naturwissenschaften (Dr. rer. nat.)

am Fachbereich Biologie
der Johannes Gutenberg-Universität Mainz

Lea Sophie Strohm
Geb. am 01.01.1994 in Siegburg
Mainz, August 2024

Dekan: Prof. Dr. Eckhard Thines

1. Berichterstatter: Univ.-Prof. Dr. rer. nat. Andreas Daiber

2. Berichterstatter: x

Tag der mündlichen Prüfung: 12.11.2024

Table of Content

List of Figures

List of Tables

List of Abbreviations

$^{\bullet}NO$	nitric oxide
2-HE	2-hydroxyethidium
3-NT	3-nitrotyrosine
4HNE	4-hydroxynonenal
ACE	angiotensin-converting enzyme
ACh	acetylcholine
ACS	acute coronary syndrome
ADMA	asymmetrical dimethyl-L-arginine
AMP	adenosine monophosphate
AMPK	AMP-activated protein kinase
AT_1R	angiotensin II receptor type 1
AT-II	angiotensin-II
ATP	adenosine triphosphate
BH_2	dihydrobiopterin
BH_4	(6R-)5,6,7,8-tetrahydro-L-biopterin
BMI	body mass index
bp	blood pressure
CaMKII	Ca^{2+}/calmodulin-dependent protein kinase II
CD	cluster of differentiation
CD40L	CD40 ligand
cGMP	cyclic guanosine monophosphate
CHD	coronary heart disease
CLPP	caseinolytic mitochondrial matrix peptidase proteolytic subunit
CPT1B	carnitine palmitoyl transferase 1B
CRP	C-reactive protein
CVD	cardiovascular disease
DAG	diacylglycerol
DALYs	disability-adjusted life years
DAMPs	damage-associated molecular patterns
DBP	diastolic blood pressure
DDAH	dimethylarginine dimethylaminohydrolase
DEG	different expressed genes
DHE	dihydroethidium
DHFR	dihydrofolate reductase
DMD	human dystrophin gene
DNA	deoxyribonucleic acid
E^+	ethidium
ECG	electrocardiogram
eNOS	endothelial $^{\bullet}NO$ synthase
ER	endoplasmatic reticulum
ET-1	endothelin-1, endothelin-1
F4/80 or EMR1	EGF-like module-containing mucin-like hormone receptor-like 1
FACS	fluorescence-activated cell sorting
FAD	flavin adenine dinucleotide
FMN	flavin mononucleotide
Gal1	galactin1
GLUT-2	glucose transporter-2
GTP	guanosine triphosphate
GTP-CH1	GTP cyclohydrolase 1
H_2O_2	hydrogen peroxide
Hbb-1b	hemoglobin, ß adult major chain
HDL	high-density lipoprotein
Het	heterozygous

HMGB1 ..... high mobility group protein B1
$HO^{\bullet}$ ..... hydroxyl radical
HO-1 ..... heme oxygenase-1
HOCl ..... hypochlorous acid
HRP ..... horseradish peroxidase
hs-CRP ..... high-sensitive CRP
Hsp90 ..... heat shock protein 90
HT ..... hypertension
ICAM-1 ..... intercellular adhesion molecule-1
ICOSLG ..... inducible T cell co-stimulatory ligand
IL-1 ..... interleukin-1
INFγ ..... interferon-γ
iNOS ..... inducible $^{\bullet}$NO synthase
INSR ..... insulin receptor
IP_3CC ..... inositol trisphosphate-regulated Ca^{2+} channels
IPA ..... ingenuity pathway analysis
IRAG ..... IP_3 receptor associated protein
KLRD ..... killer cell lectin-like receptor D
KO ..... knockout
LDL ..... low-density lipoprotein
LDL-ox ..... oxidized LDL
Ly6C or G ..... lymphocyte antigen family member C or G
MAPK ..... mitogen-activated protein kinase
MARCKS ..... myristoylated alanine-rich C kinase substrate
MCP-1 ..... monocyte chemoattractant protein-1
MEF2C ..... myocyte enhancer factor 2C
MHC ..... major histocompatibility complexes
MLCK ..... myosin light chain kinase
MMP ..... matrix metalloproteinase
MPO ..... myeloperoxidase
mRNA ..... messenger ribonclein acid
NADPH ..... nicotinamide-adenine-dinucleotide phosphate
NF-κB ..... nuclear factor κ-light-chain-enhancer of activated B cells
NIBP ..... non-invasive blood pressure
NK cells ..... natural killer cells
NK1.1 ..... killer cell lectin-like receptor subfamily B member 1C protein
NLRP3 ..... NLR family pyrin domain containing 3
nNOS ..... neuronal $^{\bullet}$NO synthase
NOS ..... $^{\bullet}$NO synthase
NOX ..... NADPH oxidase
NPX ..... normalized protein expression
Nrf2 ..... nuclear factor erythroid-2 related factor 2
NTG ..... nitroglycerine
NT-proBNP ..... N-terminal prohormone of brain natriuretic peptide
$O_2^{-\bullet}$ ..... superoxide anion
$ONOO^-$ ..... peroxynitrite
Par1 ..... proteinase-activated receptor 1
PCR ..... polymerase chain reaction
PDBu ..... phorbol 12,13-dibutyrate
PDCD ..... programmed cell death ligand
PDGF ..... platelet derived growth factor
PEA ..... Proximity Extension Assay
PGF ..... placental growth factor
$PGF_2α$ prostaglandinF2α
PGI2 ..... prostacyclin
PIP2 ..... phosphatidylinositol 4,5-bisphosphate

PKA ..... protein kinase A
PKC ..... protein kinase C
PKG ..... protein kinase G
PLC ..... phospholipase C
PPARGC1A ..... PPARG coactivator 1 α
PSLAX ..... parasternal long axis view
PVAT ..... perivascular adipose tissue
RAAS ..... renin-angiotensin-aldosterone system
RAGE ..... receptors for advanced glycation endproducts
RNA-Seq ..... RNA sequencing
RNS ..... reactive nitrogen species
RONS ..... reactive oxygen and nitrogen species
ROS ..... reactive oxygen species
SAX ..... parasternal short axis view
SBP ..... systolic blood pressure
sCD40L ..... soluble CD40 ligand
Ser ..... serine
sGC ..... soluble guanylyl cyclase
SOD ..... superoxide dismutase
T2DM ..... diabetes mellitus type 2
TCRß ..... T cell receptor beta locus
TGFß ..... transforming growth factor ß
T_H ..... T helper cells
Thr ..... threonine
TIE2 ..... angiopoietin 2 receptor
TLR ..... toll-like receptors
TNF(R)SF ..... tumor necrosis factor (receptor) super family
TNFα ..... tumor necrosis factor-α
TRAFs ..... TNF receptor-associated factors
T_{reg} ..... regulatory T cells
TRL ..... triglyceride-rich lipoprotein
Tsp1 ..... thrombospondin-1
TXA2 ..... thromboxane A2
Tyr ..... tyrosine
UlvWFs ..... ultra-large von Willebrand factors
VASP ..... vasodilator-stimulated phosphoprotein
VCAM-1 ..... vascular cell adhesion molecule-1
VEGF ..... vascular endothelial growth factor
VLDL ..... very low-density lipoprotein
WT ..... wildtype
XO ..... xanthine oxidase

1. Introduction

1.1. Cardiovascular diseases

Cardiovascular diseases (CVD) can be classified diagnostically in four major areas: coronary heart disease (CHD), cerebrovascular disease, peripheral arterial disease, and aortic atherosclerosis (1). In 2019, ischemic heart disease was the top leading cause of death globally, with 8.9 million victims (reflecting 16 % of total world deaths). Followed by strokes, which cause approximately 11 % of the world's global deaths (2). According to the global burden disease study from 2019, ischemic heart diseases and strokes have been unchanged for almost 30 years (1990-2019) as the leading causes of death. The top-ranked causes of disability-adjusted life years (DALYs) are in the group of 50-74 years and the 75 years and older group (3). High systolic blood pressure has been the leading cardiovascular risk factor for over 50 years. Also, under the top five (out of 87) risk factors are high fasting plasma glucose, high body-mass index (BMI), and high low-density lipoprotein (LDL) cholesterol levels (4). In summary, hypertension, ischemic heart disease, and cerebrovascular disease are responsible for approximately 40 % of all deaths globally. Thereby, atherosclerosis, an inflammatory vascular system disorder, is the major pathomechanism underlying almost all CVDs (see 1.4). An overview of CVD risk factors and a classification of CVDs is shown in Figure 1.

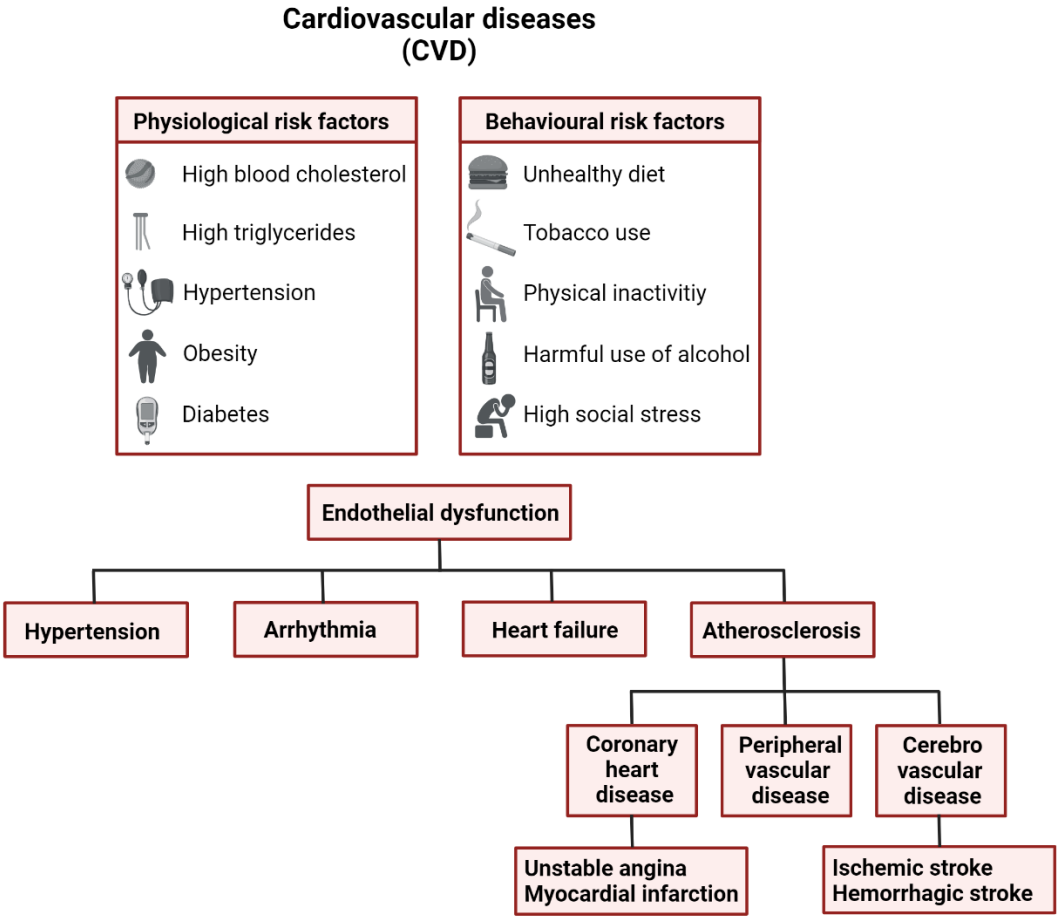

Figure 1: Risk factors of CVDs and disease classification. CVD risk factors can be classified into physiological risk factors (e.g., hypertension, obesity, and diabetes) and behavioral risk factors (e.g., unhealthy diet, smoking, and inactivity). An unhealthy lifestyle causes most of these modifiable risk factors. Endothelial dysfunction and atherosclerosis are the major pathomechanisms underlying CVD. Atherosclerosis could lead to severe outcomes in patients and is associated with myocardial infarction and stroke. Created with BioRender.com. CVD=cardiovascular disease.

1.2. Fundamental cellular and molecular mechanisms in the pathogenesis of CVD

1.2.1. Oxidative stress

Reactive oxygen species (ROS) contain at least one oxygen molecule, are highly reactive, and appear in all aerobic cells. ROS family members are free radicals or molecules with oxidizing effects. Group members are, for example, superoxide anion ($O_2^{-\bullet}$), hydroxyl radical ($HO^{\bullet}$), hydrogen peroxide (H_2O_2), or hypochlorous acid (HOCl). In addition, reactive nitrogen species (RNS) like nitric oxide ($^{\bullet}NO$) or peroxynitrite ($ONOO^-$) are also crucial in oxidative regulation. ROS and RNS are also described as reactive oxygen and nitrogen species (RONS) (5, 6). Increasing RONS levels are associated with oxidative stress and different CVDs like atherosclerosis, hypertension, or diabetes (6). Therefore, oxidative stress is defined as an imbalance between oxidants and antioxidants or failure of the organism to repair the oxidative damage. A disruption of redox signaling up to molecular damage is mediated by increasing RONS production and insufficient RONS scavenging (7). Some RONS could also act as cellular messengers essential for signaling under normal, healthy conditions. To be mentioned here is $^{\bullet}NO$-mediated signaling, which leads to beneficial vascular tone regulation and the suppression of platelet activation (see 1.2.3). Important pro-oxidant pathways and $O_2^{-\bullet}$ sources in the vascular system are the xanthine oxidase (XO), nicotinamide-adenine-dinucleotide phosphate (NADPH) oxidase, uncoupled $^{\bullet}NO$ synthase, and the mitochondrial respiratory chain. $ONOO^-$ is a highly reactive and strong oxidant produced by $^{\bullet}NO$ and $O_2^{-\bullet}$ reaction (5). A biomarker for $ONOO^-$ bioreactivity is 3-nitrotyrosine (3-NT). However, this biomarker is also formed in pro-inflammatory processes by myeloperoxidase (MPO) in the presence of peroxides and nitrite anions and is not an exclusive marker for $ONOO^-$ (8). Antioxidant defense systems in the vasculature are, for example, superoxide dismutase (SOD), catalase, glutathione peroxidase, thioredoxin, peroxiredoxins, and heme oxygenase. Also, the transcription factor erythroid-2 related factor 2 (Nrf2) is important to mention as mediating cellular anti-oxidant mechanisms (9). The following sections describe the role of RONS in developing CVD.

1.2.2. $^{\bullet}NO$ synthase (NOS) and $^{\bullet}NO$ signaling in the focus of CVD

$^{\bullet}NO$ is generated via the enzyme $^{\bullet}NO$ synthase (NOS), which has in mammals three different isoforms: neuronal NOS (nNOS), inducible NOS (iNOS), and endothelial NOS (eNOS). The

utilized substrate of all NOS isoforms is L-arginine, utilizing oxygen and NADPH as co-substrates. The following cofactors are also common among the different isoforms: flavin adenine dinucleotide (FAD), flavin mononucleotide (FMN), and (6R-)5,6,7,8-tetrahydro-L-biopterin (BH_4) (10). The structure and the catalytic mechanism of functional NOS are shown in Figure 2.

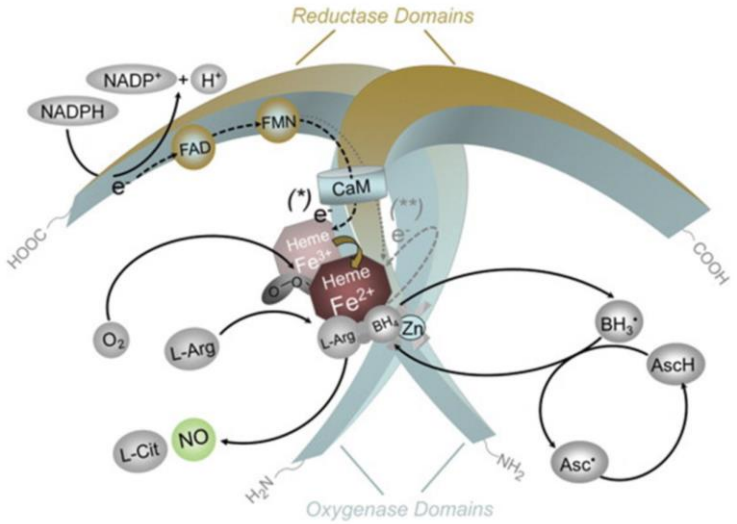

Figure 2: Structure and catalytic mechanism of coupled •NO synthase (NOS). All functional NOS isoforms are heterodimers with a reductase and an oxygenase domain on each monomer. Electrons are transferred from the co-substrate NADPH via the flavins FAD and FMN to the carboxyl-terminal reductase domain. The transfer to Heme is stimulated by increased cellular Ca^{2+} levels and calmodulin (CaM) binding. In addition to Heme, the oxygenase domain binds the cofactor BH_4, molecular oxygen, and the substrate L-arginine. The electron transfer enables the iron-containing Heme to bind molecular oxygen and reduce Fe^{3+} to Fe^{2+}. In consequence, L-arginine is oxidized to L-citrulline and •NO. Essential in •NO generation of NOS is also the binding of the cofactor BH_4. Oxidized BH_4, the BH_3• radical, is recycled either by NOS itself or by reducing agents like ascorbic acid. The electron transfer takes place at each monomer side. The figure is taken from (10) with permission.

nNOS expression is commonly associated with physiological functions like learning, memory, and neurogenesis. However, there is also evidence that nNOS is involved in blood pressure regulation. For example, the innervation of the smooth muscle cell tissues by nNOS-containing nerves could lead to •NO release, thereby modulating the tone in blood vessels (11, 12). The activity of nNOS is regulated by Ca^{2+} and calmodulin levels in the cells. Abnormal •NO signaling via nNOS is associated with primarily neurodegenerative pathologies (13). Under healthy conditions, iNOS is usually not expressed; the expression can be induced by bacterial lipopolysaccharides or cytokines, which indicate an important role of iNOS in non-specific immune responses. Because of the very tight binding of the calcium-calmodulin complex to this isoform, iNOS is not sensitive to Ca^{2+}-mediated regulation (10). In activated macrophages, iNOS expression leads to high •NO production, affecting, for example, parasites or tumor cells as a cytotoxic response. Indeed, high •NO levels lead to inhibition of iron-containing proteins, for example, in the mitochondrial electron transport chain, and further could also interfere with cellular deoxyribonucleic acid (DNA) to conduct DNA fragmentation (14, 15). Activated

macrophages are also involved in most pro-inflammatory processes or autoimmune diseases, and high •NO rates could lead to surrounding tissue damage (16). During a septic shock, excessive •NO production via iNOS leads to arterial vasodilation, hypotension, and microvascular damage, accompanied by the expression of other pro-inflammatory mediators like interleukin-1 (IL-1), tumor necrosis factor-α (TNFα), and interferon-γ (INFγ) (17). Abnormal •NO production via iNOS is associated, therefore, mainly with the mediation of inflammation and septic shock. eNOS is predominantly expressed in endothelial cells, and Ca^{2+}/calmodulin levels can regulate its expression. Further, other proteins can modulate eNOS activity, like heat shock protein 90 (Hsp90) or caveolin-1 (10). In addition, independent of Ca^{2+} increase in the cell, eNOS expression can also be activated by stimuli like fluid shear stress, which leads to enhanced •NO production and phosphorylation of the eNOS enzyme on several serine (Ser), threonine (Thr), and tyrosine (Tyr) residues. For example, Ser1177 and Thr495 phosphorylation are important for eNOS functionality and are independent mechanisms of eNOS activation (pSer1177) and inactivation (pThr495), respectively (10, 18, 19). Ser1177 phosphorylation is mediated by estrogen and vascular endothelial growth factors (VEGF) via Ser/Thr kinase Akt, by insulin via Akt and adenosine monophosphate-activated protein kinase (AMPK), by bradykinin via Ca^{2+}/calmodulin-dependent protein kinase II (CaMKII) and by shear stress via activating protein kinase A (PKA). This phosphorylation increases Ca^{2+} sensitivity and stimulates electron flux in the reductase domain of eNOS (10, 20). Phosphorylation of Thr495 via protein kinase C (PKC) is associated with eNOS dysfunction and increased eNOS activity by enhanced calmodulin binding that may lead to ROS formation (18, 21). The physiological aspects of eNOS are diverse and essential to cardiovascular function. Endothelium-produced •NO leads to vasodilation via soluble guanylyl cyclase (sGC) stimulation in smooth muscle cells (22). Further, platelet aggregation and adhesion are inhibited through •NO release into the vascular lumen (23). Important for an anti-atherosclerosis effect is also the prevention of platelet-derived growth factor release, which stimulates smooth muscle cell proliferation and matrix molecule production (24). In addition, leukocyte adhesion and vascular inflammation are inhibited by endothelial •NO. For example, endothelium-derived •NO leads to decreased monocyte chemoattractant protein-1 (MCP-1) expression and prevention of endothelial cell apoptosis stimulated by inflammatory cytokines, ROS, or angiotensin-II (AT-II) (25, 26). Also, angiogenesis, for example, after post-ischemia events and the activation of endothelial progenitor cells, is stimulated by eNOS-derived •NO production. In ischemic heart disease patients, •NO bioavailability is typically reduced and leads presumably to impaired neovascularization (26-28). In summary, eNOS is important in mediating vasodilation, vasoprotective effects, and atherosclerosis prevention.

1.2.3. ·NO mediated cGMP signaling and vasodilation

Endothelial ·NO biosynthesis is essential to mediate physiological smooth muscle relaxation in the vascular system. Further, endothelium-produced ·NO diffuses fast into smooth muscle cells and binds to sGC. ·NO leads to an activation of sGC and triggers the conversion of guanosine triphosphate (GTP) to cyclic guanosine monophosphate (cGMP). Phosphorylation of downstream targets and vasodilation is mediated by cGMP binding to protein kinase G (PKG) (29, 30). PKG phosphorylates inositol trisphosphate-regulated Ca^{2+} channels (IP_3CC) and its associated protein regulator (IRAG) on the endoplasmatic reticulum (ER), leading to inhibition of the Ca^{2+} efflux from the ER to the cytosol, which in the smooth muscle cell prevent myosin light chain kinase activation by Ca^{2+} and thereby causes reduced contractility of the myosin-actin filaments (31, 32). PKG leads to the phosphorylation of K^+ channels, resulting in K^+ influx and hyperpolarization of the cell membrane. The hyperpolarization led to the inhibition of voltage-gated Ca^{2+} channels, and therefore, the Ca^{2+} influx into the smooth muscle cells is reduced (29, 33). Further, increased cGMP levels and PKA activation in smooth muscle cells can also be induced by IL-1ß signaling, leading to suppressed smooth muscle cell proliferation (34). In addition, vasodilator-stimulated phosphoprotein (VASP) is another substrate of ·NO-cGMP signaling and is important for cell morphology changes during proliferation. Phosphorylation of VASP via PKG leads to inhibition of actin cytoskeleton reorganization of smooth muscle cells (35, 36). The signaling is terminated by converting cGMP to GMP mediated by different phosphodiesterases (29). Figure 3 shows eNOS signaling during normal vascular function.

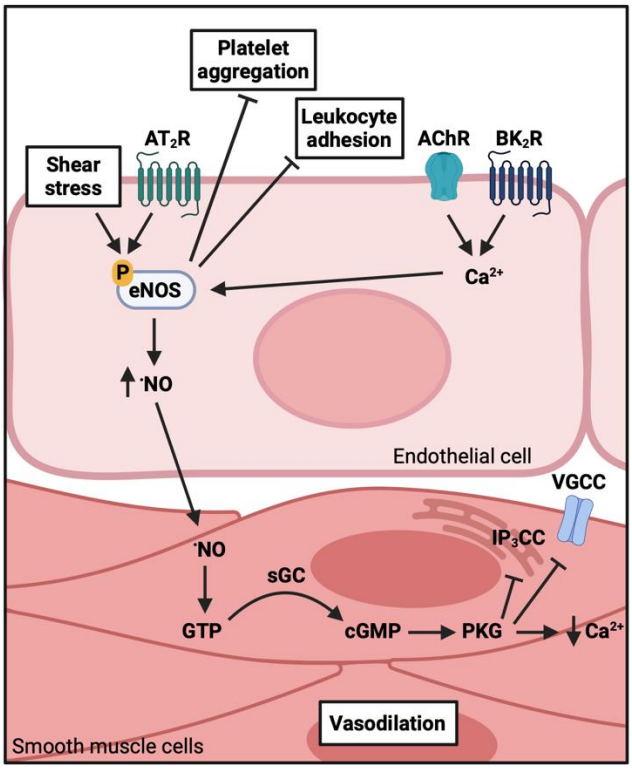

Figure 3: Coupled eNOS and •NO signaling during normal vascular function. Endothelial •NO biosynthesis regulates smooth muscle cell relaxation and vasodilation. Shear stress and other chemical stimuli like acetylcholine, bradykinin, and angiotensin-II can activate eNOS, for example, by stimulating voltage-gated Ca^{2+} channels to increase intracellular Ca^{2+} levels. •NO released by endothelial cells into the bloodstream inhibits platelet aggregation and leukocyte adhesion. In smooth muscle cells, •NO activates sGC, leading to the conversion of GTP to cGMP. Increasing cGMP levels activates kinases and leads to hyperpolarization of smooth muscle cells, followed by the closing of voltage-gated Ca^{2+} channels. Decreased intracellular Ca^{2+} levels lead to a relaxation of smooth muscle cells and vasodilation. Adapted from (37). Created with BioRender.com. Abbreviations: AT_2R=angiotensin-II receptor type 2, eNOS=endothelial •NO synthase, •NO=nitric oxide, AChR=acetylcholine receptor, BK_2R=bradykinin receptor B2, GTP=guanosine triphosphate, sGC=soluble guanylyl cyclase, cGMP=cyclic guanosine monophosphate, PKG=protein kinase G, IP_3CC=inositol trisphosphate-regulated Ca^{2+} channels, VGCC=voltage-gated Ca^{2+} channels.

1.2.4. NADPH oxidase (NOX)

NADPH oxidases (NOX) represent a group of ROS-producing enzymes identified as one of the primary ROS sources in CVDs besides mitochondria (6, 38-43). Seven NOX isoforms are known: NOX1-5, dual oxidase 1 (DUOX1), and 2 (DUOX2). All NOX isoforms share a structural homology consisting of six conserved transmembrane domains, a catalytic core with four heme-binding histidines, a dehydrogenase domain that binds FAD as a cofactor, and NADPH as substrate. The NOXs differ in cellular and tissue distributions and the regulatory system's composition/mode of action. NOX activation leads to electron transfer across the plasma membrane by reducing O_2 to $O_2^{-\bullet}$ utilizing NADPH as an electron donor (44, 45):

(I) $NADPH + 2O_2 \rightarrow 2O_2^{-\bullet} + NADP^+ + H^+$ (NOX)

The NOX2 and $p22^{phox}$ complex is localized inactive in the plasma membrane and requires the assembly of multiple subunits for its activation. The following NOX2 subunits are recruited from the cytosol, leading to NOX2 activation: $p40^{phox}$, $p67^{phox}$, and $p47^{phox}$. Further, NOX2 full activation requires the small GTPase RAC1 or RAC2 (Ras-related C3 botulinum toxin substrate) and phosphorylation of $p47^{phox}$ by PKC. NOX1 requires for activation $p22^{phox}$, RAC1, $p47^{phox}$ (or the NOX organizer 1 (NOXO1)), and NOX activator 1 (NOXA1). NOX4 activation requires $p22^{phox}$ (and is mostly regulated by NOX4 expression level), whereas NOX5 activation is Ca^{2+} dependent and requires no further subunits (Figure 4). The focus here is on the isoforms NOX1, NOX2, NOX4, and NOX5, as they are expressed in cell types belonging to the cardiovascular system (44, 45). NOX1, NOX2, and NOX5 are producing $O_2^{-\bullet}$, whereas NOX4 is mostly producing H_2O_2 (44, 46).

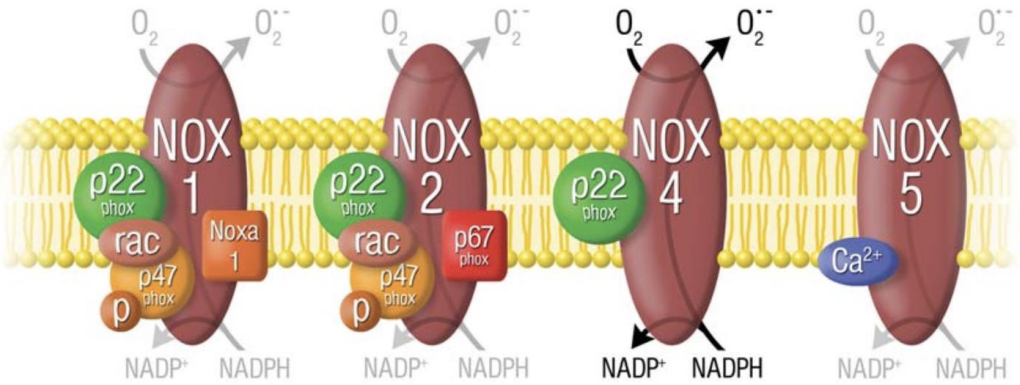

Figure 4: Assembly of different NADPH oxidase (NOX) complexes in the cardiovascular system. Four different NOX isoforms (NOX1, 2, 4, and 5) are expressed in the cardiovascular system. All NOX isoforms produce $O_2^{-\bullet}$ by electron transfer from NADPH to molecular oxygen. In addition, NOX4 also produces H_2O_2. NOX1 requires activation of different subunits like $p22^{phox}$, $p47^{phox}$ (or NOXO1), Rac, and NOXA1. NOX2 requires the same subunits except for NOXA1, which is replaced by $p67^{phox}$. While NOX4 requires only $p22^{phox}$ and NOX5 activation is only Ca^{2+} level dependent. The figure is taken from (47) with permission.

In the following, NOX signaling is described in more detail, focusing on the cardiovascular system and CVD. NOX1 is expressed in vascular smooth muscle cells and is distributed within the plasma membrane. NOX1-derived ROS is important in AT-II-induced endothelial dysfunction (acute), vascular hypertrophy, and systemic hypertension (chronic) (47-49). NOX2 is important in acute innate immune system responses and is highly expressed in phagocytic cells like neutrophils and macrophages. Besides leukocytes, NOX2 is also expressed in endothelial cells and the adventitia. NOX2 expression is enhanced after infection or in pro-inflammatory signaling (44, 47, 50). NOX4 is expressed in endothelial cells, vascular smooth muscle cells, and adventitia. NOX4 is constitutively active and is distributed in the endoplasmic reticulum of the cells. NOX4 mediates ROS signaling via direct interaction with the $^{\bullet}NO$/cGMP signaling pathway, resulting in H_2O_2 production. High H_2O_2 concentrations could lead to acute cytotoxicity (47, 50). NOX4 expression and its signaling mechanism are suggested to be involved in tissue damage, for example, after acute ischemic stroke and pressure overload in the heart. However, lower chronic NOX4 signaling is associated with more protective processes like angiogenesis or wound healing (50-52). Rodents lack the NOX5 gene; therefore, interventional studies are difficult. NOX5 expression is increased in endothelial cells and plaque-associated vascular smooth muscle cells, indicating a role of NOX5 in atherosclerotic pathology. Further, NOX5 could cause eNOS uncoupling, leading to endothelial dysfunction via enhanced ROS production (53, 54). NOX activation also promotes the activation of other oxidase systems, which causes oxidative stress like uncoupled eNOS, dysfunctional mitochondria, or xanthine oxidase (44, 45, 55, 56). This oxidative crosstalk is a major mechanism in oxidative stress generation in CVD pathologies. ROS generation, in general, starts with $O_2^{-\bullet}$ production. Spontaneous or at low pH conditions, $O_2^{-\bullet}$ dismutates rapidly to H_2O_2, a reaction that is further accelerated and catalyzed by SOD enzymes (57, 58).

(I) $2O_2^{-\bullet} + 2H^+ \rightarrow H_2O_2 + O_2$ (SOD)

Further, reactions based on H_2O_2 as a substrate are the Fenton reaction in the presence of iron and the Haber Weiss reaction. Meanwhile, H_2O_2 is degraded to H_2O by catalase or peroxidases (57).

(I) $H_2O_2 \rightarrow OH^- + OH^\bullet$ (in the presence of Fe^{2+}, Fenton reaction)
(II) $O_2^{-\bullet} + H_2O_2 \rightarrow O_2 + HO^- + OH^\bullet$ (catalyzed by Fe^{3+}, Haber Weiss reaction)
(III) $H_2O_2 \rightarrow O_2 + H_2O$ (catalase)

1.2.5. Peroxynitrite ($ONOO^-$)

$ONOO^-$ is a highly reactive non-radical, powerful, and short-lived oxidant. The fast reaction of $^\bullet NO$ with $O_2^{-\bullet}$ leads to the formation of $ONOO^-$ (59).

(I) $^\bullet NO + O_2^{-\bullet} \text{ -> } ONOO^-$

Thereby, SOD and $ONOO^-$ formation are competing kinetically for $O_2^{-\bullet}$ radicals. The ratio of this competition is crucial in the development of $^\bullet NO$ induced oxidative damage. $ONOO^-$ reacts directly in one or two electron oxidations with different metalloproteins, hemins, or glutathione protein thiols. For example, a reaction with a metal center can result in a loss of enzyme function. Further, $ONOO^-$ mediates radical reactions and leads in aqueous phases with CO_2 to nitrogen dioxide ($^\bullet NO_2$) and carbon trioxide ($^\bullet CO_3^-$) radical formation (59, 60).

(I) $ONOO^- + CO_2 \rightarrow ONOOCO_2^- \rightarrow {}^\bullet NO_2 + {}^\bullet CO_3^-$ (in aqueous phase)

These radicals are important for mediating protein tyrosine nitration, protein oxidation, DNA oxidation, and nitration. In addition, $ONOO^-$ mediates radical reactions in hydrophobic phases, which result in $ONOO^-$-mediated lipid oxidation, lipid nitration, and protein tyrosine nitration (59).

(I) $ONOO^- + H^+ \rightarrow ONOOH \rightarrow {}^\bullet NO_2 + OH^\bullet$ (in hydrophobic phase)

Important in $ONOO^-$- and $^\bullet NO_2$-mediated toxicity is the promotion of protein tyrosine nitration, which results in protein structure changes accompanied by loss or gain of a previously non-existent function (59). Physiologically, oxidant production is crucial for pathogen defense mediated by macrophages and neutrophils. However, these posttranslational protein

modifications were also observed in CVDs, neurodegenerative diseases, inflammation, and cancer (61).

1.2.6. eNOS uncoupling

Alterations of enzymatic eNOS activity in response to inflammation or CVDs could contribute to eNOS uncoupling. Thereby, eNOS uncoupling is defined as a process of electron transfer from NADPH within the reductase domain to molecular oxygen, leading to the formation of $O_2^{-\bullet}$ instead of $^{\bullet}NO$. The $O_2^{-\bullet}$ formation is accompanied by reduced vascular $^{\bullet}NO$ bioavailability (62). Different mechanisms of eNOS uncoupling concepts are described in the literature. The oxidative depletion of BH_4 should be mentioned first. BH_4 is an essential cofactor to stabilize the dimeric state of eNOS; if BH_4 is lacking, the eNOS dimer is disrupted, which results in an electron transfer to $O_2^{-\bullet}$ instead of $^{\bullet}NO$. In general, BH_4 can be generated in a de novo synthesis pathway by the enzyme GTP cyclohydrolase 1 (GTP-CH1) or via the salvage pathway by the enzyme dihydrofolate reductase (DHFR); the second one regenerates BH_4 enzymatically from its oxidized form, dihydrobiopterin (BH_2). Downstream of NOX activation, eNOS uncoupling can occur. Indeed, $ONOO^-$ could lead to oxidative degradation of BH_4 to BH_2, resulting in eNOS uncoupling (44, 62). In CVD patients, BH_4 levels seem to be decreased (63-65). Oxidants like $ONOO^-$ could also disrupt the zinc tetrathiolate (ZnS_4) cluster at the dimer interface of eNOS, which leads to eNOS uncoupling (44). Reversible S-glutathionylation of two cysteine residues within the eNOS reductase domain is another important mechanism in eNOS uncoupling. Oxidative stress promotes this protein modification, leading to increased $O_2^{-\bullet}$ generation and reduced $^{\bullet}NO$ formation (10). S-glutathionylation of eNOS is associated with different pathologies like hypertension, diabetes, and atherosclerosis (66). Another redox-sensitive modification of eNOS is represented by the phosphorylation of the enzyme. Phosphorylation of Ser1177 leads to increased eNOS productivity, and phosphorylation of Thr495 is associated with eNOS dysfunction or even uncoupling. In addition, phosphorylation of Tyr657 by the protein tyrosine kinase-2 leads to inhibition of eNOS. Both kinases mediating phosphorylation of Thr495 and Tyr657 are activated by oxidative stress and stimulated by H_2O_2 or AT-II (only Tyr657) (10, 62). A potent endogenous inhibitor of eNOS is asymmetrical dimethyl-$_L$-arginine (ADMA), which is also properly involved in eNOS uncoupling. The ADMA-generating enzyme and ADMA-degrading enzyme dimethylarginine dimethylaminohydrolase (DDAH) are redox-sensitive. Oxidative stress conditions in the vasculature lead to increased ADMA production and decreased DDAH activity, thereby diminishing ADMA degradation, resulting in higher ADMA concentrations and inhibition of eNOS activity (10, 62). The mentioned mechanisms contribute to eNOS uncoupling and are shown in Figure 5. However, not all mechanisms are fully understood or even discovered, and eNOS uncoupling needs careful elucidation.

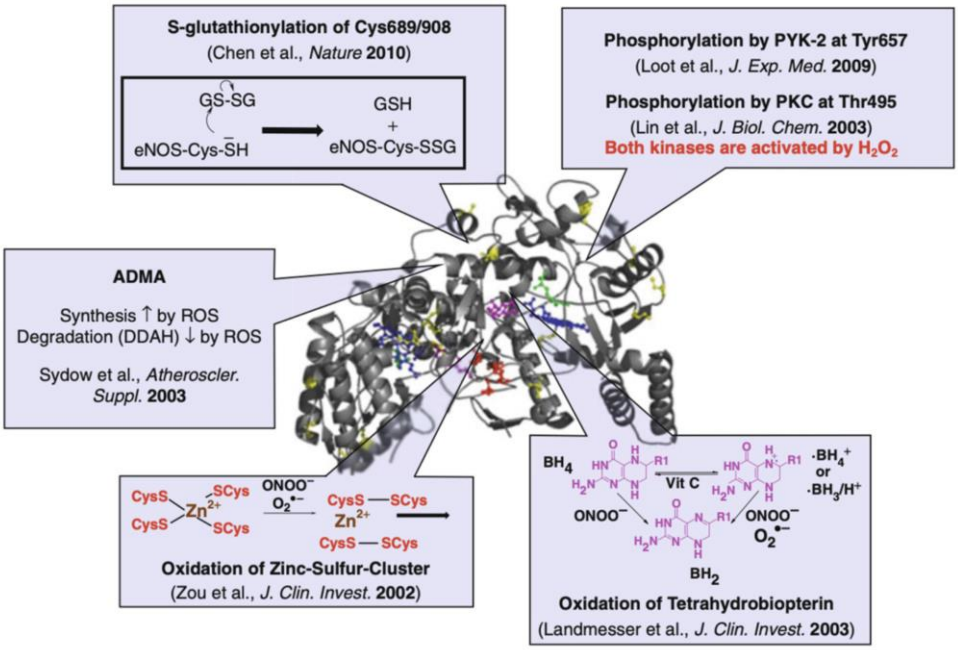

Figure 5: The main redox regulation pathways of eNOS. Five redox regulation pathways contribute mainly to eNOS dysfunction/uncoupling during oxidative stress. For example, S-glutathionylation of specific cysteine residues is associated with eNOS uncoupling, which means that eNOS produces $O_2^{-\bullet}$ instead of $^{\bullet}NO$. ROS-sensitive kinases like protein tyrosine kinase-2 (PYK-2) or protein kinase C (PKC) dependent phosphorylation induce eNOS inhibition. Another eNOS inhibiting ROS-sensitive pathway is an asymmetrical dimethyl-L-arginine (ADMA) accumulation. Oxidation of the zinc-sulfur-cluster or tetrahydrobiopterin (BH_4) is also associated with eNOS uncoupling. The figure is taken from (5) with permission.

1.2.7. Immune system and inflammation

The immune system is a network of lymphoid organs, cells, proteins, and cytokines that regulate host defense mechanisms. Abnormal immune system function could lead to reduced activity, immunodeficiency, and infections, whereas overactivity could lead to allergic or autoimmune diseases (67). The immune system can be divided into two main mechanisms: the innate immune response and the adaptive immune response. The innate immune system responds fast to infections, within minutes to hours. The response is not very specific and does not differ from repeated infections. Local tissue macrophages could detect an infection and produce cytokines. This process activates the innate immune system and induces inflammation. The cytokine gradient leads to an attraction of other immune cells to the infected tissue and the activation of phagocytic cells. Further, antimicrobial agents like ROS, proteases, or hydrolytic enzymes are produced (68). The delivery of phagocytes to the infected tissue is one of the key mechanisms of the innate immune system. As primary responders, neutrophils and macrophages are recruited to the side of infection, and both cell types clear tissue of pathogens by phagocytosis, which leads to an activation of NOX and/or iNOS, which results in RONS production. These processes result in the initiation of local inflammation (68-71). As a third phagocytotic class, dendritic cells are activated. They are processing degraded pathogens and displaying specific peptides on their cell surface. Antigen-presenting dendritic

cells migrate to lymph nodes, which results in adaptive immune system initiation via T cells (72). Further, natural killer (NK) cells are recruited to inflamed tissue responsible for targeting and destroying infected cells (73). Mast cells and basophils are tissue-resident cells. They are essential for both the innate and the adaptive immune response. Once mast cells are exposed a second time to specific antigens, they degranulate and release bioactive molecules like histamine, prostaglandins, and TNFα (68). The adaptive immune system is activated if the innate immune system activation is insufficient to fight against the infection. Activation of the adaptive immune system is slow and occurs within several days. Compared to the innate immune system, the adaptive immune system is highly specific to antigens. It has a memory, meaning the secondary response is more rapid and aggressive than the primary response (68). The adaptive immune response of T cells is mediated by two presented classes of major histocompatibility complexes (MHC). MHC class II led to activation of $CD4^+$ T helper (T_H) cells, which initiate cytokine production of target cells. Different subclasses of T_H cells mediate different immune responses. T_H1 cells target macrophages, T_H2 targets B cells, and T_H17 targets fibroblasts or epithelial cells, which leads to immunity and cytokine production (68, 74). T follicular helper (T_{FH}) cells sit in the germinal center of the lymphoid follicle and regulate B cell activation and maturation, for example, by CD40L expression (75). Regulatory T (T_{reg}) cells mediate immunosuppression by cytokine secretion, inhibiting active T and B cells (76). MHC class I presenting cells lead to the activation of cytotoxic $CD8^+$ T (T_C) cells, which are killing, for example, virus-infected cells (77). Immunological memory is also mediated via B and T cells (68). An overview of the different immune cells involved in the innate and adaptive immune responses is shown in Figure 6.

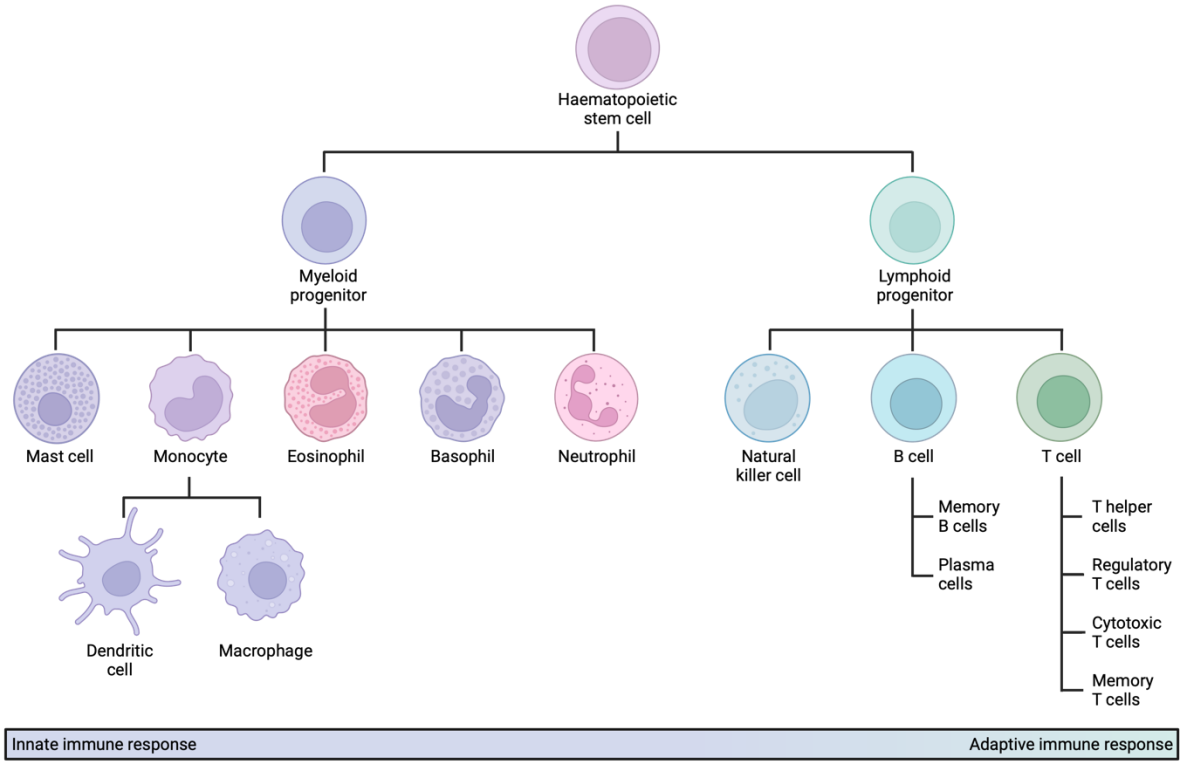

Figure 6: Different immune cells are involved in innate and adaptive immune system responses. Hematopoietic immune cells differentiate into myeloid or lymphoid progenitor cells. The innate immune system reacts fast to infections with monocyte differentiation to macrophages and dendritic cells. Further, neutrophils and natural killer cells are essential for the fast response to pathogens. The slower adaptive immune response is mainly mediated by natural killer cells, B and T cells. Natural killer cells are essential in the innate and adaptive immune response. Adapted from (78). Created with BioRender.com.

In the process of sterile inflammation, immune cells can be recruited to tissues without the involvement of pathogens. Damage-associated molecular patterns (DAMPs) can be produced by oxidative stress and ROS-mediated damage (e.g., oxidized lipids, DNA bases, free DNA, and fibrinogen) and activate the classical inflammatory cascade via pattern-recognition receptors as well as Toll-like receptors and down-stream activation of caspase/IL-1ß and TNFα signaling (79). Direct activation of key mediators of inflammation, e.g., NLRP3 and HMGB1, by oxidative modifications via RONS can further exacerbate the process of sterile inflammation (80).

1.3. Endothelial dysfunction

The endothelium is essential in maintaining vascular physiology and pathophysiology, such as regulating vascular tone, coagulation, angiogenesis, and inflammation. Indeed, endothelial dysfunction plays an important role in the pathology of atherosclerosis, hypertension, and diabetes (30, 81). Classically healthy arterial walls consist of a trilaminar structure as described in the following: (I) tunica externa or adventitia (connective tissue and vaso vasorum), (II) tunica media (external elastic lamina and smooth muscle cells), (III) tunica interna or intima (internal elastic lamina, subendothelium, and endothelium) (82). The endothelium comprises a single

layer of endothelial cells, and approximately 1.5 % of the total body mass consists of this cell type (81). The endothelium is a semi-permeable barrier covered at the luminal surface with negatively charged glycocalyx, which forms a barrier against pathogens and prevents invasion of platelets or immune cells into the intima (83). Further, hemostasis and thrombosis are regulated via endothelial cells, for example, by the expression of thrombin inhibitors. Another regulatory mechanism within the mitochondria of endothelial cells is the thioredoxin system, which prevents the formation of ROS (81). The endothelium of arteries also plays a major role in vascular tone, local blood flow, and systemic blood pressure regulation via signal integration and transduction to the tissue environment. Endothelial cells release vasodilator factors like •NO, prostacyclin (PGI2), and endothelium-derived hyperpolarizing factor (EDHF) in response to mechanical (e.g., shear stress) or chemical stimuli (e.g., bradykinin, adenosine triphosphate (ATP), acetylcholine). Bradykinin and acetylcholine (ACh) stimulate eNOS activity in endothelial cells. Endothelium-derived vasoconstrictors are thromboxane A2 (TXA2) (although primarily released by activated platelets) and endothelin-1 (ET-1). Both vasoconstriction and vasodilation are regulated by cytoplasmatic Ca^{2+} levels in the endothelial and smooth muscle cells (30, 81). An imbalance in •NO production or bioavailability could cause endothelial dysfunction, reduced vasodilator response, and the onset of pro-inflammatory signaling pathways (62). Subendothelial expression of IL-1, IL-6, TNFα, and C-reactive protein (CRP) expression leads to pro-inflammatory NF-κB signaling in endothelial cells, which leads to E-selectin, vascular cell adhesion molecule-1 (VCAM-1), and intercellular adhesion molecule-1 (ICAM-1) expression. Further, CRP is downregulating eNOS transcription, decreasing •NO bioavailability (81). Increasing oxidative stress and ROS production are essential in developing endothelial dysfunction, and decreased •NO bioavailability is associated with the onset of this pathology (6). The cellular and molecular processes of eNOS uncoupling and ROS production are described in more detail in 1.2. Hypertension stimulates endothelial injury through AT-II and aldosterone activity in addition to oxidative stress and eNOS uncoupling, which is explained in more detail in 1.5.2 (30). The development of endothelial dysfunction is shown in Figure 7.

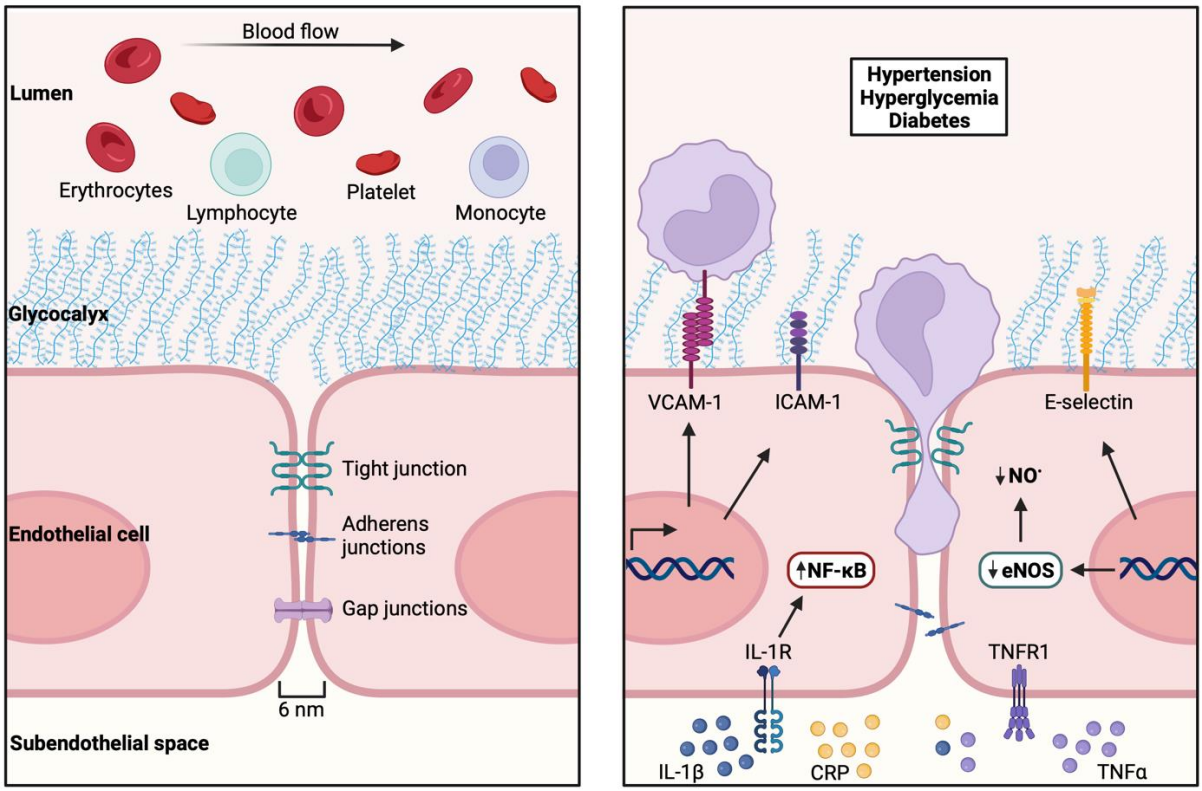

Figure 7: Development of endothelial dysfunction. The right side of the panel shows a healthy endothelium. The laminar surface of the endothelial-monolayer is covered with negatively charged glycocalyx to avoid immune cell or pathogen infiltration into the vascular wall. The left side of the panel demonstrates endothelial function after pathological stimuli, for example, triggered by hypertension, hyperglycemia, or diabetes mellitus. In response to the pathological conditions, pro-inflammatory NF-κB expression is upregulated. Different adhesion proteins (VCAM-1, ICAM-1, or E-selectin) at the surface of the endothelium promote immune cell infiltration into the subendothelial space. In addition, during the development of endothelial dysfunction, eNOS activity and •NO production are decreased, which further supports pro-inflammatory signaling and oxidative stress. Immune cells in the subendothelial space trigger the expression of pro-inflammatory proteins like IL-1β, CRP, or TNFα. Which in turn promotes further NF-κB expression in the endothelium. Adapted from (81). Created with BioRender.com. Abbreviations: VCAM-1=vascular cell adhesion protein-1, ICAM-1=intercellular adhesion molecule-1, IL-1β=interleukin-1β, CRP=c-reactive protein, TNFα=tumor necrosis factor α, eNOS=endothelial nitric oxide synthase.

1.4. Atherosclerosis

The vascular degenerative disease atherosclerosis is associated with inflammation and fibrofatty lesions in the artery wall. Atherosclerosis is initiated, for example, by endothelial dysfunction, injury of arterial walls, and vascular exposure to lipid proteins (82, 84). The pathogenesis of atherosclerosis can be categorized into three phases: initiation, progression, and complications (82, 84). Cumulative exposure to cholesterol-rich LDLs could lead to LDL accumulation in the artery intima, thereby initiating atherosclerotic plaque formation. Further, LDL particles in the intima are protected from plasma antioxidants, which cause LDL modification and oxidation (82, 85, 86). Indeed, predominantly NOX1 and NOX2-derived ROS could promote LDL oxidation (LDL-ox) in atherosclerosis initiation and progression (82, 85). The innate immune system also plays a crucial role in atherosclerosis initiation. Monocytes and macrophages are the initial recruited immune cells to the vasculature (82, 84, 87). Monocytes can be divided into two subclasses: the inflammatory Ly6C^{high} monocytes and the

resident/patrolling Ly6C^{low} monocytes. Both monocyte subclasses can differentiate into macrophages and dendritic cells (88, 89). Scavenger receptors on macrophages mediate ox-LDL particle uptake and promote the conversion of macrophages to foam cells (82, 85). Besides that, macrophages are also crucial for mediating plaque inflammation. Activated macrophages regulate monocyte and T cell migration further by inflammatory chemokine and cytokine production (82, 87). Different polarized macrophage subtypes are present in atherosclerotic plaques, for example, M1 and M2 macrophages. M1 macrophages are stimulated by toll-like receptor ligands (TLR), secrete IL-1ß, IL-6, IL12, or TNFα, and produce killing agents like iNOS. Therefore, M1 macrophages are involved in pro-inflammatory and pro-atherogenic processes and appear in the center of atherosclerotic plaques (87, 90). On the contrary, M2 macrophages are present far away from the lipid core. They are stimulated by IL-4 or IL-13 and secrete IL-10 and transforming growth factor ß (TGFß), which promote tissue repair and anti-inflammatory cytokine expression (91, 92). Also, neutrophil granule proteins contribute to plaque growth and local inflammation (93). The role of the adaptive immune system with antigen-presenting dendritic cells and the activation of T and B cells is described in more detail in 1.2.7. Besides inflammatory processes, oxidative stress also influences atherosclerosis pathogenesis. For example, NOX4-derived H_2O_2 production seems to have a protective role in atherogenesis by inhibiting inflammatory processes. Meanwhile, NOX5 activity appears to increase the proliferation of vascular smooth muscle cells, and NOS-derived $^{\bullet}NO$ mediates cardiovascular protection (anti-inflammatory, anti-apoptotic, anti-remodeling, inhibition of platelet aggregation, and vasodilation) (44). However, in the presence of other oxidants, for example, NOX-derived $O_2^{-\bullet}$, $ONOO^-$ is formed, leading to further modification of lipid proteins. Also, eNOS uncoupling and decreased $^{\bullet}NO$ production are observed during atherosclerosis (44, 61).

Further, endothelial function is affected by the hemodynamic environment; for example, blood flow disturbance also promotes plaque formation (94). Atherosclerosis pathogenesis is primarily studied in ApoE$^{-/-}$ or LDLr$^{-/-}$ mouse models. ApoE$^{-/-}$ mice develop atherosclerosis without dietary intervention and demonstrate a spontaneous hyperlipidemic profile, while LDLr$^{-/-}$ mice develop atherosclerotic pathologies after high-fat diet treatment (87). Figure 8 displays the initiation phase of atherosclerotic plaque development.

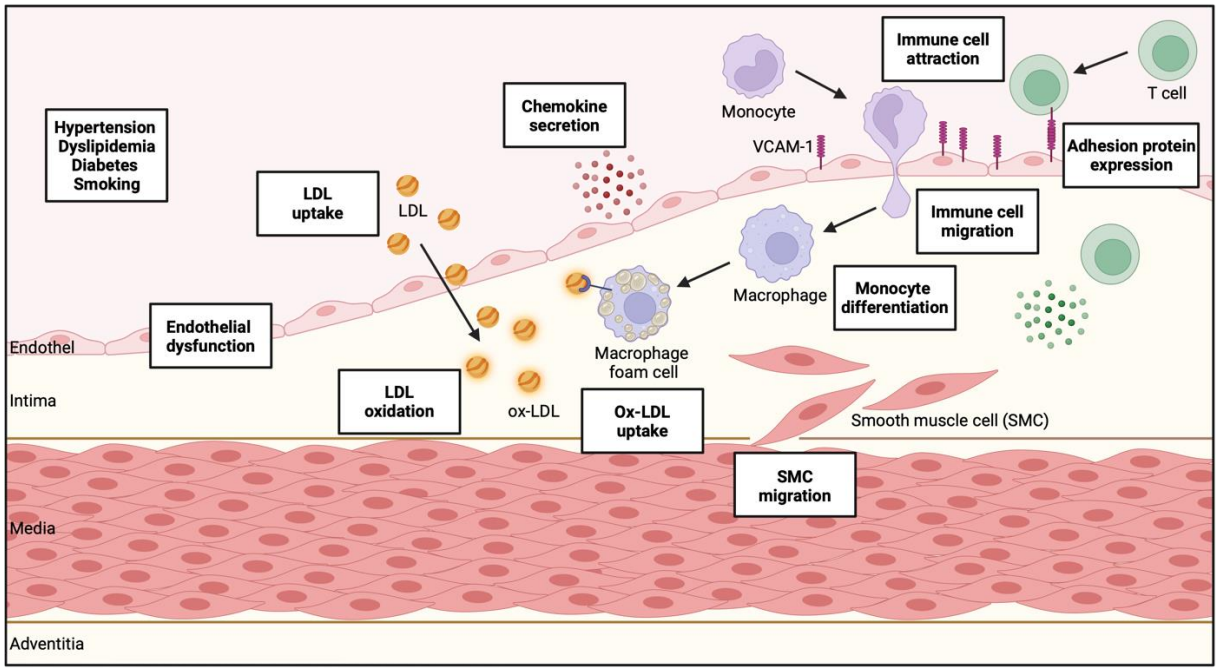

Figure 8: Initiation phase of atherosclerotic plaques. Atherosclerotic plaque formation is promoted by endothelial dysfunction, which is induced by hypertension, dyslipidemia, diabetes, or smoking. LDL particle oxidation is promoted in the intima of blood vessels. Macrophages take up the oxidized LDL particles, which differentiate them into foam cells. Endothelial dysfunctions promote further the onset of inflammation and oxidative stress in the vasculature. Endothelial cells secrete in response to inflammation or oxidative stress chemokines to attract immune cells. In addition, the adhesion protein expression in endothelial cells is increased to allow immune cell migration into the intima. In the intima, monocytes are differentiating, for example, into macrophages. Also, the smooth muscle cell migration to the intima is enhanced in the initiation phase of atherosclerotic plaque formation. Adapted from (82). Created with BioRender.com. Abbreviations: LDL=low-density lipoprotein, ox-LDL=oxidized LDL, SMC=smooth muscle cells, VCAM-1=vascular cell adhesion protein-1.

The progression of atherosclerotic plaques is characterized by more lipid and lipid-engorged cell accumulation. Leukocytic mediators lead to smooth muscle cell migration from the media into the intima, which leads to an accumulation and proliferation of smooth muscle cells in the growing atherosclerotic plaque. Further, recruited smooth muscle cells produce extracellular matrix proteins like collagen, elastin, or proteoglycans, which lead to more lipoprotein trapping and growing plaque sizes in the intima (95). The lipid-rich necrotic core formation is promoted by impaired clearance of dead macrophages and smooth muscle cells (96, 97). Increased risk of plaque rupture is promoted by thinning and structural weakening of the fibrotic cup mediated by T cell mediators, which hampers collagen synthesis of smooth muscle cells and macrophagic matrix metalloproteinase (MMP) secretion, which leads to collagen degradation (82, 98, 99). Figure 9 shows the progression of atherosclerotic plaques. Clinically relevant complications of atherosclerosis are growing plaques into the arterial lumen, which could impair arterial perfusion or plaque rupture and cause acute thrombosis (100).

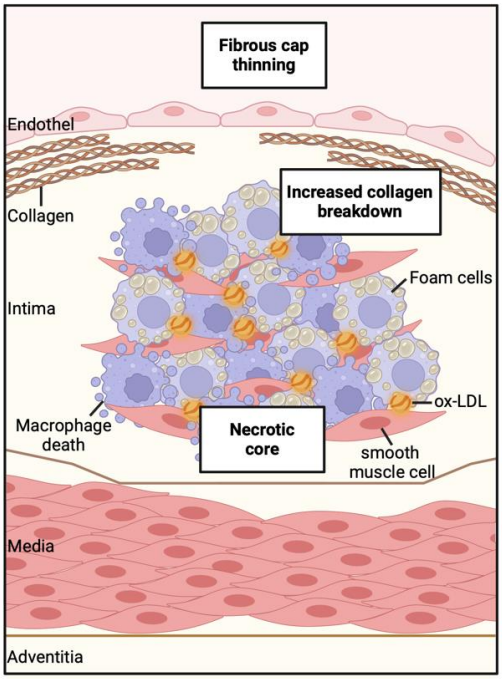

Figure 9: Progression of atherosclerosis and necrotic core formation. Necrotic cores comprise accumulated lipids, lipid-engorged cells, and smooth muscle cells. Further, impaired clearance of dead macrophages and smooth muscle cells promotes necrotic core formation. Smooth muscle cells recruited from the media into the intima produce collagen, elastin, and proteoglycans, which build a fibrous cap. Activated macrophages produce matrix metalloproteinases, which could promote collagen breakdown and fibrous cap thinning, increasing the risk of plaque rupture. Adapted from (82). Created with BioRender.com. Abbreviations: ox-LDL=oxidized low-density lipoprotein.

One of the most important primary interventions to prevent atherosclerosis onset is lifestyle modification, which includes a healthy diet, physical activity, and avoiding tobacco use (101). Guideline-directed pharmacological therapy is recommended in addition to lifestyle modifications for high-risk patients. For example, lipid-lowering therapy with statins could lead to a 30-50 % reduction of LDL/cholesterol levels; in combination with ezetimibe, the LDL/cholesterol levels could be further reduced by 15-20 % (102-104). In addition, antiplatelet drugs, such as aspirin, are crucial in the therapy of thrombotic processes, which are also associated with atherosclerosis pathogenesis. These drugs belong to the secondary treatment strategy as they are associated with a risk of bleeding (105, 106). Also, targeting low-grade inflammation, which is indicated, for example, by elevated plasma CRP levels, could decrease cardiovascular risk and is being investigated in different clinical trials. Canakinumab, an IL-1ß antibody, was the subject of investigation in the CANTOS trial and improved the cardiovascular outcome in patients after myocardial infarction (107, 108). Another study using colchicine as an unspecific anti-inflammatory agent also indicates a lower risk of ischemic events among patients with recent myocardial infarction (COLCOT study) (109). Meanwhile, methotrexate (folic acid antagonist) treatment did not reduce cardiovascular events in the CIRT trial (110). Until now, no anti-inflammatory drugs have been approved for cardiovascular protection.

1.5. Hypertension

Hypertension is a disease of the cardiovascular system associated with permanently increased pressure in the arterial vessels. Worldwide, approximately 1.28 billion adults (30-79 years) have hypertension, and 46 % of them are unaware that they have this disease. Only 1 in 5 (21 %) adults who know about the disease have it under control. Unless hypertension is a major cause of premature death worldwide, patients tend to underestimate the risk of hypertension because noticeable symptoms do not necessarily accompany it (111). According to the European guideline, hypertension is classified as systolic blood pressure (SBP) values >140 mmHg and diastolic blood pressure (DBP) >90 mmHg. However, correlations of cardiovascular and renal events have already been observed with SBP >115 mmHg and DBP >75 mmHg. The modifiable risk factors are like those of CVDs, including overweight, physical inactivity, high salt diet, and alcohol consumption (112). Recently, environmental factors like exposure to air pollution or noise have become increasingly important as hypertension and CVD risk factors (113, 114). Uncontrolled hypertension is related to the risk of serious cerebral, cardiovascular, and renal damage. Hypertension can be divided into a primary or secondary form. Primary hypertension is the predominant form triggered by genetic background or various environmental factors. Whereas the secondary form concerns only a small percentage of the overall hypertension prevalence and is caused by other diseases (for example, primary aldosteronism). The pathophysiology of hypertension is regulated by alterations in the renin-angiotensin-aldosterone system (RAAS), sympathetic nervous system, endothelin system, arginine-vasopressin peptide hormone expression, metabolomic pathways, and immune inflammation (112).

1.5.1. The Renin-Angiotensin-Aldosterone System (RAAS)

Vascular tone, blood volume, and electrolyte homeostasis are regulated via the RAAS. Therefore, RAAS plays an important role in the development and maintenance of arterial hypertension. RAAS is recognized as a medium-term regulator of blood pressure, whereas baroreceptor regulation is assigned to short-term mediation and altered blood volume to long-term regulation. Classically, the endocrine and paracrine RAAS comprise renin, angiotensinogen, angiotensin-converting enzyme (ACE), AT-II, and AT-II receptors (AT_1R and AT_2R). Targeted organs and RAAS members' expression occur in the brain, heart, vessel walls, liver, kidney, and adrenal glands (112, 115, 116).

The enzyme renin, which specifically mediates angiotensinogen cleavage to AT-I, is expressed and secreted mainly from juxtaglomerular cells of the kidney. Low blood pressure (systemic or renal), low sodium levels, or sympathetic nervous system activity led to increased renin expression and secretion. AT-I is converted from ACE to AT-II. In comparison to renin, ACEs are not substrate-specific and cleave other substrates besides AT-I, such as bradykinin (a

vasodilator). Further, ACEs are not sensitive to AT-II concentration changes. AT-II is the major bioactive peptide of the RAAS. AT-II binding to AT_1R triggers vasoconstriction, resulting in increased blood pressure, whereas AT-II binding to AT_2R leads to vasodilation and decreased blood pressure. Further, ACE2 metabolizes AT-II into AT1-7 and is an important regulator in the pathophysiology of hypertension, CVD, and renal diseases. AT-II signaling also mediates the release of the aldosterone hormone, which also increases blood pressure, as it stimulates kidneys to store sodium and potassium excretion. The increased sodium storage also increases water retention and blood volume (112, 115, 117). Figure 10 shows the RAAS structure. The role of the RAAS in cardiovascular diseases is described in more detail in the next section.

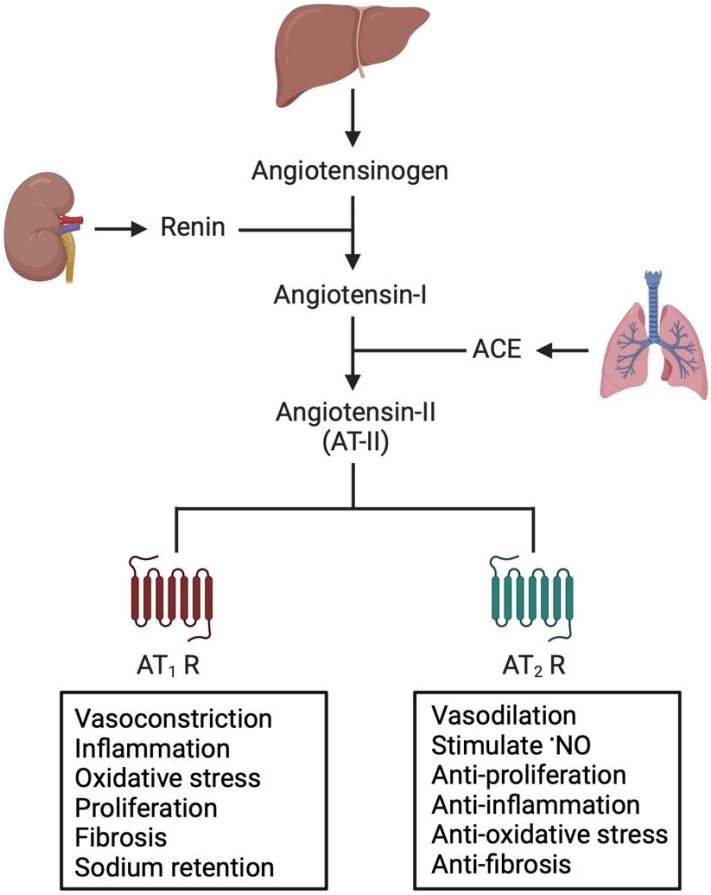

Figure 10: The composition of the renin-angiotensin-aldosterone system (RAAS). Pro-inflammatory signaling leads to an upregulation of RAAS and AT-II synthesis. Renin mediates the cleavage of angiotensinogen to angiotensin-I and is predominantly expressed in the kidney. AT-I is further processed by the angiotensin-converting enzyme (ACE) to AT-II. AT-II binding to AT_1 receptors mediates vasoconstriction and other blood pressure-increasing processes. Meanwhile, AT-II binding to AT_2 receptors leads to vasodilation and blood pressure lowering. Especially in the progression of CVD, AT-II signaling plays a central role. Created with BioRender.com. Abbreviations: RAAS=renin-angiotensin-aldosterone system, ACE=angiotensin converting enzyme, AT-II=angiotensin-II, AT_1R=angiotensin-II receptor type 1, AT_2R=angiotensin-II receptor type 2, CVD=cardiovascular disease.

Lifestyle adjustments like reduced salt intake, increased potassium intake, moderate alcohol consumption, smoking cessation, physical activity, and weight loss are recommended for all patients suffering from hypertension. In addition, five drug classes are recommended as first-line antihypertensive medication: ACE inhibitors (ACEis), AT-II receptor blockers (ARBs), calcium channel blockers (CCBs), Thiazide/Thiazide-like diuretics and beta-adrenoreceptor blockers (BBs). In many patients, blood pressure cannot be controlled with monotherapy, and a combined antihypertensive drug therapy is necessary. ACEis and ARBs targeting directly the RAAS. CCBs block calcium channels of smooth muscle cells and lead to vasodilation. Thiazide diuretics inhibit Na^+ and Cl^- cotransporters in renal tubes, promoting increased Na^+ and water excretion over the urine. Lastly, BBs reduce cardiac output, heart rate, renin release, and adrenergic nervous system effects, which also reduce blood pressure (112, 117).

1.5.2. Angiotensin-II (AT-II) is an important bioactive peptide in hypertension and atherosclerosis

The strong vasoconstricting agent AT-II is the major bioactive peptide of the RAAS and contributes to multiple cardiovascular, physiological, and pathophysiological mechanisms (115, 118). The widely expressed G-protein-coupled AT_1R mediates intracellular pathways by activating NOX, different protein kinases, and other growth factor receptors or directly interacting with associated proteins. The closest homolog to human AT_1R in mice is the $AT_{1A}R$ (118).

AT-II signaling leads to NOX activation, which promotes ROS formation (especially $O_2^{-\bullet}$ and H_2O_2) in the vasculature. Different signaling pathways are activated by ROS, like mitogen-activated protein kinases, tyrosine kinases, phosphatases, calcium channels, and redox-sensitive transcription factors (44, 118). Activating these pathways could produce extracellular matrix proteins, cell growth, and expression of pro-inflammatory genes, up to phenotype switch from contractile to proliferative vascular smooth muscle cells (119). The redox imbalance could also lead to eNOS uncoupling, promoting vasoconstriction (10, 119). Further, AT_1R activation in a G protein-dependent manner leads to activation of phospholipase C (PLC) and hydrolyzation of phosphatidylinositol 4,5-bisphosphate (PIP2), which results in IP3 and diacylglycerol (DAG) genesis. The second messenger, IP3, binds to its receptor IP3R on the ER or sarcoplasmic reticulum and leads to Ca^{2+} release into the cytosol. The second messenger, DAG, leads to PKC activation and $p47^{phox}$ phosphorylation, which leads to NOX2 activation and ROS production (119-121). Another example of ROS-mediated pathways is the activation of Rho kinases, which mediate via the inhibition of myosin light chain phosphatase and activation of myosin light chain kinase (MLCK) vascular smooth muscle cell constriction. MLCK activity is Ca^{2+}-dependent and promotes vasoconstriction, endothelial dysfunction, $^{\bullet}NO$ imbalance, hypertension, oxidative stress, and inflammation (118, 122). AT-II and increasing

cellular ROS stimulate the expression of NOX2/4, AT_1R, and receptors for advanced glycation endproducts (RAGE) via PKC-NF-κB signaling (123). Oxidative stress development and mediated signaling are described in more detail in section 1.2. AT-II signaling via AT_1R mediates inflammatory and mitogenic processes, besides vasoconstriction, demonstrated in mitogen-activated protein kinases (MAPK) activation and phosphorylation of protein tyrosine (118, 124). The transcriptional NF-κB protease-dependent VCAM-1 activation is also AT-II-induced and is important in atherosclerosis development (125). Further, AT_1R signaling mediates G protein-independent ß-arrestin activation and promotes vascular remodeling via MAPK signaling (126). Toll-like receptor 4 (TLR4) dependent signaling pathways are also activated via AT-II, which leads to up-regulation of pro-inflammatory NF-κB signaling, resulting in cardiac dysfunction, hypertension, fibrosis, and hypertrophy (118, 123). In monocytes, TLR4 signaling leads to upregulating MCP-1, IL6, and ROS (127). In summary, AT-II signaling mediates cell communication, apoptosis, growth, remodeling, and cardiovascular contractility. AT_1 signaling includes the crosstalk of other signaling cascades in addition to direct protein or receptor interaction and is, therefore, very complex. AT_1R signaling contributes to vascular remodeling, endothelial dysfunction, CVD, atherosclerosis, and organ damage (118, 119, 128). Figure 11 summarizes the AT-II receptor signaling mediated by AT_1R.

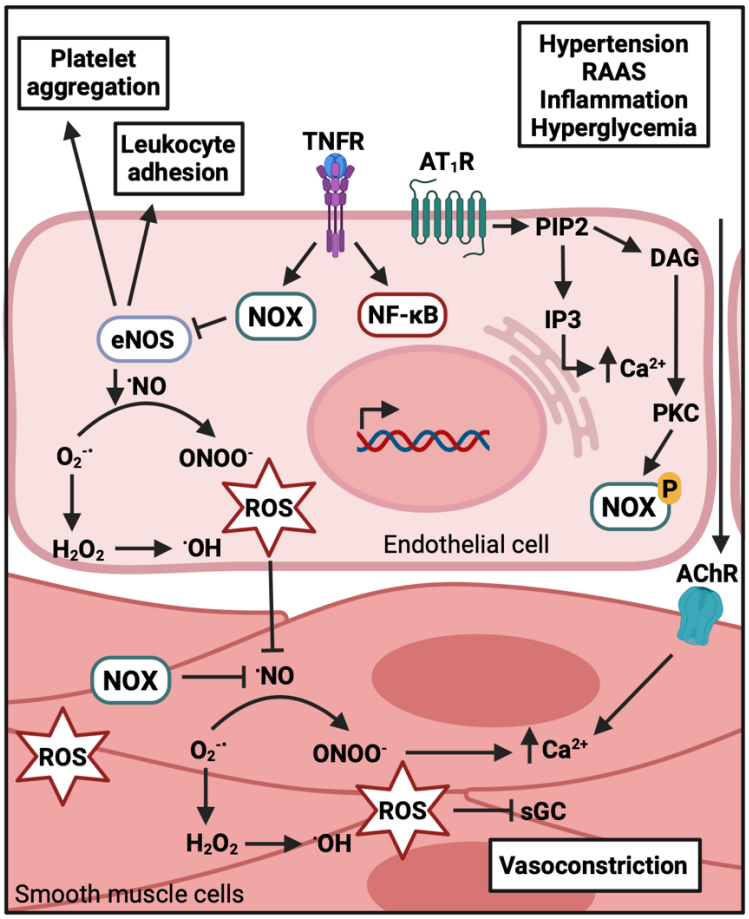

Figure 11: Angiotensin-II signaling promotes oxidative stress and eNOS uncoupling in endothelial cells. Pathological conditions like hypertension, inflammation, and hyperglycemia stimulate RAAS and angiotensin synthesis. Angiotensin-II signaling via AT_1 receptors promotes NOX activation and ROS generation in endothelial cells. AT_1R activation in a G protein-dependent manner leads to PIP2 hydrolysis, resulting in IP3 and DAG genesis as second messengers. IP3 mediates Ca^{2+} releases from the endoplasmic reticulum into the cytosol, and DAG activates PKC, leading to $p47^{phox}$ phosphorylation and NOX activation. The redox imbalance in the cells could lead to eNOS uncoupling, which means that eNOS produces $O_2^{-\bullet}$ instead of $^{\bullet}NO$. $O_2^{-\bullet}$ could react further in different steps to $ONOO^-$, H_2O_2, or $OH^{\bullet}$. Decreased $^{\bullet}NO$ diffusion could lead to platelet aggregation and leukocyte adhesion. In addition, pro-inflammatory signaling via, for example, TNF receptors supports NOX activation, NF-kB activation, and onset of pro-inflammatory protein expression. Decreased $^{\bullet}NO$ diffusion into the media results in vasoconstriction and increased blood pressure. NOX also generates ROS in smooth muscle cells, preventing hyperpolarization and soluble guanylyl cyclase blockage. Beginning endothelial dysfunction increases the endothelium's permeability for immune cell infiltration or messenger proteins. For example, acetylcholine diffuses across the semi-permeable endothelial barrier and induces Ca^{2+} signaling in smooth muscle cells. Adapted from (37, 120). Created with BioRender.com. Abbreviations: TNFR=tumor necrosis factor receptor, AT_1R=angiotensin-II receptor type 1, NOX=NADPH oxidase, eNOS=endothelial nitric oxide synthase, ROS=reactive oxygen species, PIP2= phosphatidylinositol 4,5-bisphosphate, IP3= inositol trisphosphate, DAG=diacylglycerol, PKC=protein kinase C, P=phosphorylation, sGC=soluble guanylyl cyclase, AChR=acetylcholine receptor.

1.6. Diabetes mellitus

Diabetes is a chronic metabolic disease accompanied by hyperglycemia, which causes severe damage to nerves and the vasculature. In 2019, diabetes caused 1.5 million deaths globally, and elevated blood glucose levels caused 20 % of cardiovascular deaths. In addition, diabetes caused 460000 kidney disease deaths globally in 2019. Diabetes mortality rates by age increased between 2000 and 2019 by around 3 % (3, 129). In 2021, diabetes affected 537 million individuals worldwide, which indicates a prevalence of 10.5 %, and this prevalence is expected to rise by 2045 to 12.2 % (783 million cases) (130, 131). Depending on the diabetes type, symptoms like polydipsia, frequent urination, blurred vision, fatigue, or losing weight can occur suddenly or can take many years to be noticed. Over time, diabetes can cause blindness, kidney failure, heart attacks, stroke, and lower limb amputation (129). Diabetes is classified into different types: diabetes mellitus type 1 (T1DM), diabetes mellitus type 2 (T2DM), gestational diabetes, monogenic diabetes, and secondary diabetes or stress hyperglycemia. Approximately 5-10 % of individuals with diabetes are suffering from T1DM. A characteristic of T1DM is the pancreatic ß-cell deconstruction by autoimmune processes, which results in deficient insulin production. Patients with T1DM need daily insulin administration. T2DM causes more than 90 % of the diabetes population. Patients with T2DM develop insulin resistance, which causes raised blood glucose levels. Often, T2DM is asymptomatic for years. Monogenic diabetes is accompanied by many mutations that cause glucose mishandling and do not fit in the class of T1DM or T2DM. Secondary diabetes and stress hyperglycemia occur secondary to different conditions and therapies, like in hospitalized patients with acute coronary syndrome (ACS) or heart failure. Lastly, gestational diabetes occurs during pregnancy, mainly in the second or third trimester (129, 131).

1.6.1. Pathophysiology of diabetes mellitus type 2

T2DM pathology is associated with defective insulin secretion of pancreatic ß-cells and insulin resistance (132). In healthy individuals, ß-cells produce insulin and store it in secretory vesicles. Insulin secretion is triggered in response to high glucose levels. Glucose transporter 2 (GLUT-2) at the surface of ß-cells is a glucose sensor and transporter. Glucose uptake leads to increased ATP/ADP concentrations, triggering the closing of ATP-dependent potassium channels. This, in turn, leads to the opening of voltage-dependent Ca^{2+} channels, and increasing intracellular Ca^{2+} leads to insulin exocytosis (132-134). In ß-cells, hyperlipidemia and hyperglycemia are inducing oxidative stress and ROS generation. ROS signaling leads to the inhibition of Ca^{2+} mobilization and activation of proapoptotic signals. Increasing free fatty acid levels and hyperglycemia generate ER stress by activating apoptotic unfolded protein response (UPR) (132, 135). Further, high glucose levels in ß-cells lead over time to increased biosynthesis of insulin precursor proteins. Accumulation and misfolding of these precursor proteins lead to ROS generation and IL-1ß release, attracting macrophages to ß-cell islets. Enhanced local islet inflammation and oxidative stress in ß-cells are associated with ß-cell dysfunction and ß-cell death (136, 137). Figure 12 shows essential signaling pathways in ß-cell physiology and ß-cell dysfunction.

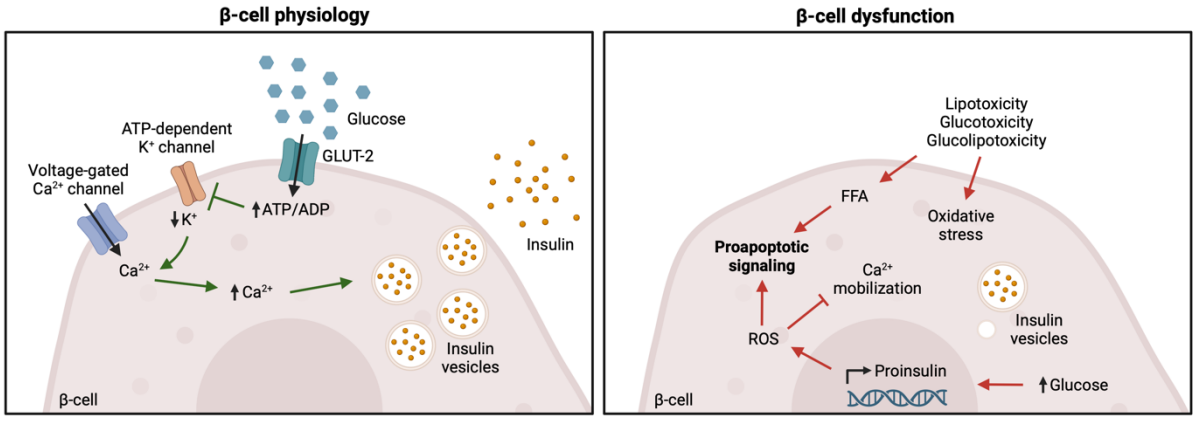

Figure 12: Insulin signaling of ß-cells and mechanisms which are causing ß-cell dysfunction. The first panel shows the physiological insulin secretion of ß-cells in response to high glucose levels. Glucose is taken up into ß-cells via glucose transporter (GLUT-2). Increasing glucose levels in the cells also lead to evaluated ATP/ADP levels and to the opening of ATP-depended potassium channels. The depolarization of the cell leads to the opening of voltage-gated Ca^{2+} channels. A high intracellular calcium level promotes insulin secretion. The left panel shows ß-cell dysfunction, for example, induced via lipotoxicity, glucotoxicity, or glucolipotoxicity. Free fatty acid and induced oxidative stress in ß-cells cause proapoptotic signaling. Further, high intracellular glucose levels lead to enhanced insulin precursor transcription. Accumulation of misfolded insulin precursor proteins leads in addition to increasing ROS production and proapoptotic signaling in ß-cells. Adapted from (132). Created with BioRender.com. GLUT-2=glucose transporter 2, FFA=free fatty acids, ROS=reactive oxygen species.

The main insulin-sensitive organs (besides the pancreas) are skeletal muscles, adipose tissue, and the liver. These organs are important in systemic insulin resistance development and T2DM progression (132). Physiologically, insulin signaling stimulates glucose uptake in skeletal muscles via glucose transporter-4 (GLUT4) and promotes glycogen synthesis (138).

Environmental factors contribute to T2DM and insulin resistance. For example, physical inactivity reduces blood flow in skeletal muscles, decreasing glucose utilization (139). Further, obesity is associated with chronic skeletal muscle inflammation, contributing to insulin resistance (140). In adipose tissue, insulin signaling leads to glucose uptake and triglyceride synthesis under physiological conditions. Insulin signaling suppresses triglyceride hydrolysis to free fatty acids and glycerol uptake in adipocytes (132). Impaired response to insulin causes impaired lipolysis and glucose uptake. In addition, adipocytes release free fatty acids to the plasma, accumulating in other organs like the liver (141). Obesity causes adipocyte hypoxia and hypertrophy, resulting in adipose tissue dysfunction and systemic low-grade inflammation. Under insulin stimulation, hypertrophic adipose tissue showed decreased glucose uptake and triglyceride synthesis, whereas free fatty acid release and pro-inflammatory signaling are increased (132, 142). Adipokine imbalance is related to insulin resistance in T2DM and could cause endothelial dysfunction, inflammation, and atherogenesis (132). In the liver, insulin is involved in glucose production and affects lipid metabolism. Hepatic glucose production is induced by glucagon, while enhanced plasma insulin levels inhibit hepatic glucose production and utilization (132, 143). Hepatic insulin resistance results in impaired glycogen synthesis, impaired suppression of glucose production, and increases pro-inflammatory signaling (144). In summary, insulin resistance causes reduced glucose uptake in skeletal muscles, adipose tissue, and the liver, whereas glucose production in the liver is increased. Further, diabetes-associated chronic inflammation is an important risk factor for atherosclerosis progression (132, 145).

1.6.2. Cardiovascular risk and diabetes mellitus type 2

T2DM is an important risk factor for atherosclerosis and CVDs. The pathological hyperglycemia, hyperinsulinemia, and insulin resistance in T2DM lead to endothelial dysfunction, diabetic dyslipidemia, and inflammation, as summarized in Figure 13 (131, 132).

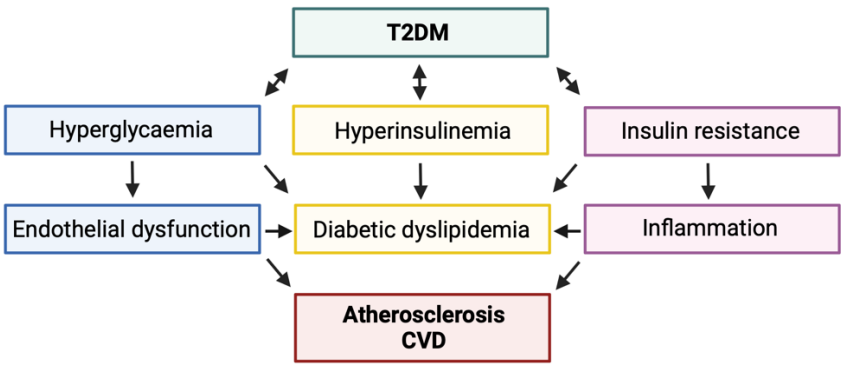

Figure 13: Type 2 diabetes mellitus (T2DM) is associated with a high cardiovascular risk. Adapted from (132). Created with BioRender.com. Abbreviations: T2DM=type 2 diabetes mellitus, CVD=cardiovascular disease.

Diabetic dyslipidemia is characterized by reduced high-density lipoprotein (HDL) levels and increased levels of triglycerides, triglyceride-rich lipoproteins (TRLs), and LDL particles (146). Insulin resistance led to impaired fat storage in adipocytes and free fatty acid release, which are taken up in hepatocytes. In hepatocytes, the free fatty acid can undergo ß-oxidation, lead to increased gluconeogenesis and worsening of hyperglycemia, or re-assimilate into triglycerides. These triglycerides can be stored, which leads to hepatic steatosis, or assemble into very low-density lipoproteins (VLDL) (132, 143, 147). Impaired metabolism and clearance of VLDLs are observed in T2DM and insulin resistance conditions. VLDLs undergo lipolysis to TRLs and smaller LDL particles, which causes cholesterol deposition and inflammation in arterial walls (132, 148, 149). Enhanced plasmatic TRL levels are associated with atherosclerosis progression and CVD risk (150, 151). Figure 14 summarizes the role of different lipoproteins and the development of atherosclerosis associated with T2DM pathology.

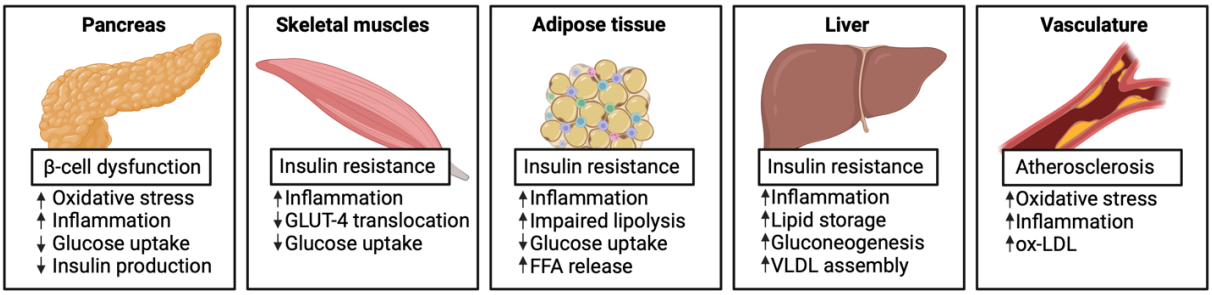

Figure 14: Type 2 diabetes mellitus (T2DM) pathology is associated with a high risk of atherosclerosis. The pathophysiology of T2DM promotes atherosclerosis progression. ß-cell dysfunction in the pancreas and impaired glucose uptake in skeletal muscles and adipose tissue due to insulin resistance, leading to enhanced glucose uptake in the liver. Further, inflammation and impaired lipolysis of adipocytes lead to increased release of free fatty acids to the circulation. In hepatocytes, free fatty acids can undergo re-assimilation into triglycerides. In T2DM pathology, enhanced VLDL assembly and release into the circulation is observed. These VLDL particles undergo lipolysis to TRL and finally to LDL particles. LDL particles promote atherosclerosis progression and are oxidized in the vascular. Created with BioRender.com. Abbreviations: T2DM=diabetes mellitus type 2, ox-LDL=oxidized low-density lipoproteins, TRL=triglyceride rich proteins, VLDL=very low-density lipoprotein, FFA=free fatty acids, GLUT-4=glucose transporter 4.

Further, chronic hyperglycemia induces endothelial dysfunction. Glucose can passively diffuse through endothelial cells and is metabolized in the sorbitol pathway, indirectly activating NADPH oxidation and reduction of NAD+. Those mechanisms change the cells' redox state, causing PKC activation, decreased $^{\bullet}NO$ levels, increased $O_2^{-\bullet}$ production, increased LDL oxidation, and enhanced cytotoxic effects (132, 152). The principles of endothelial dysfunction are further described in section 1.3.

In addition, increased RAAS activation is further increasing oxidative stress. Local RAAS upregulation is involved in the development and progression of insulin resistance and is positively correlated with T2DM (153). In skeletal muscles, increased AT-II bioavailability led to oxidative stress and suppression of insulin receptor phosphorylation via kinase blocking. The

translocation of GLUT-4 to the cell membrane is prevented, which results in impaired glucose uptake and insulin resistance. The resulting hyperglycemia also leads to increased local AT-II generation in other organs (153-155). Increased AT_1R-mediated signaling in adipose tissue leads to lipogenesis and impaired adipocyte proliferation. This results in adipose tissue overload with fat, which reduces the adipose fat buffering capacity and leads to fat storage in other organs like the liver (153-155). Enhanced triglyceride synthesis in the liver contributes to the development of insulin resistance, and dyslipidemia is associated with heart and kidney damage. Local upregulated RAAS is associated with morphological changes affecting kidney function, and further, in T2DM, RAAS is positively correlated with proteinuria and hypertension (153, 156, 157). Local RAAS upregulation in T2DM in the heart is associated with cell growth, cell proliferation, apoptosis, oxidative stress, inflammation, and fibrosis. These pathomechanisms contribute over time to cardiac remodeling and atherosclerosis development (153, 158). The role of local RAAS in T2DM pathology is summarized in Figure 15.

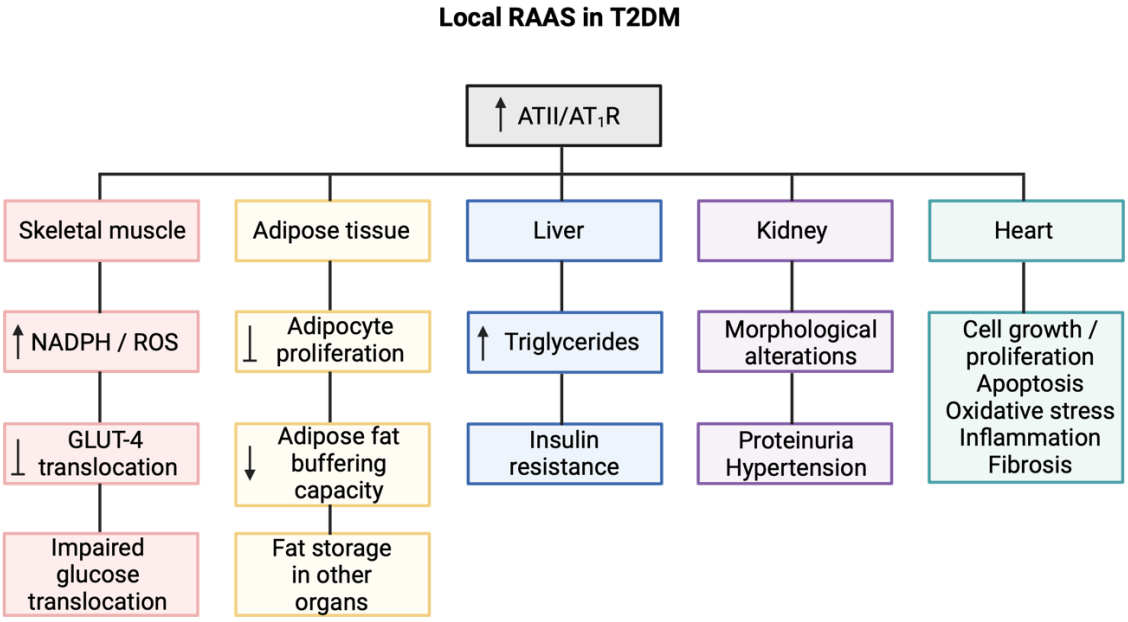

Figure 15: Local renin-angiotensin-aldosterone system (RAAS) signaling in type 2 diabetes mellitus (T2DM). Enhanced local RAAS-mediated AT-II signaling via AT_1 receptors contributes to T2DM and associated comorbidity progression. Regarding T2DM, the RAAS-mediated signaling could particularly affect organs like skeletal muscle, adipose tissue, liver, kidney, and heart. Elevated AT-II signaling generally promotes oxidative stress, inflammation, and insulin resistance, which can lead to organ damage. Adapted from (153). Created with BioRender.com. Abbreviations: RAAS=renin angiotensin aldosterone system, AT-II=angiotensin-II, T2DM=diabetes mellitus type 2, AT_1R=angiotensin type receptor 1, ROS=reactive oxygen species, GLUT-4=glucose transporter-4.

Modifiable risk factors of diabetes are lifestyle adaptations like weight reduction, change in diet or nutrition, smoking cessation, increasing physical activity, and exercise. Important for diabetic patients is also the monitoring of CVDs (129, 131). Cardiovascular efficacy was demonstrated

in cardiovascular outcome trials for glucose-lowering medications like sodium-glucose co-transporter-2 (SGLT2) inhibitors or glucagon-like peptide-1 receptor agonists (GLP1 RAs) (159-163). Other glucose-lowering medications like dipeptidyl peptidases-4 (DPP-4) inhibitors and insulin showed cardiovascular safety but no additional efficacy in cardiovascular outcome trials (164-167). Some older glucose-lowering medications like metformin or sulphonylureas were not tested in cardiovascular outcome trials considering CVDs (131).

1.7. CD40L-CD40-TRAF signaling is linked to inflammation and cardiovascular diseases

CD40L-CD40 signaling pathway has been recognized as a key player in developing inflammatory and autoimmune diseases like atherosclerosis, diabetes mellitus, rheumatoid arthritis, lupus erythematosus, and allograft rejection (168). Crucial physiological immunological and pathological inflammatory processes are mediated by CD40L-CD40 signaling. Since CD40L signaling is involved in beneficial and harmful signaling paths, developing a suitable treatment strategy targeting low-grade inflammation or atherosclerosis is challenging (169, 170).

1.7.1. Non-classical CD40L-integrin signaling

CD40L (CD154 or gp39) belongs to the TNF receptor superfamily. It is expressed by cells belonging to the immune/hemopoietic system (like T cells, B cells, basophils, eosinophils, monocytes, macrophages, Kupffer cells, natural killer cells, platelets, mast cells, and dendritic cells) as well as the vascular system (like endothelial cells, smooth muscle cells, and epithelial cells). Meanwhile, the human gene expression of CD40L is the highest in hemopoietic cells, T cells, and megakaryocytes (progenitors of erythrocytes) (171). Mutations within the CD40L (or CD40) gene could lead to the development of the X-linked hyper IgM syndrome, a rare disorder affecting the immune system. Due to inborn immune suppression like defective T cell priming, macrophage activation, and lack of other immune globulins than IgM, this defect could increase the risk of opportunistic infections, possibly leading to death (172). CD40L is present in two different isoforms: (I) a 33 kDa version, which forms predominantly trimeric complexes at the cell surface, and (II) an 18 kDa soluble version (sCD40L), which lacks the transmembrane domain (171, 173). Four different receptor proteins of CD40L are described in the literature (see Figure 16): the integrins $\alpha_M ß_2$ (or MAC-1), $\alpha_5 ß_1$ (or VLA-5), and $\alpha_{IIb} ß_3$, as well as CD40 (174). The interaction of CD40L-MAC-1 results in pro-inflammatory signaling, such as mediation of monocyte adhesion, migration, and MPO secretion. Indeed, *in vivo* Mac-1 inhibition results in reduced macrophage invasion into atherosclerotic lesions, which slowed down the progression of atherosclerosis in a high-cholesterol mouse model (175). In different human cell cultures, it was demonstrated that (s)CD40L-VLA-5 signaling mediates

inflammasome activation by expression and secretion of IL-1ß, IL-6, IL-8, and MCP-1 (176-178). Platelet activation and spreading are induced in an sCD40L-$\alpha_{IIb}ß_3$-depended manner, leading to arterial thrombi stabilization *in vivo*. Additionally, platelet aggregation is promoted under high shear stress by sCD40L (179). Furthermore, in response to shear stress or injury, CD40L-CD40 interaction at endothelial cells could lead to a deposit of ultra-large von Willebrand factors (UlvWFs), multimeric glycoproteins with high thrombogenic potential. Besides UlvWFs deposition, CD40L-CD40 mediates monocyte recruitment and platelet adhesion to endothelial cell walls, critical steps in atherogenesis (180). In summary, CD40L-Integrin signaling and CD40L-induced UlvWF formation are key players in vascular inflammation, thrombus initialization, and stabilization.

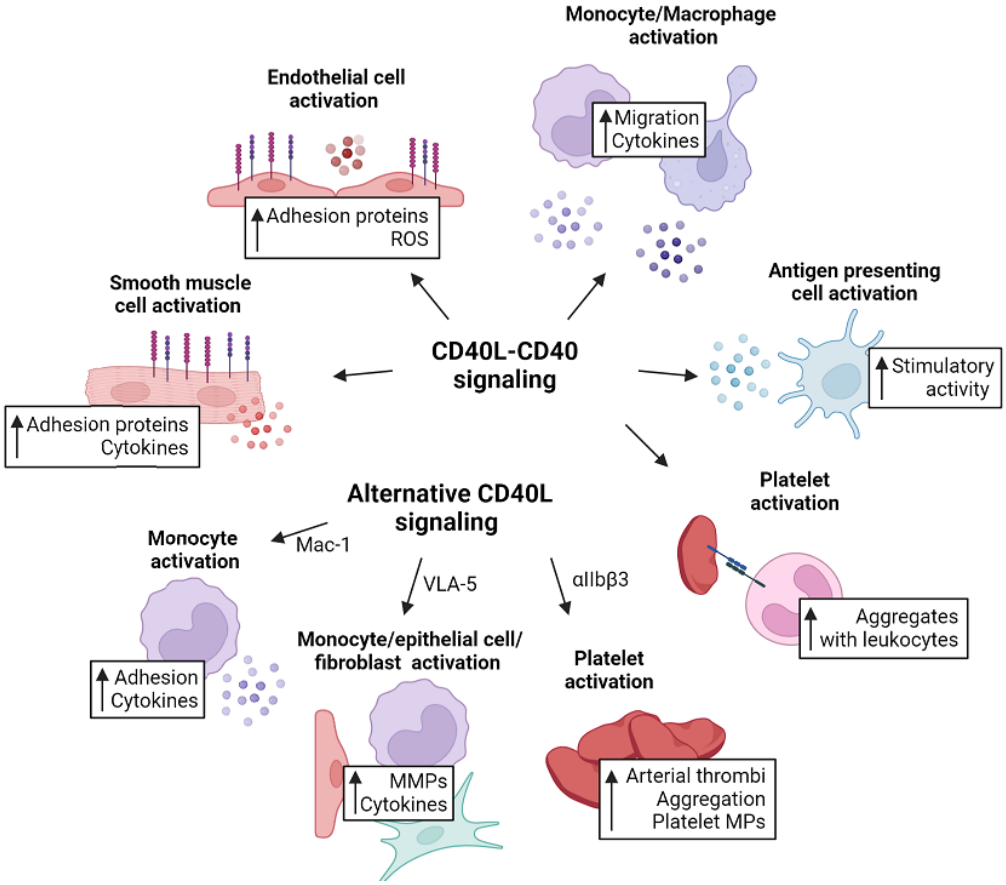

Figure 16: A broad overview of CD40L-mediated pro-inflammatory signaling. CD40L could bind to three different integrins ($\alpha_M ß_2$/MAC-1, $\alpha_5 ß_1$/VLA-5, and $\alpha_{IIb} ß_3$) and CD40. CD40L mediates pro-inflammatory signaling, which involves monocyte adhesion and migration, pro-inflammatory protein expression, and the release of chemokines and cytokines. Furthermore, CD40L signaling also plays an important role in thrombus initialization and stabilization. The scheme was adapted from (169). Created with BioRender.com. Abbreviations: MAC-1=macrophage antigen 1, VLA-5=very late antigen 5.

1.7.2. Classical CD40L-CD40-TRAF signaling

CD40 is the classical binding partner of CD40L, which also belongs to the TNF receptor superfamily, and together, they play a major role in immune system response (Figure 16). CD40 is like CD40L expressed by cells belonging to the immune/hemopoietic system (like

thrombocytes, B cells, dendritic cells, neutrophils, activated T cells, macrophages, and fibroblasts) as well as the vascular system (like endothelial cells and smooth muscle cells). The highest human gene expression was observed in dendritic cells and intermediate in B cells and megakaryocytes (171, 181). As CD40L, CD40 trimerizes at the cell surface. CD40 has no intrinsic signal capabilities and needs small adaptor proteins for signal transduction, named TNF receptor-associated factors (TRAFs) (182). CD40 contains two binding sites at its cytosolic tail for TRAFs: (I) a distal binding site for TRAF2/3/5 and (II) a proximal binding site for TRAF6 (183, 184).

TRAF1, TRAF2, and CD40 form heterotrimers, which lead to pro-inflammatory signaling by NF-κB and p38 MAPK pathway activation (185, 186). TRAF1 gene expression is mainly limited to activated immune cells via NF-κB (187, 188). Global TRAF1$^{-/-}$ mice are viable and fertile. Also, normal lymphocyte development was observed. Indeed, this mouse model showed enhanced TNF signaling in T lymphocytes, and the skin of the mice was hypersensible to TNF-induced necrosis, which indicates that TRAF1 negatively regulates TNF signaling (189). In another study, TRAF1$^{-/-}$ mice were combined with LDL receptor deficiency mice (TNFR1$^{-/-}$/LDLR$^{-/-}$). These mice developed smaller atherosclerotic lesions containing fewer macrophages, reduced adhesion of monocytes, and reduced expression of adhesion molecules (ICAM-1, VCAM-1) in endothelial cells, and macrophage was observed. The authors conclude after these findings that TRAF1 could be a potential treatment target for atherosclerosis. Further, TRAF1 levels were elevated in the blood of ACS patients (190). Taken together, TRAF1-mediated signaling seems to have a pro-inflammatory role and could play an important role in atherosclerosis pathogenesis.

CD40-TRAF2 homodimer formation activates NF-κB, c-Jun N-terminal kinases (JNK), or p38 MAPK signaling (191, 192). TRAF2 is essential for normal adaptive immune response, lymphocyte homeostasis, and for mediating cell survival. Global TRAF2$^{-/-}$ mice lead to premature lethality due to chronic inflammation and impaired T cell homeostasis (193, 194). More precisely, TRAF2 deficiency in mice leads to NF-κB activation, evaluated TNF levels in serum, and increased sensitivity of TNF-induced cell death of thymocytes and hematopoietic progenitors (194). TRAF2 also plays a role in cardiovascular inflammation and cardiac hypertrophy (192). In mice, TRAF2 expression is upregulated in atherosclerotic plaques and failing hearts (175). Cardiac-specific overexpression in mice leads to cardiac remodeling, such as hypertrophy and left ventricular dysfunction (195, 196). Like TRAF2, CD40-TRAF3 interaction activates NF-κB signaling (197, 198). Global TRAF3$^{-/-}$ mice showed postnatal lethality (within ten days) due to functionally defective T cells and permanent activation of NF-κB, resulting in multi-organ inflammation (192, 198). In humans and mice, TRAF3 expression levels are upregulated during cardiac hypertrophy. Cardiac-specific TRAF3$^{-/-}$ mice showed in response to pressure overload protection from cardiac hypertrophy; therefore, TRAF3 seems

to be a positive regulator of pathological cardiac hypertrophy (199). In cell culture experiments using endothelial cells, it was shown that TRAF3 expression is upregulated by shear stress, thereby preventing CD40-mediated endothelial activation by inhibiting pro-inflammatory cytokine expression and tissue factors (200). Until now, no evidence exists that TRAF4 is involved in inflammation or pathological processes in the cardiovascular system (201). CD40-TRAF5 interaction could be forced by the homodimer formation of TRAF3 and TRAF5, activating NF-κB and JNK signaling (202, 203). After myocardial infarction, $TRAF5^{-/-}$ mice exhibit more serious heart damage, inflammatory response, and apoptosis. Also, TRAF5 overexpression in hypoxia/reoxygenation-treated cardiomyocytes leads to less inflammation and apoptosis. Therefore, TRAF5 expression seems to be protective in myocardial ischemia-reperfusion models (204). $TRAF5^{-/-}LDLR^{-/-}$ mice consuming a high-cholesterol diet developed larger atherosclerotic plaques containing more lipids and macrophages than TRAF5-expressing control animals. TRAF5 deficiency leads to increasing inflammatory cell recruitment and foam cell formation. Further, significantly lower amounts of TRAF5 mRNA in blood were observed in ACS patients (190, 205). $TRAF5^{-/-}$ mice consuming a high-fat diet showed enhanced weight gain and fasting blood glucose levels. Further, increased leukocyte infiltration and pro-inflammatory protein expression were observed in visceral adipose tissue from these mice. These data indicate that TRAF5 could promote anti-inflammatory and obesity-preventing signaling in adipose tissue (206). In addition, TRAF5 deficiency in a pressure overload mouse model leads to cardiac hypertrophy and dysfunction aggregation, indicating that TRAF5 acts as an intrinsic cardioprotective factor (207). In addition, it was demonstrated that TRAF2/3/5 signaling does not affect atherosclerosis or neointima formation (208, 209).

CD40-TRAF6 interaction promotes NF-κB signaling (210). Through TRAF2-TRAF6 binding, JNK and p38 MAPK signaling are also activated (211). $TRAF6^{-/-}$ mice have an impaired immune system, like inflammatory cell accumulation in organs, thymic atrophy, and lack of secondary lymphatic organs (201, 212). In contrast to TRAF2/3/5, TRAF6 is more involved in pro-inflammatory processes. It was demonstrated that CD40-TRAF6 deficiency abolish atherosclerosis in $ApoE^{-/-}$ mice. Indeed, defective CD40-TRAF6 signaling leads to impaired recruitment of monocytes to arterial walls, reduced inflammatory cytokine production, and macrophage polarization toward an anti-inflammatory state (209). In contrast to endothelial TRAF6 deficiency in $ApoE^{-/-}$ mice, a myeloid cell-specific TRAF6 deficiency led to exacerbated atherosclerosis with larger plaques, reduced capability to clear apoptotic cells and impaired expression of the athero-protective cytokine IL-10. In conclusion, TRAF6 in endothelial cells promotes atherosclerosis, whereas TRAF6 regulates pro-survival and athero-protective mechanisms in myeloid cells (213). Also, in human atherosclerotic plaques, TRAF6 levels are elevated (209). Cardiac-specific TRAF6 overexpression leads in response to pressure overload or AT-II to pathological exacerbate cardiac hypertrophy. Further, in response to ROS

production, TRAF6 expression is enhanced in human and murine hypertrophic hearts and mediates the effects of TRAF6 on cardiac remodeling (214). Until now, no evidence exists that TRAF7 signaling is involved in inflammation or pathological processes in the cardiovascular system (201).

In summary, TRAF2/3/5 seems to have a more regulatory role in the immune system concerning atherosclerosis. It has been shown that the signaling seems to be protective and anti-inflammatory. In contrast, TRAF6 signaling appears to be the main driver in macrophage-activated pro-inflammatory signaling in atherosclerosis, promoting tissue damage and cell death. The role of TRAF signaling in atherosclerosis is summarized in Figure 17.

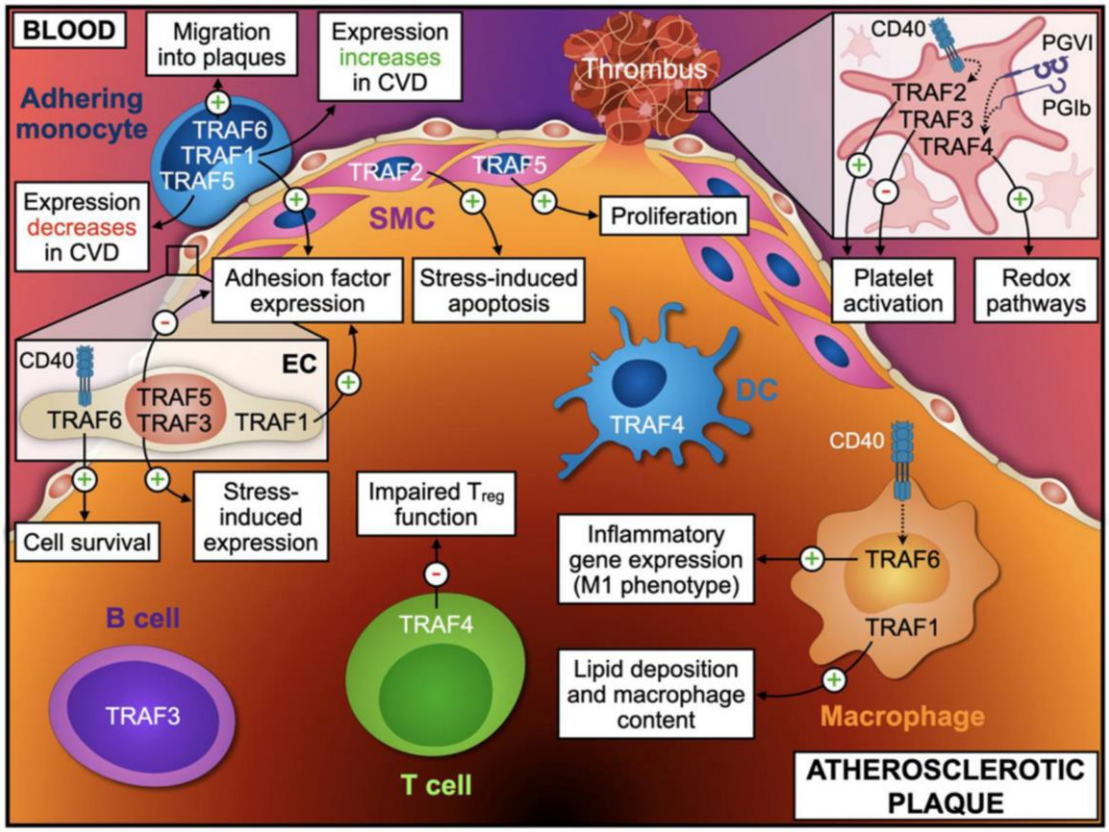

Figure 17: TRAF signaling in atherosclerotic plaques. Different TRAF isoforms (TRAF1, 2, 3, 4, 5, and 6) have been identified to be involved in atherosclerotic plaque formation and growth. TRAF1 expression is increased in CVD and is associated with pro-inflammatory signaling, such as adhesion factor expression and immune cell infiltration into the vascular wall. Lipid deposition by tissue macrophages is also associated with TRAF1 expression. TRAF2 expression in the smooth muscle cells promotes stress-induced apoptosis and is crucial for CD40-mediated platelet activation. Meanwhile, TRAF3 expression in platelets is inhibiting platelet activation. In endothelial cells, TRAF3 is mediating stress-induced protein expression. TRAF4 is expressed in dendritic cells and regulatory T cells in the inflamed vascular wall. In addition, TRAF4 promotes redox pathways in platelets. Adhering monocytes demonstrate decreased TRAF5 expression during CVD. Further, TRAF5 in endothelial cells inhibits adhesion factor expression and promotes the proliferation of smooth muscle cells. TRAF6 expression in adhering monocytes promotes migration into the vascular wall, and in endothelial cells, CD40-TRAF6-mediated signaling promotes cell survival. CD40-TRAF6 mediated macrophage signaling mediates inflammatory gene expression and M1 phenotype transition. Taken from (201) and created initially with BioRender.com. Abbreviations: TRAF=tumor necrosis factor associated factor, CVD=cardiovascular disease, SMC=smooth muscle cell, DC=dendritic cell, PGVI=platelet glycoprotein VI, PGIb=platelet glycoprotein Ib.

1.8. CD40L-CD40-TRAF signaling as a potential therapeutic target in atherosclerosis

1.8.1. Global CD40L or CD40 inhibition

$CD40L^{-/-}$ mice are viable and fertile but have a phenotype like the human hyper IgM syndrome and are exposed to an increased risk of infections (215). CD40L deficiency positively influences AT-II-induced vascular dysfunction and hypertension in mice. It was demonstrated that hypertensive $CD40L^{-/-}$ mice have an improved endothelial function. Further, CD40L deficiency reduces platelet monocyte interaction in blood and decreases oxidative stress in the cardiovascular system (216). CD40L deficiency in high-fat diet-treated mice leads to a normalization of weight gain, blood cholesterol levels, endothelial function, expression of inflammatory markers, and platelet activation (217). In contradiction of these positive effects, CD40L deficiency also carries some risks. As described in 1.7.1, sCD40L has a crucial role in arterial thrombi stabilization in an $\alpha_{IIb}ß_3$ dependent manner. This results in unstable thrombi formation in $CD40L^{-/-}$ mice mesenteric arterioles, leading to a higher risk of thrombus rupture and embolism (179, 218). Unfortunately, these adverse effects were also observed in a clinical trial, including patients suffering from lupus nephritis. The clinical trial was terminated after thromboembolic events occurred among the study participants, who were treated with a CD40L antibody (BG9588) (219). Thromboembolic events were also observed in a monkey kidney allograft model after CD40L monoclonal antibody treatment (220). After these events, CD40L antibodies were adjusted to prevent thromboembolic side effects. The first successfully described adjusted CD40L antibody (CDP7657) lacking the functional Fc region did not induce thrombotic events but simultaneously inhibited CD40L-mediated immune responses in monkeys (221). A clinical trial is currently in progress (phase 3; NCT04294667) using the adapted CD40L antibody (dapirolizumab pegol) as a treatment strategy for lupus erythematosus suffering patients. Until now, no severe side effects (only mild or moderate), thromboembolic events, or deaths occurred within the treatment groups (222, 223). Another clinical study (phase 1) using a humanized monoclonal CD40L antibody (toralizumab/IDEC-131) is ongoing in multiple sclerosis patients and seems safe and well tolerated (224).

$CD40^{-/-}$ mice are viable and fertile, but again, like $CD40L^{-/-}$ mice, they develop a similar phenotype to the human hyper IgM syndrome and exhibit impaired germinal center formation (225). In contrast to high-fat-diet-treated $CD40L^{-/-}$ mice, $CD40^{-/-}$ mice had no protective phenotype. They displayed worsened insulin resistance and excessive inflammation of adipose tissue. More detailed investigations showed that only CD40-TRAF2/3/5 signaling seems protective against metabolic dysfunction and obesity-associated inflammation, whereas CD40-TRAF6 signaling leads to a contrary effect (226). CD40 deficiency reduces atherosclerosis in $CD40^{-/-}ApoE^{-/-}$ mice, associated with decreased inflammatory cell content, reduced plaque macrophages, and higher fibrotic plaque quality (209). Also, clinical trials with

CD40 antibodies are currently ongoing. For example, in phase 1, an anti-CD40 monoclonal antibody (ASKP1240) was tested regarding safety, tolerability, pharmacokinetics, and -dynamics in addition to standard immunosuppressant after kidney transplantation or plaque psoriasis patients. No cytokine release syndrome or thromboembolic events were observed after CD40 antibody treatment in the study groups (227-229). Various other clinical trials are taking place in phase 1 or 2 to investigate whether CD40 antibodies are a potential novel treatment strategy for autoimmune diseases like lupus nephritis, systemic lupus erythematosus, rheumatoid arthritis, or Crohn's disease (230-233).
In summary, it is still unclear whether CD40L or CD40 blockade via antibodies is appropriate for treating atherosclerosis or inflammatory diseases. A step in the right direction encompasses thromboembolisms (CD40L). Still, it remains to be investigated if the strong immunosuppression accompanying CD40 antibody application is a suitable treatment strategy for atherosclerosis or if the side effects tend to predominate.

1.8.2. Tissue specific CD40L or CD40 inhibition

A long-term treatment to prevent atherosclerosis with CD40L or CD40 antibodies seems unsuitable due to previously (see 1.8.1) mentioned effects of strong immunosuppression or thromboembolic events. One possibility to avoid these side effects would be a more targeted treatment strategy, for example, with nano pharmaceuticals or developing cell-type specific antibodies (234, 235). Several *in vivo* studies regarding cell type-specific knockout of CD40(L) are ongoing. Some of them are described here in more detail. $ApoE^{-/-}$ mice with induced endothelial-specific CD40 deficiency showed a more stable plaque phenotype characterized by improved plaque lipid deposit, increased collagen, and smooth muscle content. Further, inflammatory cell recruitment to atherosclerotic lesions was indicated by decreased expression of adhesion proteins (e.g., ICAM-1 or VCAM-1) followed by impaired leukocyte adhesion (236). In $CD4^+$ T cell-specific CD40L deficient mice on an $ApoE^{-/-}$ background, smaller atherosclerotic plaques, decreased INFγ expression, and impaired T_H1 cell polarization were observed. A similar phenotype was expressed in a $CD11c^+$ dendritic cell-specific CD40 deficiency in mice on an $ApoE^{-/-}$ background (237). In line with these findings, in human plasma of patients with cerebrovascular disease, the sCD40L/CD40 expression levels correlate with INFγ expression and atherosclerotic plaques (237). Deficiency of CD40L in $Pf4^+$ platelets did not affect atherosclerotic plaque development or phenotype, whereas atherothrombosis progression was influenced by reduced platelet deposit and fibrinogen content in thrombi (237). Mice lacking myeloid-specific CD40 expression on an $ApoE^{-/-}$ background showed a less activated immune cell profile, reduced atherosclerosis, and increased alternative macrophage activation (238). Also, CD40 deficiency specific on leukocytes in high-fat diet-treated $LDLR^{-/-}$ mice leads to impaired macrophage migration and thereby reduced atherosclerosis (209). CD40

adipocyte-specific deficiency in mice with ApoE$^{-/-}$ background results in fewer lymphoid progenitors, increased T cell activation, decreased B cells in lymphoid organs, and decreased atherosclerotic lesion size but induced necrotic core formation (239).

CD40L-CD40 signaling in endothelial, T, dendritic, and myeloid cells is crucial in atherogenesis, pro-inflammatory signaling, and cell migration. On the other hand, CD40L expressed on platelets is more involved in atherothrombotic processes. Further, adipocytic CD40 signaling is an important regulator in hematopoiesis and pro-inflammatory signaling. The generation of cell-specific CD40L or CD40 deficiency is an important tool for better understanding the molecular mechanisms of the signaling cascade in inflammatory processes and the progression of atherosclerosis. Targeting CD40(L) blocking is a promising treatment strategy for atherosclerosis, which could eliminate the side effects of general protein blocking.

1.8.3. CD40-TRAF inhibition

Another possibility for reaching a more selective CD40 blockade to eliminate side effects is the analysis of downstream targets. In 1.7.2, it is already described that CD40-TRAF6 signaling and not CD40-TRAF2/3/5 signaling is important in activating pro-inflammatory processes and atherosclerosis pathogenesis (209). Therefore, a cell-permeable compound that targets TRAF6 at the C terminal domain and disrupts its functional coupling with CD40 was developed. The propanone compound (6877002) targets TRAF6 via direct affinity interaction (K_d = 97 µM) and has the following chemical formula $C_{17}H_{17}NO$. The biological evaluation of the top seven inhibitor hits was performed via IL-6 and IL-1ß mRNA expression analyses and LPS-induced NF-κB assay in stimulated bone marrow-derived macrophages. *In vivo*, the TRAF6 inhibitor was first tested in high-fat diet-fed animals to analyze its influence on metabolic function. The mice displayed after the treatment improved insulin sensitivity, decreased inflammation in adipose tissue through less pro-inflammatory macrophage polarization, and reduced hepatosteatosis. These results indicate that pharmacological CD40-TRAF6 inhibition could be suitable to ameliorate obesity-related metabolic complications (226, 240). After TRAF6 inhibitor treatment in diabetic mice (db/db), decreased levels of oxidative stress, inflammatory markers, and improved endothelial function were observed (217). In ApoE$^{-/-}$ mice, pharmacological TRAF6 inhibition prevents the initiation of atherosclerosis (241). Further, the progression of atherosclerosis is prevented by this treatment via reduced leukocyte recruitment and macrophage activation. Important is that the classical CD40-mediated immune responses seem to be not impaired; no interference with Ig isotype switching, antigen-specific T cell proliferation, antibacterial response, and only minor effects on the activation status of B and T cells were observed (241). Figure 18 shows CD40(L) signal transduction via different TRAFs and the impact of specific TRAF inhibition.

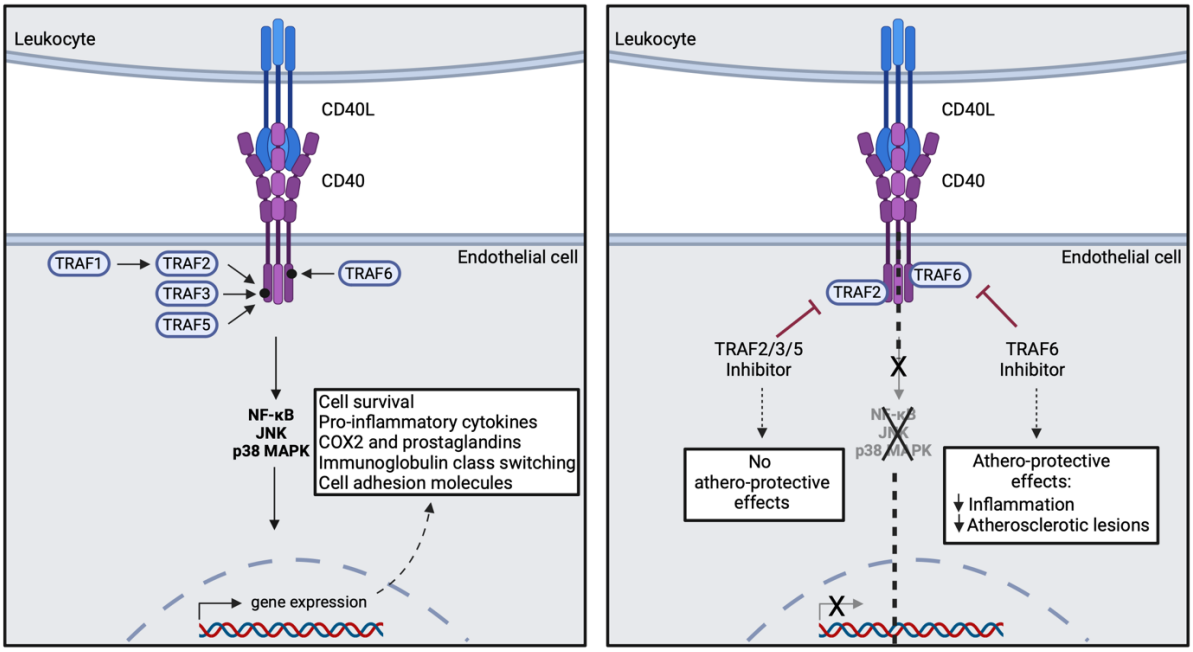

Figure 18: CD40(L) signal transduction via TRAFs. CD40 has no intrinsic signaling capabilities and needs; small adaptor proteins are called the so-called TRAFs. CD40 contains two binding sites for TRAFs: a more distal binding site for TRAF2/3/5 and a proximal binding site for TRAF6. TRAF1 is binding via TRAF2 to CD40. TRAFs activate different signal cascades like NF-κB, JNK, or p38 MAPK. These signaling cascades activate gene expression and regulate, for example, cell survival, inflammation, or immunoglobulin class switching. The left panel is focused more on TRAF inhibition. TRAF2/3/5 inhibition in an ApoE$^{-/-}$ mouse model displayed no athero-protective effects, whereas a selective TRAF6 inhibition showed athero-protective effects like reduced inflammation and atherosclerotic lesion size. The scheme was summarized from (241) and published in (170). The original scheme was created with BioRender.com. Abbreviations: TRAF=tumor necrosis factor associated factor, JNK=c-Jun N-terminal kinase, p38 MAPK=p38 mitogen-activated protein kinase, NF-κB=nuclear factor kappa B, COX2=cyclooxygenase 2.

Further improvement is the development of a nanoparticle therapy that targets macrophage-specific TRAF6 inhibition via recombinant HDLs. In atherosclerotic mice (ApoE$^{-/-}$), the nano immunotherapy reduces plaque volumes, and anti-inflammatory effects are achieved, reflected by less monocyte migration. In addition, a safety assessment regarding the pharmacokinetics and biodistribution of targeted TRAF6 nano therapy was performed in non-human primates. The advantage of this therapy method would be a reduced treatment frequency and reduced cumulative dosage compared to a non-targeted TRAF6 inhibitor therapy (226, 242).

In general, TRAF6 inhibitor treatment is frequently tested as a potential new treatment strategy also for other inflammation-related diseases like breast cancer (243), bone cancer (244), multiple sclerosis (245), or heart failure (244, 246). TRAF6 inhibition is considered a promising tool to overcome the limitations of a CD40 antibody treatment by not impairing classical immune responses.

2. Aim

The CD40L-CD40 signaling pathway has been recognized as a key player in developing autoimmune diseases and CVD. The signaling cascade is crucial for physiological, immunological, and pathological inflammatory processes. However, whether targeting the signaling cascade is beneficial or harmful is still controversial. First therapeutic approaches in patients have not fulfilled safety standards and showed major side effects. Particularly in relation to CVD risk factors that trigger low-grade inflammation in the progression of atherosclerosis, pharmacological treatment is still challenging, and no therapy targeting the CD40L-CD40 dyad is available (169). With this study, we want to provide a better understanding of the CD40L-CD40 cascade as a target to prevent and modulate chronic vascular inflammation, with a spotlight on modifiable metabolic risk factors of CVD in different hypertensive and diabetic mouse models.

The study aims to characterize the cardio- and vasoprotective effects of global and tissue-specific CD40 knockout in hypertensive mice. Arterial hypertension was induced via AT-II administration in different genetically modified mice. The global CD40 knockout mouse model is used to evaluate the effects of the tissue-specific CD40 knockout and put them in relation to each other. The role of CD40 signaling in adipose tissue in hypertension-induced vascular inflammation was examined in adipocyte-specific CD40 knockout mice. Systolic blood pressure, vascular function, and DHE staining were performed to analyze the hypertensive phenotype. Unfortunately, we did not observe a significantly improved phenotype in the genetically modified mice, so the study was continued with a pharmacological TRAF6 inhibition in C57BL6/J mice. The beneficial effects of TRAF6 inhibition in hypertensive mice were examined with isometric tension studies, flow cytometry of aortic tissue lysates, and echocardiography as functional read-outs and various biochemical markers of inflammatory pathways and oxidative stress. The cardio- and vasoprotective effects of TRAF6 inhibition were also analyzed in diabetic mice (db/db) via protein expression analysis utilizing different inflammatory, oxidative stress, and apoptotic markers. Lastly, as a translational approach, vascular tissue and plasma of coronary heart disease patients with or without the comorbidities hypertension or diabetes plus hypertension are examined in relation to the role of CD40L-CD40 signaling. Therefore, plasma proteomics and transcriptomic analysis of the remaining bypass tissue were performed to analyze protein and mRNA expression of inflammatory and oxidative stress markers.

This study was performed to highlight the importance of CD40L-CD40 signaling in pathological inflammatory processes and the possibility of targeted therapy as a promising treatment strategy.

3. Material

3.1. Chemicals

Table 1: Used chemicals.

Product	Company	Product No.
2-Mercaptoethanol (ß-ME)	Sigma	M6250
Acetic acid (glacial) 100%	AppliChem	A2354
Acetonitrile	Honeywell	34967
Acetylcholine chloride	Sigma	A6625
Acrylamid/Bis solution 40 %, 29:1	Bio-Rad	1610146
Agarose	Invitrogen	16500-100
Albumin Fraktion V (BSA)	Roth	8076.3
Ammonium persulfate (APS)	Sigma	A3678
Angiotensin-II acetate salt	Bachem	4006473
Aprotinin	Sigma	A6279
Braunol	Braun	3864065
Bromophenol Blue sodium salt	Sigma	B8026
$CaCl_2$	Sigma	21102
DEPC (diethylpyrocarbonate)-treated water, nuclease-free and autoclaved	Roth	T143.3
D-glucose	Roth	6780.1
Dihydroethidium 95 % (DHE)	Sigma	37291
DMSO (Dimethylsulfoxid)	Honeywell	34943
EDTA-free protease inhibitor cocktail, cOmplete™	Roche	11873580001
Ethanol	Sigma	32205
Ethylendiamintetraacetic acid (EDTA)	Sigma	E9884
Ethylene glycol-bis(ß-aminoethylether)-N,N,N´,N´-tetraacetic acid (EGTA)	Sigma	E4378
Fetal calf serum (FCS)	Thermo Scientific	10270106
Glycerol	Roth	3783.1
Glycine	Roth	3908.2
HBSS, Hanks balanced salt solution with calcium and magnesium	Sigma	55037C
Heparin-Natrium-25000	Ratiopharm	
HEPES sodium salt hydrate	Sigma	H2393
Indometacin	Sigma	I-7378
Isofluran	Abbot	B506

Isopropanol	AppliChem	A3465
KCl	AppliChem	7447-40-7
Ketamine hydrochloride/xylazine hydrochloride solution	Sigma	K113
$KHCO_3$	Merck	104854
K_2HPO_4	Roth	16788-57-1
L-012 (8-amino-5-chloro-7-phenylpyrido[3,4-d]pyridazine-1,4-(2H,3H)dion) sodium salt	Wako Chemicals	120-04891
Leupeptin hydrochloride	Sigma	L0649
Lucigenin	Sigma	M8010
Methanol, 99.8 %	Sigma	322415
$MgSO_4$	Roth	7487-88-9
Midori Green	NIPPON Genetics	MG04
Milk powder	Roth	T145.2
N,N,N´,N´-Tetramethylethylenediamine (TEMED)	Sigma	T9281
Na_2HCO_3	Applichem	131638
Na-Acetate	Merck	127-09-3
NaCl	Roth	7647-14-5
Na-HEPES	Roth	75277-39-3
Na_2HPO_4	Merck	1.06576.5000
NaOH	Merck	106462
NH_4Cl	Sigma	A9434
Nitroglycerin, NITRO Carino Infus	Carinopharm	
OCT (Otimal Cutting Temperature)-resin Tissue-Tek®	Sakura	4583
PBS (1x), Dulbecco´s Phosphate Buffered Saline without calcium and magnesium	Sigma	D8537
PDBu	Sigma	37558-16-0
Pepstatin A	Sigma	P5318
Phenylmethanesulfonyl (PMSF)	Sigma	P7626
Phosphatase inhibitor cocktail	Sigma	P2850
Ponceau S	Sigma	P5288
Prostaglandin F2alpha	Sigma	16010
Protease inhibitor cocktail	Sigma	P8340
ROTI®-Quant	Roth	K015.1
Sodium dodecyl sulfate (SDS)	Merck	822050

Sucrose	Sigma	57-50-1
TRAF6 inhibitor compound 6877002	Tocris	5602
Tris-hydrochlorid (Tris-HCl)	Roth	9090.2
Tris(hydroxymethyl)-aminomethane (Tris-base)	Sigma	252859
TritonX-100	Sigma	93420
Trypan blue	Bio Rad	1450021
Tween 20	Sigma	P2287
Zymosan A	Sigma	Z4250

3.2. Media and Buffers

3.2.1. Alkaline lysis buffer (DNA extraction)

NH_4Cl	150 mM
$KHCO_3$	10 mM
EDTA pH 7.2	0.1 mM

3.2.2. FACS buffer

Fetal calf serum (FCS)	2 % (v/v)
in PBS	

3.2.3. Homogenization buffer

Tris-HCl	20 mM
Sucrose	250 mM
EGTA	3 mM
EDTA	20 mM
pH 7.5	

3.2.4. Homogenization solution

Tris-HCl	20 mM
Sucrose	250 mM
EGTA	3 mM
EDTA	20 mM
PMSF	0,5 mM
Protease inhibitor cocktail	1 % (v/v)
Phosphatase inhibitor cocktail	1 % (v/v)
TritonX-100	1 % (v/v)
pH 7.5	

3.2.5. Lämmli buffer

Tris HCl	188 mM
Glycerol	30 % (v/v)
SDS	6 % (w/v)
2-mercaptoethanol	15 % (v/v)
Bromphenol blue	0.01 % (w/v)
pH 6.8	

3.2.6. Krebs-Hepes buffer (KH buffer)

NaCl	99.01 mM
KCl	4.69 mM
$CaCl_2$	2.5 mM
$MgSO_4$	1.2 mM
$NaHCO_3$	25 mM
K_2HPO_4	1.03 mM
Na-Hepes	20 mM
D-glucose	11 mM
pH 7.35	

3.2.7. Organ bath buffer

NaCl	99.01 mM
KCl	4.69 mM
$CaCl_2$	2.5 mM
$MgSO_4$	1.2 mM
$NaHCO_3$	25 mM
K_2HPO_4	1.03 mM
Indometacin	18 mg
D-glucose	11 mM
pH 7.35	

3.2.8. PBS 10x

NaCl	1.37 M
Na_2HPO_4	100 mM
KCl	27 mM
KH_2PO_4	17.6 mM
pH 7.4	

3.2.9. PBS-T 1x

1x PBS	
Tween 20	0.1 % (v/v)

3.2.10. Protease-Inhibitor buffer

KH buffer with:	
Aprotinin	1 % (v/v)
Leupeptin	5 µg/ml
Pepstatin	8 µg/ml

3.2.11. SDS-Page resolving gel buffer

Tris-HCl	1.5 M
pH 8.8	

3.2.12. SDS-Page running buffer

Tris-base	250 mM
Glycine	192 mM
SDS	35 mM

3.2.13. SDS-Page stacking gel buffer

Tris-HCl	0.5 M
pH 6.8	

3.2.14. TAE (Tris-Acetate-EDTA) buffer 50x

Tris-base	0.5 M
Acetic acid (glacial)	1.5 M
EDTA	50 mM
pH 8.5	

3.2.15. TBS 10x

Tris-base	200 mM
NaCl	1.5 M
pH 7.6	

3.2.16. TBS-T

1x TBS	
Tween 20	0.1 % (v/v)

3.2.17. Transfer buffer

Tris-base	250 mM
Glycin	192 mM
Methanol	25 % (v/v)

3.3. Reagents and kits

Table 2: Used reagents and kits.

Product	Company	Product No.
ACK-Lyse buffer	Gibco	A1049201
BD Fc Block™ anti-CD16/CD32 (mouse)	BD Biosciences	553142
GoTaq® Master Mix	Promega	M7123
Pierce™ ECL Western Blotting Substrate	Thermo Fisher	32106
RNeasy Mini kit	Qiagen	74104
SuperSignal™ West Femto Maximum Sensitivity Substrate	Thermo Fisher	34095

3.4. Enzymes and standards

Table 3: Used enzymes and standards.

Product	Company	Product No.
100 bp DNA ladder	New England Biolabs	N3231L
BenchMark™ Unstained Protein ladder	Invitrogen	10747012
Bovine Serum Albumin Standard Ampules	Thermo Scientific	23309
Der bunte Tobias	German Research Product	GRP13284
Liberase™ (Thermolysin Medium)	Roche	5401127001
Precision Plus Protein™ WesternC™	Bio-Rad	1610376

3.5. Antibodies

3.5.1. Primary antibodies

Table 4: Primary Antibodies used for Dot Blot and Western blot analysis. Monoclonal antibodies are labeled in the table with (M) and polyclonal as (P).

Product	Blocking medium	Anti IgG	Dilution	Company	Product No.
(M) anti-TSP-1	3 % BSA in PBS-T	mouse	1:250	Santa Cruz	sc-59886
(M) anti-VCAM-1	3 % BSA in PBS-T	mouse	1:200	Santa Cruz	sc-13160
(M) anti-ET-1	3 % BSA in PBS-T	mouse	1:250	Santa Cruz	sc-517436
(M) anti-eNOS	3 % BSA in TBS-T	mouse	1:1000	BD bioscience	610297

(M) anti-p47^{phox}	3 % BSA in PBS-T	mouse	1:250	BD bioscience	610354
(M) anti-NOX2	3 % BSA in TBS-T	mouse	1:500	BD bioscience	611414
(M) anto-PAR1	3 % BSA in TBS-T	mouse	1:300	BD bioscience	611522
(M) anti-CD40L	3 % BSA in PBS-T	rabbit	1:5000	NovusBio	NB110-57627
(M) anti-HO-1	3 % BSA in TBS-T	rabbit	1:2000	Abcam	Ab68477
(M) anti-CD68	3 % BSA in TBS-T	mouse	1:1000	Abcam	Ab31630
(P) anti-ß-actin	3 % BSA in TBS-T	rabbit	1:2500	Sigma	A5060
(P) anti-caspase-3	3 % BSA in TBS-T	rabbit	1:1000	Cell Signaling	9662S
(P) anti-RAGE	3 % BSA in PBS-T	rabbit	1:1000	Cell Signaling	42544
(P) anti-pMARCKS	3 % BSA in TBS-T	rabbit	1:1000	Cell Signaling	2741
(P) anti-3NT	5 % Milk in PBS-T	rabbit	1:2000	Millipore	06-284
(P) anti-4HNE	5 % Milk in PBS	goat	1:1000	Millipore	Ab5605

3.5.2. Secondary antibodies

Table 5: Secondary antibodies used for Dot Blot and Western blot analysis. Secondary antibodies were diluted in the same blocking medium as the respective primary antibodies. All secondary antibodies are peroxidase-labeled.

Product	Dilution	Company	Product No.
anti-mouse IgG	1:10000	Vector lab	PI-2000
anti-rabbit IgG	1:10000	Vector lab	PI-1000
anti-goat IgG	1:5000	Santa Cruz	Sc-2354

3.5.3. Fluorescence labeled antibodies

Table 6: Fluorescence-labeled antibodies used for FACS. All FACS antibodies were diluted in FACS buffer (2 % FCS in PBS). Monoclonal antibodies are labeled with (M).

Product	Fluorophore conjugates	Dilution	Company	Product No.
Fixabel Viability Dye	eFluor506	1:1000	BD Bioscience	65-0866
(M) anti-CD11b	PE	1:100	BD Bioscience	553311
(M) anti-CD45	APC-efluor 780	1:100	eBioscience	47-0451-82
(M) anti-F4/80	APC	1:50	eBioscience	17-4801-82
(M) anti-Ly6C	PerCP-Cy.5.5	1:100	BD Bioscience	560525
(M) anti-Ly6G	FITC	1:100	BD Bioscience	552460
(M) anti-NK1.1	PE-Cy7	1:100	eBioscience	25-5941-81
(M) anti-TCRß Chain	V450	1:100	DB Bioscience	560706

3.6. Oligonucleotides used for genotyping

All primers were ordered from Eurofins Genomics and prediluted before use 1:10 in DEPC-treated water.

Table 7: Primer Sequences which were used for genotyping PCRs of transgenic mice.

Name	Sequence
AdipoqCre fw	5´-GGA TGT GCC ATG TGA GTC TG-3´
AdipoqCre rv	5´-ACG GAC AGA AGC ATT TTC CA-3´
Noxa fw	5´-GGA GGG CAT AAA TGG GCA ATG AC-3´
Noxa rv	5´-GAT GCT TCT TGG GTG CAC CCA CA-3´
CD40fl/wt fw	5´-TCT TTG GGA GCA CTG AAG AG-3´
CD40fl/wt rv	5´-TTC CAC CGG CAT GTT GAA AG-3´
CD40fl/fl fw	5´-GAT CGT TGA AGA AGG AGG TG-3´
CD40 Com/J	5´-GTG AGA TGC TAG CCC TCC TG-3´
CD40 WT rev/J	5´-CAC GTC ATC TGC TGG TTT TC-3´
CD40 Mut rev/J	5´-CGT GCA ATC CAT CTT GTT CA-3´

3.7. Consumables

Table 8: Used Consumables.

Product	Company	Product No.
Blood glucose test strips	Roche	6114963
Cell Counting Slides for TC20 Cell Counter	Bio-Rad	1450015
Cell Strainer 40 µm	Falcon® Corning	352340
Cell Strainer 70 µm	Falcon® Corning	352350
Centrifuge tube 15 ml	Greiner	188271
Centrifuge tube 50 ml	Greiner	227261
Coverslips 24 x 50 mm	Diagonal	LD2450
epT.I.P.S Standard 0.1-10 µl	Eppendorf	0030000811
epT.I.P.S Standard 2-200 µl	Eppendorf	0030000889
epT.I.P.S Standard 100-1000 µl	Eppendorf	0030000927
FACS tubes	Falcon® Corning	352052
Gel blotting paper	Whatman	9057077
Glass petri dish	Duran	237554805
Hair removal cream	SNÄ Epil	02186115
Inject®-F 1 ml	B. Braun	9166017V
Micro osmotic pumps	Alzet	1007D

Microlance™ 3 24 G cannula	Becton Dickinson	304100
Microlance™ 3 26 G cannula	Becton Dickinson	303800
Microplate 96 well F-bottom transparent	Greiner	655101
Microplate 96 well U-bottom transparent	Greiner	650101
Microscope slides superfrost plus	Thermo Scientific	J1800AMNZ
Mini-trans-blot filter paper	Bio-Rad	1703932EDU
Nitrocellulose Blotting membrane Amersham 0.45 µm	GE Healthcare	GE10600002
PCR tubes, 0.2 ml	Kisker Biotech	G003-A
Petri dish sterile	Greiner	632181
Safe-Lock microcentrifuge tubes 0.5 ml	Eppendorf	0030121023
Safe-Lock microcentrifuge tubes 1.5 ml	Eppendorf	0030120086
Safe-Lock microcentrifuge tubes 2.0 ml	Eppendorf	0030120094
Suture clip Michel 7.5 x 1.75 mm	B. Braun	BN507R
S-Monovette® 10 ml 9NC	Sarstedt	02.1067.001
S-Monovette® 1.2 ml K3E	Sarstedt	06.1664.001
Sonosid® ultrasound gel	Asid Bonz	782010

3.8. Technical Devices

Table 9: Used Technical Devices.

Device	**Company**
Automated Cell Counter TC20	Bio-Rad
Attune NxT Flow Cytometer	Thermo Fisher
Benchtop centrifuge ROTOFIX 32	Hettich
Bridge amplifier	CB Science / ADInstuments
Chemiluminescence plate reader Mithras^2 LB943	Berthold Technologies
ChemiLux Imager	Intas
Cold light lamp KL 1500	Schott
Cryostat CM3050 S	Leica Biosystems
Fluorescence microscope Axiovert 40CFL with Axiocam MRm	Zeiss
Force transducer	Kent Scientific
Heraeus Megafuge 16R	Thermo Scientific
Infrared lamp IL21 150 Watt	Breuer
Luminometer Lumat LB 9507	Berthold Technologies
Mini Trans-Blot Electrophoretic Transfer Cell (Blotting apparatus)	Bio-Rad

Mini-Protean 3 Cell (Electrophoresis apparatus)	Bio-Rad
Minifold I vacuum dot-blot system device	Whatman® Schleicher&Schuell
MiniSpin® Centrifuge	Eppendorf
MRXII plate reader	Dynex Technologies
Non-invasive Blood Pressure (NIBP) System CODA®	Kent Scientific
Organ bath chamber	Radnoti
Pipette Eppendorf 0.1 – 2.5 µl	Eppendorf
Pipette Eppendorf 0.5 – 10 µl	Eppendorf
Pipette Eppendorf 2 – 20 µl	Eppendorf
Pipette Eppendorf 10 – 100 µl	Eppendorf
Pipette Eppendorf 20 – 200 µl	Eppendorf
Pipette Eppendorf 100 – 1000 µl	Eppendorf
PowerPac™ Basic power supply	Bio-Rad
Refrigerate benchtop centrifuge Mikro 22R	Hettich
Shaver ECO XS	Tondeo
SimpliAmp Thermal Cycler	Thermo Fisher
Stereomicroscope MSZ 5400	Krüss
Thermomix comfort	Eppendorf
TissueLyser LT	Qiagen
Transferpipette 200 µl	Brand GmbH
UV transilluminator iX	Intas
Vortex-Genie™ 2	Scientific Industries
Wide Mini-Sub Cell GT Cell (DNA electrophoresis apparatus)	Bio-Rad

3.9. Surgical instruments

Table 10: Used surgical instruments.

Product	**Company**	**Product No.**
Extra Fine Bonn Scissor Straight, 8.5 cm	Fine Science Tools	14084-08
Extra Fine Graefe Forceps Curved 10 cm	Fine Science Tools	11152-10
Graefe Forceps Straight 10 cm	Fine Science Tools	11050-10
Michel Suture Clip Applying Forceps 12.5 cm	Fine Science Tools	12018-12
Noyes Spring Scissors Curved 12 cm	Fine Science Tools	15011-12
Scissors Curved Blunt 12 cm	Fine Science Tools	14003-12
Strabismus Scissors Tungsten Carbide Curved 9 cm	Fine Science Tools	14575-09

3.10. Software

Table 11: Used software.

Name	Company
Adobe Photoshop 2024	Adobe Systems GmbH
Axiovision Rel 4.3	Carl Zeiss Vision GmbH
BioRender (medical illustrations)	BioRender
ChromPass Chromatography	Jasco
CODA data acquisition	Kent Scientific Corporation
EndNote 20	Clarivate Analytics
FlowJo v10	FlowJo LLC
Gel Pro Analyser 6.0	Media Cybernetics
Grammarly 1.70.1.0	Grammarly Inc.
GraphPad Prism 9.5.0	GraphPad Software, Inc.
Image ProPlus 7.0	Media Cybernetics
ImageJ	Wayne Rasband
Microsoft Office 16.81	Microsoft 365
Organbad Chart 5	ADInstruments GmbH
Revelation 4.25	Dynex Technologies
Vevo Lab	VisualSonics

4. Methods

4.1. Human samples

All human studies followed the Declaration of Helsinki. The DZHK Heart Bank provided human aortic and plasma samples from bypass surgeries at the “Deutsches Herzzentrum der Charité” in Berlin under ethical permission No.: EA4/035/18 and EA4/032/23. The patients are fully characterized regarding clinical chemistry parameters (for example, blood cholesterol, triglycerides, and glucose) and clinical functional parameters (for example, blood pressure, heart rate, and BMI). The patient’s characteristics are listed in Table 18. In total, samples of 20 coronary heart disease (CHD) patients without comorbidities, 49 CHD patients with arterial hypertension (HT), and 25 CHD patients with HT and type 2 diabetes mellitus (T2DM) were used in this thesis. Figure 19 summarizes the human study.

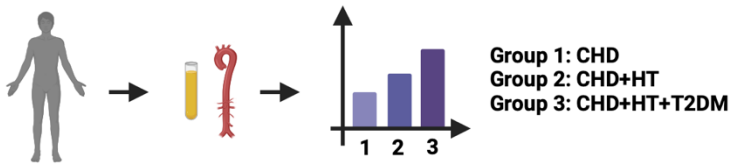

Figure 19: Human study overview. Aortic tissue and plasma samples from bypass surgeries were provided by the DZHK Heart Bank. RNA-Seq (aortic tissue) and Olink proteomics (plasma) analysis were performed. Created with BioRender.com. Abbreviations: CHD=cardiovascular disease, HT=hypertension, T2DM=type 2 diabetes mellitus.

4.2. *In vivo* animal studies

All animals were treated according to the Guide of Care and Use of Laboratory Animals as adopted and promulgated by the U.S National Institute of Health. The Ethics Commission permitted animal experiments according to the German Law on the Protection of Animals (Landesuntersuchungsamt Rheinland-Pfalz, Koblenz, Germany; No.: G19-1-068 and extension from March 2022 for hypertensive (AT-II) mice; No.: 23-177-07/G 11-1-020 and extension from June 2016 for diabetic (db/db) mice).

4.2.1. Laboratory animals

All animals were used according to the German Animal Welfare Act with §4 Abs. 1 and §8 Abs. 1. For the study, only male animals at the age of 10-12 weeks were used, whereas male db/db mice were used at the age of 14 weeks (stored samples from a published study (217)). AdipoqCre wildtype mice were crossed with AdipoqCre Het mice to generate control and tissue-specific knockout (KO) littermates. AdiCD40$^{-/-}$ mice and the CD40$^{-/-}$ mice were bred in-house at the Translational Animal Research Center Mainz (TARC). All used mouse lines are described in Table 12.

Table 12: Summary of all used mouse strains with description and origin.

Mouse strain	Description	Origin
C57BL/6J (WT)	Inbreed strain	Charles River (Stock #632)
B6.129P2-Cd40^{tm1Kik}/J (CD40KO or CD40$^{-/-}$)	Inbreed strain on C57BL/6J background, neomycin cassette was inserted into exon 3, targeted mutation, homozygous mutant, deficient of CD40 antigen and exhibit impaired immunoglobulin class switching (225)	Jackson lab (Stock #002928), bred in-house (TARC)
BKS.CgTemoin (WT)	Inbreed strain on C57BL/6J background	Charles River
BKS.Cg-Dock7^{m}+/+Lepr^{db}/J (db/db)	Inbreed strain on C57BL/6J background, homozygous for diabetes spontaneous point mutation (Lepr^{db}), obesity starts around three to four weeks, plasma insulin elevations start at 10 to 14 days and blood sugar at four to eight weeks (247, 248)	Charles River (Stock #607)
AdipoqCre x CD40fl/fl (AdiCD40$^{-/-}$)	Inbreed strain on C57BL/6J background, tissue specific knockout of CD40 on adipocytes generated by crossbreeding of CD40fl/fl (237) mice with AdipoqCre mice from Jackson lab, strain B6.FVB-Tg-1Evdr/J (249), Cre wildtype littermates were used as controls, Cre heterozygous littermates were used as tissue specific knockout model	Breed in house (TARC), provided by Esther Lutgens, Mayo Clinic, Rochester, Minnesota, USA

4.2.2. Implantation of osmotic minipumps

Miniosmotic pumps from Alzet® were required to guarantee continuous and accurate subcutaneous dosing of the drugs into the laboratory animals. The pumps operate with an osmotic layer, setting up an osmotic pressure between a compartment in the pump and the tissue environment where the pump is implanted. High osmolarity causes water influx into the pump, which induces pressure on a flexible reservoir; by this process, the drug is continuously released out of the pump (250, 251).

The pumps were filled according to the company instructions with either AT-II or TRAF6 inhibitor compound 6877002. The agents' concentrations were adjusted to a dose of 1 mg/kg/d

in 0.9 % NaCl for AT-II for seven days and 2.5 mg/kg/d in 25 % DMSO for TRAF6 inhibitor for seven days (WT mice) or 14 days (db/db mice). Because of the different solubility of AT-II and TRAF6 inhibitor, double pump implantations were performed in WT animals to administer both drugs simultaneously. The surgery was performed under sterile conditions, and the animals were anesthetized with Ketamine/Xylazine (120 mg/kg; 16 mg/kg in 0.9 % NaCl; injected volume 0.1-0.2 ml). In preparation, the dorso-caudal area of the mice was shaved, followed by disinfection with Braunol. A small skin incision of approximately 1 cm was set in this dorsal area, and a small subcutaneous pocket was prepped to insert the pump. The wound was closed with a clamp seam. Postoperative analgesia is provided by applying lidocaine ointment to the wound. To ensure reproducibility, the pumps were implanted for each experiment at the same time (10-11 am). Control animals (Sham) underwent the same surgery procedure, and the pumps were implanted without the drug containing only the dilution solution of 0.9 % NaCl or 25 % DMSO. After pump implantation, *in vivo* measurements were performed, such as blood pressure (bp) or echocardiography. The mice were sacrificed after seven (AT-II mice) or 14 days (db/db mice), and the organs or tissues were collected (4.3.1). Figure 20-22 show the different treatment schemes.

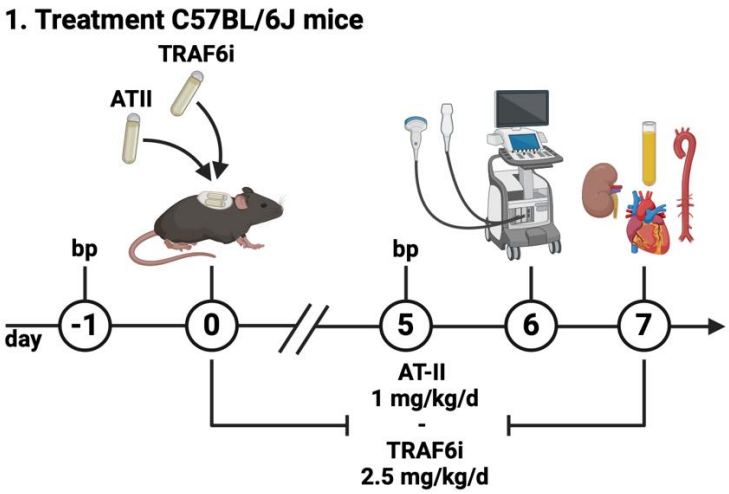

Figure 20: Treatment scheme for C57B6/J mice. AT-II (1mg/kg/d) and TRAF6 inhibitor (2.5 mg/kg/d) were applied to the animals via osmotic minipumps for seven days. Only male mice were used in the study and sacrificed in an age range of 10-12 weeks. The blood pressure was measured one day before the treatment started and after five days of the treatment. Echocardiography was performed on day six after the treatment started. Created with BioRender.com. Abbreviations: AT-II=angiotensin-II, TRAF6i=TRAF6 inhibitor, bp=blood pressure.

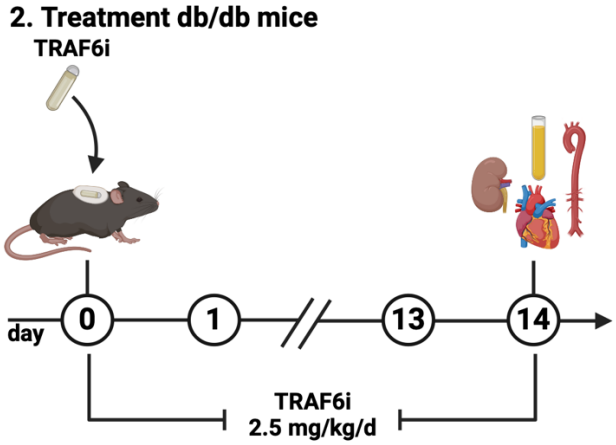

Figure 21: Treatment scheme for db/db mice. TRAF6 inhibitor (2.5 mg/kg/d) was applied to the animals via osmotic minipumps for seven days. Only male mice were used in the study, and they were sacrificed at the age of 14 weeks. Created with BioRender.com. Abbreviations: db/db=BKS.Cg-Dock7^{m}+/+Lepr^{db}/J mice, TRAF6i=TRAF6 inhibitor.

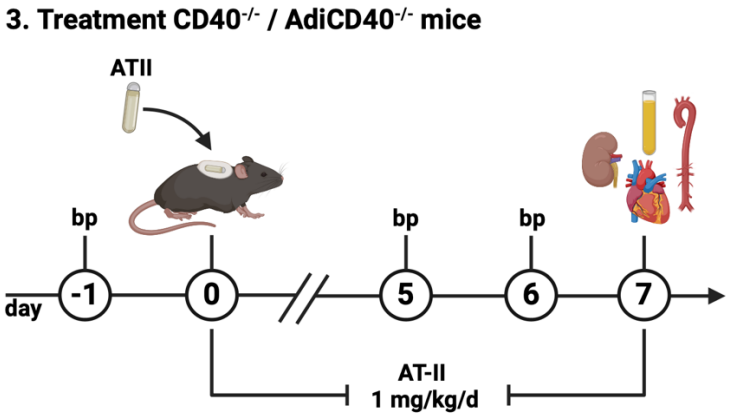

Figure 22: Treatment scheme for CD40$^{-/-}$ and AdiCD40$^{-/-}$ mice. AT-II (1 mg/kg/d) was applied to the animals via osmotic minipumps for seven days. Only male mice were used in the study and sacrificed in an age range of 10-12 weeks. The blood pressure was measured one day before the treatment started and on days five and six of the treatment. Created with BioRender.com. Abbreviations: AT-II=angiotensin-II, TRAF6i=TRAF6 inhibitor, bp=blood pressure.

4.2.3. Non-invasive blood pressure (NIBP) measurement

Blood pressure was measured non-invasively by tail cuffs, determining the tail blood volume by volume pressure recordings (VPR). A CODA® High Throughput 2 Noninvasive Blood Pressure System (Kent Scientific) was utilized for the experiments. The occlusion cuff at the tail of the mice is inflated and deflated, which causes either no or returning blood flow. The changes in blood tail volume, characteristic of the underlying blood pressure, are recorded by a VPR sensor in the system (252). With this method, only the systolic blood pressure can be used as a reliable value. Compared to telemetry, similar systolic blood pressure values (<10

mmHg) can be achieved via tail cuff if the mice were handled correctly and trained beforehand (253).

Before the actual measurement, the mice were placed three times in the restrainers for training purposes to achieve habituation and reduce stress. For training and measurement purposes, the mice were placed in a holder at a heating platform (32°C) with the tail cuffs at their tails. NIBP was measured on days minus one, five, and six. The measurement started with a resting phase, and the mice were placed in the holders for 15 min at the heating platform. Per animal, 10 NIBP measurements were performed. The first three measurements were discarded as acclimatization cycles, the remaining NIBP values were evaluated, and a mean value was taken. Figure 23 shows how the mice were sitting fixated in the restrainers.

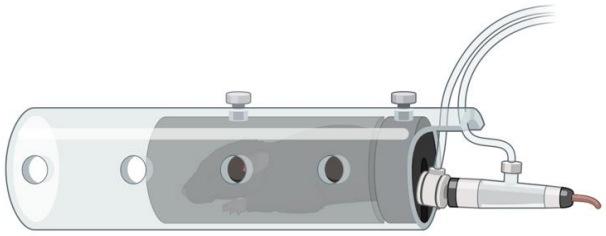

Figure 23: Tail cuff blood pressure measurement system with fixated mouse in a restrainer. Created with BioRender.com.

4.2.4. Transthoracic echocardiography (TTE)

A specially designed echocardiography for mice has been established in the platform laboratory at the Centrum of Thrombosis and Hemostasis (CTH) in Mainz and was performed together with Alexander Czarnowski (MD candidate, Laboratory for Molecular Cardiology, University Medical Center Mainz). Cardiac function was measured non-invasively using high-frequency small animal echocardiography with a 30 MHz transducer (254, 255). The Vevo3100 device (VisualSonics, FUJIFILM, Toronto, Canada) was provided at the CTH. The focus of the examination was the left ventricular assessment and the systolic function. Echocardiography was initially taught by Dr. med. Michael Molitor (Cardiology I, University Medical Center Mainz).

Anesthesia was induced via inhalation of 2-3 % isoflurane by volume at an inspiratory oxygen fraction of 0.35 (FiO_2 35 %). Sedation during the experiment is maintained by inhalation of 1-2 vol. % isoflurane using a breathing mask. Under sedation, the mice were placed supine on a warming plate in the sonography examination station. An eye ointment is then applied to protect the eyes, and the paws of the mice are fixed to electrocardiogram (ECG) electrodes using plaster stripes. The abdominal-thorax area of the mice was depilated by shaving and then applying a depilatory cream. Finally, the shaved thorax is disinfected. The ultrasound gel

is pre-heated to body temperature and applied to the shaved area. The transducer is placed on the corresponding spot on the abdomen of the test animals without pressure and with light contact with the ultrasound gel. During the examination, the temperature is constantly monitored using a rectal probe, and the ECG and respiratory rate are continuously monitored via the contact electrodes. The parasternal long axis view (PSLAX) and parasternal short axis view (SAX) were each performed in M- and B-Mode as described in the following text and the Guide to Small Animal Echocardiography using the Vevo® Imaging Systems. The optimal animal position to conduct the PSLAX is to tilt the platform to elevate the animal's head and tilt it slightly to the left side. Further, the transducer is placed parallel to the sternum and rotated (approximately 15-35°) clockward to the animal's right shoulder. The animal remains in the same position for the SAX. But the transducer is rotated 90° clockwise starting from the PSLAX position. The examination takes about 10-20 min per animal. The mice wake up entirely within a few minutes after being transferred back into the cage. Echocardiography was performed on day six after the osmotic minipumps were inserted and filled with AT-II or TRAF6 inhibitor. Figure 24 shows representative B-mode images of the mouse heart and provides an anatomical description.

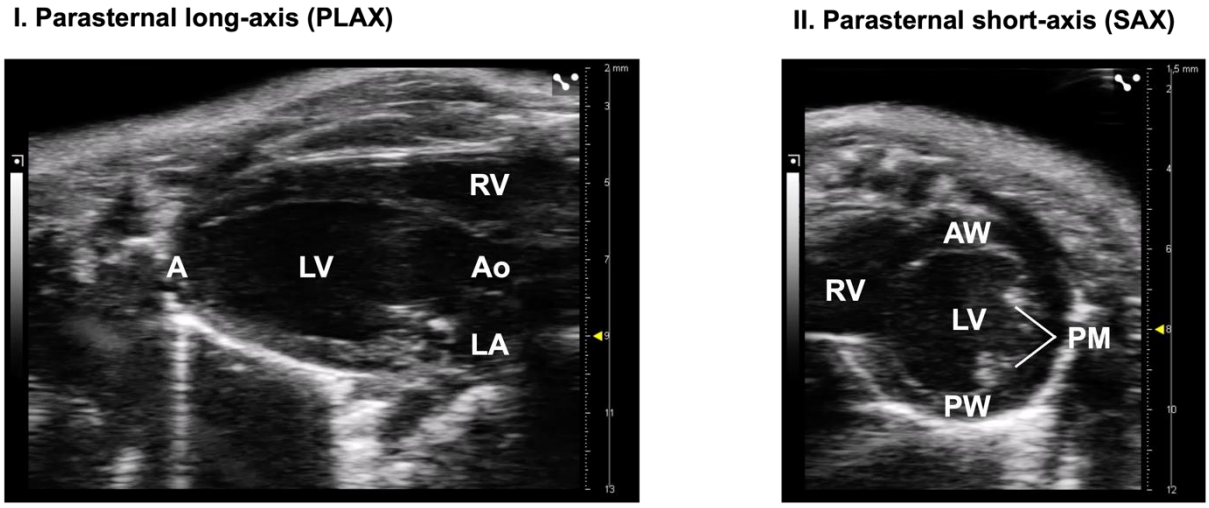

Figure 24: B-Mode images of a mouse heart. Exemplary pictures of B mode images in the (I) Parasternal long-axis (PLAX) view and (II) the parasternal short-axis (SAX) view. Abbreviations: A=apex, RV=right ventricle, LV=left ventricle, Ao=aorta, LA=left atrium, AW=anterior wall, PW=posterior wall, PM=papillary muscles.

4.3. *Ex vivo* animal studies

4.3.1. Blood, organ, and tissue harvesting from mice

Blood, organs, and tissue were harvested according to the German Animal Welfare Act with §4 Abs. 1 and §8 Abs. 1. The animals were anesthetized with ketamine/xylazine (120 mg/kg and 16 mg/kg in 0.9 % NaCl). An intermediate toe reflex was performed before opening the abdomen to ensure that the anesthesia was deep enough. The abdominal cavity was opened beginning from distal to proximal. At first, the urine was taken directly out of the urinary bladder

with a 1 ml syringe and a 26G cannula. Afterward, the diaphragm and the rips were opened to perform a cardiac puncture. The blood was taken directly out of the bumping heart with a 1 ml syringe and a 26G cannula. The blood was mixed with either citrate or collected in EDTA monovettes depending on the following experiment. To prevent intravascular anticoagulation 200 µl heparin (200 IE) was injected into the left ventricle. The following tissues and organs were collected: heart, EWAT, liver, spleen, kidney, adrenal gland, aorta, lung, and brain. The tissue and organs were stored on ice in Krebs-HEPES buffer until further processing for experiments or freezing in liquid nitrogen for storage. The perivascular adipose tissue (PVAT) was removed carefully on ice from the aortas to ensure an intact endothelium. The EDTA blood monovettes were centrifuged at 3600 rpm for 10 min at room temperature, and the plasma was taken and frozen in liquid nitrogen for long-term storage at -80°C.

4.3.2. Quantification of whole blood oxidative stress

This method analyzes the leukocyte-dependent hydrogen peroxide formation, mainly in whole blood samples. Thereby, hydrogen peroxide formation is mostly driven by the NADPH oxidase NOX2. L-012 is a luminol analog and chemiluminescent probe for reactive oxygen and nitrogen species (256). Myeloperoxidases convert hydrogen peroxide into highly reactive oxygen-metal complexes, which lead to the oxidation of L-012 and chemiluminescent light emission. The blood samples were stimulated with Zymosan A to initiate inflammation by macrophage activation. In addition, the samples were stimulated with phorbol 12,13-dibutyrate (PDBu) to activate the PKC with subsequent phosphorylation of $p47^{phox}$ and NOX2 activation leading to oxidative burst (257, 258).

As previously described, the protocol was performed in cooperation with Dominika Mihalikova (PhD candidate, Laboratory of Molecular Cardiology, University Medical Center Mainz) (256, 259). Fresh citrate blood was diluted 1:50 in PBS containing Ca^{2+} and Mg^{2+} at room temperature and mixed with 100 µM of L-012. The blood was stimulated either with 50 µg/ml Zymosan A or 10 µM PDBu. Chemiluminescence (ECL) was measured using a Mithras^2 chemiluminescence plate reader (Berthold Technologies), and the results were expressed as counts per minute after 10 min (PDBu) or after 55 min (Zymosan A).

4.3.3. Quantification of dihydroethidium (DHE) staining in tissue cryosections

Oxidative stress in cryosections of different tissues (PVAT, aorta, heart, or kidney) was analyzed by dihydroethidium (DHE) staining, which allows rapid and specific detection of intracellular stress as a result of $O_2^{-\bullet}$ production. DHE is a lipophilic, cell-permeable dye oxidized by $O_2^{-\bullet}$ to 2-hydroxyethidium (2-HE). 2-HE intercalates into the DNA, changes thereby its fluorescence properties, and could be detected when excited. If other oxidants are present,

DHE could also be oxidized simultaneously non-specifically to ethidium (E^+). E^+ also intercalates into the DNA and is excited with an overlapping wavelength compared to 2-HE (Figure 25). Therefore, it is impossible to distinguish 2-HE and E^+ fluorescence signals with this microscopy method, which is used to visualize all ROS products in the analyzed tissue (260, 261).

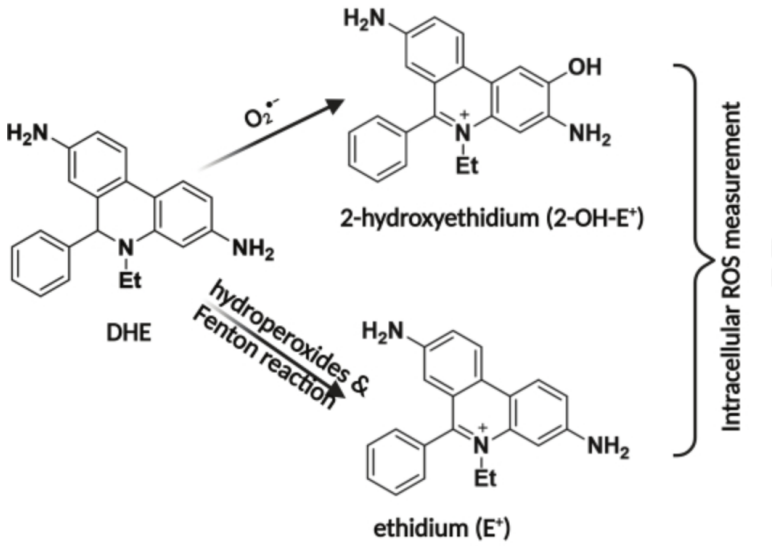

Figure 25: Oxidation products of dihydroethidium (DHE). DHE reacts with $O2^{-\bullet}$ to 2-hydroxyethidium or is oxidized with H_2O_2 and metal catalysis to ethidium (Fenton reaction). Due to overlapping fluorescence spectra from 2-hydroxyethidium and ethidium, it is impossible to distinguish these reaction products with common filters in fluorescence microscopy. The figure is taken from (262) with permission.

Heart tips, 3 mm aortic pieces (thoracic part with PVAT), and kidney poles (freed of fat) were incubated in KH buffer containing inhibitors for 10 min at 37°C at 300 rpm. The tissue was embedded in an OCT compound and frozen in liquid nitrogen. A cryostat cut the tissue into 8 µm thick slices, which were placed on a microscopy glass slice and frozen at -80°C until further processing. To achieve comparability, tissue from all treatments and controls within a group was applied to one object slice. The staining was performed on the object slice at 37°C for 30 min in the dark with DHE solution (1 µM DHE in PBS). Afterward, the excess solution was removed, and the tissue was embedded under a coverslip. Because of the photosensitive staining, which is only stable for approximately 1 h, the fluorescence signal was immediately measured by a fluorescence microscope (Zeiss) with a rhodamine filter (excitation: 546 nm, emission: ≥ 590 nm). The autofluorescence signal of aortic collagen fibers was measured with a FITC filter (excitation: 450-490 nm, emission: 515-565 nm). Images were quantified using ImageJ by mean grey value measurements of the region of interest.

4.3.4. Superoxide anion detection in aortic tissue by lucigenin-derived chemiluminescence

Lucigenin has been identified as an $O_2^{-\bullet}$-specific chemiluminescence probe. The method was used mainly to measure NADPH oxidase-derived $O_2^{-\bullet}$ production in small aortic pieces. Figure 26 shows the reactions involved in developing lucigenin-enhanced chemiluminescence (ECL). The assay was performed as previously described (216, 263).

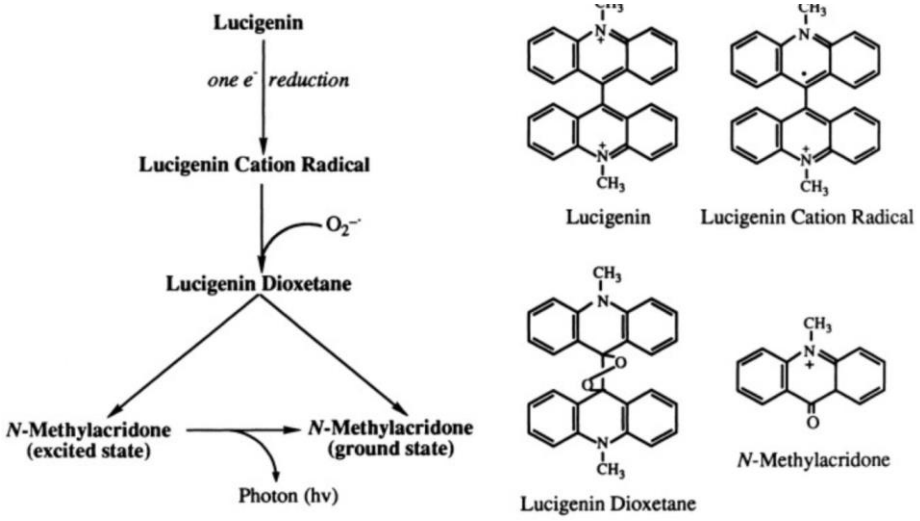

Figure 26: Scheme of the lucigenin reaction pathway. Lucigenin reacts specifically with $O_2^{-\bullet}$ and is used as a chemiluminescence probe to determine oxidative stress in different tissues, such as aortic tissue. The figure is taken from (263, 264).

Aorta pieces (3 mm, thoracic part) were incubated one by one in 500 µl KH buffer on a heater for 20 min at 37°C at 350 rpm. After the incubation, the aorta pieces were placed in vials containing 5 µM lucigenin in PBS. The vials were put into a counter (Lumat LB 9507, Berthold Technologies) with the following setting: measuring time 60 s, total measuring time 1230 s, and delay between measurement 2 s. Aortic rings were removed after the measurement and dried overnight to determine their dry weight. The chemiluminescence value was normalized to the dry weight of aortic rings.

4.3.5. Vascular isometric tension studies

Vascular function *ex vivo* was measured by isometric tension studies of small aortic rings. ACh was used to analyze the functionality of the endothelium. Under healthy conditions, ACh leads to vasodilation via activating muscarinic receptors in the endothelium, which leads to eNOS-catalyzed $^{\bullet}NO$ production (265, 266). The functionality of the vascular musculature was analyzed with nitroglycerine (NTG), an organic nitrate, and $^{\bullet}NO$ donor. With NTG dose-response curves, a vasodilation independent of eNOS catalyzed $^{\bullet}NO$ formation could be observed (267).

Vascular isometric tension studies were performed as already published (268, 269). The aorta was freed from PVAT, under avoidance of dragging, to ensure that the endothelium stayed intact. Small 3 mm pieces of the thoracic aortic part were mounted between two wire triangles connected to a transducer in an organ bath chamber. The buffer in the organ bath chamber was preheated to 37°C and gassed with 95 % CO_2 / 5 % O_2 to simulate a physiological environment. The rings are manually pre-tensioned to create a baseline (stepwise from 0.2 g to 1.1 g). Endothelial function measurement starts with pipetting a dosing effect curve with potassium chloride (KCl, 5 mM to 80 mM). High KCl concentrations cause altered cell membrane polarization, affecting Ca^{2+} channels and leading to a Ca^{2+} uptake from the buffer into the cells, which provides optimal conditions for contraction. Vascular pre-contraction is performed with the vasoactive substance prostaglandin F_{2alpha} ($PGF_2\alpha$, 10mMol), followed by a relaxation-response curve measurement with ACh (1 nM to 3.2 µM). A second relaxation-response curve was performed with NTG (1nM to 32 µM). Figure 27 shows the organ bath chamber setup. Jörg Schreiner (Laboratory of Molecular Cardiology, University Medical Center Mainz) performed the isometric tension studies with technical assistance.

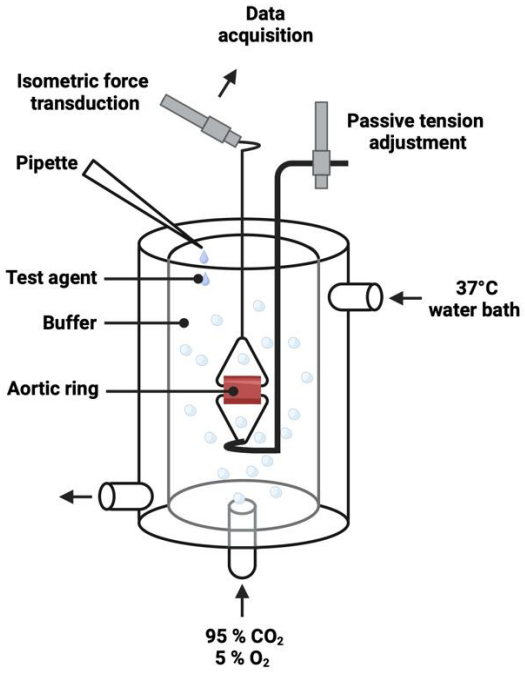

Figure 27: Scheme of the tissue bath system required for isometric tension studies. Small thoracal aortic pieces are mounted between two triangles, connected to an isometric force transducer and a device to adjust the passive tension initially. The inner chamber is filled with organ bath buffer and gassed with 95 % CO_2/5 % O_2. A 37°C water bath surrounds the inner chamber to simulate physiological conditions. Created with BioRender.com. Adapted from (270).

4.3.6. Flow cytometric quantification of vascular immune cell infiltration

Vascular immune cell infiltration was determined with fluorescence-activated cell sorting (FACS) using an Attune NxT Flow Cytometer (Thermo Fisher Scientific) with up to 14 colors

provided from the platform lab at the Centrum of Thrombosis and Hemostasis (University Medical Center Mainz). The protocol was performed as previously described (257, 271). This laser-based technique distinguishes different cell types in a suspension by their size, granulocytic, and fluorescence antibody-based staining of specific surface markers (272). Table 13 shows the utilized antibodies with their respective immune cell targets.

Table 13: Fluorescence-labeled antibodies used for FACS with respective immune cell targets. Table 6 gives an overview of antibody dilutions.

Antibody	**Target**
Fixabel Viability Dye-eFluor506	Live/dead cells
CD11b-PE	Myeloid cells
CD45-APC-efluor 780	Leukocytes
F4/80-APC	Macrophages, monocytes, cytotoxic T-cells
Ly6C-PerCP-Cy.5.5	Macrophages, monocytes, granulocytes, (neutrophils)
Ly6G-FITC	Granulocytes, (neutrophils)
NK1.1-PE-Cy7	Natural killer cells
TCRß Chain-V450	T-cells

4.3.6.1. Preparation of splenic cells for single staining

Single staining for compensation was performed with splenic cell lysates. At first, the whole spleen was freed from fat. A 40 µm cell strainer was placed on a 50 ml falcon and rinsed with 1 ml PBS/FCS. Afterward, the spleen was placed on it and rubbed through the cell strainer with a 1 ml syringe stamp. The cell strainer was rinsed three to four times with 1 ml PBS/FCS, and the cell suspension was transferred into a 15 ml Falcon. Followed by 6 min centrifugation at 300 g at 4°C. The supernatant was removed, and the pellet was resuspended in 3 ml of ACK-Lyse buffer. After 3 min of incubation at room temperature, the reaction was immediately stopped by adding 3 ml PBS/FCS into the Falcons and centrifugation for 6 min at 300 g at 4°C. The supernatant was removed, and the pellet was resuspended in 5 ml of PBS/FCS. The cells were diluted 1:1 with trypan blue and counted with the TC20 automated cell counter from BioRad. Per well, 1 million spleen cells were pipetted into a well of a U-bottom-shaped 96-well plate. The number of wells corresponds to the number of the used dyes plus one unstained control.

4.3.6.2. Preparation of aortic cell lysates for extracellular staining

Immune cell composition and infiltration into the aortic wall were analyzed in aortic cell lysates. In preparation, fat and blood were removed from the aortas (see 4.3.1). The tissue was stored

on ice in KH buffer, and the length of the aortas was measured. Before the tissue preparation, the liberase stock solution of 5 mg/ml was diluted 1:4 with $HBSS^{+/+}$, and for each aorta, a 2 ml Eppi containing 1 ml of diluted liberase solution was provided. Afterward, the tissue was placed in one drop of diluted liberase in glass Petri dishes and chopped into small pieces by sharp razor blades. The tissue was transferred with rounded tweezers into the liberase containing Eppis, and the glass petri dish was rinsed with a cut-off blue tip to collect all remaining cells. The digestion was started by placing the tissue containing Eppis from ice in a heater for 30 min at 37°C at 500 rpm. During the incubation, the tissue was pipetted up and down every 10 min with a cut-off blue tip. A 70 µm cell filter was placed on a 50 ml falcon for each aorta and rinsed with 1 ml PBS/FCS. After the incubation, the digestion was stopped by adding 1 ml PBS/FCS to the cell suspensions and transferring the Eppis to ice. The cell suspension was pipetted onto the cell strainer and rubbed with a 1 ml syringe stamp. The cell strainer was rinsed three to four times with 1 ml PBS/FCS, and the suspension was transferred into a 15 ml falcon for 6 min centrifugation at 300 g at 4°C. In the last step, the supernatant was removed after centrifugation, and the cell pellet was resuspended in 200 µl PBS/FCS. The cells were counted with the TC20 automated cell counter from BioRad and transferred into a U-bottom-shaped 96-well plate.

4.3.6.3. Extracellular staining

The 96-well plate containing all cell suspensions was centrifuged for 6 min at 300 g at 4°C. Afterward, the supernatant was removed, and the cell pellets were resuspended in 50 µl Fc-block followed by 10 min incubation in the dark at 4°C. The incubation was stopped by adding 100 µl PBS/FCS into the wells and a centrifugation step for 6 min at 300 g at 4°C. The supernatant was again removed, and the cell pellets were resuspended with the extracellular staining-master mix (40 µl per pellet, containing a mixture of eight antibodies see Table 6) or the respective single stainings for compensation (40 µl per pellet), followed by 30 min incubation in the dark at 4°C. The extracellular staining master mix contains a mixture of the fluorescence-labeled antibodies summarized in Table 6. The reaction was stopped by adding 100 µl PBS/FCS, and the 96-well plate was centrifuged again for 6 min at 300 g at 4°C followed by supernatant removal. The pellets were washed with 100 µl PBS/FCS and centrifuged for a last time for 6 min at 300 g at 4°C followed by supernatant removal. All samples were resuspended in 200 µl PBS/FCS. The samples incubated in the extracellular staining-master mix remained in the 96-well plate. In contrast, the single staining samples for compensation were transferred into FACS tubes and filled up with an additional 300 µl PBS/FCS. The cell composition was analyzed using an Attune NxT Flow Cytometer. The applied gating strategy is shown in Figure 28. For each sample, the number of stained cells was normalized to the number of living cells and the length of the aorta.

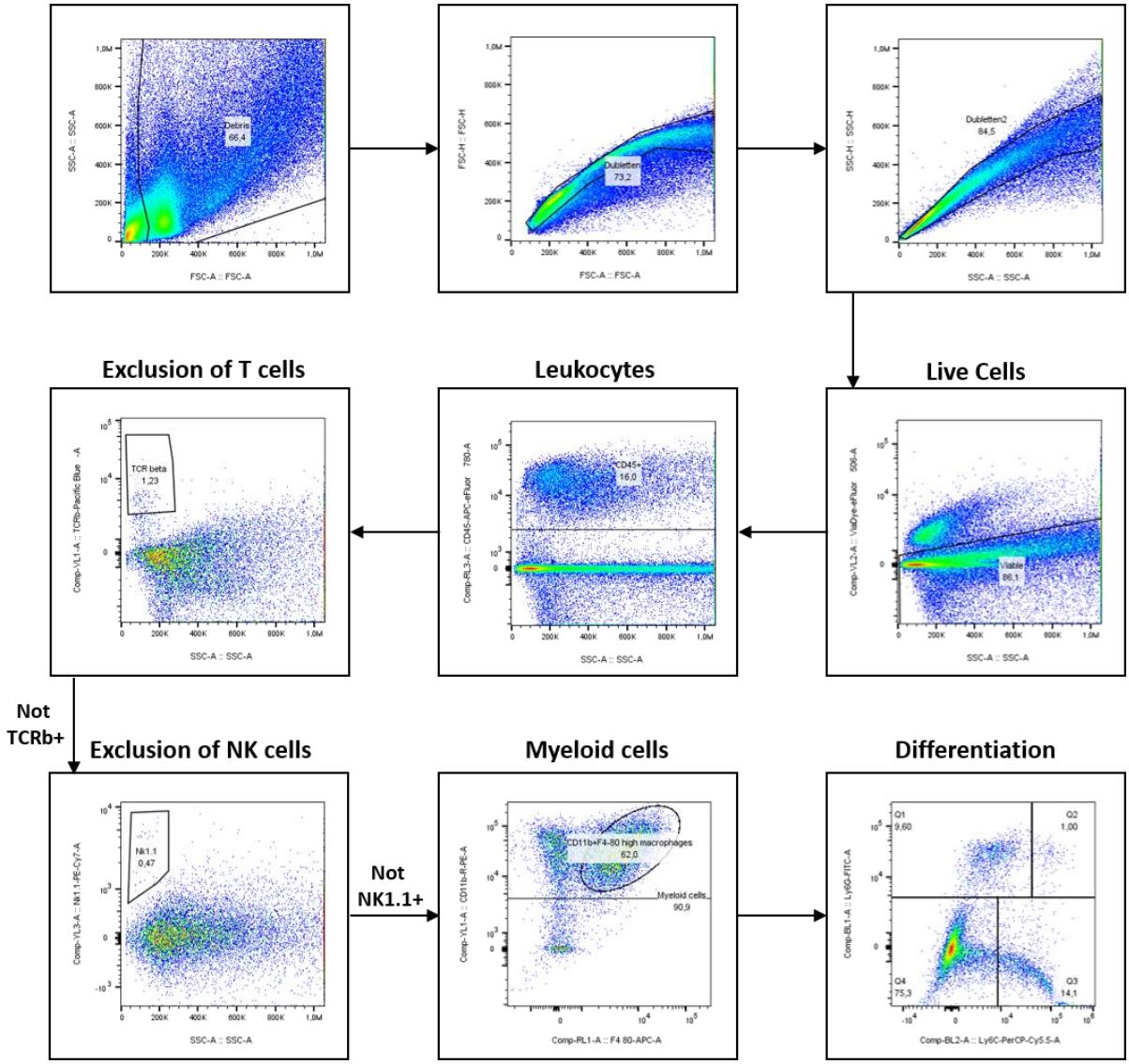

Figure 28: Gating strategy to determine different immune cell subtypes in aortic tissue. Cell debris, doublets, and dead cells were excluded in the first steps of the analysis. Subsequently, the leukocytic (CD45+) population was identified to exclude T (TCRß+) and NK (NK1.1+) cells from further analysis in the following step. Myeloid cells (CD11b+) and macrophages (CD11b+ F4/80+) were then identified. As a last step, the myeloid cell gate was utilized to differentiate neutrophils (Ly6G+ Ly6C+) and inflammatory monocytes (Ly6C high).

4.4. Molecular biological methods

4.4.1. DNA isolation for genotyping

The genotype of the transgenic mice was determined by isolating genomic DNA from ear biopsies using the “HotShot” DNA preparation method (273). Ear biopsies were taken from the freezer (-20°C) and placed on a 95°C preheated thermocycler in 75 µl lysis buffer for 45 min at 500 rpm. Afterward, the microtubes were cooled down for 10 min, and 75 µl neutralization buffer was added. The tubes were mixed by vortexing and frozen at -20°C until further processing. The extracted DNA can be used without further purification for the genotyping PCR analysis.

4.4.2. Genotyping by using polymerase chain reaction (PCR)

The PCR method was used to amplify distinct DNA fragments to determine the genotype from transgenic mice. Extracted DNA from ear biopsies was mixed with GoTaq master mix, and distinct primers and the PCR programs were performed as described in Table 14, Table 15 and Table 16.

Table 14: PCR reaction mix and program for CD40$^{-/-}$ mice.

PCR reaction mix [µl]	
GoTaq Green Master mix 2x	12.5
Primer CD40 Com/J	1.25
Primer CD40 WT rev/J	1.25
Primer CD40 Mut rev/J	1.25
DEPC treated water	6.25
Genomic DNA	2
	25

PCR program		
95°C	3 min	1x
95°C	15 s	35x
60°C	15 s	
72°C	15 s	
72°C	7 min	1x
4°C	∞	

Genotyping of the CD40$^{-/-}$ mouse line was unnecessary, but it was performed at least four times within a year as verification and quality control. In the agarose gel, a signal at 685 bp indicates a homozygous global knockout of CD40.

Table 15: PCR reaction mix and program for AdipoqCre mice.

PCR reaction mix [µl]	
GoTaq Green Master mix 2x	12.5
Primer AdipoqCre fw	1.5
Primer AdipoqCre rv	1.5
Primer Noxa fw	1.5
Primer Noxa rv	1.5
DEPC treated water	4.5
Genomic DNA	2
	25

PCR program		
95°C	2 min	1x
95°C	30 s	35x
60°C	30 s	
72°C	1 min	
72°C	5 min	1x
4°C	∞	

Table 16: PCR reaction mix and program for CD40fl/fl mice.

PCR reaction mix CD40fl/fl [µl]	
GoTaq Green Master mix 2x	12.5
Primer CD40fl/wt fw	1.5
Primer CD40fl/wt rv	1.5
Primer CD40fl/fl fw	1.5
DEPC treated water	6
Genomic DNA	2
	25

PCR program		
95°C	2 min	1x
95°C	30 s	35x
60°C	30 s	
72°C	1 min	
72°C	5 min	1x
4°C	∞	

Genotyping of the AdiCD40$^{-/-}$ mice was mandatory. A breeding scheme was applied in which Cre wildtype (WT) animals were crossed with Cre heterozygous (Het) animals to obtain both genotypes. Indeed, Cre WT mice were used as control animals and Cre Het animals as tissue-specific CD40 knockout mice. In an agarose gel, a Cre Het animal showed signals at 220 bp and 190 bp, whereas a signal at only 190 bp was observed for Cre WT mice. CD40fl/fl genotyping was performed as a verification and quality control. For CD40fl/fl mice, a signal at 380 bp was observed.

4.4.3. Agarose gel electrophoresis

The PCR products were analyzed using agarose gel electrophoresis. Therefore, 2.5 g of agarose was diluted in 100 ml 1x TAE buffer and heated in the microwave. Before pouring the gel into a horizontal chamber, 5 µl Midori green was added to the hand-warm solution and gently mixed. 10 µl of the samples, controls, and a 100 bp ladder were pipetted into the gel pockets. The gel ran in 1x TAE buffer for 90 min at 62 V. Midori green is a DNA intercalating agent that could be visualized via UV light.

4.4.4. RNA Sequencing

RNA sequencing (RNA-Seq) was performed to analyze total mRNA expression in CHD patients' bypass material and examine altered gene expression levels due to the influence of different co-morbidities. The RNA was isolated in our lab and sent for RNA-Seq to Novogene Bioinformatics Technology Co., Ltd., in Cambridge (274-276).

According to the manufacturer's instructions, aortic mRNA was isolated using the RNeasy Mini kit (Qiagen, Germany). Novogene performed RNA quality control, mRNA library preparation (poly A enrichment), NovaSeq PE150 sequencing (9 G raw data per sample), and data quality control. CLC genomic workbench (22.0.2) and IPA were used for data analysis (Qiagen, Germany). The data (fastq.gz) were imported in the CLC data (.clc) format, and the reads were

trimmed as recommended by the manufacturer (quality score: 0.05, maximum number of ambiguities: 2). The trimmed data were mapped to the human (Homo_sapiens_hg38-2022-11-25-22-33, ENSEMBL) using the following parameters (Mismatch cost: 3; Insertion cost: 3; Deletion cost: 3; Length fraction: 0.9; Similarity fraction: 0.9; Maximum number of hits for a read: 10). Calculation of the fold enhancement of the mRNA expression was performed with the rpkm data. Followed by upload to the IPA server to analyze relevant changes in signal pathways (upload $p < 0.05$, analysis $p < 0.05$). The CLC genomic workbench created volcano plots (Figure 47). Meanwhile, the canonical pathway analysis results were produced using IPA (Figure 48-52). RNA isolations were performed in co-operation with PhD Marin Kuntic, and Novogene performed the RNA-Seq. Data analysis was performed in collaboration with Prof. Dr. Hartmut Kleinert (Pharmacology Department, University Medical Center Mainz).

4.5. Protein biochemical methods

4.5.1. Purification of protein from murine tissue

Protein isolations were performed from frozen tissue or organs stored at -80°C. The frozen tissue/organ pieces were transferred into a precooled 2 ml microcentrifuge tube in liquid nitrogen containing one stainless steel bead (5 mm diameter) and were incubated for 15 min. The tubes were placed into the Tissue Lyser LT adapter and incubated at room temperature for 2 min to avoid freezing of the buffer. Afterward, the homogenization buffer was added to 100-400 µl depending on the sample size. The adapters were attached to the tissue lyser, and the samples were disrupted at 50 Hz for 5 min, followed by 1 h incubation on ice and two centrifugation steps at 8000 g and 10000 g each for 10 min at 4°C. The protein-containing supernatant was taken after each centrifugation step and transferred to a fresh 1.5 ml microcentrifuge tube. The protein was stored after purification at -20°C, and the protein content was determined using Bradford assay.

4.5.2. Protein quantification by Bradford assay

The Bradford assay is used as a photometric method for quantitatively determining proteins. When the Coomassie brilliant blue-containing dye is added to the sample, the proteins form complexes with it, which leads to a shift of the absorption maximum from 465 nm to 595 nm. Changes in absorption depend on the amount of protein in the sample (277). Standard curve samples with concentrations of 0, 1, 5, 10, 20, 30, and 50 µg/ml bovine albumin serum in ddH_2O were prepared. The samples were diluted in ddH_2O (kidney and heart 1:800, plasma 1:2000), and respectively of each sample, 80 µl were pipetted in a 96-well plate as quadruplicates. In the end, 200 µl Roti®Quant solution was added to the samples, and the absorption was immediately measured in an MRX-II plate reader at 595 nm. Protein concentrations were calculated with Revelation 4.25.

4.5.3. Protein separation by SDS polyacrylamide gel electrophoresis

One-dimensional SDS polyacrylamide gel electrophoresis allows the separation of proteins regarding the molecular weight in an electric field. In preparation, the protein samples were diluted in Laemmli buffer containing SDS, which covers the intrinsic charge of the proteins and ensures a constant negative charge distribution. In addition, the buffer comprises β-mercaptoethanol to split disulfide bridges by reduction. The secondary and tertiary protein structures were destroyed by heating the samples at 95°C. This sample treatment leads to a denaturation of the proteins and a uniform charge. Consequently, the separation on the gel is independent of charge and only proportional to their molecular weight (278, 279). Figure 29 shows the protein denaturation and SDS gel electrophoresis setup.

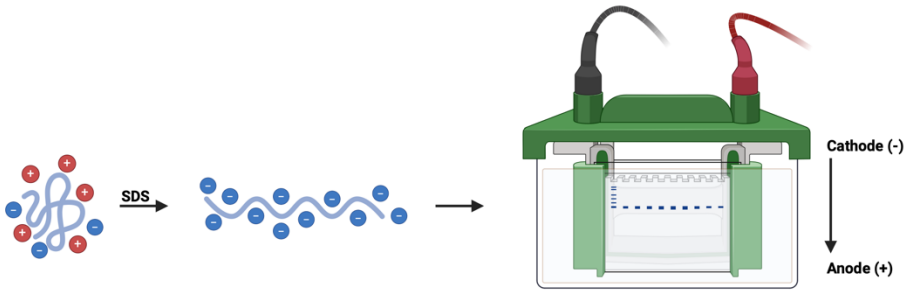

Figure 29: Protein separation by SDS polyacrylamide gel electrophoresis. Heat and SDS treatment lead to protein denaturation and uniformly negative protein charge. The proteins are separated according to their molecular size via SDS polyacrylamide gel electrophoreses. Created with BioRender.com.

The SDS gels were prepared in a vertical gel electrophoresis chamber. At first, a 10 % resolving gel was poured into the chamber. After complete polymerization, the 4 % stacking gel pouring followed. The composition of running and stacking gels is shown in Table 17. A comb was inserted into the liquid stacking gel. The samples were adjusted to a uniform protein amount (15-30 µg), mixed with Laemmli buffer, and heated at 95°C for 10 min. The gel was inserted in a holder, and the electrophoresis chamber was filled with a running buffer. The chamber was placed in an ice-filled box. After pre-running at 30 V for 10 min, samples and protein markers were loaded into the pockets of the SDS-PAGE. Electrophoresis was performed at first for 15 min at 60 V and afterward at 120 V, and it was stopped after an effective separation of the proteins was observed.

Table 17: Composition of running and stacking gels used for SDS gel electrophoresis.

	10 % Resolving gel	**4 % Stacking gel**
ddH_2O	4.8 ml	3.2 ml
40 % Acrylamide/bis (29:1)	2.5 ml	0.5 ml
1.5 M Tris-HCl, pH 8.8	2.5 ml	-
0.5 M Tris-HCl, pH 6.8	-	1.2 ml
10 % SDS	100 µl	50 µl
10 % APS	100 µl	50 µl
TEMED	10 µl	5 µl

4.5.4. Immunological detection of proteins by Western blotting

Western blotting is called the electrophoretic transfer of proteins from a polyacrylamide gel onto a nitrocellulose membrane. The pattern of electrophoretic separation is preserved, and the proteins adhere to the membrane surface due to hydrophobic interactions (280). In preparation, the Western blot cassette was placed in an ice-cold blotting buffer (-20°C), sucked fiber pads, and a Whatman filter paper was put on top. The gel was removed from the chamber, washed with ddH_2O, and laid on the filter paper. Further, the nitrocellulose membrane (0.45 mm) was carefully placed on top of the gel, and the assembly ended with adding another filter paper and a fiber pad. The cassette was closed and put in a blotting tank filled with ice-cold blotting buffer. The cassette must be aligned correctly between the anode and cathode to transfer the negatively charged proteins to the membrane. The assembly of the Western blot cassette is also shown in Figure 30. The blotting tank was placed with a cooling pack in the fridge, and the protein transfer took place overnight at 90 mA.

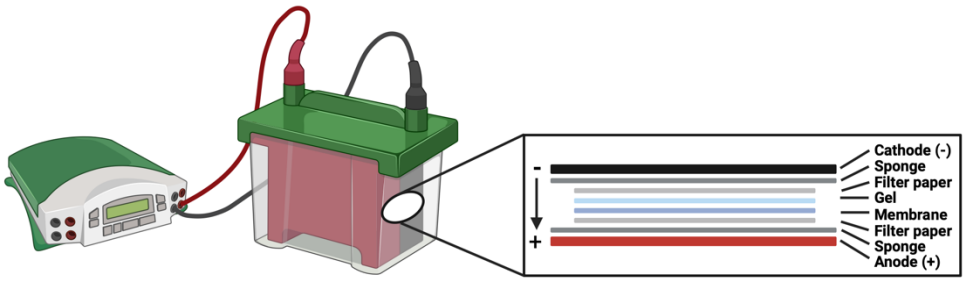

Figure 30: Assembly of the Western blot cassette. Created with BioRender.com.

The next day, the blotting efficiency was verified with Ponceau S staining, which was used as total protein staining. The dye can easily be washed off with the respective washing buffers (PBS-T or TBS-T) and does not interfere with the following immunological detection (281). Unspecific antibody binding is reduced by blocking the membranes in respective blocking solutions for 1 h at room temperature. The membranes were incubated overnight at 4°C under

gentle movement with the diluted primary antibodies. The following day, the membranes were washed three times for 10 min at room temperature under gentle shaking. As secondary antibodies, horseradish peroxidase (HRP) conjugated antibodies were used, and the membranes were incubated for 2 h with them at room temperature. Afterward, they were washed again three times for 10 min in washing solutions. HRP-conjugated protein complexes are visualized by chemiluminescence, which can be detected because HRP catalyzes the conversion of luminol into its oxidized form. The membranes were incubated for 1 min (Pierce™ECL Western Blotting Substrate) or 3 min (SuperSignal™West) in a 1:1 mixture of luminol/hydrogen peroxide. Chemiluminescence signals were recorded with a digital imaging system (ChemiLux Imager, Intas). Densitometric quantification of the protein bands was conducted using the Gel-Pro Analyzer 6.0 software, and the protein expression was normalized against a housekeeping protein (ß-actin).

4.5.5. Immunological detection of proteins by Dot Blot

Dot blotting was used to analyze antigen content from tissue samples without previous separation by gel electrophoresis. In preparation, proteins were purified as described in 4.5.1 and diluted to 30 µg/well in PBS containing 0.1 % SDS. The Minifold I vacuum dot blot system was assembled with a prewetted Whatman filter and a prewetted Nitrocellulose membrane. Under constant vacuum, the 96 wells of the top frame were washed twice with 200 µl PBS. Afterward, the samples were loaded, and the wells were washed again twice with 200 µl PBS. The vacuum was removed, and the membrane was dried for 1 h at 60°C to fix the proteins in the membrane. Ponceau S staining was performed. The immunological detection and antibody incubation were performed as described above in 4.5.4.. The quantification was executed with the Gel-Pro Analyzer Software, and the protein expression was normalized to its total protein count (Ponceau S staining).

4.5.6. Targeted Olink proteomics analysis

Targeted Olink proteomics analysis was performed to analyze the role of co-morbidities in the severity of CHD in patients' plasma samples. The Olink T96 IMMUNO-ONCOLOGY panel was utilized to measure 92 CVD-related human protein biomarkers using the Proximity Extension Assay (PEA) technology (Olink Biosciences, Sweden) (276, 282-284).

Once-thawed EDTA-blood plasma was used for analysis. After antibody binding and unspecific preamplification, a quantification by qPCR followed, resulting in a C_t-value for each protein (Fluidigm Real-Time PCR Analysis Software, Version 4.3.1, USA). C_t-values were converted into normalized protein expression (NPX) units using the Olink® NPX Manager software (Version 1.1.4.0, Sweden). NPX units represent relative quantifications of protein

concentrations on a log2-scale. Olink measurement and generation of processed raw data was performed in collaboration with Prof. Dr. Imo Hoefer (Central Diagnostic Laboratory, UMC Utrecht, Utrecht, The Netherlands). The Perseus software suite was used to group the samples and to perform differential expression analysis. Student t-test with a cut-off of $p<0.05$ was applied, and differentially expressed proteins in at least one group were kept for analysis. To visualize expression changes across the groups, the mean value was determined, Z-normalized, and proteins were clustered using Euclidean distance. Network analysis and data representation were performed using Cytoscape, and differentially expressed proteins were mapped onto a network generated by String. Edges represent interactions based on genetic, experimental, biochemical, and text-mining data using a threshold of >0.4. The bioinformatical analysis were performed in co-operation with Dr. Roopesh Krishankutty and Dr. Alex von Kriegsheim (Institute of Genetics and Cancer, University of Edinburgh, UK).

4.6. Statistics

Data are represented as mean values (Ø) ± standard derivation (SD). The statistical analysis was performed using Graph Pad Prism Software (9.5.0). If not previously mentioned, the Shapiro-Wilk test was used as a normality test. If the normality test failed, the Kruskal-Wallis test with Dunn's multiple comparison test was performed. If the normality test passed, one-way ANOVA with Tukey´s multiple comparison test or a two-way ANOVA with Dunnett´s multiple comparison test, depending on the group design, were performed. Outliers were identified and removed with the ROUT (1 %) method. P-values <0.05 were considered statistically significant and labeled as *$p\leq0.05$, **$p\leq0.01$, ***$p\leq0.001$, and ****$p\leq0.0001$. The patient's characteristics were analyzed using SPSS Statistic software provided by Dr. Omar Hahad (Laboratory of Molecular Cardiology, University Medical Center Mainz). A cross-tabulation analysis and a person's chi-squared test were performed for categorical variables. In the case of continuous variables, a descriptive statistic, a test of normal distribution, and an ANOVA were performed.

5. Results

This study was performed to better understand the CD40L-CD40 cascade as a pharmacological target to prevent and modulate chronic vascular inflammation. The focus here is set on modifiable metabolic risk factors of CVD, like hypertension or diabetes mellitus, in different mouse models. Further, aortic tissue and plasma from CVD patients were analyzed to determine the role of CD40L-CD40 signaling and inflammation. We want to highlight the importance of CD40L-CD40 signaling in pathological inflammatory processes and that targeted therapy could be a promising treatment strategy. Some of the results presented here have already been published (276).

5.1. The role of global CD40 knockout in a hypertensive mouse model

5.1.1. CD40 deficiency does not significantly improve the hypertensive phenotype in mice

If CD40 deficiency has beneficial effects on vascular function and oxidative stress in a mouse model of arterial hypertension is examined first. WT (C57BL/6J) and global CD40$^{-/-}$ (CD40 KO, B6.129P2-Cd40^{tm1Kik}/J) mice were treated with AT-II (1 mg/kg/d) for seven days. No significant differences in body weight were observed between the groups after seven days of treatment (WT Ø 26 g, WT+AT-II Ø 27 g, CD40$^{-/-}$ Ø 26 g, and CD40$^{-/-}$+AT-II Ø 26 g) (Figure 31 A). Whereas, compared to WT animals (Ø 111 mg), the heart weight was significantly increased in both AT-II treated groups (WT+AT-II Ø 139 mg and CD40$^{-/-}$+AT-II 127 mg). Interestingly, the AT-II-induced heart weight gain in CD40$^{-/-}$ mice was lower than in WT mice (Ø 9 mg vs. Ø 28 mg) (Figure 31 B). This trend was also reflected in the calculation of the heart-to-body weight ratio (Figure 31 C)

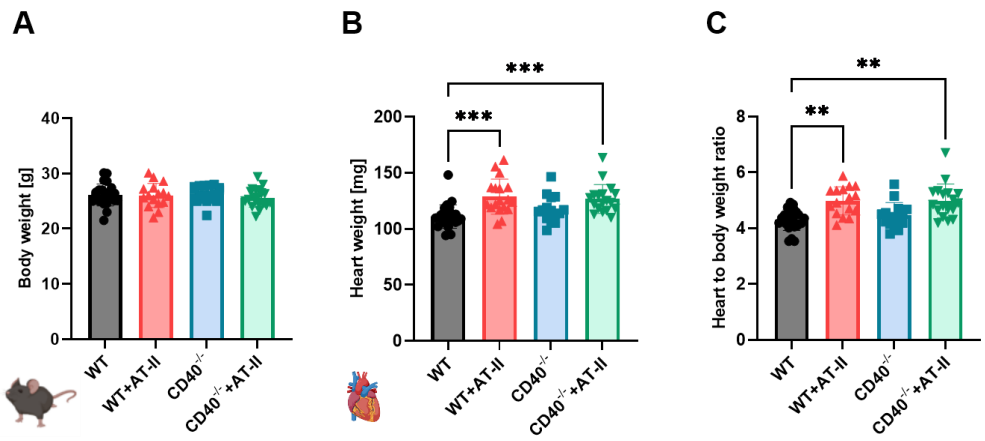

Figure 31: Global CD40$^{-/-}$ does not prevent cardiac hypertrophy development in hypertensive mice. WT (C57BL6/J) and CD40$^{-/-}$ (B6.129P2-Cd40^{tm1Kik}/J) mice were treated with AT-II (1 mg/kg/d) via osmotic minipumps for seven days to induce arterial hypertension. After seven days of treatment, the body (A) and heart weight (B) were measured to calculate the heart-to-body weight ratio (C). Data are presented as mean values ±SD of n=15-26 (A-C) animals per group. *p≤0.05, **p≤0.01, ***p≤0.001, and ****p≤0.0001. One-way ANOVA with Tukey´s

multiple comparison test was performed. Icons were created with BioRender.com. Abbreviations: WT=C57BL6/J mice, CD40$^{-/-}$=B6.129P2-Cd40^{tm1Kik}/J, AT-II=angiotensin-II.

Systolic blood pressure was measured by noninvasive tail-cuff measurement. AT-II treatment significantly increased the systolic blood pressure in WT (WT Ø 133 mmHg and WT+AT-II Ø 162 mmHg) and CD40$^{-/-}$ mice (CD40$^{-/-}$ Ø 131 mmHg and CD40$^{-/-}$+AT-II Ø 148 mmHg). Overall, in WT animals, AT-II treatment caused a higher systolic blood pressure increase than in CD40$^{-/-}$ mice (29 mmHg vs. 17 mmHg) (Figure 32 A). In addition, the relaxation of aortic rings in response to different ACh concentrations was recorded to analyze the endothelial function in isometric tension studies. At the time point of maximal relaxation, both hypertensive groups demonstrate an impaired endothelial function with Ø 57 % (WT+AT-II) and Ø 59 % (CD40$^{-/-}$+AT-II) compared to the respective control group (Ø 83 % WT and Ø 74 % CD40$^{-/-}$). This data indicates that the endothelial function in CD40$^{-/-}$ animals did not deteriorate as much as in the WT animals by AT-II treatment, considering that the CD40$^{-/-}$ mice already showed a worse endothelial function than WT mice (Figure 32 B). A similar trend was observed for the smooth muscle cell function measured in small aortic rings by relaxation in response to different NTG concentrations. At the time point of maximal smooth muscle cell function, a maximal relaxation of Ø 87 % WT, Ø 82 % WT+AT-II, Ø 88 % CD40$^{-/-}$, and Ø 84 % CD40$^{-/-}$+AT-II were measured. Compared to WT animals, smooth muscle cell function of both hypertensive groups was significantly impaired (Figure 32 C). Concerning this data, only systolic blood pressure is statistically improved by the absence of CD40.

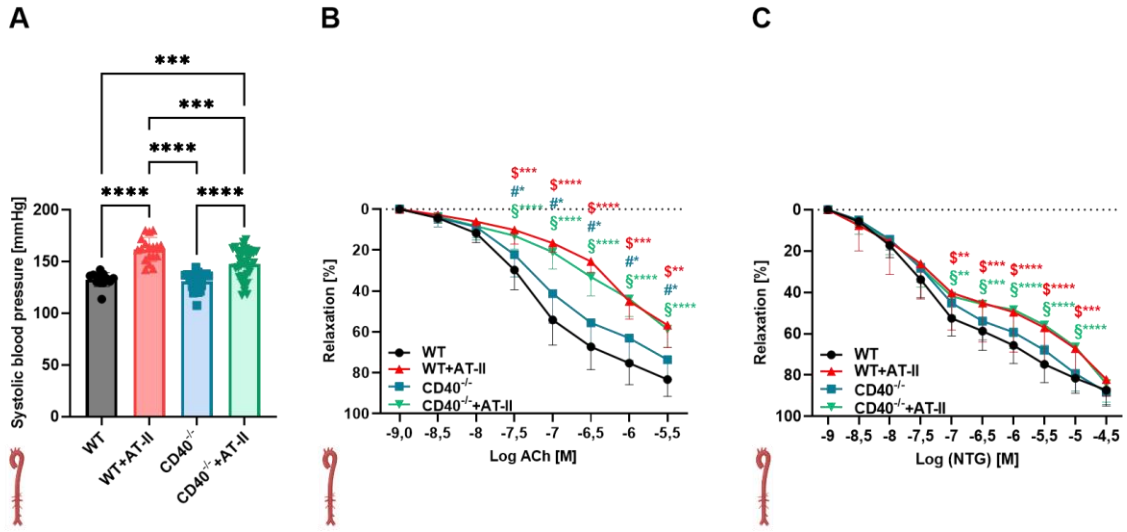

Figure 32: Absence of CD40 only slightly reduces systolic blood pressure but does not improve vascular function in hypertensive mice. WT (C57BL6/J) and CD40$^{-/-}$ (B6.129P2-Cd40^{tm1Kik}/J) mice were treated with AT-II (1 mg/kg/d) via osmotic minipumps for seven days to induce arterial hypertension. (A) Systolic blood pressure was measured via the noninvasive tail-cuff method. Aortic segments were used to measure endothelial (B) and smooth muscle cell function (C) in isometric tension studies. Data are presented as mean values ±SD of n=13-26 (A) and n=6-18 animals per group. *p≤0.05, **p≤0.01, ***p≤0.001, and ****p≤0.0001. One-way ANOVA with Tukey´s multiple

comparison test was performed. Icons were created with BioRender.com. Abbreviations: WT=C57BL6/J mice, CD40$^{-/-}$=B6.129P2-Cd40^{tm1Kik}/J, AT-II=angiotensin-II, ACh=acetylcholine, NTG=nitroglycerine.

5.1.2. CD40 deficiency does not significantly diminish oxidative stress in the blood and aortic tissue of hypertensive mice

Oxidative stress formation in cryosections of aortic and cardiac tissue was analyzed with DHE stainings. The overall ROS production was increased in AT-II-treated animals (Ø 148 % WT+AT-II and Ø 180 % CD40$^{-/-}$+AT-II) compared to the control groups (Ø 100 % WT and Ø 121 % CD40$^{-/-}$) in aortic tissue. No genotypic improvement in aortic oxidative stress generation in hypertensive CD40$^{-/-}$ animals was observed (Figure 33 A). Whereas, in cardiac tissue, a significant improvement in ROS formation was shown in hypertensive CD40$^{-/-}$ mice (Ø 80% CD40$^{-/-}$ vs. Ø 116 % CD40$^{-/-}$+AT-II) compared to the control group (Ø 100 % WT vs. 175 % WT+AT-II) (Figure 33 B). In addition, representative pictures of the staining are shown below the bar graphs in Figure 33. The fluorescence of aortic and cardiac ROS is reflected in red, and the autofluorescence of aortic laminae is represented in green. In addition, whole-blood oxidative burst measurements were performed to analyze the mostly leukocyte-dependent H_2O_2 formation. The oxidative burst was detected by chemiluminescence resulting from L-012 oxidation in either PDBu (Figure 33 C) or zymosan A (Figure 33 D) stimulated samples. No significant increase of oxidative burst in the PDBu-stimulated blood samples was observed after AT-II treatment, despite a noticeable trend of increased ROS formation in WT mice (Ø 357 counts/s WT, Ø 595 counts/s WT+AT-II, Ø 357 counts/s CD40$^{-/-}$, and Ø 465 counts/s CD40$^{-/-}$+AT-II). Also, no significant improvement was observed by CD40 deficiency. In zymosan A stimulated AT-II treated WT animals (Ø 1602 counts/s), the oxidative burst was significantly elevated compared to both control groups (Ø 657 counts/s WT and Ø 520 counts/s CD40$^{-/-}$). In CD40$^{-/-}$+AT-II mice (Ø 1171 counts/s), the oxidative burst increased by trend compared to the untreated groups. These data showed that CD40 deficiency largely did not improve oxidative stress in different tissues to the expected amount.

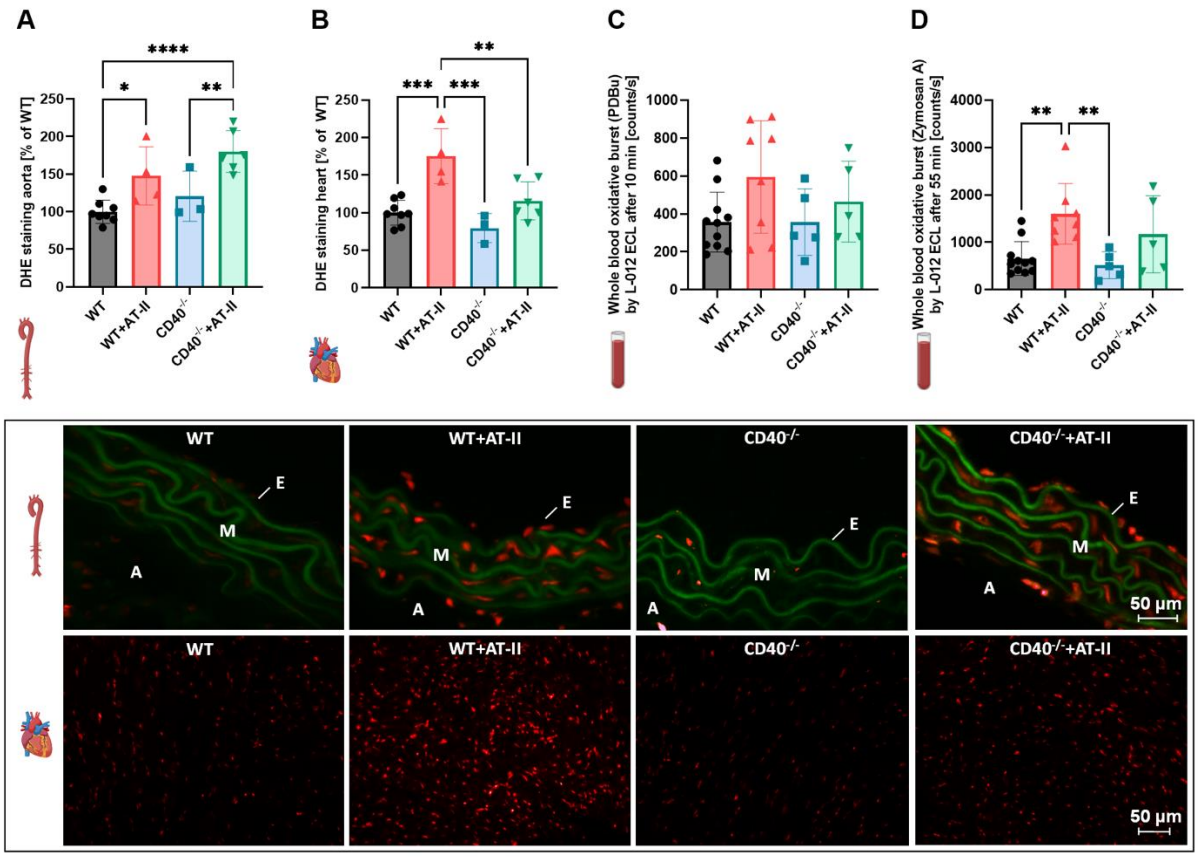

Figure 33: Absence of CD40 largely does not improve oxidative stress in different tissues of hypertensive mice. WT (C57BL6/J) and CD40$^{-/-}$ (B6.129P2-Cd40^{tm1Kik}/J) mice were treated with AT-II (1 mg/kg/d) via osmotic minipumps for seven days to induce arterial hypertension. DHE stainings in cryosections of aortic (A) and cardiac tissue (B) were performed to analyze the overall ROS production. Representative pictures of aortic stainings are shown below the bar graphs. The green color reflects the autofluorescence of aortic laminae, whereas the red color reflects the fluorescence from ROS. The chemiluminescence of L-012 oxidation was utilized to analyze the mainly leukocyte-dependent H_2O_2 production in whole blood samples. Previously, the blood was stimulated with PDBu for 10 min (C) or with zymosan A for 55 min (D). Data are presented as mean values ±SD of n=3-8 (A+B) and n= 5-11 (C+D) animals per group. *p≤0.05, **p≤0.01, ***p≤0.001, and ****p≤0.0001. One-way ANOVA with Tukey´s multiple comparison test was performed. Icons were created with BioRender.com. Abbreviations: WT= C57BL6/J mice, CD40KO=B6.129P2-Cd40^{tm1Kik}/J mice, AT-II=Angiotensin-II, DHE=dihydroethidium, PDBu=phorbol 12,13-dibutyrate, ECL=electrochemiluminescence, A=adventitia, M=media, E=endothelium.

5.2. The role of adipocyte-specific CD40 knockout in a hypertensive mouse model

5.2.1. Adipocyte-specific CD40 knockout does not lead to a vasoprotective phenotype in hypertensive mice

It is important to understand further the function and the contribution of different cell types in CD40L-CD40-mediated inflammatory signaling. Among vascular and immune cells, CD40 is expressed from adipocytes, which play an important role in the modulation of immune cell responses, especially in the progression of cardiovascular and metabolic diseases. The role of adipocytes in low-grade inflammation was studied here with an adipocyte-specific CD40 knockout (AdiCD40$^{-/-}$, AdipoqCre x CD40fl/fl) mouse model, which was generated and provided by a partner lab for this study (see 4.2.1). AdiCD40$^{-/-}$ and respective control (Ctr) mice were treated for seven days with 1 mg/kg/d AT-II to induce arterial hypertension and vascular

inflammation. Thereby, Cre WT animals were used as a control (Ctr). A significant increase was observed when the heart-to-body weight ratio of Ctr mice was compared with that of AT-II-treated mice. Nevertheless, no significant difference was shown in the heart-to-body weight ratio of AT-II-treated Ctr and AdiCD40$^{-/-}$ mice. Cardiac hypertrophy was not improved in AdiCD40$^{-/-}$ mice (Figure 34 A). In addition, systolic blood pressure was measured after six days of treatment via the tail-cuff method. Again, the two control groups (Ø 132 mmHg Ctr and Ø 135 mmHg AdiCD40$^{-/-}$) showed no significant difference in systolic blood pressure. In contrast, a significant increase in the two AT-II treated groups (Ø 167 mmHg Ctr+AT-II, Ø 158 mmHg AdiCD40$^{-/-}$+AT-II) was observed compared to the control groups. Interestingly, the systolic blood pressure was by trend reduced in AdiCD40$^{-/-}$+AT-II mice compared to Ctr+AT-II mice (Figure 34 B). The endothelial and smooth muscle cell function of small aortic rings was measured via isometric tension studies. But again, neither in the endothelial-dependent nor in the independent relaxation of aortic rings was a significant difference observed between the two AT-II-treated groups (WT vs. AdiCD40$^{-/-}$) (Figure 34 C+D). At the maximal relaxation, endothelial function was significantly impaired in the AT-II-treated groups (Ø 65 % Ctr+AT-II and Ø 59 % AdiCD40$^{-/-}$+AT-II) compared to the control animals (Ø 77 % Ctr and Ø 73 % AdiCD40$^{-/-}$). Also, the smooth muscle cell function was partially significantly impaired in the two AT-II-treated groups compared to the control mice without any improvement by the cell-specific knockout of CD40 (Figure 34 C+D). At the maximal smooth muscle cell relaxation potential, no significant differences were observed between the groups (Ø 89 % Ctr, Ø 84 % Ctr+AT-II, Ø 89 % AdiCD40$^{-/-}$, and Ø 85 % AdiCD40$^{-/-}$+AT-II). Cell-specific CD40$^{-/-}$ did not improve the endothelial or smooth muscle cell function as hypothesized in the beginning (Figure 34 C+D).

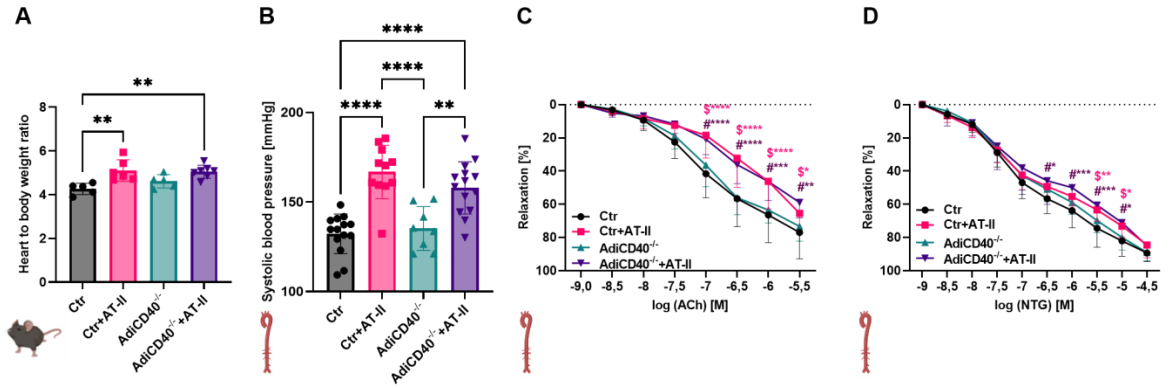

Figure 34: Systolic blood pressure and endothelial function are not improved in angiotensin-II (AT-II) treated adipocyte-specific CD40 knockout mice. Adipocyte-specific CD40$^{-/-}$ mice (AdiCD40$^{-/-}$) and respective control mice (Ctr) were treated for seven days with AT-II (1 mg/kg/d) via osmotic minipumps. (A) The body and heart weights were taken from the mice on day seven, and a ratio was calculated. (B) Systolic blood pressure was determined via non-invasive blood pressure measurement at the tail of the mice. (C+D) Endothelial function in response to acetylcholine and smooth muscle cell function in response to nitroglycerine were measured by isometric tension studies. Data are presented as mean values ±SD of n=5-7 (A), n=8-14, and n=9-14 (C+D) animals per group. *p≤0.05, **p≤0.01, ***p≤0.001, and ****p≤0.0001. Icons were created with BioRender.com. Abbreviations: Ctr= AdiCD40$^{-/-}$ (Cre WT), AT-II=Angiotensin-II, ACh=Acetylcholine, NTG=nitroglycerine.

Oxidative stress in cryosections of different tissues was analyzed via DHE stainings. The overall ROS production in PVAT was significantly increased in the Ctr+AT-II group (Ø 164 %) compared to the control group (Ø 100 %). No significant differences between the untreated tissue-specific CD40$^{-/-}$ mice (Ø 129 %) or AT-II-treated mice (Ø 125 %) were observed. Indeed, comparing the two AdiCD40$^{-/-}$ groups, no significant increase by AT-II treatment was observed (Figure 35 A). In cardiac tissue, the ROS production was significantly increased in Ctr+AT-II mice (Ø 167 %) compared to the control groups (Ø 100 % Ctr and Ø 90 % AdiCD40$^{-/-}$). Interestingly, the ROS production in the adipocyte-specific CD40$^{-/-}$ mice (Ø 118 % AdiCD40$^{-/-}$ +AT-II) was, by trend, reduced compared to the Ctr+AT-II group (Figure 35 B). Representative pictures of cardiac tissue are shown below the bar graphs (Figure 35). In addition, whole-blood oxidative burst measurements were performed to analyze the mostly leukocyte-dependent H_2O_2 formation. The oxidative burst was not significant, but by trend increased in Ctr+AT-II mice compared to the other groups. The adipocyte-specific CD40 knockout seems beneficial and reduces oxidative stress (Figure 35 C). These results must be interpreted cautiously as the n number is relatively low, and mostly no significant differences between the groups were observed.

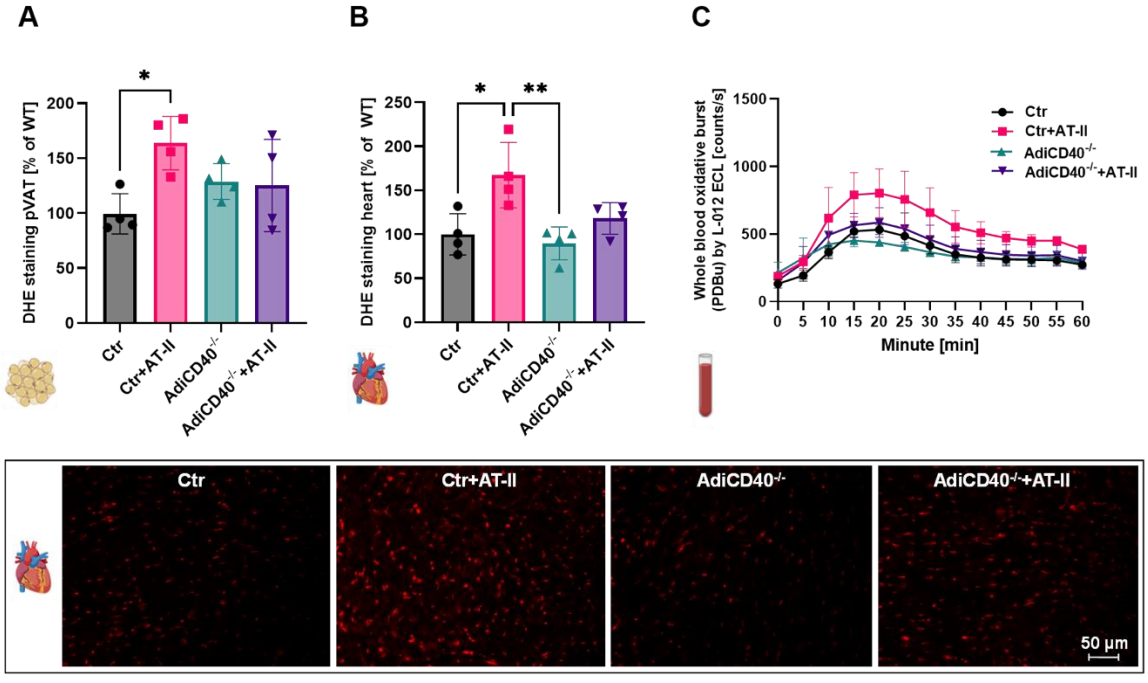

Figure 35: Oxidative stress seems to be reduced in different tissues of angiotensin-II (AT-II) treated adipocyte-specific CD40 knockout mice. Adipocyte-specific CD40$^{-/-}$ mice (AdiCD40$^{-/-}$) and respective control mice (Ctr) were treated for seven days with AT-II (1mg/kg/d) via osmotic minipumps. Cryosections and DHE stainings of PVAT (A) and cardiac tissue (B) were performed to analyze the overall ROS production. (C) In addition, an oxidative burst of whole blood samples was performed to determine the mostly leukocyte-dependent H_2O_2 production. Data are presented as mean values ±SD of n=4 (A+B) and n=2-4 (C) animals per group. *p≤0.05, **p≤0.01, ***p≤0.001, and ****p≤0.0001. Icons were created with BioRender.com. Abbreviations: Ctr=AdiCD40$^{-/-}$ (Cre WT), AT-II=Angiotensin-II, DHE=dihydroethidium, PVAT=perivascular adipose tissue, PDBu=phorbol 12,13-dibutyrate, ECL=electrochemiluminescence.

5.3. The role of CD40-TRAF6 inhibition in a hypertensive mouse model

5.3.1. TRAF6 inhibition improves endothelial function and reduces systolic blood pressure in hypertensive mice

Downstream of CD40, different TRAFs are meditating simultaneously, beneficial and harmful signaling. Especially CD40-TRAF6 signaling was identified to be involved in pathological signaling. Selective pharmacological inhibition of CD40-TRAF6 interaction potentially provides a more targeted treatment strategy than CD40L or CD40 inhibition. This inhibitor (compound 6877002, Tocris, Wiesbaden) was tested in a hypertensive mouse model. Arterial hypertension in WT mice (C57BL/6J) was induced through AT-II treatment (1 mg/kg/d) applied for seven days via osmotic minipumps. In addition, in the hypertensive mice, TRAF6 inhibitor (2.5 mg/kg/d) was applied via a second osmotic pump for seven days. In this intervention group, double pump implantation was necessary due to the different solubilities of the substances. Untreated WT animals, only AT-II, and only TRAF6i-treated animals served as experimental control groups. The systolic blood pressure of the mice was measured on day five of the treatment via noninvasive tail-cuff measurement. AT-II-treated animals (WT+AT-II Ø 151 mmHg) showed a significantly increased systolic blood pressure compared to the untreated WT mice (WT Ø 122 mmHg). Interestingly, the TRAF6 inhibitor treatment in hypertensive animals (WT+AT-II+TRAF6i Ø 132 mmHg) significantly reduces the systolic blood pressure compared to the hypertensive group. Whereas only TRAF6 inhibitor-treated mice also showed a slight increase in systolic blood pressure (WT+TRAF6i Ø 134 mmHg), and the difference to the WT+AT-II group was only reflected in a trend ($p=0.0819$) but not significantly (Figure 36 A). Isometric tension recordings were performed to analyze the endothelial and smooth muscle cell function of the aortic segments. The endothelial function of WT+AT-II mice with a maximal relaxation potential of Ø 57 % was significantly impaired compared to the control group with Ø 83 %. Comparing the maximal relaxation potential of WT+TRAF6i (Ø 69 %) and WT+AT-II+TRAF6i (Ø 64 %) mice with WT+AT-II mice, these two groups displayed an improved endothelial function. Nevertheless, WT+TRAF6i and WT+AT-II+TRAF6i showed, compared to the control animals, still an impaired endothelial function (Figure 36 B). All groups showed, on average, an impaired smooth muscle cell function compared to the control animals. However, as follows, no significant differences were observed at the maximal relaxation potential after nitroglycerine treatment: WT Ø 87 %, WT+TRAF6i Ø 84 %, WT+AT-II Ø 82 %, and WT+AT-II+TRAF6i Ø 81 % (Figure 36 C).

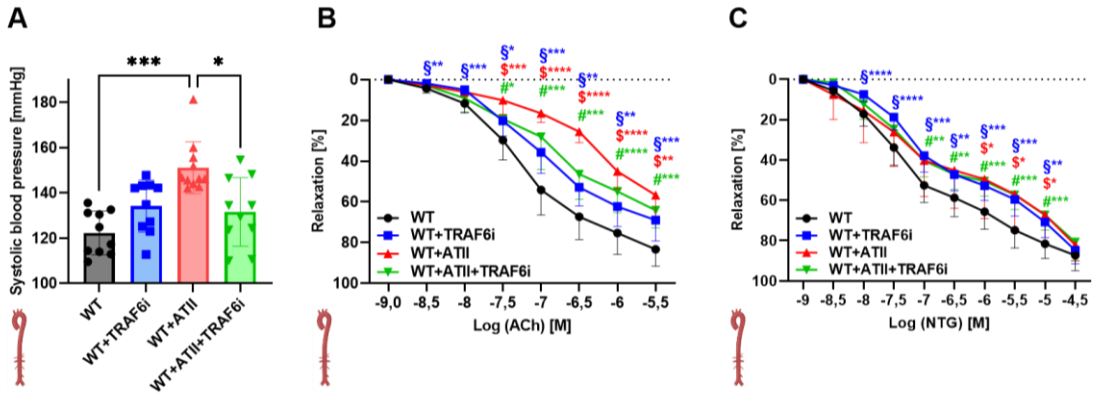

Figure 36: CD40-TRAF6 inhibition leads to phenotypic improvement in hypertensive mice. WT animals (C57BL6/J) were either treated with TRAF6i (2.5 mg/kg/d), AT-II (1 mg/kg/d), or AT-II and TRAF6i via osmotic minipumps for seven days. (A) The systolic blood pressure of the mice was measured by the noninvasive tail-cuff method. (B+C) Endothelial function in response to acetylcholine and smooth muscle cell function in response to nitroglycerine were measured via isometric tension studies. Data are presented as mean values ±SD of n=10-11 (A) and n=6-16 (B+C) animals per group. *p≤0.05, **p≤0.01, ***p≤0.001, and ****p≤0.0001. One-way ANOVA with Tukey´s multiple comparison test (A) and a two-way ANOVA with Dunnett´s multiple comparison test (B+C) were performed. Icons were created with BioRender.com. Abbreviations: WT=C57BL6/J mice, TRAF6i=TRAF6 inhibitor, AT-II=angiotensin-II, ACh=Acetylcholine, NTG=nitroglycerine.

5.3.2. TRAF6 inhibition diminishes oxidative stress in hypertensive mice

The ROS species $O_2^{-\bullet}$ and H_2O_2 genesis were analyzed in cryosections of aortic, PVAT, cardiac, and renal tissue via DHE staining. AT-II treated mice showed a significant increase in ROS development in aortic, cardiac, and renal tissue compared to the other groups. Indeed, compared to WT mice (Ø 100 %), the ROS signal was increased by Ø 48 % in the aorta, by Ø 46 % in PVAT, by Ø 75 % in the heart, and by Ø 51 % in the kidney. No significant differences were observed from the control group to WT+TRAF6i mice (aorta Ø 105 %, PVAT Ø 120 %, heart Ø 76%, and kidney Ø 96 %) and WT+AT-II+TRAF6i (aorta Ø 97 %, PVAT Ø 104 %, heart Ø 77 %, and kidney Ø 99 %). This indicates that ROS production was significantly reduced in this tissue after TRAF6 inhibitor treatment in hypertensive mice (Figure 37 A, C, D). This is also reflected in the representative pictures of stained aortic cryosections below the bar graphs in Figure 37. In PVAT, no significant differences could be determined within the groups, but by trend, the oxidative stress is also reduced in this tissue by TRAF6 inhibitor treatment in hypertensive mice, although the overall pattern/trend was similar compared to the other tissues (Figure 37 B).

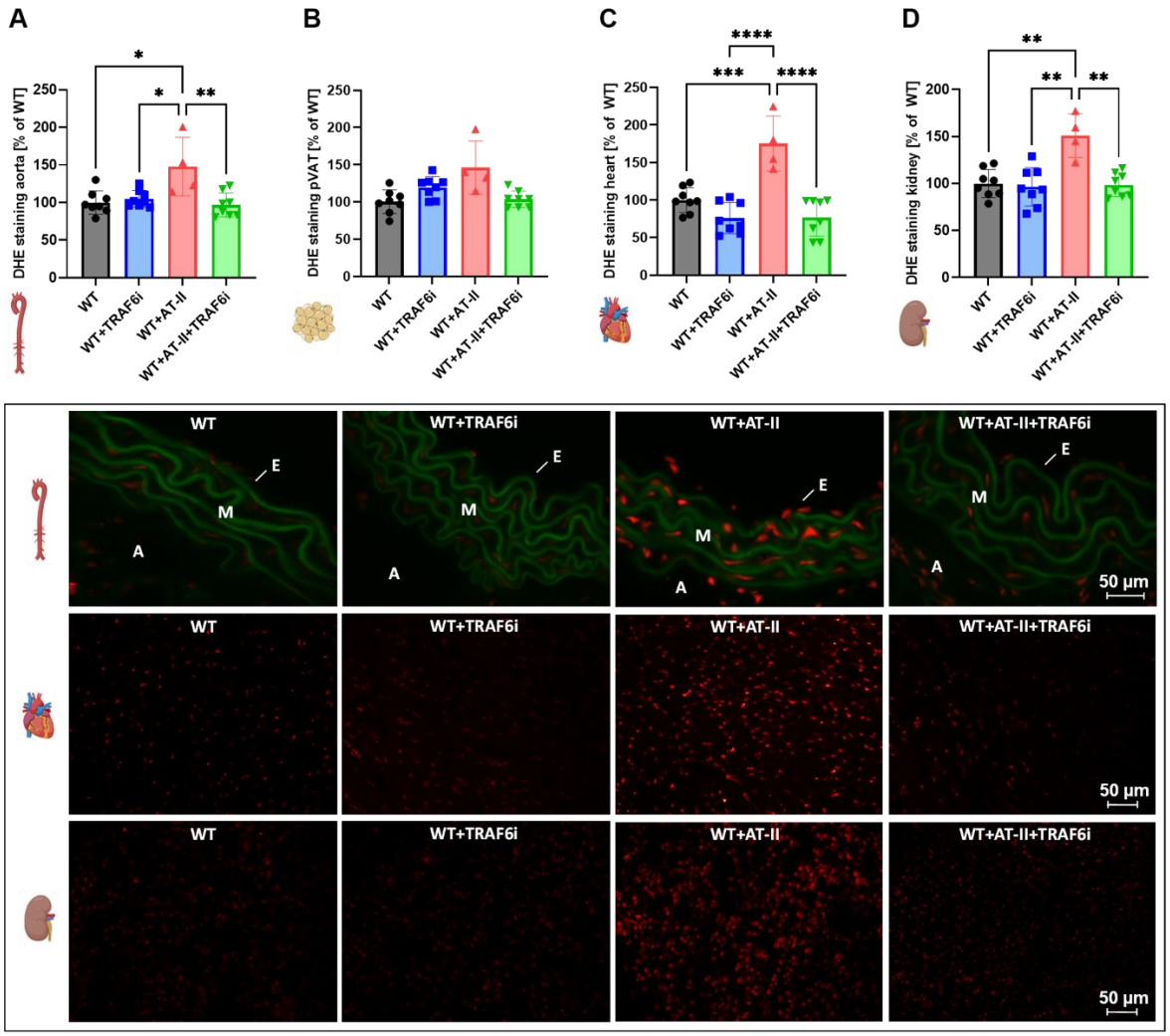

Figure 37: TRAF6 inhibition leads to reduced $O_2^{-\bullet}$ and H_2O_2 formation in different tissues of hypertensive mice. WT animals (C57BL6/J) were either treated with TRAF6i (2.5 mg/kg/d), AT-II (1 mg/kg/d), or AT-II and TRAF6i via osmotic minipumps for seven days. The overall ROS production was analyzed in cryosections via DHE staining in different tissues: aorta (A), PVAT (B), heart (C), and kidney (D). Representative pictures of aortic stainings are shown below the bar graphs. The green color reflects the autofluorescence of aortic laminae, whereas the red color reflects the fluorescence from ROS. Data are presented as mean values ±SD of n=4-8 (A-D) animals per group. *p≤0.05, **p≤0.01, ***p≤0.001, and ****p≤0.0001. One-way ANOVA with Tukey´s multiple comparison test was performed. Icons were created with BioRender.com. Abbreviations: WT=C57BL6/J mice, TRAF6i=TRAF6 inhibitor, AT-II=angiotensin-II, DHE=dihydroethidium, PVAT=perivascular adipose tissue, E=endothelium, M=media, A=adventitia.

In addition to the DHE staining, whole blood oxidative burst measurements were conducted to analyze the leukocyte-dependent H_2O_2 production mainly mediated by NOX2. The samples were stimulated either with PDBu (Figure 38 A) or zymosan A (Figure 38 B), which is detected by chemiluminescence resulting from L-012 oxidation. After 10 min incubation with PDBu, no significant differences were observed between the groups (WT Ø 357 counts/s, WT+TRAF6i Ø 346 counts/s, WT+AT-II Ø 595 counts/s, and Ø 344 counts/s). Meanwhile, the oxidative burst slightly increased by a trend in WT+AT-II mice compared to the other groups (Figure 38 A). The oxidative burst after 55 min of zymosan A stimulation was significantly increased in hypertensive mice (Ø 1602 counts/s) compared to control animals (Ø 657 counts/s). Compared

to WT+TRAF6i mice (Ø 986 counts/s) and WT+AT-II+TRAF6i mice (Ø 1166 counts/s), the hypertensive mouse group showed by trend an increased oxidative burst (Figure 38 B). Lastly, aortic rings were incubated with the chemiluminescent $O_2^{-\bullet}$ sensitive probe lucigenin. Significantly increased counts/min/mg were observed in WT+AT-II animals (Ø 5356 counts/min/mg) compared to WT mice (Ø 3182 counts/min/mg) and WT+AT-II+TRAF6i mice (Ø 3165 counts/min/mg). The $O_2^{-\bullet}$ production in WT+TRAF6i (Ø 4249 counts/min/mg) animals increased slightly by trend compared to the control group (Figure 38 C).

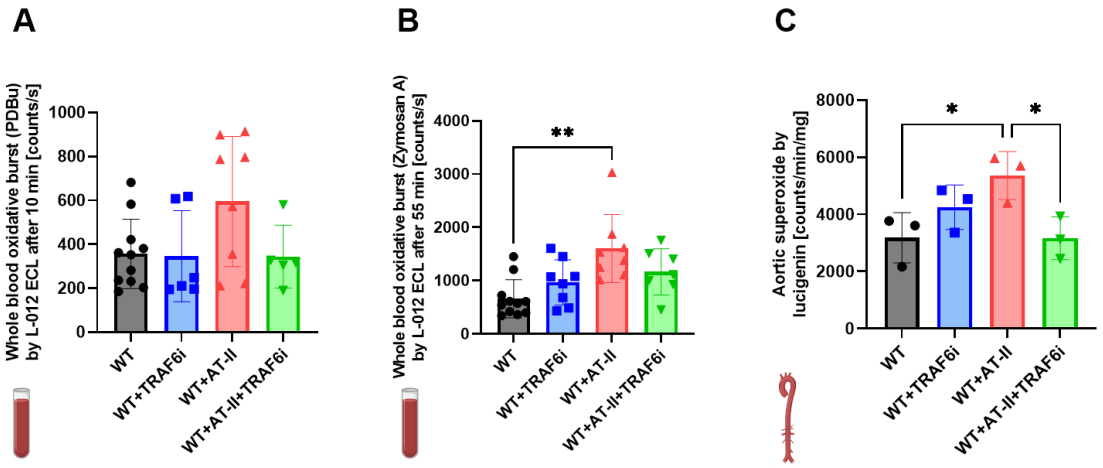

Figure 38: TRAF6 inhibition reduced ROS production in hypertensive mice whole blood and aortic tissue. WT animals (C57BL6/J) were either treated with TRAF6i (2.5 mg/kg/d), AT-II (1 mg/kg/d), or AT-II and TRAF6i via osmotic minipumps for seven days. The chemiluminescence of L-012 oxidation was utilized to analyze the mainly leukocyte-dependent H_2O_2 production in whole blood samples. Previously, the blood was stimulated with PDBu for 10 min (A) or with zymosan A for 55 min (B). (C) Aortic $O_2^{-\bullet}$ production was analyzed by using the chemiluminescent probe lucigenin. Data are presented as mean values ±SD of n=5-11 (A+B) and n=3 (C) animals per group. *p≤0.05 and **p≤0.01. One-way ANOVA with Tukey´s multiple comparison test was performed. Icons were created with BioRender.com. Abbreviations: ROS=reactive oxygen species, WT=C57BL6/J mice, TRAF6i=TRAF6 inhibitor, AT-II=angiotensin-II, PDBu=phorbol 12,13-dibutyrate, ECL=electrochemiluminescence.

Different methods were taken together to analyze the overall ROS production in the organs of hypertensive animals. Interestingly, TRAF6 inhibition leads in hypertensive aortic, cardiac, and renal tissue to a significantly reduced $O_2^{-\bullet}$ as well as ROS generation, which indicates that TRAF6 inhibition can reduce oxidative stress in these mice.

5.3.3. TRAF6 inhibition minimizes vascular immune cell infiltration in hypertensive mice

Vascular immune cell content and infiltration were determined via flow cytometric measurements to assess the impact of TRAF6 inhibition on vascular inflammation in hypertensive mice. The vascular inflammation of AT-II-treated animals was reflected through high leukocyte (CD45+), myeloid (CD11b+), neutrophil (Ly6G+/Ly6c+), and inflammatory monocyte (Ly6C high) cell count. TRAF6 inhibition reduces the leukocyte count by trend

(p=0.0504) in hypertensive mice compared to the WT+AT-II group (WT Ø 3425 cells/cm vs. WT+TRAF6i Ø 3269 cells/cm vs. WT+AT-II Ø 13491 cells/cm vs. WT+AT-II+TRAF6i Ø 5940 cells/cm, Figure 39 A). A similar trend (p=0.0534 and p=0.0836) is observed for myeloid cells (WT Ø 2688 cells/cm vs. WT+TRAF6i Ø 2886 cells/cm vs. WT+AT-II Ø 12352 cells/cm vs. WT+AT-II+TRAF6i Ø 5391 cells/cm, Figure 39 B) and inflammatory monocytes (WT Ø 67 cells/cm vs. WT+TRAF6i Ø 58 cells/cm vs. WT+AT-II Ø 1099 cells/cm vs. WT+AT-II+TRAF6i Ø 163 cells/cm, Figure 39 C). In addition, neutrophil occurrence was significantly decreased in the WT+AT-II+TRAF6i group compared to WT+AT-II mice (WT Ø 3 cells/cm vs. WT+TRAF6i Ø 4 cells/cm vs. WT+AT-II Ø 73 cells/cm vs. WT+AT-II+TRAF6i Ø 4 cells/cm, Figure 39 D). Representative flow cytometry plots are shown below the bar graphs, and the area of interest is marked with a red box. These results indicate that TRAF6 inhibition has vasoprotective properties and reduces vascular immune cell infiltration in hypertensive mice.

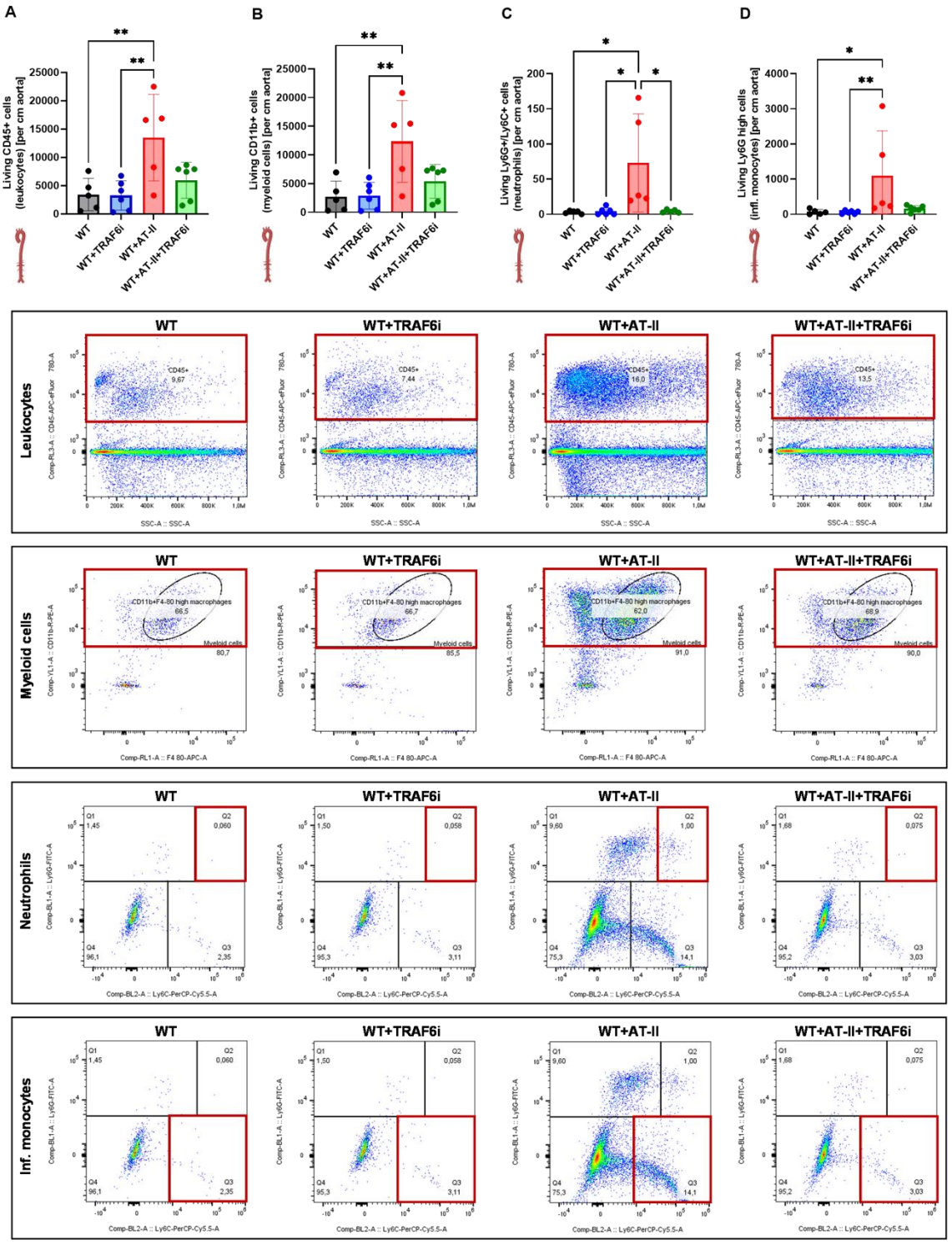

Figure 39: TRAF6 inhibition reduces vascular immune cell infiltration in hypertensive animals. WT animals (C57BL6/J) were either treated with TRAF6i (2.5 mg/kg/d), AT-II (1 mg/kg/d), or AT-II and TRAF6i via osmotic minipumps for seven days. Flow cytometric analysis with different fluorophore-tagged antibodies was performed to analyze the immune cell content in aortic tissue lysates. To distinguish between different immune cell subtypes, the following antibodies were used: (A) anti-CD45 (leukocytes), (B) anti-CD11b (myeloid cells), (C+D) anti-Ly6G and anti-Ly6C (inflammatory monocytes and neutrophils). Representative counter blots are shown below the bar graphs, and the interested area is marked with a red box. Data are presented as mean values ±SD of n=5-6 (A-D) animals per group. *p≤0.05 and **p≤0.01. One-way ANOVA with Tukey´s multiple comparison test was performed. Icons are created with BioRender.com. Abbreviations: WT=C57BL6/J mice, TRAF6i=TRAF6 inhibitor, AT-II=angiotensin-II.

5.3.4. TRAF6 inhibition does not reduce left ventricular hypertrophy in hypertensive mice

The consequences of arterial hypertension in the cardiovascular system are further analyzed by left ventricular function measurements using transthoracic small animal echocardiography. The left ventricular ejection fraction (LV-EF) indicates how effectively a heart pumps into the systemic circulation. The LV-EF was significantly increased in WT+AT-II mice (Ø 69 %) compared to WT and WT+TRAF6i animals (Ø 60 % and Ø 57 %). WT+AT-II+TRAF6 mice showed a EF of Ø 61 %, which did not significantly differ from the other treatment groups, although showing a minor trend of reduced ejection fraction (Figure 40 A). LV mass is a parameter reflecting the weight of the LV. Interestingly, LV mass is not significantly but slightly increased in WT+AT-II (Ø 111 mg) and WT+AT-II+TRAF6i (Ø 117 mg) animals compared to WT (Ø 97 mg) and WT+TRAF6i (Ø 97 mg) mice (Figure 40 B). The LV posterior wall (LVPW) is significantly thicker in the AT-II-treated animals than in the control groups, and TRAF6 inhibitor treatment did not improve the wall thickening in hypertensive mice (WT Ø 1.128 mm, WT+TRAF6i Ø 1.076 mm, WT+AT-II Ø 1.452 mm, and WT+AT-II+TRAF6i Ø 1.491 mm) (Figure 40 C).

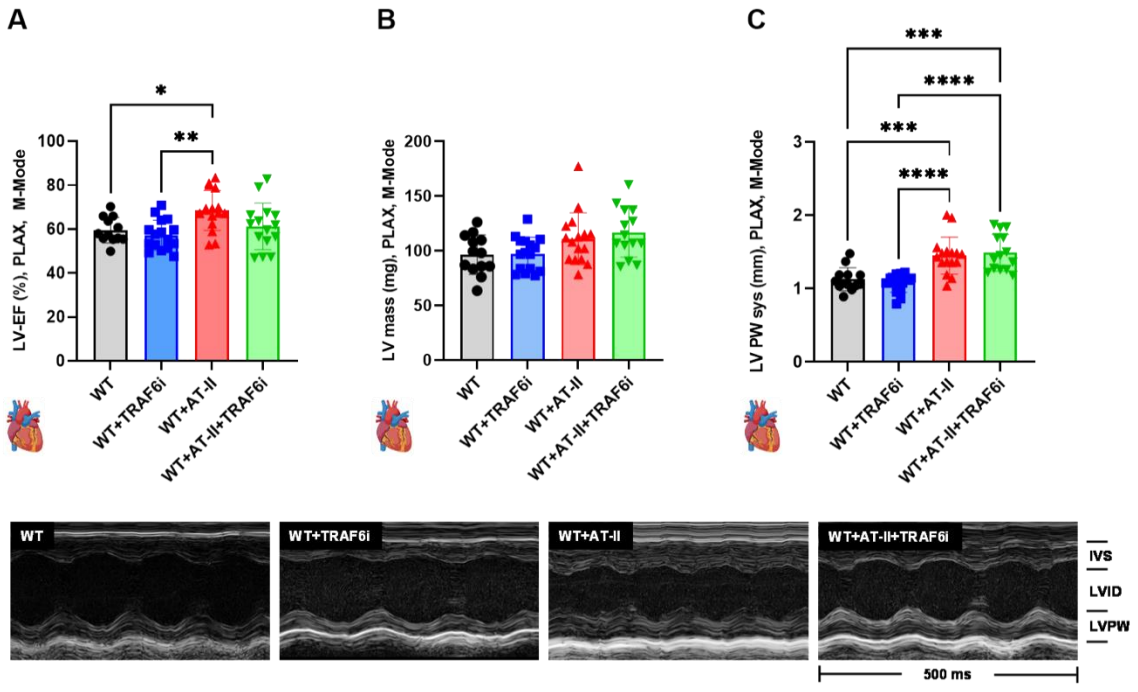

Figure 40: TRAF6 inhibition does not improve left ventricular function in hypertensive mice. WT animals (C57BL6/J) were either treated with TRAF6i (2.5 mg/kg/d), AT-II (1 mg/kg/d), or AT-II and TRAF6i via osmotic minipumps for seven days. Transthoracic echocardiography for small animals was utilized to determine left ventricular (LV) function. The following parameters were calculated with the Vevo Lab 3100 software: (A) LV-EF, (B) LV mass, and (C) LV PW (systolic). Representative M-Mode pictures are shown below the bar graphs. Data are presented as mean values ±SD of n=12-16 (A-C) animals per group. *p≤0.05, **p≤0.01, ***p≤0.001, and ****p≤0.0001. One-way ANOVA with Tukey´s multiple comparison test was performed. Icons are created with BioRender.com. Abbreviations: WT=C57BL6/J mice, TRAF6i=TRAF6 inhibitor, AT-II=angiotensin-II, LV=left ventricle, EF=ejection fraction, PLAX=parasternal long axis view, M-mode=motion mode, PW=posterior wall,

sys=systole, IVS=intraventricular septum, LVID=left ventricular internal diameter, LVPW=left ventricular posterior wall.

The echocardiography results are further supported by measuring body weight, heart weight, and the ratio of heart to body weight. The body weight of the mice does not differ significantly between the groups (WT Ø 26.13 g vs. WT+TRAF6i Ø 27.18 g vs. WT+AT-II Ø 26.04 g vs. WT+AT-II+TRAF6i Ø 27.47 g, Figure 41 A). In contrast, the hearts of AT-II treated mice independent of TRAF6 inhibitor treatment gained significantly more weight than the control group (WT Ø 111 mg vs. WT+TRAF6i Ø 117 mg vs. WT+AT-II Ø 129 mg vs. WT+AT-II+TRAF6i Ø 132 mg, Figure 41 B). Consequently, the heart-to-body weight ratio in WT+AT-II and WT+AT-II+TRAF6i mice is significantly increased compared to WT and WT+TRAF6 animals, and the TRAF6 inhibition does not improve cardiac hypertrophy (Figure 41 C).

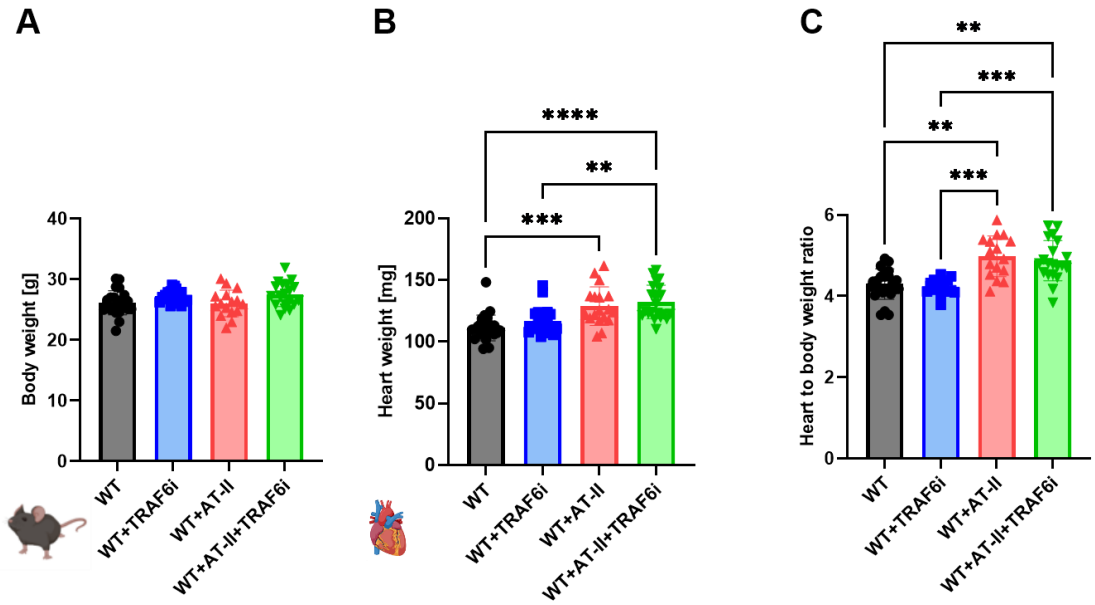

Figure 41: Cardiac hypertrophy is not improved by TRAF6 inhibitor treatment in hypertensive mice. WT animals (C57BL6/J) were either treated with TRAF6i (2.5 mg/kg/d), AT-II (1 mg/kg/d), or AT-II and TRAF6i via osmotic minipumps for seven days. At the end of the treatment, the body (A) and heart weight (B) of the mice were measured to calculate a heart-to-body weight ratio (C). Data are presented as mean values ±SD of n=15-26 (A-C) animals per group. *p≤0.05, **p≤0.01, ***p≤0.001, and ****p≤0.0001. One-way ANOVA with Tukey´s multiple comparison test was performed. Icons are created with BioRender.com. Abbreviations: WT=C57BL6/J mice, TRAF6i=TRAF6 inhibitor, AT-II=angiotensin-II.

5.4. TRAF6 inhibition in diabetic mice

5.4.1. TRAF6 inhibition reduces protein expression of different inflammatory, oxidative stress, and apoptotic markers in diabetic mice

Db/db mice were used as a model for type 2 diabetes and obesity. They were treated for 14 days with 2.5 mg/kg/d TRAF6 inhibitor via osmotic minipumps. TRAF6 inhibition in diabetic mice has already been shown to attenuate the inflammatory phenotype (217). In addition to

this study, the following focus is on changes in protein expression levels in cardiac and renal tissue by Western or Dot blot. Cardiac protein expression of different inflammatory, apoptotic, and oxidative stress markers was significantly increased in db/db mice compared to the control mice. After TRAF6 inhibition, the cardiac protein expression of NOX2, eNOS, $p47^{phox}$, CD40L, and RAGE significantly decreased (Figure 42 A-D, G). The protein expression of the inflammatory and apoptotic markers like thrombospondin-1 (Tsp1), proteinase-activated receptor 1 (Par1), VCAM-1, and caspase3 was not significantly decreased in TRAF6 inhibitor-treated db/db mice compared to untreated db/db mice (Figure 42 E, F, H, I). For VCAM-1 expression, a reduced protein expression by trend ($p=0.0612$) was observed in TRAF6 inhibitor-treated db/db mice (Figure 42 H). TRAF6 inhibitor treatment in control animals did not significantly affect the protein expression of the utilized markers.

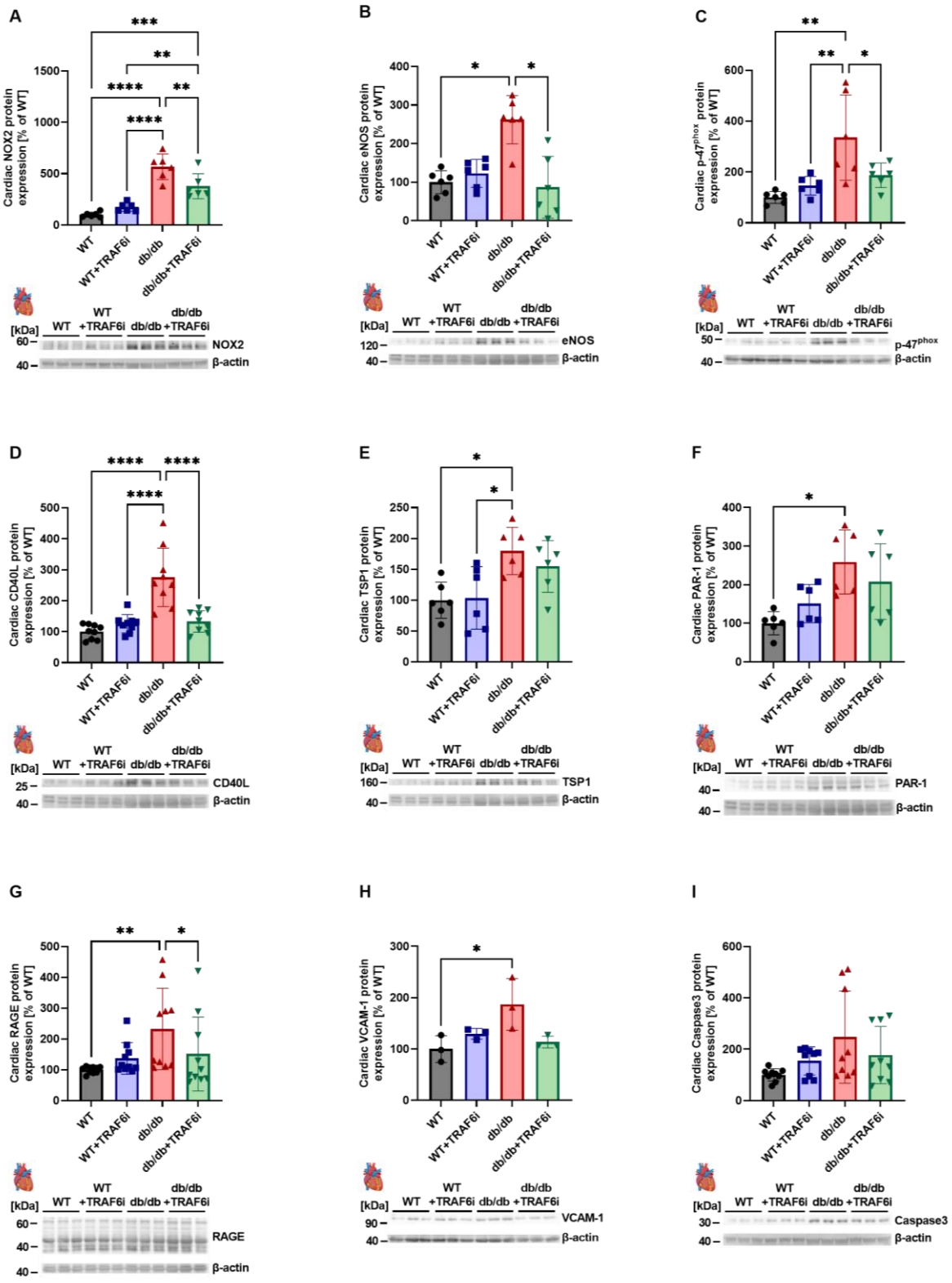

Figure 42: In hearts of diabetic (db/db) mice, TRAF6 inhibition causes decreased protein expression of different inflammatory, apoptotic, and oxidative stress markers. WT and db/db mice were treated for 14 days with a TRAF6 inhibitor (2.5 mg/kg/d) via osmotic minipumps. Then, cardiac tissue was immunoblotted. The following markers for inflammation, apoptosis, and oxidative stress were used for the protein expression analyses: NOX2 (A), eNOS (B), p47^{phox} (C), CD40L (D), TSP1 (E), PAR-1 (F), RAGE (G), VCAM-1 (H), and caspase3 (I). The original representative blots are shown below the densiometric quantification. Data are mean ±SD of n=6 (A, B, C), n=9 (D), n=6 (E, F), n=10 (G), n=3 (H), and n=9 (I) animals per group. * p≤0.05, ** p≤0.01, *** p≤0.001, and **** p≤0.0001. One-way ANOVA with Tukey´s multiple comparison test was performed. Icons are created with BioRender.com.

Data are already published (276). WT=wild type (BKS.CgTemoin mice), TRAF6i=tumor necrosis factor receptor-associated factor 6 inhibitor, TSP1=thrombospondin-1, eNOS=endothelial nitric oxide synthase, $p47^{phox}$ NCF1=neutrophil cytosol factor 1, NOX2=NADPH oxidase 2, PAR-1=protease activated receptor 1, RAGE=receptor for advanced glycation endproducts, VCAM-1=vascular cell adhesion molecule 1.

Further, renal protein expression of eNOS, myristoylated alanine-rich C kinase substrate (pMARCKS), heme oxygenase-1 (HO-1), and endothelin-1 (ET-1) was significantly decreased in TRAF6 inhibitor-treated db/db mice compared to untreated db/db mice (Figure 43 A-D). No significant decrease was observed in the expression of oxidative stress markers like 3NT and 4-hydroxynonenal (4HNE) in the serum and kidney of TRAF6 inhibitor-treated db/db mice (Figure 43 E-G). Representative Western blot pictures are shown below the respective graphs (Figure 43 A-D), whereas all representative Dot blot pictures are shown in Figure 43 H.

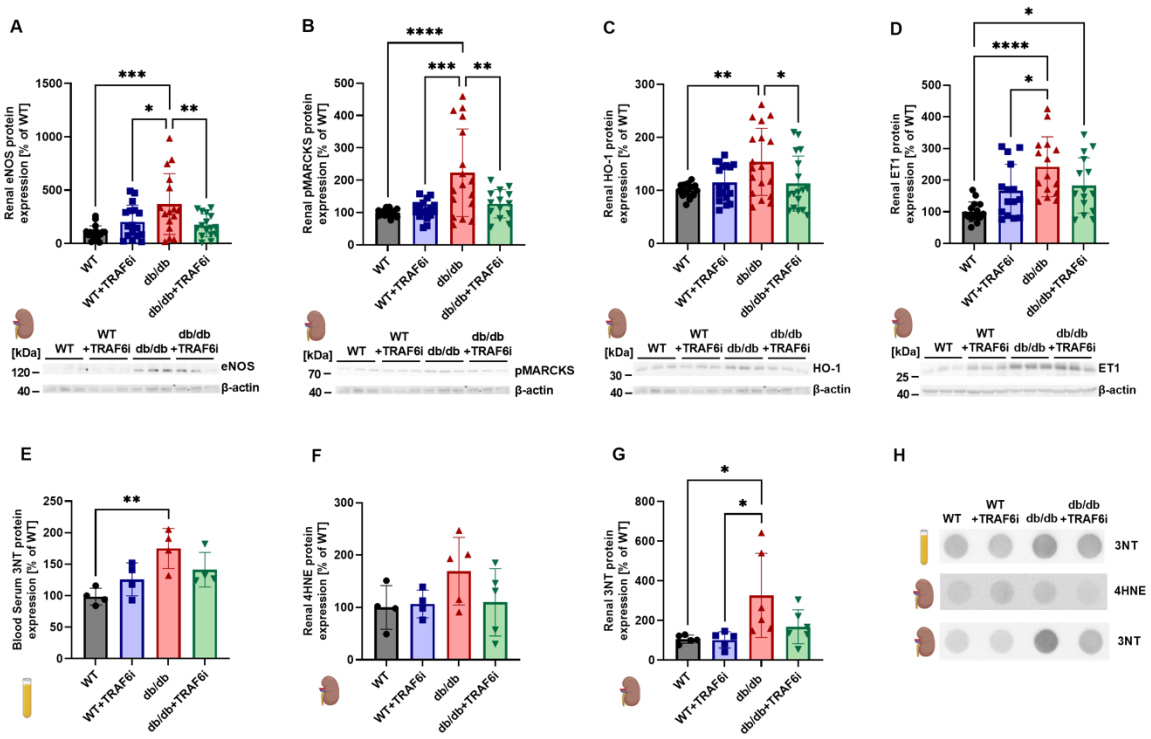

Figure 43: TRAF6 inhibition in db/db mice decreases protein expression of different inflammatory and oxidative stress markers in the kidney and plasma. WT and db/db mice were treated for 14 days with a TRAF6 inhibitor (2.5 mg/kg/d) via osmotic minipumps. Then, renal tissue and plasma were immunoblotted. The following markers for inflammation and oxidative stress were used for the protein expression analyses: eNOS (A), pMARCKS (B), HO-1 (C), ET1 (D), 3NT (E), 4HNE (F), and 3NT (G). The original representative blots are shown below the densiometric quantification and in (H). Data are mean ±SD of n=15-18 (A-D) and n=4-6 (E-G) animals per group. * p≤0.05, ** p≤0.01, *** p≤0.001, and **** p≤0.0001. One-way ANOVA with Tukey´s multiple comparison test was performed. Icons are created with BioRender.com. Data are already published (276). WT=wild type (BKS.CgTemoin mice), TRAF6i=tumor necrosis factor receptor-associated factor 6 inhibitor, eNOS=endothelial nitric oxide synthase, pMARCKS= myristoylated alanine-rich C kinase substrate, HO-1=heme oxygenase-1, ET1=endothelin1, 3NT=3 nitrotyrosine, 4HNE=4-hydroxynonenal.

5.5. The role of inflammatory signaling pathways, including the CD40L-CD40-TRAF signaling cascade in CHD patients suffering from hypertension and diabetes

This study utilized plasma and aortic tissue remaining from bypass surgeries for further analysis. Three different groups of CHD patients were included: (1) CHD patients without comorbidities, (2) CHD patients with hypertension (+HT), and (3) CHD patients with hypertension and type 2 diabetes mellitus (+HT+T2DM) as comorbidity. The patient's characteristics regarding physiological parameters, laboratory parameters, and medication are summarized in Table 18.

Table 18: Patient characteristics. Published in (276).

	CHD n=20	**CHD+HT n=49**	**CHD+HT+T2DM n=25**	*p*-value
General parameters				
Age [y] (SD)	64 (10)	58 (6)	60 (5)	0.001
Sex (male)	70% (14/20)	84% (41/49)	72% (18/25)	0.34
Current Smoker	40% (8/20)	45% (21/47)	38% (9/24)	0.891
Ex-smoker	20% (4/20)	17% (8/47)	29% (7/24)	0.489
Physiological parameters				
Height [cm] (SD)	173 (8)	176 (8)	171 (9)	0.104
BMI [kg/m^2] (SD)	25 (4)	28 (3)	31 (4)	<0.001
SBP [mmHg] (SD)	125 (15)	136 (26)	143 (17)	0.02
DBP [mmHg] (SD)	70 (7)	75 (13)	75 (10)	0.155
Heart rate [bpm] (SD)	73 (13)	68 (11)	74 (11)	0.107
CHD				
Multivessel disease	100% (20/20)	96% (47/49)	100% (25/25)	0.391
LMCA affected	40% (8/20)	31% (15/49)	36% (9/25)	0.735
Comorbidities				
HT	0% (0/20)	100% (49/49)	100% (25/25)	
T2DM	0% (0/20)	0% (0/49)	100% (25/25)	
Laboratory parameters				
Cholesterol [mg/dl]	190 (9/20)	158 (28/49)	173 (15/25)	0.284
Creatinin [mg/dl]	0.91 (20/20)	0.99 (49/49)	1.09 (25/25)	0.038
CRP [mg/dl]	1.32(18/20)	1.4 (38/49)	0.48 (22/25)	0.269
Glucose [mg/dl]	113 (20/20)	111 (49/49)	246 (25/25)	<0.001
HDL [mg/dl]	40 (9/20)	36 (28/49)	36 (15/25)	0.784
LDL cholesterol [mg/dl]	124 (9/20)	95 (28/49)	103 (15/25)	0.247
Triglycerides [mg/dl]	169 (9/20))	143 (28/49)	209 (14/25)	0.082
Medication				
ASS	65% (13/20)	51% (25/49)	76% (19/25)	0.104
ACEi/ARB	50% (10/20)	88% (43/49)	80% (20/25)	0.003
BB	65% (13/20)	84% (41/49)	76% (19/25)	0.234
Nitrates	15% (3/20)	20% (10/49)	28% (7/25)	0.558
CCB	0% (0/20)	14% (7/49)	36% (9/25)	0.005

MRA	20% (4/20)	29% (14/49)	16% (4/25)	0.444
Statin	75% (15/20)	78% (38/49)	84% (21/25)	0.733
Sulfonylureas	0% (0/20)	0% (0/49)	12% (3/25)	0.014
Thiazide/distal loop	10% (2/20)	14% (7/49)	24% (6/25)	0.399
Loop diuretic	15% (3/20)	22% (11/49)	16% (4/25)	0.695
RA Insulin	0% (0/20)	0% (0/49)	60% (15/25)	<0.001
LA Insulin	0% (0/20)	0% (0/49)	48% (12/25)	<0.001
Metformin	0% (0/20)	0% (0/49)	36% (9/25)	<0.001
SGLT2i	0% (0/22)	0% (0/49)	4% (1/25)	0.248
DPP4i	0% (0/20)	0% (0/49)	12% (3/25)	0.014
GLP1i	0% (0/20)	0% (0/49)	8% (2/25)	0.06

* Abbreviations: BMI=body mass index. SBP=systolic blood pressure, DBP=diastolic blood pressure, CHD=coronary heart disease, LMCA=left main coronary artery, HT=arterial hypertension, T2DM=type 2 diabetes, LDL=low density lipoprotein, ASS=acetylsalicylic acid, ACEi=angiotensin converting enzyme inhibitor, ARB=angiotensin receptor blocker, BB=beta blockers, CCB=calcium channel blocker, MRA=mineralocorticoid receptor antagonist, RA Insulin=rapid-acting insulin, LA insulin=long-acting insulin, SGLT2i=sodium-glucose cotransporter-2 inhibitors, DPP4i=dipeptidyl peptidase-4 inhibitors, GLP1=glucagon-like peptide-1 antagonist.

5.5.1. Plasma proteomic analysis of CHD patients with hypertension or hypertension and diabetes as comorbidity showed increased expression of oxidative stress and inflammatory markers

Plasma proteomic analysis was performed to analyze the expression pattern of CD40L-CD40 signaling cascade members and associated pathways in CHD patients suffering from comorbidities like HT or HT+T2DM. The Olink IMMUNO-ONCOLOGY panel was utilized to identify upregulated protein targets. DR6 (TNFRSF21) and CD27 belong to the TNF(R)SF family and are stepwise increased in CHD patients with HT and HT+T2DM compared to CHD patients without comorbidities (Figure 44 A, M). A similar pattern was observed expressing other inflammatory markers like TNFα, IL12, C-C motif chemokine ligand-4 (CCL4), and CCL3 (Figure 44 B, G-I). In addition, some immune cell markers, including CD5, CD83, CD244, killer cell lectin-like receptor D (KLRD1), and inducible T cell co-stimulatory ligand (ICOSLG), were also stepwise increased in patients with HT or HT+T2DM (Figure 44 C-E, J, K), such as galactin1 (Gal1) and angiopoietin 2 receptor (TIE2) (Figure 44 F, L). In total, 13/92 markers showed a significant increase in expression associated with the number of comorbidities, which indicates a more severe phenotype in these CHD patient groups.

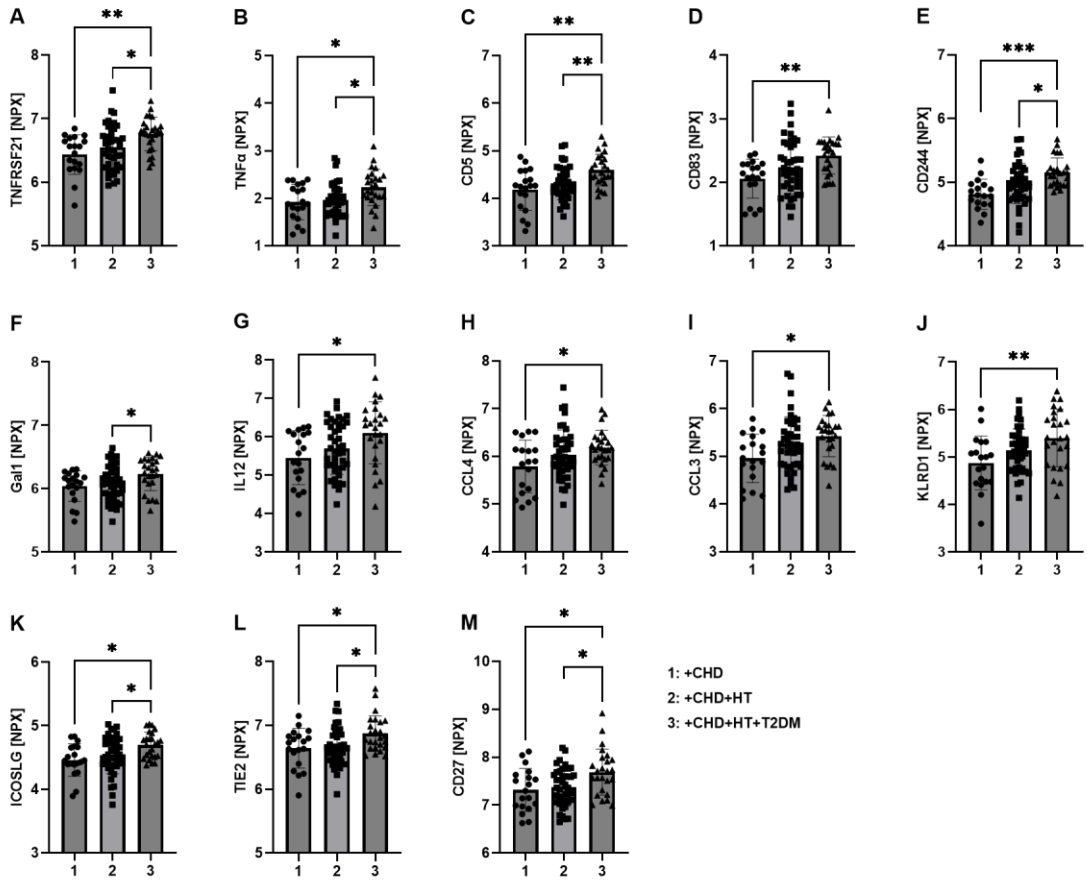

Figure 44: A stepwise increased pattern of selected low-grade inflammatory markers is shown in the plasma of CHD patients with hypertension or hypertension and diabetes as comorbidity. Olink analysis of patient's plasma was performed in three different groups: CHD patients without prior comorbidities (1), CHD patients with hypertension (2), and CHD patients with hypertension and diabetes (3) as comorbidity. The following significantly (or at least by trend) increased markers were identified: TNFRSF21 (A), TNFα (B), CD5 (C), CD83 (D), CD244 (E), Gal1 (F), IL12 (G), CCL4 (H), CCL3 (I), KLRD1 (J), ICOSLG (K), TIE2 (L), and CD27 (M). One-way ANOVA (with Tukey's test) or Kruskal-Wallis test (with Dunn's correction) were performed. Data are mean±SD. CHD n=19, CHD+HT n=42, and CHD+HT+T2DM=25 patients per group. * p≤0.05, ** p≤0.01, and *** p≤0.001. Outliers were identified and removed with the ROUT (Q=1 %) method. Abbreviations: CHD=coronary heart disease, HT=hypertension, T2DM=type 2 diabetes mellitus, TNFRSF=tumor necrosis factor receptor superfamily, TNF=tumor necrosis factor, Gal1=galectin1, CCL=C-C motif chemokine ligand, KLRD=killer cell lectin-like receptor D, ICOSLG=inducible T cell co-stimulatory ligand, TIE2=angiopoietin 1 receptor. Published in (276).

Cluster analyses were performed using Olink data, which revealed that T2DM as a comorbidity causes the most significant changes in CHD patients' plasma. In total, three different clusters were identified (Figure 45 A). The first cluster consists of downregulated proteins by T2DM, the second cluster includes proteins that are induced by HT and T2DM, and the third cluster contains proteins that are upregulated by T2DM. Indeed, the third cluster includes cytokines linked to TNFα, immune cell surface markers, and interleukins. The network analysis showed that T2DM significantly altered the plasma proteome expression in CHD patients (Figure 45 B-D). Four closely connected subnetworks were detected in a comparison of CHD to CHD+HT+T2DM. These subnetworks contain growth factors (e.g., TGFB1, PGF, PDGF), chemokines (e.g., CCL2, CCL3), or cell surface proteins (e.g., TNF receptors, PDCD1, CD5).

The network analysis identified the cytokine/adipokine TNFα as a potential central player in altered protein expression patterns linked to T2DM.

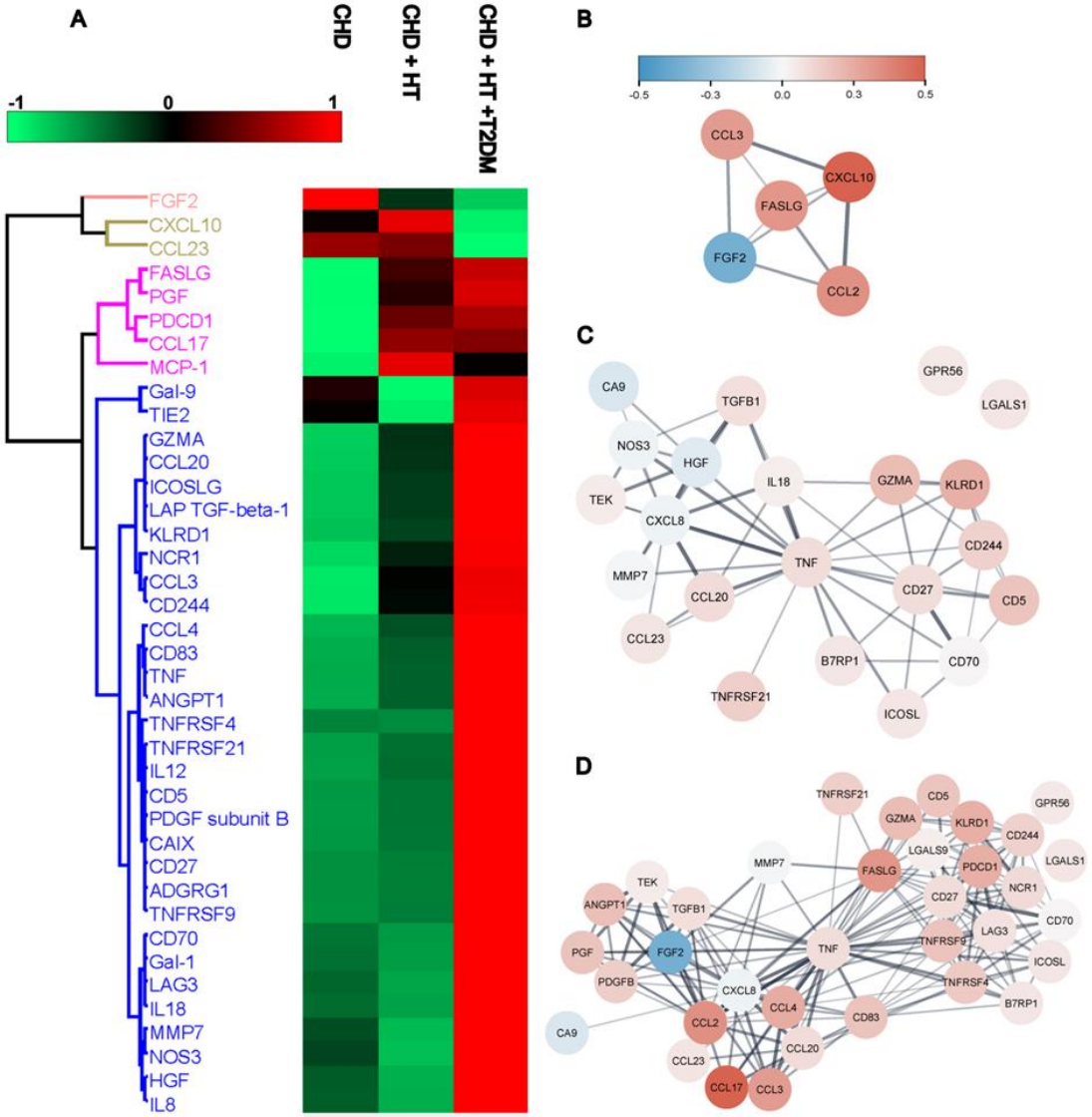

Figure 45: The expression of specific low-grade inflammatory markers increases in the plasma of CHD patients with hypertension or hypertension and diabetes as comorbidities. Olink analysis of patient's plasma was performed in three different groups: CHD patients without prior comorbidities (CHD), CHD patients with hypertension (CHD+HT), and CHD patients with hypertension and diabetes (CHD+HT+T2DM) as comorbidity. The dataset was filtered for differentially expressed proteins; mean values were determined, and Z-normalized (A). Euclidean clustering of median expression is shown in B-D. The protein network of differentially expressed proteins comparing CHD to CHD+HT (B), CHD+HT to CHD+HT+T2DM (C), and CHD to CHD+HT+T2DM (D). Data are mean±SD CHD n=21, CHD+HT n=42, and CHD+HT+T2DM=25 patients per group. Abbreviations: FGF=fibroblast growth factor, CXCL=C-X-X motif chemokine ligand, CCL=C-C motif chemokine ligand, FASLG=Fas ligand, PGF=placental growth factor, PDCD=programmed cell death ligand, MCP=monocyte chemoattractant protein, Gal=galectin, TIE2=angiopoetin receptor-2, GZMA=granzyme A, ICOSLG=inducible T cell co-stimulatory ligand, LAP TGF=latency-associated peptide transforming growth factor, KLRD=killer cell lectin-like receptor D, NCR=natural cytotoxicity triggering receptor, CD=cluster of differentiation, TNF=tumor necrosis factor, ANGPT1=angiopoetin-1, TNFRSF=tumor necrosis factor receptor superfamily, IL=interleukin, PDGF=platelet derived growth factor, CAIX=carbonic anhydrase, ADGRG1=adhesion G-protein-coupled receptor, LAG=lymphocyte activation gene, MMP=matrix metalloproteinase, NOS=nitric oxide synthase, HGF=hepatocyte growth factor. Published in (276).

Additionally, Dot blot analysis with patients' plasma was performed. Oxidative stress was increased in CHD patients suffering from comorbidities, as shown with NOX2 expression, and the stepwise by trend increased (p=0.0787) expression pattern (Figure 46 A). CD40L is utilized as an inflammatory marker protein, but its expression showed only a similar pattern and was not significantly increased by comorbidities in CHD patients (Figure 46 B). The cell adhesion protein CD68 is associated with macrophages and used as an inflammatory marker protein. CD68 expression significantly increases in CHD patients' plasma with T2DM (Figure 46 C). 3-NT expression is associated with cellular or tissue-specific changes in H_2O_2/nitrite levels, and enhanced expression is related to oxidative stress. In patients, plasma 3-NT expression levels significantly increase in CHD+HT+T2DM patients compared to CHD+HT patients (Figure 46 D).

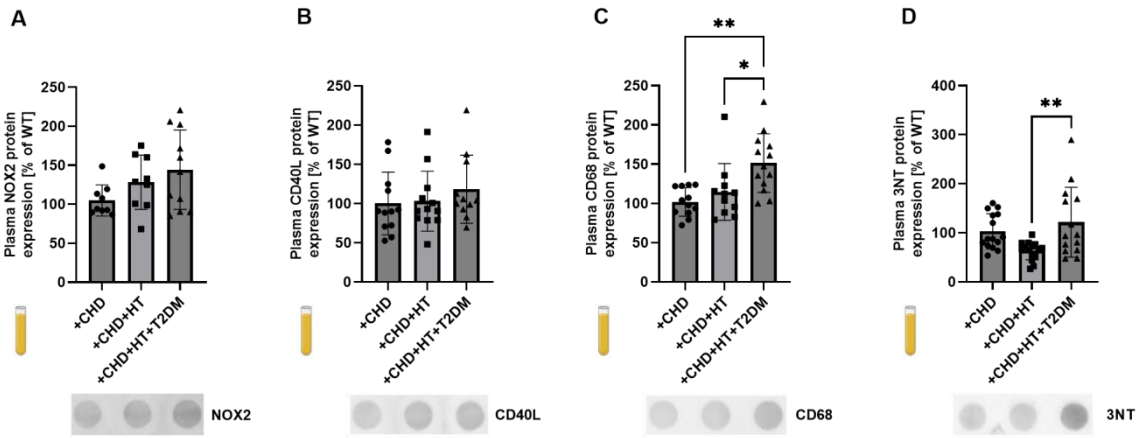

Figure 46: Oxidative stress and inflammatory protein marker expression are increased in the plasma of CHD patients with hypertension and diabetes. Protein expression of NOX2 (A), CD40L (B), CD68 (C), and 3-NT (D) in plasma of CHD patients without comorbidity, hypertension, or hypertension and T2DM were analyzed via dot blot analysis**.** Original representative blots are shown below. Data are mean±SD CHD n=8-15, CHD+HT n=9-15, and CHD+HT+T2DM n=11-14 patients per group. * p≤0.05 and ** p≤0.01. Abbreviations: CHD=coronary heart disease, HT=hypertension, T2DM=type 2 diabetes mellitus, NOX2=NADPH oxidase 2, 3NT=3-nitrotyrosine. Published in (276).

In summary, the CHD patient's plasma proteomic and protein expression analysis revealed that comorbidities like HT and T2DM lead to elevated expression of low-grade inflammatory and oxidative stress protein markers. In addition, the altered protein expression profiles are also linked to the CD40L-CD40 co-stimulatory dyad. Especially in CHD+HT+T2DM patients compared to CHD patients, the expression of many low-grade inflammatory markers was upregulated and closely related to TNFα expression.

5.5.2. mRNA gene expression levels of multiple genes are altered in CHD patients with comorbidities like hypertension or hypertension and diabetes

Aortic tissue remaining from bypass surgeries of CHD patients was utilized for RNA isolation and total mRNA expression analysis. RNA-Seq was performed to examine altered gene expression due to the influence of different comorbidities in CHD patients. The data were analyzed with CLC genomics workbench and illustrated in Volcano blots (Figure 47 A-C). In a comparison of CHD+HT vs. CHD, 2074 different expressed genes (DEG, $p<0.05$) were identified, 1695 DEGs for CHD+HT+T2DM vs. CHD, and 2928 DEGs for CHD+HT+T2DM vs. CHD+HT.

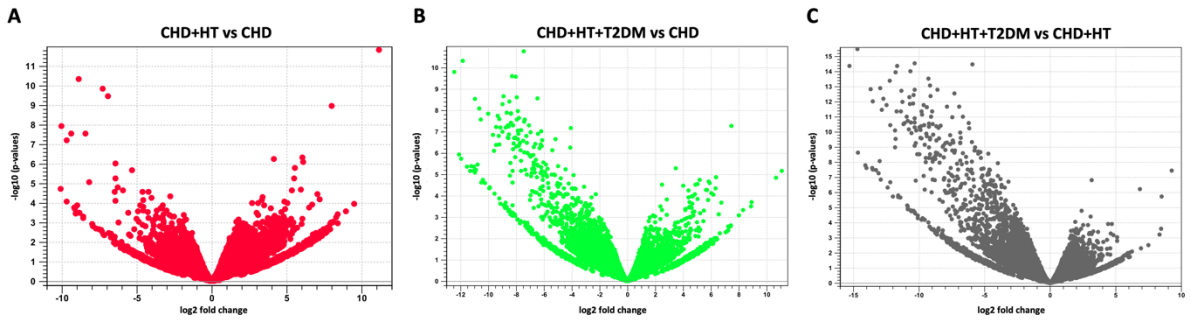

Figure 47: Comparison of gene expression in aortic tissue of CHD patients with hypertension or hypertension and diabetes as comorbidity. RNA was isolated from the aortic tissue of CHD patients, CHD+HT patients, or CHD+HT+T2DM patients. The tissue samples were analyzed regarding the total mRNA expression using the RNA-Seq method. The analysis was performed with the CLC genomics workbench and shown as volcano blots (provided by the CLC workbench). Total mRNA comparison is shown as follows: (A) CHD+HT vs. CHD, (B) CHD+HT+T2DM vs. CHD, and (C) CHD+HT+T2DM vs. CHD+HT. Abbreviations: CHD=coronary heart disease, HT=hypertension, T2DM=type 2 diabetes mellitus. Published in (276).

The identified DEGs are associated with different signaling clusters like CD40L-CD40-TRAF, immune system, hemostasis, muscle contraction, metabolism of lipids, and apoptosis, as published in the supplement data of Strohm et al. (276). Further, the DEGs were utilized to perform pathway analysis via the Ingenuity Pathway Analysis (IPA from Qiagen). An overview of the IPA analysis is shown in Figure 48-50. Comparing CHD+HT versus CHD patients, many pathways are indicated as activated. Interestingly, pathways centered around CD40L and INFγ are predicted to be activated. CD40L and INFγ signaling is closely associated with the onset and the progression of tissue inflammation. Indeed, indirectly, they are involved in cell movement, activation, interaction, binding, and adhesion of leukocytes. CD40L and INFγ are upregulating the response of myeloid cells and phagocytes, which play an important role in atherosclerosis progression. Further, predicted activated pathways bind blood cells, which is important in clot formation. Also, T lymphocytes are indicated to be activated, which is relevant for adaptive immune system responses (Figure 48).

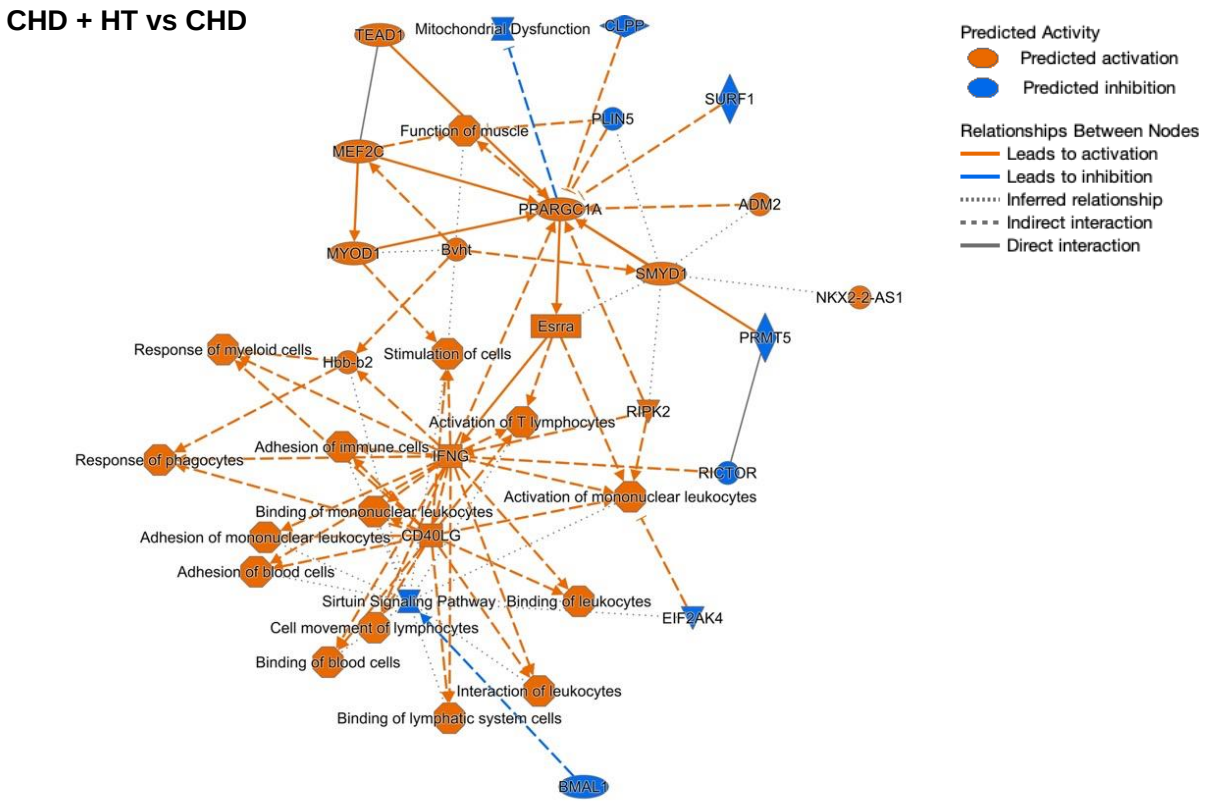

Figure 48: Activated gene expression of pathways centered around CD40L and INFγ has been identified in the aortic tissue of CHD patients with hypertension compared to CHD patients without a comorbidity. Aortic tissue samples of CHD and CHD+HT patients were analyzed for total mRNA expression using the RNA-Seq method. The data were analyzed with the CLC genomics workbench, and the reported DEG ($p<0.05$) list was imported into the ingenuity software and analyzed. The graphical summary of the ingenuity software is shown in this figure. Activated pathways are shown in orange, and inhibited pathways are shown in blue. Abbreviations: CHD=coronary heart disease, HT=hypertension, INFγ=interferon-γ. Published in (276).

When comparing the gene expression profiles of CHD+HT+T2DM patients with those of CHD patients, more pathways are predicted to be downregulated. The comorbidity of T2DM seems to change the regulating pathways and indicates to inhibit the function and contractility of different muscles. Indeed, T2DM alters the calcium signaling in muscle cells (Figure 49).

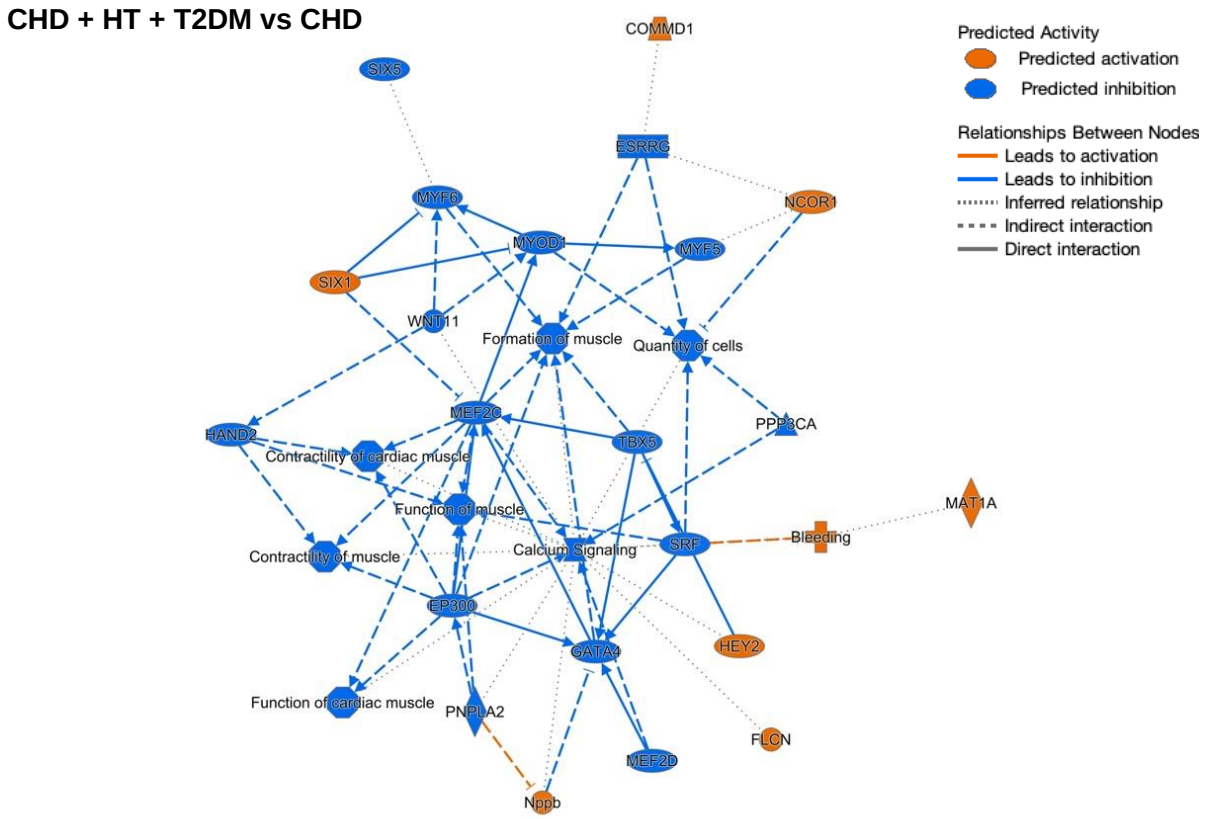

Figure 49: Inhibited gene expression of pathways centered around muscle function and contractility has been identified in the aortic tissue of CHD patients with hypertension and diabetes compared to CHD patients without comorbidity. Aortic tissue samples of CHD and CHD+HT+T2DM patients were analyzed for total mRNA expression using the RNA-Seq method. The data were analyzed with the CLC genomics workbench, and the reported DEG ($p<0.05$) list was imported into the ingenuity software and analyzed. The graphical summary of the ingenuity software is shown in this figure. Activated pathways are shown in orange, and inhibited pathways are shown in blue. Abbreviations: CHD=coronary heart disease, hypertension, T2DM=type 2 diabetes mellitus. Published in (276).

Also, compared to CHD+HT+T2DM versus CHD+HT patients, most pathways are downregulated, especially the function and contractility of muscles, which are predicted to be inhibited. Further, oxygen consumption was inhibited, impacting mitochondrial function and oxidative stress. Lastly, many downregulated pathways in these groups are associated with VEGF-A signaling. This growth factor signaling molecule was predicted to be inhibited and led to negative regulation of angiogenesis and vasodilation in these patients' groups (Figure 50).

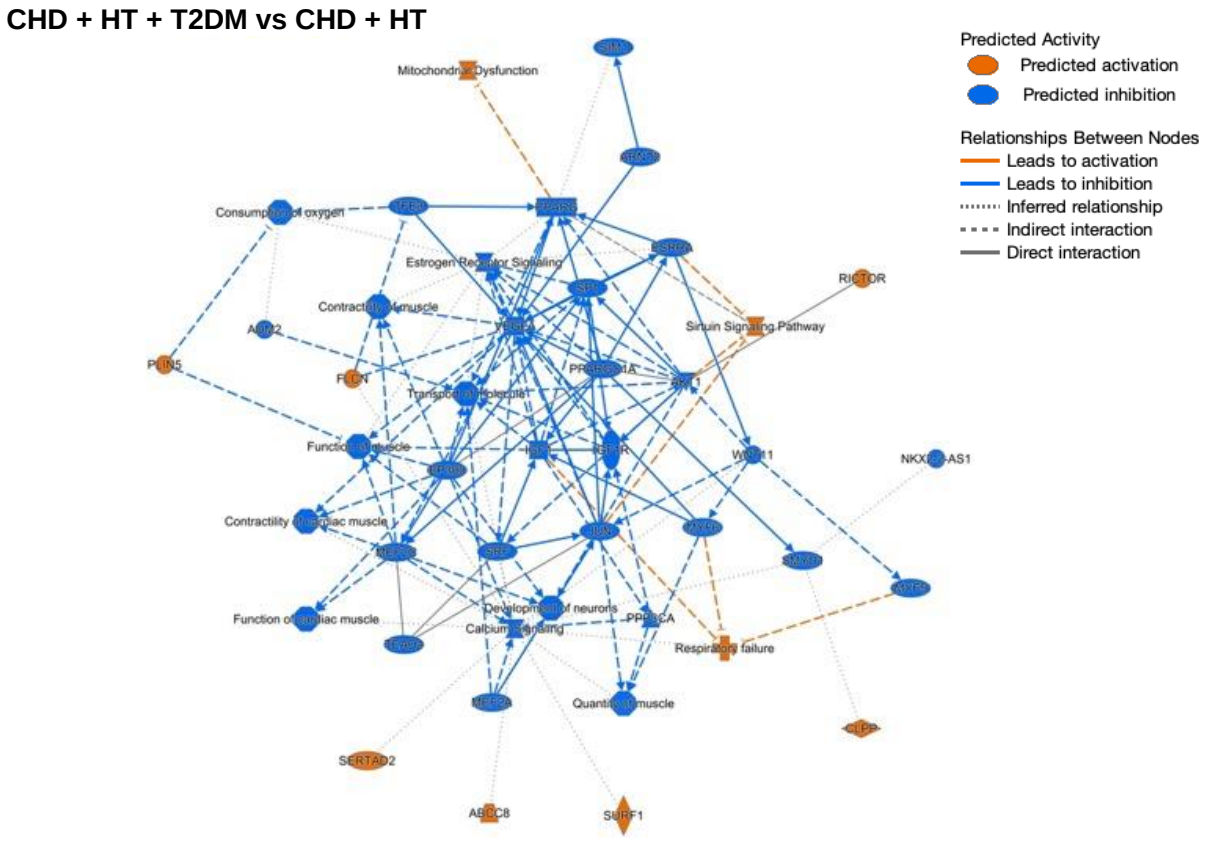

Figure 50: Inhibited gene expression of pathways centered around muscle contractility and vascular endothelial growth factor A signaling molecule has been identified in the aortic tissue of CHD patients with hypertension and diabetes compared to CHD patients with hypertension patients. Aortic tissue samples of CHD+HT and CHD+HT+T2DM patients were analyzed for total mRNA expression using the RNA-Seq method. The data were analyzed with the CLC genomics workbench, and the reported DEG ($p<0.05$) list was imported into the ingenuity software and analyzed. The graphical summary of the ingenuity software is shown in this figure. Activated pathways are shown in orange, and inhibited pathways are shown in blue. Abbreviations: CHD=coronary heart disease, HT=hypertension, T2DM=type 2 diabetes mellitus, VEGF-A=vascular endothelial growth factor A. Published in (276).

The identified DEGs (Figure 47) were also utilized to determine the top 5 canonical pathways. Comparing CHD+HT and CHD patients, the top 5 enhanced regulated pathways are mitochondrial dysfunction, oxidative phosphorylation, sirtuin pathways activation, neutrophil extracellular trap-dependent signaling, and granzyme A activity (Figure 51 A). The upregulation of these pathways is associated with loss of electron chain transport efficacy, metabolic dysfunction, thrombosis, apoptosis, and oxidative stress. Whereas comparing mRNA gene expression of aortic tissue of CHD+HT+T2DM and CHD patients, the top 5 regulated canonical pathways are enhanced agranulocyte diapedesis, reduced calcium pathway activity, reduced dilated cardiomyopathy, enhanced hepatic fibrosis, and reduced effects of sildenafil (Figure 51 B). The dysregulation of these pathways is accompanied by inflammation, immune cell migration, abnormal wound healing, and impaired muscle contractility and function. Lastly, comparing CHD+HT+T2DM with CHD+HT patients, the top 5 regulated pathways are reduced

oxidative phosphorylation, mitochondrial dysfunction, sirtuin signaling, estrogen receptor activity, and calcium pathway activity (Figure 51 C).

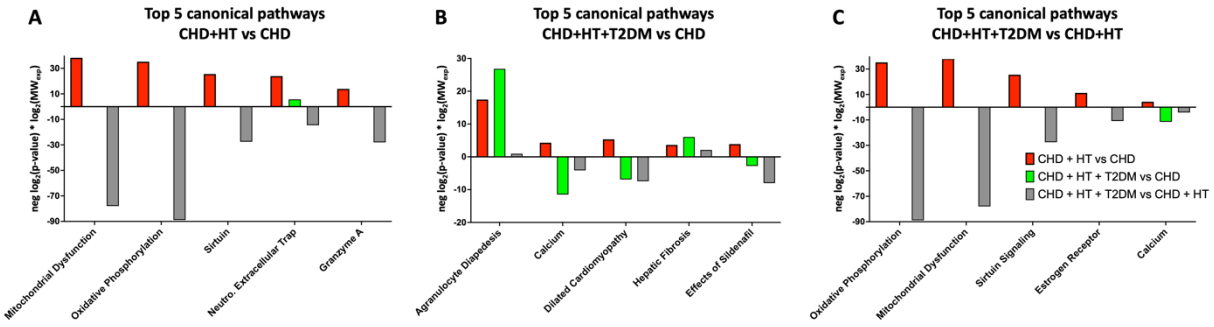

Figure 51: Top 5 regulated signaling pathways identified in aortic tissue of CHD patients with hypertension or hypertension and diabetes as comorbidities. Aortic tissue samples were analyzed for total mRNA expression using the RNA-Seq method. The data were analyzed with the CLC genomics workbench, and the reported DEG ($p<0.05$) lists were imported into the ingenuity software and analyzed for the top 5 regulated canonical signaling pathways. The following patients' groups were compared to each other: (A in red) CHD+HT vs. CHD, (B in green) CHD+HT+T2DM vs. CHD, and (C in grey) CHD+HT+T2DM vs. CHD+HT. The negative $\log_2$ p-values were multiplicated with the $\log_2$ expression values for normalization. Further, in each graph, the values of the other comparisons were also included. Abbreviations: CHD=coronary heart disease, HT=hypertension, T2DM=type 2 diabetes mellitus, VEGF-A=vascular endothelial growth factor A. Published in (276).

The RNA-Seq dataset (Figure 48-50) was further analyzed regarding the top 5 upstream regulators. Compared to the CHD control group, CHD+HT patients showed enhanced activity of the factors TEAD1 (TEA family member 1, transcription factor), PPARGC1A (PPARG coactivator 1 α, transcriptional coactivator), CD40, INSR (insulin receptor), and Hbb-1b (hemoglobin, ß adult major chain) which were identified in the IPA as top 5 upstream regulators (Figure 52 A). Further, by comparing CHD+HT+T2DM patients with CHD patients, the top 5 upstream regulators are enhanced effects of SIX1 (SIX homeobox 1, transcription factor). In contrast, the activities of DMD (human dystrophin gene), MYOD1 (myogenic differentiation, transcription factor), MEF2C (myocyte enhancer factor 2C, transcription factor), and beta-estradiol (sex hormone) were reduced (Figure 52 B). Finally, decreased activity of TEAD1 and DMD, as well as increased effects of SIX1, CLPP (caseinolytic mitochondrial matrix peptidase proteolytic subunit), and CPT1B (carnitine palmitoyl transferase 1B) were observed as top 5 upstream regulators comparing CHD+HT+T2DM patients with CHD+HT patients (Figure 52 C).

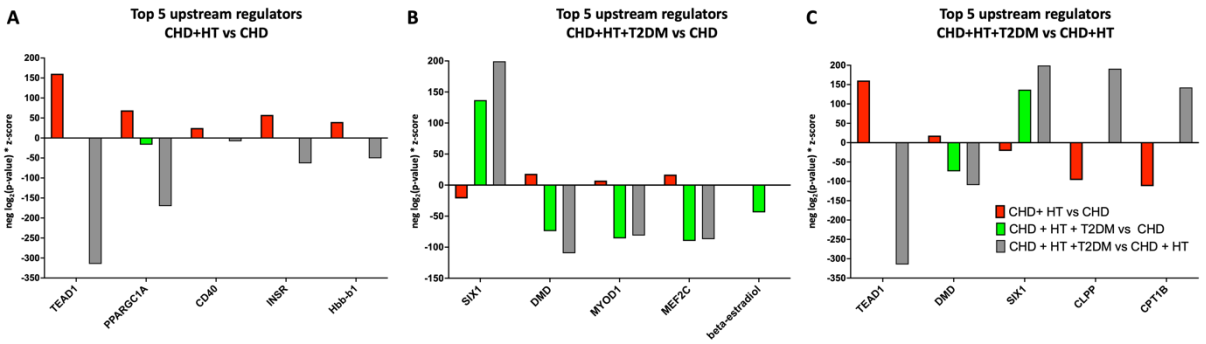

Figure 52: Top 5 upstream regulating factors identified in aortic tissue of CHD patients with hypertension or hypertension and diabetes as comorbidities. Aortic tissue samples were analyzed for total mRNA expression using the RNA-Seq method. The data were analyzed with the CLC genomics workbench, and the reported DEG ($p<0.05$) lists were imported into the ingenuity software and analyzed for the top 5 upstream regulating factors. The following patients' groups were compared to each other: (A in red) CHD+HT vs. CHD, (B in green) CHD+HT+T2DM vs. CHD, and (C in grey) CHD+HT+T2DM vs. CHD+HT. The negative $\log_2$ p-values were multiplicated with the z-score values for normalization. Further, the other comparisons' values were also included in each graph. Abbreviations: CHD=coronary heart disease, HT=hypertension, T2DM=type 2 diabetes mellitus, VEGF-A=vascular endothelial growth factor A. Published in (276).

In summary, comparing CHD patients with the CHD+HT group RNA-Seq analysis identified a network of upregulated pathways around CD40L and further CD40 under the top five upstream regulators. Conversely, by comparing CHD+HT+T2DM with the control group and the CHD+HT group, CD40L-CD40 signaling cascade members were not found under the upstream regulators or in the network analysis.

6. Discussion

6.1. Mouse data

This study provides new insights into the role of CD40L-CD40-TRAF6 signaling as a pharmacological target for preventing and modulating chronic vascular inflammation. The focus is set hereby on modifiable risk factors of CVD, like hypertension and type 2 diabetes mellitus. A general CD40 deficiency and a tissue-specific knockout of CD40 showed here no protective effects in a mouse model of arterial hypertension, whereas TRAF6 inhibition has beneficial effects in diabetic and hypertensive mouse models.

6.1.1. The role of global and tissue-specific CD40 deficiency in the progression of CVD

Chronic low-grade inflammation is an important pathology in various metabolic and cardiovascular diseases, and its incidence increases with age (285). The complex interplay of lipids, metabolism, immune cells, and inflammation in the pathogenesis of CVD makes general treatment difficult, and a combination of different drugs is required tailored to the patient's pre-existing conditions. Researchers are currently trying to find more effective drugs to limit disease progression and reduce the risk of cardiovascular events (107, 174).

The co-stimulation of the CD40L-CD40 dyad reflects an important immune checkpoint in inflammation. Depending on the inflammatory environment, different cell types regulate the immune response (237, 286). The immune checkpoint proteins CD40L or CD40 deficiency have various effects in obese and atherosclerotic mouse models (208, 216, 217, 237, 238, 287-291). For example, $CD40L^{-/-}$ in high-fat diet-treated obese mice ameliorates metabolic manifestations like the development of diet-induced obesity, insulin resistance, and adipose tissue inflammation (287). Further, obesity-associated vascular inflammation, oxidative stress, and endothelial dysfunction are improved in CD40L-deficient mice (217). Another study demonstrated that CD40L in a mouse model of arterial hypertension contributes to the induction of a pro-thrombotic state, vascular inflammation, oxidative stress, and endothelial dysfunction (216). This study was also performed in our lab, and some key data are shown in Figure 53.

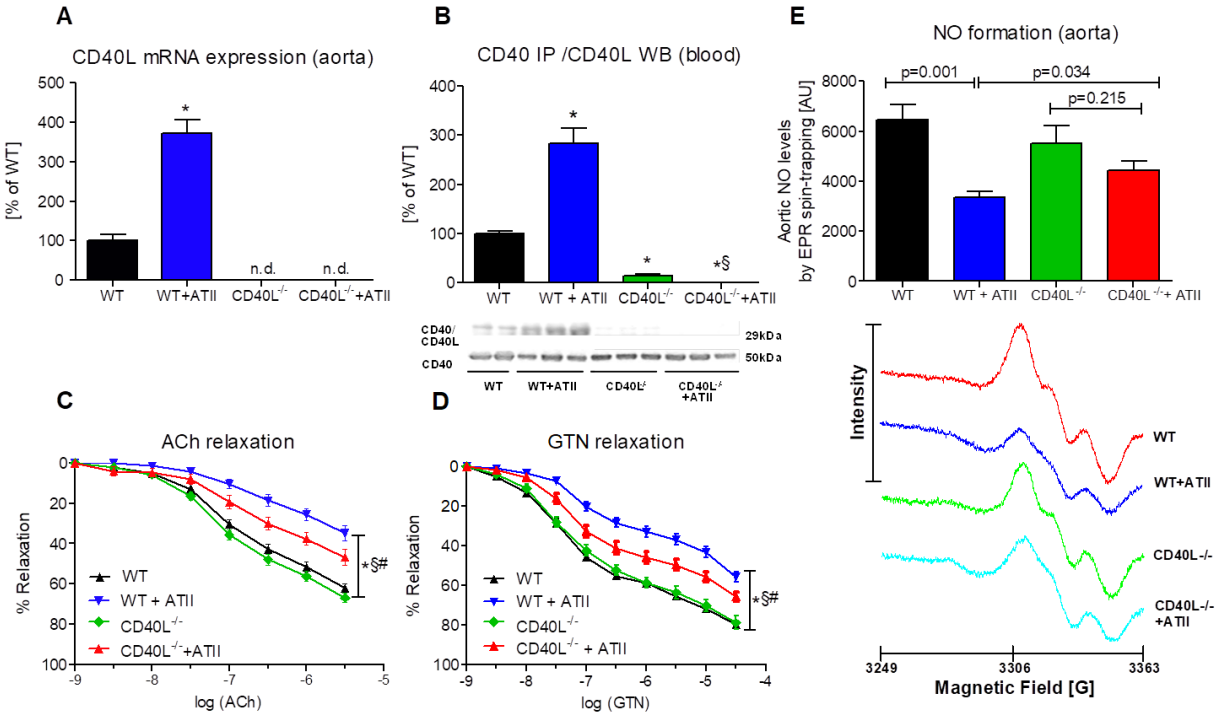

Figure 53: CD40L deficiency led to improved vascular function in hypertensive mice. WT (C57BL6/J) and CD40L$^{-/-}$ mice were treated with AT-II (1 mg/kg/d) via osmotic minipumps to induce arterial hypertension for seven days. (A) Aortic CD40L mRNA expression levels were measured via RT-PCR. (B) In citrate, mixed blood, CD40L-CD40 protein interaction analysis was performed via immunoprecipitation of CD40 followed by CD40L Western blot detection. Original representative blots are shown below. Aortic segments were used to measure endothelial (C) and smooth muscle cell function (D) in isometric tension studies. (E) Electron paramagnetic resonance spin trapping using Fe(DETC)$_2$ colloid was performed to determine aortic $^{\bullet}$NO bioavailability. Data are presented as mean values ±SEM of n=4 (A+B), n=10-12 (C+D), and n=8-12 (E) animals per group. * p≤0.05 vs WT, § p≤0.05 vs WT+AT-II, and # p≤0.05 vs CD40L$^{-/-}$. Abbreviations: WT=C57BL6/J mice IP=immunoprecipitation, AT-II=angiotensin-II, ACh=acetylcholine, NTG=nitroglycerine, n.d.=not detectable. The figure is taken from (216) with permission.

Impaired T_H1 polarization was observed in atherosclerosis-prone mice with T cell-specific CD40L deficiency reflected by reduced INFγ production and smaller atherosclerotic plaque size (237). Meanwhile, diet-induced obesity in T cell-specific CD40L$^{-/-}$ mice did not affect weight gain or insulin resistance and showed, in general, only minor beneficial effects on metabolic dysfunction (288). CD40$^{-/-}$ mice showed impaired remodeling capabilities after ligating carotid arteries, a smaller total vascular tone, reduced collagenase activity, and decreased vascular immune cell infiltration (208). Also, a reduced atherosclerotic phenotype was observed in macrophage and dendritic cell-specific CD40 deficient mice (237, 238). Contradictory high-fat diet-induced obesity in CD40$^{-/-}$ mice leads to worsening metabolic dysfunction like increased adipose tissue inflammation and insulin resistance (289, 290). Macrophages seems to be not the main driver of the induced metabolic dysfunction as analyzed in macrophage-specific CD40 deficient high-fat treated mice. No changes in body weight, insulin resistance, or triglyceride levels were observed (291).

Also, in this study, only minor beneficial effects were observed in CD40$^{-/-}$ mice after the onset of arterial hypertension. The heart-to-body weight ratio of CD40$^{-/-}$ AT-II-treated mice was not

significantly lower than in the AT-II-treated control animals. Therefore, the absence of CD40 did not improve the hypertension-induced cardiac hypertrophy. The systolic blood pressure was significantly reduced in $CD40^{-/-}$+AT-II animals compared to WT AT-II-treated mice. However, the mice were still hypertensive, with an average systolic blood pressure of 148 mmHg. Only a minor effect on vascular function improvement was observed in AT-II-treated CD40 deficient mice. Also, the ROS production in the aorta, heart, and blood showed no uniform beneficial trend. In summary, the data here did not show the expected beneficial effect of CD40 absence in the progression of arterial hypertension.

The mouse model of arterial hypertension was chosen in this project because it was demonstrated earlier in this lab that CD40L deficiency prevents major complications (216). As an important bioregulator in the cardiovascular system, AT-II mediates ROS production of different NADPH oxidases in vascular and cardiac cells (292). AT-II induces vascular inflammation and oxidative stress, especially in the mouse model utilized here and physiologically. AT-II binding to AT_1R triggers a pro-inflammatory response by activating the transcription factor NF-κB in different immune and vascular cells (292). Also, CD40L-CD40 expression can be regulated by either inflammation or NF-κB signaling (170, 293). Indeed, in smooth muscle cells, CD40 expression is modulated by AT-II stimulus (294). CD40L-CD40 and AT-II-mediated pathways seem closely connected; however, the link between these pathways is not fully understood. In conclusion, from our data, we don't think a general CD40 blockade is suitable as a treatment strategy for chronic low-grade inflammation in the vasculature.

We further hypothesized that a more targeted inhibition of CD40, as in a tissue-specific knockout mouse model, may benefit arterial hypertension. Previously, it was demonstrated that CD40 expressed on adipocytes can modulate immune cell activation (286). Adipocytes in young, healthy individuals are important for storing and metabolizing lipids. During aging and metabolic diseases, adipocytes are expanding. Cellular stress leads to the dysfunction of adipocytes and the secretion of pro-inflammatory signaling molecules like adipokines, TNFα, CCL2, or IL-6 (239, 295). Further, adipocytes play a key role in inflammation by presenting antigens like MHCII or the immune checkpoint protein CD40 (286, 296). Indeed, here we investigate further the role of adipocytes in CD40L-CD40 signaling and their contribution to low-grade vascular inflammation. Unfortunately, in our study, the hypertensive phenotype in mice was not improved by selective adipocyte-specific CD40 deficiency. As no positive effects on endothelial function, oxidative stress levels, or systolic blood pressure were observed, we did not investigate protein expression levels in PVAT or other fat tissues in more detail. Recently, another study utilizing different adipocyte-specific CD40-deficient mouse models was published. It stated that adipocytes control hematopoiesis and inflammation through CD40

signaling (239). Indeed, the lymphoid organs of adipocyte CD40-deficient mice (22 weeks old) showed altered immune cell decomposition, including increased T cell activation and decreased hematopoiesis. Further, aging in these mice (52 weeks old) was associated with features like fewer lymphoid progenitor cells and a compensatory increase in bone marrow effector memory T cells. In addition, a decrease of B cells in lymphoid organs and bone marrow was observed (239). The adipocyte-deficient mice were backcrossed with $ApoE^{-/-}$ mice and fed a high-cholesterol diet to analyze further the role of CD40 signaling in atherosclerosis. No significant changes in body weight, plasma lipid levels, or triglyceride levels were observed. Again, the systemic immune cell composition was affected in these mice. In addition, enhanced hypercholesterolemia, associated with myelopoiesis and lymphopoiesis, was observed. Interestingly, these mice showed a decreased atherosclerotic lesion size but an induced necrotic core formation. Lastly, to mimic conditions of a metabolic syndrome or obesity, the adipocyte-specific CD40-deficient mice were fed a high-fat diet. A decreased weight gain, more activated T cells, fewer immune cells in adipose tissue, and increased fat oxidation were observed in obese mice (239). Global $CD40L^{-/-}$ or pharmacological inhibition of the CD40/TRAF6 pathway significantly suppresses obesity-induced vascular damage and atherosclerotic changes (217). A mouse model associated more with lipid dysfunction and storage, like an atherosclerotic, aging, diabetic, or obesity model, would be more suitable to analyze the effect of adipocytic CD40 signaling during disease than the hypertensive mouse model. Further, the focus of analysis must be set more on the cellular regulation of the immune system.

In summary, neither the $CD40^{-/-}$ nor the adipocyte-specific CD40 deficiency mice showed the expected cardiovascular protective phenotype during short-term AT-II treatment. The CD40L-CD40 signaling pathway is complex and mediates beneficial and harmful signaling simultaneously. In the following, we focused more on proteins downstream of CD40 signaling to identify a more selective treatment target.

6.1.2. Selective CD40-TRAF6 inhibition in hypertension and diabetes

As mentioned before, in atherosclerotic and diabetic mouse models, CD40L deficiency seems to be a promising treatment strategy (216, 217, 287). However, in clinical trials utilizing a CD40L antibody treatment, prothrombotic events were observed as severe side effects in the probands (220). This probably happened due to the property of CD40L to stabilize arterial thrombi by $\alpha_{IIb}ß_3$ integrin-dependent mechanism (179). An alternative approach would be the antagonization of CD40. The results here and other studies, for example, in atherosclerotic $Ldlr^{-/-}$ mice, demonstrated that CD40 deficiency did not lead to smaller atherosclerotic lesions or improved vascular function (175). Meanwhile, in $CD40^{-/-}ApoE^{-/-}$ mice, atherosclerotic lesion

size was reduced, and less plaque inflammation was observed (209). Based on the controversial results of either CD40L or CD40 blockade in mice, the focus moved to downstream mediators in the signaling cascade.

CD40L modulates TRAF1, 2, 3, 5, and 6 differentially in endothelial cells, which are functionally important in pro-inflammatory signaling (205). Analyzing neointima formation and arterial remodeling in CD40 deficient mice, CD40-TRAF6 signaling was identified as a key regulator (208). The role of different TRAFs was further examined in an atherosclerotic model by backcrossing CD40-T2/3/5$^{-/-}$ or CD40-T6$^{-/-}$ mice with ApoE$^{-/-}$ mice. Interestingly, TRAF2/3/5 signaling does not affect atherosclerosis. Even higher amounts of distinct T cells and resident dendritic cells were observed in the vasculature. Meanwhile, inhibiting CD40-TRAF6 signaling abolished atherosclerosis, leading to macrophage polarization toward regulatory M2 phenotype (209). A specific inhibitor for CD40-TRAF6 interaction was developed (240). A beneficial effect of small-molecule CD40-TRAF6 inhibition has already been observed in pathologies such as insulin resistance (226), obesity (297), diabetes (217), atherosclerosis (241), bone disorders (244), heart failure (246), breast cancer (243), and neuroinflammation (245). Based on these previous results, we tested the CD40-TRAF6 inhibition in a mouse model of arterial hypertension.

Our data revealed that the systolic blood pressure was significantly reduced after the TRAF6 inhibitor treatment in hypertensive mice. The TRAF6 inhibitor treatment also improved vascular function. Further, ROS production was reduced in blood, aortic, adipose, cardiac, and renal tissue of hypertensive TRAF6 inhibitor-treated mice. Via flow cytometric analysis, we revealed that aortic tissue lysates contain fewer immune cells in TRAF6 inhibitor-treated hypertensive mice than in only AT-II-treated mice. This data indicates that CD40-TRAF6 inhibition prevents immune cell infiltration into the vascular wall during hypertension, which is also associated with less inflammation. The measured LV-EF in small animal cardiography of untreated WT animals (Ø 60%) fit published data. For example, an LV-EF of 58-62% is described in the literature as physiological for C57BL/6J mice (298, 299). Interestingly, the observed hypertrophy of the cardiac muscle induced by AT-II treatment reflected in the heart-to-body weight measurement and LV mass was not improved by TRAF6 inhibitor treatment. Also, the LV PW thickening was not improved. Indeed, the calculated average LV-EF did not differ significantly between control and WT+AT-II+TRAF6 animals, but the average mean values are approximately the same (Ø 60% WT vs Ø 61% WT+AT-II+TRAF6i). A previous study using a similar hypertensive mouse model also demonstrated that AT-II treatment in C57BL/6J mice leads to increased LV-EF, cardiac remodeling, and wall thickening, which is also reflected in our study (300). Further, in a mouse model of induced heart failure via transverse aortic constriction, TRAF6 inhibitor

treatment over ten weeks leads to improved cardiac function. This was presumably mediated by reduced macrophage and T-cell infiltration into the myocardium accompanied by decreased cardiac hypertrophy and fibrosis (246). Since this pressure overload model positively affects cardiac function through TRAF6 inhibitor treatment, we hypothesized that long-term treatment with TRAF6 inhibitor in a hypertensive model could be beneficial. Investigating the long-term TRAF6 inhibitor treatment and its effects on the immune system would be interesting. In addition, the AT-II dosage utilized here induces a quite harsh hypertensive phenotype in the mice, and TRAF6 inhibition does not block the signaling of AT receptors. Further, FACS analysis addressing the immune cell composition in the heart of hypertensive TRAF6 inhibitor-treated animals would be interesting.

Chronic inflammation also plays an important role in the pathology of obesity and metabolic dysfunction (301, 302). Indeed, CD40L-CD40 signaling is associated with obesity-induced inflammation (303). Stimulation of CD40 expressed on adipocytes by CD40L reduces IRS-1 and GLUT4 expression and further enhances adipokine secretion (304). CD40L-stimulated adipocytes also activate endothelial cells (305). In obese patients, elevated plasma levels of CD40L are observed (217, 306). In a mouse model of diet-induced obesity, CD40 deficiency induces insulin resistance and adipose tissue inflammation (226). In addition, CD40L deficiency improved endothelial dysfunction, oxidative stress, and inflammatory parameters in high-fat diet mice (217). Whereby the pharmacological TRAF6 inhibition ameliorates these obesity-related metabolic complications (226, 297). As shown in Figure 54, TRAF6 inhibition in a diabetic mouse model (db/db) improves blood glucose levels, body weight gain, vascular function, and oxidative stress (217). This study was also performed in our institute, and some key data are shown in Figure 54.

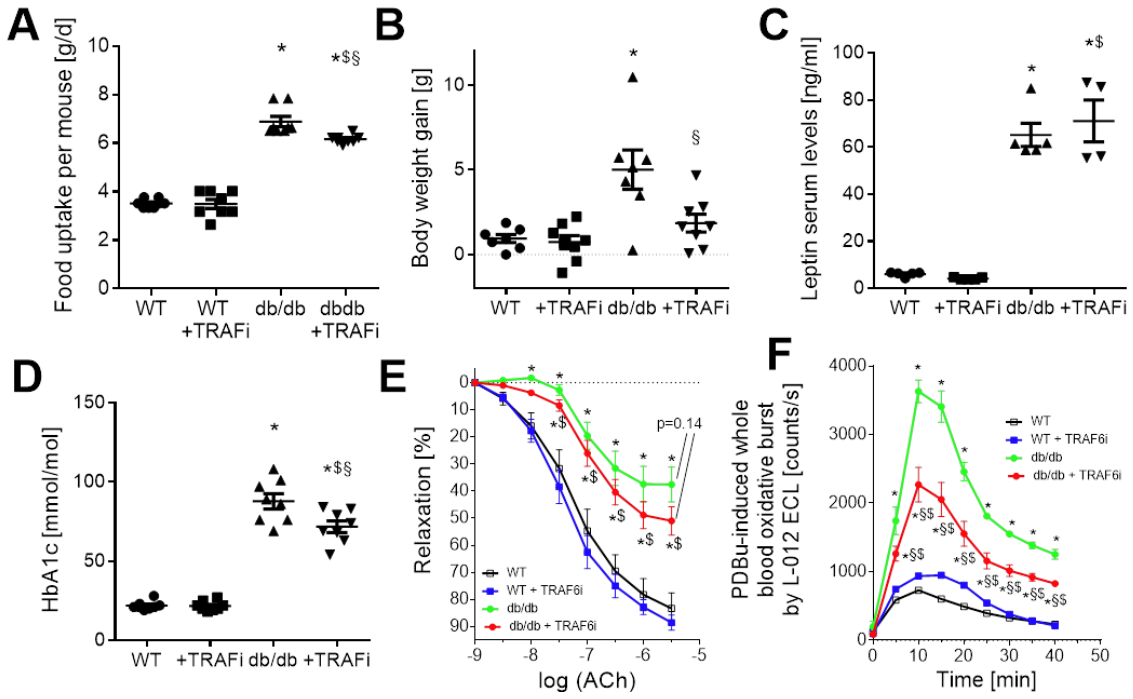

Figure 54: TRAF6 inhibition in db/db mice improves vascular function and decreases oxidative stress. WT and db/db mice were treated for 14 days with a TRAF6 inhibitor (2.5 mg/kg/d) via osmotic minipumps. The food uptake per mouse (A) and the body weight gain (B) were monitored during the two weeks of treatment. After the treatment, leptin serum levels (C) and whole blood HbA1c levels (D) were measured. (E) Aortic segments were used to determine endothelial function in isometric tension studies. (F) Whole blood oxidative burst was performed with PDBu and measured by L-012 chemiluminescence. Data are mean ±SEM of n=8 (A-D), n=6-8 (E), and n=5 (F) animals per group. Abbreviations: WT=wild type (BKS.CgTemoin mice), TRAF6i=tumor necrosis factor receptor-associated factor 6 inhibitor, HbA1c=hemoglobin A1c, ACh=acetylcholine, PDBu=phorbol 12,13-dibutyrate, ECL=enhanced chemiluminescence. The figure is taken from (217) with permission.

In this study, we further analyze the effects of TRAF6 inhibition in diabetic mice and provide new additional protein expression analysis to complete already published data. Significantly decreased protein expression was observed in the cardiac tissue of diabetic mice treated with TRAF6 inhibitor for the oxidative stress and inflammation markers NOX2, eNOS, $p47^{phox}$, RAGE, and CD40 compared to untreated db/db mice. Further renal expression of eNOS, pMARCKS, HO1, and ET1 was also significantly reduced after TRAF6 inhibitor treatment in diabetic mice. The protein expression analysis indicates less inflammatory, oxidative stress, and apoptotic activity in renal and cardiac tissue by TRAF6 inhibitor treatment. Figure 55 summarizes the vaso-protective effects of TRAF6 inhibition in mouse models of hypertension and diabetes.

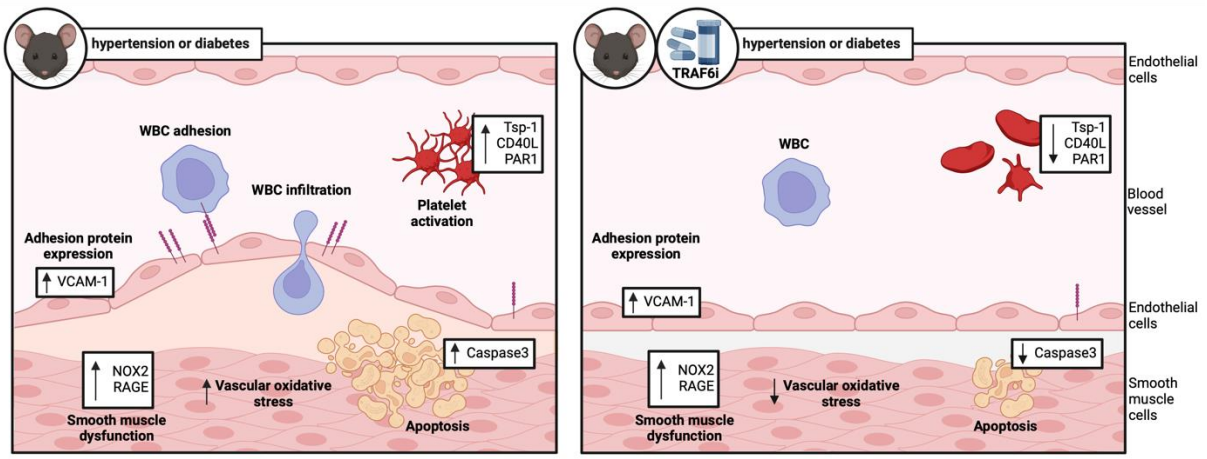

Figure 55: The role of the inflammatory TRAF6 inhibition in hypertensive and diabetic mouse models. The left panel shows the central pathomechanisms associated with CD40L-CD40-TRAF signaling in hypertensive and diabetic mice. The right panel shows the protective effects of TRAF6 inhibitor treatment in hypertensive and diabetic mice. Created with BioRender.com. Adapted from (276). Abbreviations: WBC=white blood cell, Tsp-1=thrombospondin-1, CD=cluster of differentiation, CD40L=CD40 ligand, PAR1=protease-activated receptor 1, VCAM-1=vascular cell adhesion molecule-1, TXNIP=thioredoxin-interacting protein, NOX2=NADPH oxidase 2, RAGE=receptor for advanced glycation endproducts.

The CD40L-CD40 dyad is a powerful mediator in inflammation and immunity. To circumvent potential side effects over a full CD40L/CD40 blockade, a partial CD40 blockade via TRAF6 inhibition seems to be a promising treatment strategy for low-grade tissue inflammation. With this study, we provide new insights into the beneficial effects of TRAF6 inhibition in hypertension and diabetes. Indeed, we could show in a hypertensive and diabetic mouse model that TRAF6 inhibition suppresses inflammation and oxidative stress in different tissues. Therefore, CD40-TRAF6 inhibition is a promising candidate for treating low-grade inflammation to prevent cardiovascular events.

6.1.3. Limitations of the mouse data

The hypertensive mouse model utilized in this study does not represent a uniform model, as AT-II is only one possible pathway to induce hypertension. Other signaling pathways, like diet-induced or genetically-induced hypertension, are not considered here. In patients, the origin of hypertension is multifactorial, but the RAAS with AT-II signaling plays a definitive central role (276). Treatment with 1 mg/kg/d AT-II for seven days is too short to reflect hypertension-triggered end-organ damage, for example, in the kidney or heart. Therefore, we could not test the impact of TRAF6 inhibition on end-organ damage. Previously, it was already demonstrated that CD40L deficiency prevents major complications in arterial hypertension induced by AT-II (216). Indeed, the study indicates that the immigration of CD40L-expressing inflammatory cells primarily drives the AT-II model. AT-II-induced arterial hypertension in mice is further negatively influencing vascular function and leads to excessive blood pressure increase, which is also well-published already (216, 257, 307, 308). Therefore, this model seems suitable for analyzing the CD40L-CD40-TRAF6 signaling during inflammation and oxidative stress in the

cardiovascular system. Normally, the pathophysiology of arterial hypertension is frequently studied in mouse or rat models with short-term AT-II treatment (1 to 2 weeks), which causes already hypertension and a drastic increase in inflammation and oxidative stress.

As shown previously, diabetic db/db mice develop a severe vascular phenotype reflected in increased inflammation, oxidative stress, and endothelial dysfunction (217). The correlation of this phenotype in 14-week-old mice with the actual clinical situation of patients could be weak. However, we could demonstrate that even a short-term CD40/TRAF6 inhibitor treatment in db/db mice leads to significantly reduced expression of inflammatory and oxidative stress markers, which indicates the strengths of this treatment strategy. In addition, previous studies supporting these results showed that CD40/TRAF6 inhibitor treatment in db/db mice gained less body weight, decreased HbA1c levels, and improved endothelial function (217, 276).

6.2. Human data

Patients suffering from systemic or chronic inflammatory diseases exhibit an increased risk of cardiovascular complications (309, 310), which promotes the classification of CVDs as an inflammatory-related entity (311). This association was also shown in a clinical study with ACS patients, where statin treatment was associated with lower CRP levels and better clinical outcomes than in patients with higher CRP levels (312). Further, this concept is utilized to develop new pharmacological agents, such as canakinumab (IL-1ß antagonist) in the CANTOS trial, which targets inflammation and improves clinical outcomes in high cardiovascular-risk patients (107). Colchicine in the COLCOT trial is also currently tested as an anti-inflammatory agent. The data indicate that a low dose of colchicine decreases the risk of major adverse cardiac events after a myocardial infarction (109). The impact of canakinumab and colchicine therapy on cardiovascular events or mortality is published (313) and shown in Figure 56.

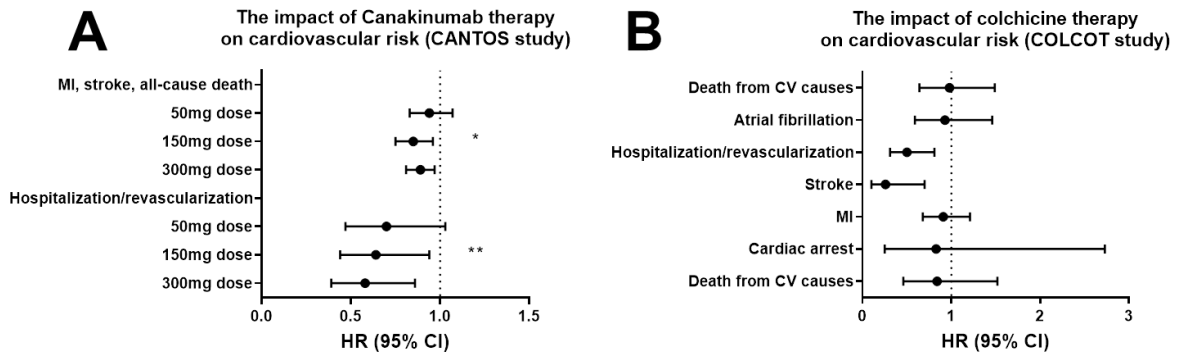

Figure 56: Impact of anti-inflammatory canakinumab and colchicine therapy on cardiovascular risk and mortality. (A) 10061 patients with previous myocardial infarction and CRP levels >2 mg/l were included in the CANTOS study. The patients were divided into four groups: placebo n=3344, 50 mg canakinumab n=2170, 150 mg canakinumab n=2284, or 300 mg canakinumab n=2263. The risk of cardiovascular events or mortality after different

dosages of canakinumab therapy was calculated via hazard ratios. Original data are taken from (107). (B) 4745 patients were included in the COLCOT study, where 2366 patients received colchicine therapy, and 2379 received a placebo. The original published data calculated hazard ratios regarding cardiovascular events and mortality (109). Abbreviations: MI=myocardial infarct, HR=hazard ratio, CI=confidence interval, CV=cardiovascular. The figure is taken from (313).

In addition to inflammation, oxidative stress is recognized as an essential factor in the pathogenesis of CVDs, characterized by an imbalance of ROS generation and scavenging (314, 315). This imbalance was observed, for example, by the positive correlation between glutathione peroxidase-1 levels and outcomes in CVD patients, as well as the association between markers of oxidative stress and cardiovascular mortality (316).

6.2.1. Human proteomics data

The plasma proteomic analysis in CHD patients revealed several stepwise increased targets associated with the number of their comorbidities (CHD<CHD+HT<CHD+HT+T2DM). In the following, the role of altered protein expression is discussed in more detail concerning their role in inflammatory signaling and the reference to the CD40L-CD40 signaling cascade. The cluster analysis showed upregulated protein expression for TNF receptor superfamily members like TNFRSF9 (CD137 / 4-1BB) and TNFRSF4 (CD134 / ox40) in CHD patients with HT and T2DM as comorbidities. These proteins are expressed on the surface of activated T cells. Like CD40 (TNFRSF5), TNFRSF9 and TNFRSF4 are directly interacting with TRAF2, which leads to NF-κB activation (317-319). Moreover, pro-inflammatory stimuli via CD40 or IL12 lead to enhanced TNFRSF9 expression, which promotes its T cell co-stimulatory function (320). CD27, another TRAF-interacting receptor, facilitates T-T and T-B cell interactions. Like other co-stimulatory receptors, it activates NF-κB through TRAF2/5 signaling (321). Inflammatory cytokines like TNFα are also part of the TRAF interacting protein group, and it was significantly upregulated in CHD+HT+T2DM patients compared to CHD patients. In addition to TRAF2-mediated signaling, TNFα can trigger apoptosis via caspase8/caspase3 signaling (322). Furthermore, TNFRS21 (DR6) expression significantly increases in the plasma of CHD patients with T2DM as a comorbidity. TNFRS21 contains a death domain and induces apoptosis via NF-κB. As a TNF receptor superfamily member, TNFRS21 might also contribute to inflammation and regulation of the immune system (323).

Further, the cluster analysis identified TNFα as a central player for altered protein expression patterns in CHD patients suffering from HT or T2DM. This also indicates an involvement of the CD40L-CD40 signaling pathway in upregulated pro-inflammatory signaling. Previously, it was shown that activated platelets promote pro-inflammatory signaling and bind via CD40L-CD40 interaction to monocytes, forming aggregates. These monocytes further secreted IL-1ß and TNFα in a CD40/TRAF6/NF-κB dependent manner, promoting immune cell migration. A

blockade of CD40L/CD40 or silencing of CD40/TRAF6 leads to a lack of monocytic TNFα secretion due to the absence of phosphorylation and nuclear translocation of NF-κB. Also, the monocytic secretion of CCl2 (MCP-1) was reduced by utilizing CD40L or CD40 blocking antibodies (324). In patients with diabetic retinopathy, CD40 expression is upregulated, accompanied by increased ICAM-1 (CD54), CCL2, TNFα, and IL-1ß expression (325). During HIV infection, CD40L and other TNFRSF members play a central role in the regulation of immune responses (326). In mouse models of arthritis, TRAF6 inhibition led to suppression of RANKL, CD40L, and IL-1ß expression and had anti-inflammatory effects (244). Enhanced CD68 expression is co-stimulated with CD40L-CD40 signaling. CD40L-CD40 signaling leads to the expression of different cytokines and the recruitment of monocytes and macrophages to the inflammation side. An increasing number of macrophages is associated with the incidence of the macrophagic marker CD68 (243, 327).

In addition to TNF superfamily members, other proteins linked to the CD40L-CD40 signaling cascade are upregulated in CHD patients suffering from additional comorbidities. Like IOSLG, it is expressed on germinal center B cells and is upregulated in CHD+HT+T2DM patients. It interacts with its receptor ICOS on T follicular T helper cells and mediates calcium flux. This promotes the externalization of CD40L, which triggers the binding of germinal center B cells via CD40 and leads to increased ICOSLG expression in a positive feedback loop-dependent manner. Upregulated ICOSLG expression via CD40 signaling is important for bone marrow plasma cell development and establishing T follicular helper cell-mediated, long-lasting immunity (328). Gal1 protein expression is also upregulated in CHD+HT+T2DM patients and is associated with T-cell apoptosis. Gal1 is expressed and secreted by activated B cells, which interact via CD40L-CD40 binding with T cells. This interaction of CD40L-CD40 could lead to T-cell apoptosis and enhanced cytokine production in B cells. Therefore, CD40L-CD40 interaction and Gal1 expression seem to regulate B-cell mediated function and survival of T-cells (329). A novel subset of B cells expressing CCL4/CCL3 chemokine has been identified recently in human tonsils. The activation and expression of these chemokines are positively correlated with CD40 co-stimulation in this B-cell subset (330). These data indicate that evaluated plasma levels of CCL4/CCL3 in CVD patients could be mediated by CD40L-CD40 signaling. CD40 expressed on macrophages could mediate contrary immune responses. On the one hand, strong CD40 stimulation led to p38 MAPK pathway activation, resulting in iNOS induction, IL-12, and INFγ secretion as pro-inflammatory immune responses to recruit other immune cells to fight against infections. On the other hand, weak CD40 signal activation led to ERK1/2 pathway activation, causing IL-10 cytokine expression, which promotes infections by inhibiting other immune cell recruitment (331). KLRD1 and CD244 expression is also upregulated in the plasma of CHD+HT+T2DM patients compared to the CHD group. These

proteins are involved in NK cell function and NK cell-mediated immunity. However, their involvement in CD40L-CD40 signaling remains unclear (332). Figure 57 summarizes the results of the proteomic analysis.

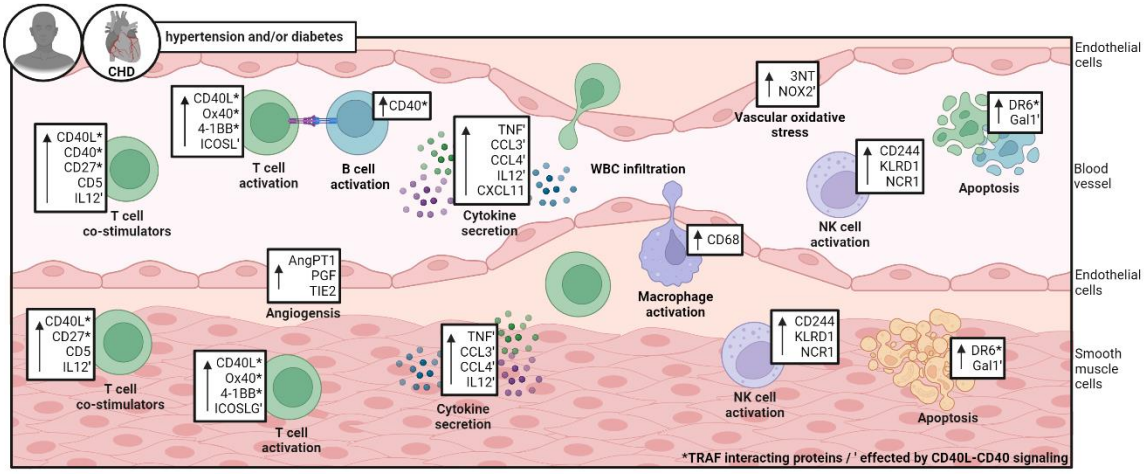

Figure 57: The role of the inflammatory CD40L-CD40 signaling cascade in CHD patients with diabetes and hypertension. The panel shows that different inflammatory markers in CHD patients with additional comorbidities like hypertension and diabetes are upregulated. Directly, TRAF6 interacting proteins are marked with *, and proteins affected by CD40L-CD40-TRAF signaling are marked with '. Some of the targets mentioned here have only changed according to the trend in proteomic analysis. Created with BioRender.com. Adapted from (276). Abbreviations: CD=cluster of differentiation, CD40L=CD40 ligand, TNF=tumor necrosis factor, CHD=coronary heart disease, IL12=interleukin-12, TNFRSF4 (or ox40 or CD134)=TNF receptor superfamily member-4, TNFRSF9 (or 4-1BB or CD137)=TNF receptor superfamily member-9, ICOSL=inducible costimulator ligand, AngPT1=angiopoetin-1, PGF=placental growth factor, TIE2=angiopoetin receptor-2, CCL3/CCL4=C-C motif chemokine ligand-3/-4, CXCL11=C-X-C motif chemokine ligand-11, 3NT=3-nitrotyrosine, KLRD1=killer cell lectin like receptor D-1, NCR1=natural cytotoxicity triggering receptor-1, DR6=death receptor-6, Gal1=galactin-1, NK=natural killer cell.

The proteomic data are further supported by protein expression analysis performed via dot blotting. In patients, plasma protein expression associated with oxidative stress (e.g., NOX2, 3-NT) and inflammation (e.g., CD40L, CD68) is enhanced, as in the performed proteomic and transcriptomic analyses.

6.2.2. Human transcriptomic data

Proteomic analysis in the plasma and mRNA expression analysis of aortic tissue showed only a minor target overlap, which is unsurprising and discussed in more detail. Whereas the plasma proteomic analysis allows conclusions on the whole body, the RNA-Seq analysis represents only conclusions on tissue-specific local gene expression alterations. Regarding the proteomic data in CHD+HT+T2DM patients compared to the CHD group without comorbidities, increased aortic gene expression was observed for cytokines/chemokines (e.g., TNFα, CCL3, CCL4), markers associated with T-cell activation (e.g., TNFRSF4, TNFRSF9, ICOSLG, CD5), apoptotic markers (e.g., Gal1, TNFRSF21), angiogenic markers (e.g., AngPT1, TIE2) and NK cell-specific markers (e.g., KLRD1, CD244).

IPA analysis identified the top 5 canonical pathways and top 5 upstream regulators within the different patient groups. Comparing CHD+HT with CHD patients, the top 5 upregulated canonical pathways are involved in pro-inflammatory and pro-oxidative mechanisms, which are important in CVD pathogenesis. Upregulated mitochondrial dysfunction and oxidative phosphorylation in CHD+HT patients are associated with the pathogenesis of chronic diseases (e.g., atherosclerosis and cardiomyopathy), reduced ATP synthesis, and loss of electron transport chain efficiency, which results in ROS generation and uncoupling of proteins (333). Especially, eNOS uncoupling is to be mentioned as involved in endothelial dysfunction and progression of hypertension. Mitochondrial dysfunction also promotes apoptosis and plaque rupture (334). Another pathway upregulated in CHD+HT patients compared to CHD patients was the sirtuin pathway. Sirtuins are NAD^+-dependent enzymes that control inflammation, mitochondrial function, cellular metabolism, and DNA repair. For example, Sirt1 activation is associated with cell survival and cellular resistance against oxidative stress. Indeed, Sirt1-mediated AMPK activation eliminates oxidative stress by controlling insulin sensitivity, metabolism, fatty acid oxidation, and mitochondrial biogenesis. NF-κB induced gene expression is inhibited by Sirt1 activity, which promotes cell survival. Upregulated sirtuin signaling also has protective characteristics in ischemia/reperfusion injury of cardiac tissue. Lastly, Sirt1 acts as an anti-atherosclerotic factor by protecting endothelial cells from oxidative stress, improving endothelial function, and inhibiting smooth muscle cell hypertrophy, which is critical in atherosclerosis progression (335, 336). Fourthly, the neutrophil extracellular trap (NET) pathway is upregulated in CHD patients. NETs consist of predominantly DNA strings released by neutrophils and provide a link between inflammation, innate immunity, thrombosis, and oxidative stress in CVD patients. NETs are present in atherosclerotic lesions and contribute to plaque destabilization. Further, oxidative stress contributes to NETosis. Also, NET formation is important in activating the coagulation system and mediation of arterial thrombosis (337). The fifth upregulated pathway in comparing CHD+HT with CHD patients is granzyme A, a serine protease. Extracellular granzymes promote matrix degradation and induce vascular dysfunction, inflammation, and plaque instability in atherosclerosis (338).

The top 5 upstream regulators for the observed gene expression changes in comparing CHD+HT patients with CHD patients are TEAD1, PPARGC1A, CD40, INSR, and Hbb-b1. The protein-coding transcription factor TEAD1 promotes vascular smooth muscle cell differentiation and is important in vascular development. Yes-associated protein (YAP1) signaling depends on TEAD1 binding and is involved in AT-II-mediated vascular remodeling in hypertensive rats (339, 340). PPARGC1A is a protein-coding gene linked to energy metabolism, which may affect the heart and smooth muscle cell function. In previous studies, PPARGC1A dysregulation was observed in heart failure (341, 342), and further, it was associated with the regulation of

endothelial function (343) and generation of atherosclerotic lesions (344). The upregulation of CD40 aligns with our mouse data and already published data (216, 217). Also, enhanced INSR gene expression in hypertension is in accordance with published literature (345). The upregulation of the Hbb-b1 gene could be associated with social stress and may affect vascular dysfunction in mice (346).

The IPA analysis of CHD+HT+T2DM versus CHD patients revealed enhanced agranulocyte diapedesis and hepatic fibrosis, reduced calcium, dilated cardiomyopathy, and the effect of sildenafil as the top five canonical pathways. Enhanced agranulocyte (lymphocytes or monocytes) adhesion and migration are frequently observed in chronic diseases like atherosclerosis (82, 87). Hepatic liver fibrosis is another pro-inflammatory-driven pathological entity partially mediated by atherosclerosis identified in a multiethnic cohort study (347). During the development of atherosclerosis, calcium signaling may also play an important regulatory role in aortic gene expression. Imbalance of intracellular calcium homeostasis could promote atherosclerotic lesion development (348). Dilated cardiomyopathy is characterized by left ventricular or biventricular dilation that is caused by, for example, CHD, heart attack, hypertension, or diabetes (349). In rat renal ischemia/reperfusion models, sildenafil activates antioxidant and antiapoptotic genes. Further, sildenafil inhibits pro-inflammatory cytokine genes, and its reduced effects would probably promote inflammation and oxidative stress (350).

Comparing CHD+HT+T2DM versus CHD patients, the IPA identified SIX1 as an upregulated upstream regulator. The homeobox transcription factor SIX1 is associated with regulatory protein expression of organ development, differentiation, and cancer (351). Unfortunately, nothing is published about how SIX1 is involved in CHD, hypertension, or diabetes. Interestingly, most of the top five upstream regulators (DMD, MYOD1, MEFC1, and ß-estradiol) are downregulated compared to CHD+HT+T2DM versus CHD patients. This unexpected result correlates with using glucose-lowering drugs like metformin or insulin in the CHD+HT+T2DM cohort. It is well established that high glucose levels are associated with pro-inflammatory and pro-oxidative signaling (352). A pharmacological reduction of blood glucose levels could lead to reversal glucose gene expression alterations. Furthermore, anti-oxidative effects through AMPK activation and mTOR pathway inhibition were reported for metformin (353, 354). Also, insulin exhibits anti-oxidative effects via $^{\bullet}$NO signaling (355). These mechanisms may also promote the reversal of gene expression patterns in CHD+HT+T2DM patients if compared to the CHD group. Mutations in the cytoskeletal/membrane protein DMD could lead to dilated cardiomyopathy and muscle dystrophy. Dystrophin and dystrophin-associated proteins serve as mechanical stabilization of muscle sarcolemma and prevent contraction-related injuries. If

dystrophin is missing, the dystrophin-associated protein complex is degraded, which leads to mitochondrial dysfunction, impaired potassium signaling, pro-inflammatory signaling, and muscle degradation (356). The transcription factor MYOD1 prevents cardiac remodeling and fibrosis development in hypertensive rats. Reduced MYOD1 gene expression is observed during hypertension in cardiac and aortic tissue, which aligns with our results and may indicate severe aortic damage in CHD+HT+T2DM patients (357). In the cardiovascular system, the transcription factor MEF2C is important for cellular phenotypic modulation and is involved in cell proliferation, smooth muscle cell differentiation, migration, and homeostasis. A dysregulation of MEF2C is linked to hypertension-related vascular remodeling (358, 359). Estrogen treatment is described as a possible therapeutic approach to reduce atherosclerosis. The vasoprotective properties of estrogen are caused by its ability to enhance eNOS activity, resulting in increased •NO bioavailability. Therefore, estrogen causes vasodilation, suppresses arterial collagen secretion and extracellular matrix deposition, and decreases the secretion of inflammatory cytokines (360, 361). However, using estrogen as a potential new treatment for CVD is still controversially discussed in the literature (362, 363).

Comparing CHD+HT+T2DM patients with CHD+HT patients, the top five reduced canonical pathways involved oxidative phosphorylation, mitochondrial dysfunction, sirtuin signaling, estrogen receptor signaling, and calcium homeostasis. The role of these pathways in relation to CVD is previously discussed in the text. The IPA revealed that under the top 5 upstream regulators, TEAD1 and DMO activity decreased, and SIX1, CLPP, and CPT1B activity was enhanced by comparing CHD+HT+T2DM patients with CHD+HT patients. Also, in high-fat diet-treated animals, systemic insulin resistance leads to enhanced CLPP expression in slow-twitch muscles. Insulin sensitivity in skeletal muscle is related to mitochondria hemostasis, and enhanced CLPP activity may be involved in mechanisms that cause mitochondrial dysfunction (364). The fatty acid oxidation enzyme CPT1B seems to be involved in T2DM pathogenesis. Indeed, CPTB1-deficient mouse models were protected from diet-induced insulin resistance (365). Further, T2DM patients with gastric bypass surgeries had improved whole-body insulin sensitivity by increased expression of CPT1B (366). Lastly, the transcription of the CPT1B gene is related to cardiac hypertrophy (367).

6.2.3. Limitations of the human data

Individual variabilities in CHD patient's plasmatic protein or aortic RNA expression could arise from factors beyond the known comorbidities, such as environmental stressors, age, diet, circadian rhythms, or other known and unknown factors. The utilized cohort size of 88 CHD patients for the plasma proteome analysis was too small to account for these confounding factors. Also, the number of patients in the three groups is limited, and we cannot exclude unexpected confounding factors. Lastly, we could only screen for a limited number of proteins

in a targeted fashion, limiting the breadth of the analysis. Compared to inbreed mouse strains, human tissue transcriptomes exhibit greater heterogeneity, reflected by lower p-values among healthy and diseased individuals. The higher genetic variance could cause some transcriptional disease-related changes to remain undetected. A larger sample size would reduce this limitation. The availability and utilization of healthy aortic tissue is ethically problematic. However, the IPA revealed in comparing CHD+HT patients with CHD patients that the CD40L-CD40 pathway is a main regulator, which also fits our mouse data. For the transcriptomic analysis, whole aortic tissue was utilized, including different cell types (like endothelial cells, smooth muscle cells, immune cells, etc.); therefore, cell type-specific effects could not be analyzed. The immune cell composition could be affected by additional infections. All study patients were previously treated with different drugs, which partially overlap between the groups; nevertheless, the effects of these drugs could also affect the gene expression and mask disease-related transcriptional changes. Because of the small sample size, the human study was performed as an exploratory pilot study. The lack of a CHD+T2DM patient cohort may further limit this study (276).

6.3. Clinical impact

In the last decades, treatment strategies associated with CVD risk factors, such as lifestyle changes, hypertension, and dyslipidemia, have been well established. In addition, lipid-lowering therapy (e.g., statins) could reduce CVD risk by 30 % (see 1.4) (169, 368). Nevertheless, patients still suffer from atherosclerotic complications, and treating the associated chronic systemic low-grade inflammation is still challenging (369). Indeed, high-sensitive CRP (hs-CRP) is used classically in the clinic as a cardiovascular risk marker. Elevated hs-CRP levels are associated with inflammation and serve, for example, as an indicator for MI-induced mortality in ACS patients (312, 370). Further studies have identified other inflammatory CVD risk loci, supporting that inflammation is a major independent cardiovascular risk factor (371, 372). For example, some circulating cytokines (e.g., TNFα, IL-6, IL-18) or closely related factors (e.g., MMP-9) and sCD40L have also been established in the literature as independent cardiovascular risk factors (107, 373, 374). Recent clinical trials like the COLCOT (109) or CANTOS (107) study demonstrated that anti-inflammatory drug therapy reduces cardiovascular risk by suppressing different inflammatory pathways. However, clinically well-established classical cardiovascular risk markers are still more powerful tools than new inflammatory markers and seem to provide a better risk assessment until now, as demonstrated in Figure 58 (169). Besides hsCRP, well-established risk markers are, for example, systolic blood pressure, LDL, and N-terminal prohormone of brain natriuretic peptide (NT-proBNP) (169).

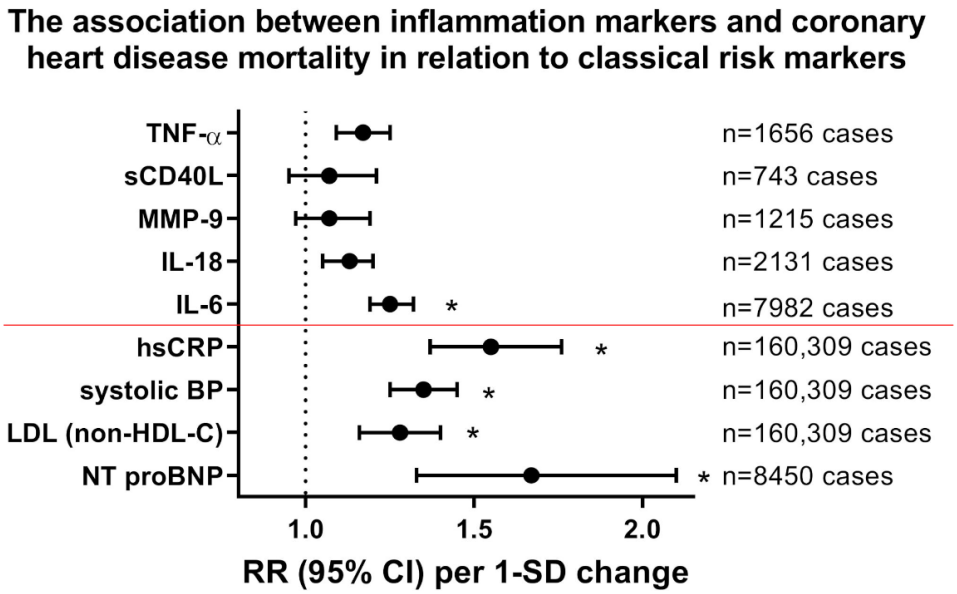

Figure 58: Association of coronary heart disease mortality to inflammatory and classical risk markers. A meta-analysis was performed to obtain the relative risk (RR) of CHD mortality correlated with inflammatory markers like TNFα, sCD40L, MMP-9 IL-18, and IL-6. These inflammatory risk markers were compared to classical CVD risk markers like hs-CRP, systolic BP, LDL, and NT-proBNP. The red line separates inflammatory and classical risk markers. Significant differences to the respective control groups are marked with *. Original data are taken from (374-377). Abbreviations: TNFα=tumor necrosis factor α, sCD40L=soluble CD40 ligand, MMP-9=matrix metalloproteinase-9, IL=interleukin, hs-CRP=high sensitive C-reactive protein, BP=blood pressure, LDL=low-density lipoproteins, HDL=high-density lipoprotein, NT proBNP=N-terminal prohormone of brain natriuretic peptide, RR=relative risk. The figure is taken from (169).

CD40L-CD40 signaling pathway has been recognized as a key player in developing autoimmune diseases and CVD. However, whether targeting the cascade is harmful or beneficial is still controversial (169). This study showed that CD40L-CD40 signaling is linked to leukocyte activation, oxidative stress, and inflammation. Further, we could demonstrate that CD40-TRAF6 signaling is associated with major pathomechanism in the progression of diabetes and hypertension. From these mouse data, we conclude that especially CD40-TRAF6-mediated signaling seems to be important in mediating cardiovascular complications. CD40L-CD40 cascade members and associated proteins are upregulated also in CHD patients (Figure 57). In addition, TNFα has been identified as a key mediator in the proteomic and genomic analysis of CHD patients' tissue. However, in this study, we could not clarify if the CHD patient's comorbidities or other factors (for example, sincerity of cardiovascular event, other pre-existing diseases, patient’s lifestyle, or age) lead to the observed step-wise increase of inflammatory markers. Nevertheless, it is well known that hypertension and lipid metabolic disorders are important cardiovascular risk factors promoting atherothrombotic vascular diseases like MI and stroke. The targeted CD40-TRAF6 inhibitor therapy could provide a new therapeutic strategy for these diseases, which may circumvent the side effects of a general CD40L or CD40 blockade. It remains unclear if a long-term CD40-TRAF6 inhibitor treatment also provides some risk and if it would also be beneficial in hypertensive or diabetic patients. Further experiments in animals and humans are needed to clarify these questions.

7. Summary

Cardiovascular diseases are the leading cause of disease burden and death worldwide and are fueled by vascular inflammation. Inflammatory pathways involving the CD40L-CD40-TRAF axis play a role in atherosclerosis progression and affect coronary heart disease pathogenesis. TRAF6 has already been identified as being involved in pro-inflammatory processes in atherosclerosis. The present study investigates the involvement of adipocytes in CD40L-CD40-driven inflammation. We used a tissue-specific CD40KO mouse model to answer this question and assessed the impact on hypertension. In addition, CD40-TRAF6 inhibition was tested as a potential therapeutic target to suppress cardiovascular inflammation in hypertensive and diabetic mice. As a translational aspect, we further characterized the CD40L-CD40-TRAF cascade and major markers of thrombosis and inflammation in vascular bypass material and sera from patients with coronary heart disease (CHD) with or without diabetes and/or hypertension as comorbidity.

Arterial hypertension in mice was induced via angiotensin-II (AT-II) infusion by s.c. osmotic minipumps. The hypertensive global and tissue-specific CD40KO mouse models showed only a minor effect on endothelial function, systolic blood pressure, and oxidative stress in aortic tissue. Therefore, we conclude that adipocytes are not the main drivers of CD40L-CD40-TRAF6-mediated inflammation. We suggest focusing more on macrophage-driven inflammation in the future. In addition, hypertensive WT mice were treated with a TRAF6 inhibitor. TRAF6 inhibition showed vasoprotective and cardioprotective properties in hypertensive WT mice. Isometric tension studies demonstrated improved endothelial function. Also, decreased systolic blood pressure via tail cuff measurement, reduced inflammatory protein marker expression via Western blotting, and decreased oxidative stress levels via DHE-cryo stainings and oxidatively modified proteins were observed in the aortic or cardiac tissue of TRAF6 inhibitor-treated hypertensive animals. In addition, FACS analysis revealed that TRAF6 inhibition in hypertensive animals leads to reduced inflammation observed by reduced CD45+ leukocyte, Ly6G+/Ly6C+ neutrophil, and Ly6C high inflammatory monocyte infiltration into aortic tissue. In the diabetic mouse model (db/db mice), TRAF6 inhibition led to significantly decreased protein expression of different inflammatory and oxidative stress markers, for example, CD40L, p-47^{phox}, NOX2, and eNOS. In CHD patients, our initial Olink-targeted plasma proteomic analysis showed a stepwise increase in markers of atherothrombosis and endothelial cell activation with each additional comorbidity. In addition, specific gene clusters correlating with the comorbidities were identified in isolated aortic mRNA through next-generation sequencing.

In summary, our data shows that TRAF6 inhibition can reduce pathophysiological vascular inflammation and oxidative damage in hypertensive mice and that TRAF6 inhibition could be a suitable candidate for a therapeutic approach in hypertensive patients.

8. Zusammenfassung

Herz-Kreislauf-Erkrankungen zählen weltweit zu den häufigsten Erkrankungen bzw. Todesursachen und werden vor allem durch Gefäßentzündungen begünstigt. An den Entzündungsprozessen, die ein Fortschreiten von Atherosklerose und die Pathogenese von koronaren Herzkrankheiten beeinflussen, ist die CD40L-CD40-TRAF Signalkaskade beteiligt. Es konnte bereits gezeigt werden, dass TRAF6 maßgeblich an pro-inflammatorischen atherosklerotischen Prozessen beteiligt ist. In dieser Studie wurden die Auswirkungen einer globalen sowie Adipozyten spezifischen CD40 Deletion in einem hypertensivem Mausmodell untersucht. Darüber hinaus wurde die pharmakologische Hemmung des CD40-TRAF6 Signalweges als potenzielles therapeutisches Ziel zur Unterdrückung kardiovaskulärer Entzündungen in hypertensiven und diabetischen Mäusen untersucht. Als translationalen Ansatz wurden die CD40L-CD40-TRAF Signalkaskade, sowie Thrombose- und Entzündungsmarker in Aortengewebe und Serum von Patienten mit einer koronaren Herzerkrankung (KHK) mit oder ohne Diabetes und/oder Hypertonie als Komorbidität charakterisiert.

Im Mausmodell wurde die arterielle Hypertonie durch eine Angiotensin-II (AT-II) Infusion über s.c. osmotische Minipumpen induziert. Dabei zeigten die globalen und gewebespezifischen $CD40^{-/-}$ Mausmodelle nur einen geringen Einfluss auf die Endothelfunktion, den systolischen Blutdruck und den oxidativen Stress in Aortengewebe. Adipozyten scheinen daher nicht maßgeblich an den von CD40L-CD40-TRAF6-vermittelten Entzündungsprozessen beteiligt zu sein. In zukünftigen Studien werden wir uns auf die durch Makrophagen vermittelten Entzündungsprozesse fokussieren. Weiterhin zeigte in hypertensiven Mäusen eine TRAF6 Hemmung einen vasoprotektiven und kardioprotektiven Phänotyp. Isometrische Spannungsstudien haben eine verbesserte endotheliale Funktion gezeigt. Außerdem wurden im Aorten- und Herzgewebe von mit TRAF6-Inhibitoren behandelten hypertensiven Tieren ein verringerter systolischer Blutdruck, eine verringerte Expression von Entzündungsproteinmarkern durch Western Blotting und eine Reduktion des oxidativen Stresses durch DHE-Cryo-Färbungen und oxidativ modifizierte Proteine beobachtet. FACS-Analysen zeigten im Aortengewebe, von hypertensiven mit TRAF6 Inhibitor behandelten Tieren, eine geringe Infiltration von CD45+ Leukozyten, Ly6G+/Ly6C+ Neutrophilen und Ly6C-reichen entzündlichen Monozyten. Diese Beobachtung lässt auf eine verminderte Entzündungsreaktion schließen. Im diabetischen Mausmodell (db/db-Mäuse) führte die Hemmung von TRAF6 zu einer signifikant verringerten Proteinexpression verschiedener Entzündungs- und oxidativer Stressmarker, z. B. CD40L, p-47^{phox}, NOX2 und eNOS. Bei KHK-Patienten zeigte unsere anfängliche Olink Plasmaproteomanalyse einen schrittweisen Anstieg von Markern für Atherothrombose und Endothelzellaktivierung mit jeder zusätzlichen Komorbidität. Darüber hinaus wurde durch Sequenzierung isolierter mRNA aus Aortengewebe

spezifische Gencluster identifiziert, die mit den Komorbiditäten (Hypertonie und/oder Diabetes) korrelieren.

Zusammenfassend zeigen unsere Daten, dass die Hemmung von TRAF6 pathologische vaskuläre Entzündungen und oxidative Schäden bei hypertensiven Mäusen reduzieren kann und dass die Hemmung von TRAF6 ein geeigneter Kandidat für einen therapeutischen Ansatz bei hypertensiven Patienten sein könnte.

9. References

1. WorldHealthOrganization. Cardiovascular diseases (CVDs) https://www.who.int/news-room/fact-sheets/detail/cardiovascular-diseases-(cvds) (accessed on 26.05.2024).
2. WorldHealthOrganization. The top 10 causes of death https://www.who.int/news-room/fact-sheets/detail/the-top-10-causes-of-death (accessed on 15.02.2024).
3. Global burden of 369 diseases and injuries in 204 countries and territories, 1990-2019: a systematic analysis for the Global Burden of Disease Study 2019. Lancet. 2020;396(10258):1204-22.
4. Global burden of 87 risk factors in 204 countries and territories, 1990-2019: a systematic analysis for the Global Burden of Disease Study 2019. Lancet. 2020;396(10258):1223-49.
5. Daiber A, Oelze M, Daub S, Steven S, Schuff A, Kröller-Schön S, et al. Vascular Redox Signaling, Redox Switches in Endothelial Nitric Oxide Synthase (eNOS Uncoupling), and Endothelial Dysfunction. In: Laher I, editor. Systems Biology of Free Radicals and Antioxidants. Berlin, Heidelberg: Springer Berlin Heidelberg; 2014. p. 1177-211.
6. Cai H, Harrison DG. Endothelial dysfunction in cardiovascular diseases: the role of oxidant stress. Circ Res. 2000;87(10):840-4.
7. Sies H. Oxidative stress: a concept in redox biology and medicine. Redox Biol. 2015;4:180-3.
8. Brennan ML, Wu W, Fu X, Shen Z, Song W, Frost H, et al. A tale of two controversies: defining both the role of peroxidases in nitrotyrosine formation in vivo using eosinophil peroxidase and myeloperoxidase-deficient mice, and the nature of peroxidase-generated reactive nitrogen species. J Biol Chem. 2002;277(20):17415-27.
9. Sena CM, Leandro A, Azul L, Seiça R, Perry G. Vascular Oxidative Stress: Impact and Therapeutic Approaches. Front Physiol. 2018;9:1668.
10. Förstermann U, Sessa WC. Nitric oxide synthases: regulation and function. Eur Heart J. 2012;33(7):829-37, 37a-37d.
11. Togashi H, Sakuma I, Yoshioka M, Kobayashi T, Yasuda H, Kitabatake A, et al. A central nervous system action of nitric oxide in blood pressure regulation. J Pharmacol Exp Ther. 1992;262(1):343-7.
12. Melikian N, Seddon MD, Casadei B, Chowienczyk PJ, Shah AM. Neuronal nitric oxide synthase and human vascular regulation. Trends Cardiovasc Med. 2009;19(8):256-62.
13. Steinert JR, Chernova T, Forsythe ID. Nitric oxide signaling in brain function, dysfunction, and dementia. Neuroscientist. 2010;16(4):435-52.
14. Wink DA, Kasprzak KS, Maragos CM, Elespuru RK, Misra M, Dunams TM, et al. DNA deaminating ability and genotoxicity of nitric oxide and its progenitors. Science. 1991;254(5034):1001-3.
15. Nathan CF, Hibbs JB, Jr. Role of nitric oxide synthesis in macrophage antimicrobial activity. Curr Opin Immunol. 1991;3(1):65-70.
16. Abramson SB, Amin AR, Clancy RM, Attur M. The role of nitric oxide in tissue destruction. Best Pract Res Clin Rheumatol. 2001;15(5):831-45.
17. Lange M, Enkhbaatar P, Nakano Y, Traber DL. Role of nitric oxide in shock: the large animal perspective. Front Biosci (Landmark Ed). 2009;14(5):1979-89.
18. Fleming I, Busse R. Molecular mechanisms involved in the regulation of the endothelial nitric oxide synthase. Am J Physiol Regul Integr Comp Physiol. 2003;284(1):R1-12.
19. McCabe TJ, Fulton D, Roman LJ, Sessa WC. Enhanced electron flux and reduced calmodulin dissociation may explain "calcium-independent" eNOS activation by phosphorylation. J Biol Chem. 2000;275(9):6123-8.

20. Schleicher M, Yu J, Murata T, Derakhshan B, Atochin D, Qian L, et al. The Akt1-eNOS axis illustrates the specificity of kinase-substrate relationships in vivo. Sci Signal. 2009;2(82):ra41.
21. Lin MI, Fulton D, Babbitt R, Fleming I, Busse R, Pritchard KA, Jr., et al. Phosphorylation of threonine 497 in endothelial nitric-oxide synthase coordinates the coupling of L-arginine metabolism to efficient nitric oxide production. J Biol Chem. 2003;278(45):44719-26.
22. Ignarro LJ, Harbison RG, Wood KS, Kadowitz PJ. Activation of purified soluble guanylate cyclase by endothelium-derived relaxing factor from intrapulmonary artery and vein: stimulation by acetylcholine, bradykinin and arachidonic acid. J Pharmacol Exp Ther. 1986;237(3):893-900.
23. Alheid U, Frölich JC, Förstermann U. Endothelium-derived relaxing factor from cultured human endothelial cells inhibits aggregation of human platelets. Thromb Res. 1987;47(5):561-71.
24. Rudic RD, Shesely EG, Maeda N, Smithies O, Segal SS, Sessa WC. Direct evidence for the importance of endothelium-derived nitric oxide in vascular remodeling. J Clin Invest. 1998;101(4):731-6.
25. Zeiher AM, Fisslthaler B, Schray-Utz B, Busse R. Nitric oxide modulates the expression of monocyte chemoattractant protein 1 in cultured human endothelial cells. Circ Res. 1995;76(6):980-6.
26. Dimmeler S, Zeiher AM. Nitric oxide-an endothelial cell survival factor. Cell Death Differ. 1999;6(10):964-8.
27. Murohara T, Asahara T, Silver M, Bauters C, Masuda H, Kalka C, et al. Nitric oxide synthase modulates angiogenesis in response to tissue ischemia. J Clin Invest. 1998;101(11):2567-78.
28. Aicher A, Heeschen C, Mildner-Rihm C, Urbich C, Ihling C, Technau-Ihling K, et al. Essential role of endothelial nitric oxide synthase for mobilization of stem and progenitor cells. Nat Med. 2003;9(11):1370-6.
29. Weilue H, Maria Paula K, Eyerusalem G, Sijia L. Nitric Oxide and Oxidative Stress-Mediated Cardiovascular Functionality: From Molecular Mechanism to Cardiovascular Disease. In: Marcelo, editor. Vascular Biology. Rijeka: IntechOpen; 2019. p. Ch. 1.
30. Sabe SA, Feng J, Sellke FW, Abid MR. Mechanisms and clinical implications of endothelium-dependent vasomotor dysfunction in coronary microvasculature. Am J Physiol Heart Circ Physiol. 2022;322(5):H819-h41.
31. Schlossmann J, Ammendola A, Ashman K, Zong X, Huber A, Neubauer G, et al. Regulation of intracellular calcium by a signalling complex of IRAG, IP3 receptor and cGMP kinase Ibeta. Nature. 2000;404(6774):197-201.
32. Casteel DE, Zhang T, Zhuang S, Pilz RB. cGMP-dependent protein kinase anchoring by IRAG regulates its nuclear translocation and transcriptional activity. Cell Signal. 2008;20(7):1392-9.
33. Hofmann F, Ammendola A, Schlossmann J. Rising behind NO: cGMP-dependent protein kinases. J Cell Sci. 2000;113 (Pt 10):1671-6.
34. Cornwell TL, Arnold E, Boerth NJ, Lincoln TM. Inhibition of smooth muscle cell growth by nitric oxide and activation of cAMP-dependent protein kinase by cGMP. Am J Physiol. 1994;267(5 Pt 1):C1405-13.
35. Benz PM, Blume C, Seifert S, Wilhelm S, Waschke J, Schuh K, et al. Differential VASP phosphorylation controls remodeling of the actin cytoskeleton. J Cell Sci. 2009;122(Pt 21):3954-65.

36. Chen L, Daum G, Chitaley K, Coats SA, Bowen-Pope DF, Eigenthaler M, et al. Vasodilator-stimulated phosphoprotein regulates proliferation and growth inhibition by nitric oxide in vascular smooth muscle cells. Arterioscler Thromb Vasc Biol. 2004;24(8):1403-8.
37. Najjar RS, Schwartz AM, Wong BJ, Mehta PK, Feresin RG. Berries and Their Polyphenols as a Potential Therapy for Coronary Microvascular Dysfunction: A Mini-Review. Int J Mol Sci. 2021;22(7).
38. Matsushima S, Tsutsui H, Sadoshima J. Physiological and pathological functions of NADPH oxidases during myocardial ischemia-reperfusion. Trends Cardiovasc Med. 2014;24(5):202-5.
39. Konior A, Schramm A, Czesnikiewicz-Guzik M, Guzik TJ. NADPH oxidases in vascular pathology. Antioxid Redox Signal. 2014;20(17):2794-814.
40. Amanso AM, Griendling KK. Differential roles of NADPH oxidases in vascular physiology and pathophysiology. Front Biosci (Schol Ed). 2012;4(3):1044-64.
41. Förstermann U, Xia N, Li H. Roles of Vascular Oxidative Stress and Nitric Oxide in the Pathogenesis of Atherosclerosis. Circ Res. 2017;120(4):713-35.
42. Loperena R, Harrison DG. Oxidative Stress and Hypertensive Diseases. Med Clin North Am. 2017;101(1):169-93.
43. Cai H, Griendling KK, Harrison DG. The vascular NAD(P)H oxidases as therapeutic targets in cardiovascular diseases. Trends Pharmacol Sci. 2003;24(9):471-8.
44. Zhang Y, Murugesan P, Huang K, Cai H. NADPH oxidases and oxidase crosstalk in cardiovascular diseases: novel therapeutic targets. Nat Rev Cardiol. 2020;17(3):170-94.
45. Vermot A, Petit-Härtlein I, Smith SME, Fieschi F. NADPH Oxidases (NOX): An Overview from Discovery, Molecular Mechanisms to Physiology and Pathology. Antioxidants (Basel). 2021;10(6).
46. Helmcke I, Heumüller S, Tikkanen R, Schröder K, Brandes RP. Identification of structural elements in Nox1 and Nox4 controlling localization and activity. Antioxid Redox Signal. 2009;11(6):1279-87.
47. Münzel T, Gori T, Bruno RM, Taddei S. Is oxidative stress a therapeutic target in cardiovascular disease? Eur Heart J. 2010;31(22):2741-8.
48. Matsuno K, Yamada H, Iwata K, Jin D, Katsuyama M, Matsuki M, et al. Nox1 is involved in angiotensin II-mediated hypertension: a study in Nox1-deficient mice. Circulation. 2005;112(17):2677-85.
49. Gavazzi G, Banfi B, Deffert C, Fiette L, Schappi M, Herrmann F, et al. Decreased blood pressure in NOX1-deficient mice. FEBS Lett. 2006;580(2):497-504.
50. Altenhöfer S, Kleikers PWM, Radermacher KA, Scheurer P, Rob Hermans JJ, Schiffers P, et al. The NOX toolbox: validating the role of NADPH oxidases in physiology and disease. Cellular and Molecular Life Sciences. 2012;69(14):2327-43.
51. Kleinschnitz C, Grund H, Wingler K, Armitage ME, Jones E, Mittal M, et al. Post-stroke inhibition of induced NADPH oxidase type 4 prevents oxidative stress and neurodegeneration. PLoS Biol. 2010;8(9).
52. Datla SR, Peshavariya H, Dusting GJ, Mahadev K, Goldstein BJ, Jiang F. Important role of Nox4 type NADPH oxidase in angiogenic responses in human microvascular endothelial cells in vitro. Arterioscler Thromb Vasc Biol. 2007;27(11):2319-24.
53. Zhang Q, Malik P, Pandey D, Gupta S, Jagnandan D, Belin de Chantemele E, et al. Paradoxical activation of endothelial nitric oxide synthase by NADPH oxidase. Arterioscler Thromb Vasc Biol. 2008;28(9):1627-33.
54. Schulz E, Münzel T. NOX5, a new "radical" player in human atherosclerosis? J Am Coll Cardiol. 2008;52(22):1810-2.

55. Daiber A. Redox signaling (cross-talk) from and to mitochondria involves mitochondrial pores and reactive oxygen species. Biochim Biophys Acta. 2010;1797(6-7):897-906.
56. Daiber A, Di Lisa F, Oelze M, Kröller-Schön S, Steven S, Schulz E, et al. Crosstalk of mitochondria with NADPH oxidase via reactive oxygen and nitrogen species signalling and its role for vascular function. Br J Pharmacol. 2017;174(12):1670-89.
57. Anilkumar N, Sirker A, Shah AM. Redox sensitive signaling pathways in cardiac remodeling, hypertrophy and failure. Front Biosci (Landmark Ed). 2009;14(8):3168-87.
58. Thannickal VJ, Fanburg BL. Reactive oxygen species in cell signaling. Am J Physiol Lung Cell Mol Physiol. 2000;279(6):L1005-28.
59. Bartesaghi S, Radi R. Fundamentals on the biochemistry of peroxynitrite and protein tyrosine nitration. Redox Biol. 2018;14:618-25.
60. Zhang L, Wang X, Cueto R, Effi C, Zhang Y, Tan H, et al. Biochemical basis and metabolic interplay of redox regulation. Redox Biol. 2019;26:101284.
61. Pacher P, Beckman JS, Liaudet L. Nitric oxide and peroxynitrite in health and disease. Physiol Rev. 2007;87(1):315-424.
62. Münzel T, Daiber A. Vascular Redox Signaling, Endothelial Nitric Oxide Synthase Uncoupling, and Endothelial Dysfunction in the Setting of Transportation Noise Exposure or Chronic Treatment with Organic Nitrates. Antioxid Redox Signal. 2023;38(13-15):1001-21.
63. Laursen JB, Somers M, Kurz S, McCann L, Warnholtz A, Freeman BA, et al. Endothelial regulation of vasomotion in apoE-deficient mice: implications for interactions between peroxynitrite and tetrahydrobiopterin. Circulation. 2001;103(9):1282-8.
64. Shinozaki K, Kashiwagi A, Nishio Y, Okamura T, Yoshida Y, Masada M, et al. Abnormal biopterin metabolism is a major cause of impaired endothelium-dependent relaxation through nitric oxide/O2- imbalance in insulin-resistant rat aorta. Diabetes. 1999;48(12):2437-45.
65. Landmesser U, Dikalov S, Price SR, McCann L, Fukai T, Holland SM, et al. Oxidation of tetrahydrobiopterin leads to uncoupling of endothelial cell nitric oxide synthase in hypertension. J Clin Invest. 2003;111(8):1201-9.
66. Daiber A, Xia N, Steven S, Oelze M, Hanf A, Kröller-Schön S, et al. New Therapeutic Implications of Endothelial Nitric Oxide Synthase (eNOS) Function/Dysfunction in Cardiovascular Disease. Int J Mol Sci. 2019;20(1).
67. Parkin J, Cohen B. An overview of the immune system. Lancet. 2001;357(9270):1777-89.
68. Kellie S, Al-Mansour Z. Chapter Four - Overview of the Immune System. In: Skwarczynski M, Toth I, editors. Micro and Nanotechnology in Vaccine Development: William Andrew Publishing; 2017. p. 63-81.
69. Aderem A, Underhill DM. Mechanisms of phagocytosis in macrophages. Annu Rev Immunol. 1999;17:593-623.
70. Bogdan C. Nitric oxide synthase in innate and adaptive immunity: an update. Trends Immunol. 2015;36(3):161-78.
71. Nauseef WM, Borregaard N. Neutrophils at work. Nat Immunol. 2014;15(7):602-11.
72. Mellman I. Dendritic cells: master regulators of the immune response. Cancer Immunol Res. 2013;1(3):145-9.
73. Long EO, Kim HS, Liu D, Peterson ME, Rajagopalan S. Controlling natural killer cell responses: integration of signals for activation and inhibition. Annu Rev Immunol. 2013;31:227-58.
74. Zhu X, Zhu J. CD4 T Helper Cell Subsets and Related Human Immunological Disorders. Int J Mol Sci. 2020;21(21).

75. Crotty S. T Follicular Helper Cell Biology: A Decade of Discovery and Diseases. Immunity. 2019;50(5):1132-48.
76. Li X, Zheng Y. Regulatory T cell identity: formation and maintenance. Trends Immunol. 2015;36(6):344-53.
77. Kulinski JM, Tarakanova VL, Verbsky J. Regulation of antiviral CD8 T-cell responses. Crit Rev Immunol. 2013;33(6):477-88.
78. Torang A, Gupta P, Klinke DJ, 2nd. An elastic-net logistic regression approach to generate classifiers and gene signatures for types of immune cells and T helper cell subsets. BMC Bioinformatics. 2019;20(1):433.
79. Wenzel P, Kossmann S, Münzel T, Daiber A. Redox regulation of cardiovascular inflammation - Immunomodulatory function of mitochondrial and Nox-derived reactive oxygen and nitrogen species. Free Radic Biol Med. 2017;109:48-60.
80. Yin H, Wu M, Lu Y, Wu X, Yu B, Chen R, et al. HMGB1-activatied NLRP3 inflammasome induces thrombocytopenia in heatstroke rat. PeerJ. 2022;10:e13799.
81. Medina-Leyte DJ, Zepeda-García O, Domínguez-Pérez M, González-Garrido A, Villarreal-Molina T, Jacobo-Albavera L. Endothelial Dysfunction, Inflammation and Coronary Artery Disease: Potential Biomarkers and Promising Therapeutical Approaches. Int J Mol Sci. 2021;22(8).
82. Libby P, Buring JE, Badimon L, Hansson GK, Deanfield J, Bittencourt MS, et al. Atherosclerosis. Nat Rev Dis Primers. 2019;5(1):56.
83. Pries AR, Secomb TW, Gaehtgens P. The endothelial surface layer. Pflugers Arch. 2000;440(5):653-66.
84. Roy P, Orecchioni M, Ley K. How the immune system shapes atherosclerosis: roles of innate and adaptive immunity. Nature Reviews Immunology. 2022;22(4):251-65.
85. Navab M, Ananthramaiah GM, Reddy ST, Van Lenten BJ, Ansell BJ, Fonarow GC, et al. The oxidation hypothesis of atherogenesis: the role of oxidized phospholipids and HDL. J Lipid Res. 2004;45(6):993-1007.
86. Ference BA, Ginsberg HN, Graham I, Ray KK, Packard CJ, Bruckert E, et al. Low-density lipoproteins cause atherosclerotic cardiovascular disease. 1. Evidence from genetic, epidemiologic, and clinical studies. A consensus statement from the European Atherosclerosis Society Consensus Panel. Eur Heart J. 2017;38(32):2459-72.
87. Legein B, Temmerman L, Biessen EAL, Lutgens E. Inflammation and immune system interactions in atherosclerosis. Cellular and Molecular Life Sciences. 2013;70(20):3847-69.
88. Woollard KJ, Geissmann F. Monocytes in atherosclerosis: subsets and functions. Nat Rev Cardiol. 2010;7(2):77-86.
89. Geissmann F, Jung S, Littman DR. Blood monocytes consist of two principal subsets with distinct migratory properties. Immunity. 2003;19(1):71-82.
90. Moore KJ, Tabas I. Macrophages in the pathogenesis of atherosclerosis. Cell. 2011;145(3):341-55.
91. Chinetti-Gbaguidi G, Baron M, Bouhlel MA, Vanhoutte J, Copin C, Sebti Y, et al. Human atherosclerotic plaque alternative macrophages display low cholesterol handling but high phagocytosis because of distinct activities of the PPARγ and LXRα pathways. Circ Res. 2011;108(8):985-95.
92. Martinez FO, Sica A, Mantovani A, Locati M. Macrophage activation and polarization. Front Biosci. 2008;13:453-61.
93. Bdeir K, Cane W, Canziani G, Chaiken I, Weisel J, Koschinsky ML, et al. Defensin promotes the binding of lipoprotein(a) to vascular matrix. Blood. 1999;94(6):2007-19.

94. Chatzizisis YS, Coskun AU, Jonas M, Edelman ER, Feldman CL, Stone PH. Role of endothelial shear stress in the natural history of coronary atherosclerosis and vascular remodeling: molecular, cellular, and vascular behavior. J Am Coll Cardiol. 2007;49(25):2379-93.
95. Bennett MR, Sinha S, Owens GK. Vascular Smooth Muscle Cells in Atherosclerosis. Circ Res. 2016;118(4):692-702.
96. Clarke MC, Talib S, Figg NL, Bennett MR. Vascular smooth muscle cell apoptosis induces interleukin-1-directed inflammation: effects of hyperlipidemia-mediated inhibition of phagocytosis. Circ Res. 2010;106(2):363-72.
97. Yurdagul A, Jr., Doran AC, Cai B, Fredman G, Tabas IA. Mechanisms and Consequences of Defective Efferocytosis in Atherosclerosis. Front Cardiovasc Med. 2017;4:86.
98. Galis ZS, Sukhova GK, Lark MW, Libby P. Increased expression of matrix metalloproteinases and matrix degrading activity in vulnerable regions of human atherosclerotic plaques. J Clin Invest. 1994;94(6):2493-503.
99. Galis ZS, Muszynski M, Sukhova GK, Simon-Morrissey E, Unemori EN, Lark MW, et al. Cytokine-stimulated human vascular smooth muscle cells synthesize a complement of enzymes required for extracellular matrix digestion. Circ Res. 1994;75(1):181-9.
100. Libby P. Mechanisms of acute coronary syndromes and their implications for therapy. N Engl J Med. 2013;368(21):2004-13.
101. Piepoli MF, Hoes AW, Agewall S, Albus C, Brotons C, Catapano AL, et al. 2016 European Guidelines on cardiovascular disease prevention in clinical practice: The Sixth Joint Task Force of the European Society of Cardiology and Other Societies on Cardiovascular Disease Prevention in Clinical Practice (constituted by representatives of 10 societies and by invited experts)Developed with the special contribution of the European Association for Cardiovascular Prevention & Rehabilitation (EACPR). Eur Heart J. 2016;37(29):2315-81.
102. Stone NJ, Robinson JG, Lichtenstein AH, Bairey Merz CN, Blum CB, Eckel RH, et al. 2013 ACC/AHA guideline on the treatment of blood cholesterol to reduce atherosclerotic cardiovascular risk in adults: a report of the American College of Cardiology/American Heart Association Task Force on Practice Guidelines. Circulation. 2014;129(25 Suppl 2):S1-45.
103. Baigent C, Blackwell L, Emberson J, Holland LE, Reith C, Bhala N, et al. Efficacy and safety of more intensive lowering of LDL cholesterol: a meta-analysis of data from 170,000 participants in 26 randomised trials. Lancet. 2010;376(9753):1670-81.
104. Hammersley D, Signy M. Ezetimibe: an update on its clinical usefulness in specific patient groups. Ther Adv Chronic Dis. 2017;8(1):4-11.
105. Collaborative meta-analysis of randomised trials of antiplatelet therapy for prevention of death, myocardial infarction, and stroke in high risk patients. Bmj. 2002;324(7329):71-86.
106. Zheng SL, Roddick AJ. Association of Aspirin Use for Primary Prevention With Cardiovascular Events and Bleeding Events: A Systematic Review and Meta-analysis. Jama. 2019;321(3):277-87.
107. Ridker PM, Everett BM, Thuren T, MacFadyen JG, Chang WH, Ballantyne C, et al. Antiinflammatory Therapy with Canakinumab for Atherosclerotic Disease. N Engl J Med. 2017;377(12):1119-31.
108. Ridker PM, MacFadyen JG, Thuren T, Everett BM, Libby P, Glynn RJ. Effect of interleukin-1β inhibition with canakinumab on incident lung cancer in patients with atherosclerosis: exploratory results from a randomised, double-blind, placebo-controlled trial. Lancet. 2017;390(10105):1833-42.
109. Tardif JC, Kouz S, Waters DD, Bertrand OF, Diaz R, Maggioni AP, et al. Efficacy and Safety of Low-Dose Colchicine after Myocardial Infarction. N Engl J Med. 2019;381(26):2497-505.

110. Ridker PM, Everett BM, Pradhan A, MacFadyen JG, Solomon DH, Zaharris E, et al. Low-Dose Methotrexate for the Prevention of Atherosclerotic Events. N Engl J Med. 2019;380(8):752-62.
111. WorldHealthOrganization. Hypertension https://www.who.int/news-room/fact-sheets/detail/hypertension (accessed on 20.02.2024).
112. Mancia G, Kreutz R, Brunström M, Burnier M, Grassi G, Januszewicz A, et al. 2023 ESH Guidelines for the management of arterial hypertension The Task Force for the management of arterial hypertension of the European Society of Hypertension: Endorsed by the International Society of Hypertension (ISH) and the European Renal Association (ERA). J Hypertens. 2023;41(12):1874-2071.
113. Münzel T, Schmidt FP, Steven S, Herzog J, Daiber A, Sørensen M. Environmental Noise and the Cardiovascular System. J Am Coll Cardiol. 2018;71(6):688-97.
114. Münzel T, Miller MR, Sørensen M, Lelieveld J, Daiber A, Rajagopalan S. Reduction of environmental pollutants for prevention of cardiovascular disease: it's time to act. Eur Heart J. 2020;41(41):3989-97.
115. Wu CH, Mohammadmoradi S, Chen JZ, Sawada H, Daugherty A, Lu HS. Renin-Angiotensin System and Cardiovascular Functions. Arterioscler Thromb Vasc Biol. 2018;38(7):e108-e16.
116. Lavoie JL, Sigmund CD. Minireview: overview of the renin-angiotensin system--an endocrine and paracrine system. Endocrinology. 2003;144(6):2179-83.
117. Oparil S, Acelajado MC, Bakris GL, Berlowitz DR, Cífková R, Dominiczak AF, et al. Hypertension. Nat Rev Dis Primers. 2018;4:18014.
118. Verma K, Pant M, Paliwal S, Dwivedi J, Sharma S. An Insight on Multicentric Signaling of Angiotensin II in Cardiovascular system: A Recent Update. Front Pharmacol. 2021;12:734917.
119. Te Riet L, van Esch JH, Roks AJ, van den Meiracker AH, Danser AH. Hypertension: renin-angiotensin-aldosterone system alterations. Circ Res. 2015;116(6):960-75.
120. Dridi H, Santulli G, Gambardella J, Jankauskas SS, Yuan Q, Yang J, et al. IP3 receptor orchestrates maladaptive vascular responses in heart failure. J Clin Invest. 2022;132(4).
121. Birk M, Baum E, Zadeh JK, Manicam C, Pfeiffer N, Patzak A, et al. Angiotensin II Induces Oxidative Stress and Endothelial Dysfunction in Mouse Ophthalmic Arteries via Involvement of AT1 Receptors and NOX2. Antioxidants (Basel). 2021;10(8).
122. Wang S, Cheng M, Hu Z, Hu S, Zou Q, Lai X, et al. Angiotensin II Facilitates Matrix Metalloproteinase-9-Mediated Myosin Light Chain Kinase Degradation in Pressure Overload-Induced Cardiac Hypertrophy. Cell Physiol Biochem. 2017;44(6):2281-95.
123. Lee CY, Park HK, Lee BS, Jeong S, Hyun SA, Choi JW, et al. Novel Therapeutic Effects of Pterosin B on Ang II-Induced Cardiomyocyte Hypertrophy. Molecules. 2020;25(22).
124. Kranzhöfer R, Schmidt J, Pfeiffer CA, Hagl S, Libby P, Kübler W. Angiotensin induces inflammatory activation of human vascular smooth muscle cells. Arterioscler Thromb Vasc Biol. 1999;19(7):1623-9.
125. Tummala PE, Chen XL, Sundell CL, Laursen JB, Hammes CP, Alexander RW, et al. Angiotensin II induces vascular cell adhesion molecule-1 expression in rat vasculature: A potential link between the renin-angiotensin system and atherosclerosis. Circulation. 1999;100(11):1223-9.
126. Ma Z, Viswanathan G, Sellig M, Jassal C, Choi I, Garikipati A, et al. β-Arrestin-Mediated Angiotensin II Type 1 Receptor Activation Promotes Pulmonary Vascular Remodeling in Pulmonary Hypertension. JACC Basic Transl Sci. 2021;6(11):854-69.

127. Matsuda S, Umemoto S, Yoshimura K, Itoh S, Murata T, Fukai T, et al. Angiotensin Ⅱ Activates MCP-1 and Induces Cardiac Hypertrophy and Dysfunction via Toll-like Receptor 4. J Atheroscler Thromb. 2015;22(8):833-44.
128. Kawai T, Forrester SJ, O'Brien S, Baggett A, Rizzo V, Eguchi S. AT1 receptor signaling pathways in the cardiovascular system. Pharmacol Res. 2017;125(Pt A):4-13.
129. WorldHealthOrganization. Diabetes https://www.who.int/news-room/fact-sheets/detail/diabetes (accessed on 04.03.2024).
130. Sun H, Saeedi P, Karuranga S, Pinkepank M, Ogurtsova K, Duncan BB, et al. IDF Diabetes Atlas: Global, regional and country-level diabetes prevalence estimates for 2021 and projections for 2045. Diabetes Res Clin Pract. 2022;183:109119.
131. Marx N, Federici M, Schütt K, Müller-Wieland D, Ajjan RA, Antunes MJ, et al. 2023 ESC Guidelines for the management of cardiovascular disease in patients with diabetes. Eur Heart J. 2023;44(39):4043-140.
132. Galicia-Garcia U, Benito-Vicente A, Jebari S, Larrea-Sebal A, Siddiqi H, Uribe KB, et al. Pathophysiology of Type 2 Diabetes Mellitus. Int J Mol Sci. 2020;21(17).
133. Fu Z, Gilbert ER, Liu D. Regulation of insulin synthesis and secretion and pancreatic Beta-cell dysfunction in diabetes. Curr Diabetes Rev. 2013;9(1):25-53.
134. Boland BB, Rhodes CJ, Grimsby JS. The dynamic plasticity of insulin production in β-cells. Mol Metab. 2017;6(9):958-73.
135. Yamamoto WR, Bone RN, Sohn P, Syed F, Reissaus CA, Mosley AL, et al. Endoplasmic reticulum stress alters ryanodine receptor function in the murine pancreatic β cell. J Biol Chem. 2019;294(1):168-81.
136. Christensen AA, Gannon M. The Beta Cell in Type 2 Diabetes. Curr Diab Rep. 2019;19(9):81.
137. Halban PA, Polonsky KS, Bowden DW, Hawkins MA, Ling C, Mather KJ, et al. β-cell failure in type 2 diabetes: postulated mechanisms and prospects for prevention and treatment. Diabetes Care. 2014;37(6):1751-8.
138. Satoh T. Molecular mechanisms for the regulation of insulin-stimulated glucose uptake by small guanosine triphosphatases in skeletal muscle and adipocytes. Int J Mol Sci. 2014;15(10):18677-92.
139. Venkatasamy VV, Pericherla S, Manthuruthil S, Mishra S, Hanno R. Effect of Physical activity on Insulin Resistance, Inflammation and Oxidative Stress in Diabetes Mellitus. J Clin Diagn Res. 2013;7(8):1764-6.
140. Wu H, Ballantyne CM. Skeletal muscle inflammation and insulin resistance in obesity. J Clin Invest. 2017;127(1):43-54.
141. Gastaldelli A, Gaggini M, DeFronzo RA. Role of Adipose Tissue Insulin Resistance in the Natural History of Type 2 Diabetes: Results From the San Antonio Metabolism Study. Diabetes. 2017;66(4):815-22.
142. Maki KC, Kelley KM, Lawless AL, Hubacher RL, Schild AL, Dicklin MR, et al. Validation of insulin sensitivity and secretion indices derived from the liquid meal tolerance test. Diabetes Technol Ther. 2011;13(6):661-6.
143. Cherrington AD, Moore MC, Sindelar DK, Edgerton DS. Insulin action on the liver in vivo. Biochem Soc Trans. 2007;35(Pt 5):1171-4.
144. Leclercq IA, Da Silva Morais A, Schroyen B, Van Hul N, Geerts A. Insulin resistance in hepatocytes and sinusoidal liver cells: mechanisms and consequences. J Hepatol. 2007;47(1):142-56.
145. Hotamisligil GS. Inflammation and metabolic disorders. Nature. 2006;444(7121):860-7.

146. Vergès B. Pathophysiology of diabetic dyslipidaemia: where are we? Diabetologia. 2015;58(5):886-99.
147. Choi SH, Ginsberg HN. Increased very low density lipoprotein (VLDL) secretion, hepatic steatosis, and insulin resistance. Trends Endocrinol Metab. 2011;22(9):353-63.
148. Steinberg D, Carew TE, Fielding C, Fogelman AM, Mahley RW, Sniderman AD, et al. Lipoproteins and the pathogenesis of atherosclerosis. Circulation. 1989;80(3):719-23.
149. Bernelot Moens SJ, Verweij SL, Schnitzler JG, Stiekema LCA, Bos M, Langsted A, et al. Remnant Cholesterol Elicits Arterial Wall Inflammation and a Multilevel Cellular Immune Response in Humans. Arterioscler Thromb Vasc Biol. 2017;37(5):969-75.
150. Chapman MJ, Ginsberg HN, Amarenco P, Andreotti F, Borén J, Catapano AL, et al. Triglyceride-rich lipoproteins and high-density lipoprotein cholesterol in patients at high risk of cardiovascular disease: evidence and guidance for management. Eur Heart J. 2011;32(11):1345-61.
151. Nordestgaard BG, Varbo A. Triglycerides and cardiovascular disease. Lancet. 2014;384(9943):626-35.
152. Sena CM, Pereira AM, Seiça R. Endothelial dysfunction - a major mediator of diabetic vascular disease. Biochim Biophys Acta. 2013;1832(12):2216-31.
153. Mkhize BC, Mosili P, Ngubane PS, Sibiya NH, Khathi A. The Relationship between Renin-Angiotensin-Aldosterone System (RAAS) Activity, Osteoporosis and Estrogen Deficiency in Type 2 Diabetes. Int J Mol Sci. 2023;24(15).
154. Gutierrez-Rodelo C, Arellano-Plancarte A, Hernandez-Aranda J, Landa-Galvan HV, Parra-Mercado GK, Moreno-Licona NJ, et al. Angiotensin II Inhibits Insulin Receptor Signaling in Adipose Cells. Int J Mol Sci. 2022;23(11).
155. Ramalingam L, Menikdiwela K, LeMieux M, Dufour JM, Kaur G, Kalupahana N, et al. The renin angiotensin system, oxidative stress and mitochondrial function in obesity and insulin resistance. Biochim Biophys Acta Mol Basis Dis. 2017;1863(5):1106-14.
156. Watson AMD, Gould EAM, Moody SC, Sivakumaran P, Sourris KC, Chow BSM, et al. Disparate Effects of Diabetes and Hyperlipidemia on Experimental Kidney Disease. Front Physiol. 2020;11:518.
157. Park CH, Kim HW, Park JT, Chang TI, Yoo TH, Lee J, et al. Intrarenal Renin-Angiotensin System Activation Alters Relationship Between Systolic Blood Pressure and Progression of Chronic Kidney Disease. Hypertension. 2023;80(5):1024-34.
158. Jia G, Aroor AR, Hill MA, Sowers JR. Role of Renin-Angiotensin-Aldosterone System Activation in Promoting Cardiovascular Fibrosis and Stiffness. Hypertension. 2018;72(3):537-48.
159. Cannon CP, Pratley R, Dagogo-Jack S, Mancuso J, Huyck S, Masiukiewicz U, et al. Cardiovascular Outcomes with Ertugliflozin in Type 2 Diabetes. N Engl J Med. 2020;383(15):1425-35.
160. Gerstein HC, Colhoun HM, Dagenais GR, Diaz R, Lakshmanan M, Pais P, et al. Dulaglutide and cardiovascular outcomes in type 2 diabetes (REWIND): a double-blind, randomised placebo-controlled trial. Lancet. 2019;394(10193):121-30.
161. Hernandez AF, Green JB, Janmohamed S, D'Agostino RB, Sr., Granger CB, Jones NP, et al. Albiglutide and cardiovascular outcomes in patients with type 2 diabetes and cardiovascular disease (Harmony Outcomes): a double-blind, randomised placebo-controlled trial. Lancet. 2018;392(10157):1519-29.
162. Wiviott SD, Raz I, Bonaca MP, Mosenzon O, Kato ET, Cahn A, et al. Dapagliflozin and Cardiovascular Outcomes in Type 2 Diabetes. N Engl J Med. 2019;380(4):347-57.

163. McGuire DK, Shih WJ, Cosentino F, Charbonnel B, Cherney DZI, Dagogo-Jack S, et al. Association of SGLT2 Inhibitors With Cardiovascular and Kidney Outcomes in Patients With Type 2 Diabetes: A Meta-analysis. JAMA Cardiol. 2021;6(2):148-58.
164. Scirica BM, Bhatt DL, Braunwald E, Steg PG, Davidson J, Hirshberg B, et al. Saxagliptin and cardiovascular outcomes in patients with type 2 diabetes mellitus. N Engl J Med. 2013;369(14):1317-26.
165. Green JB, Bethel MA, Armstrong PW, Buse JB, Engel SS, Garg J, et al. Effect of Sitagliptin on Cardiovascular Outcomes in Type 2 Diabetes. N Engl J Med. 2015;373(3):232-42.
166. Bosch J, Gerstein HC, Dagenais GR, Díaz R, Dyal L, Jung H, et al. n-3 fatty acids and cardiovascular outcomes in patients with dysglycemia. N Engl J Med. 2012;367(4):309-18.
167. Marso SP, McGuire DK, Zinman B, Poulter NR, Emerson SS, Pieber TR, et al. Efficacy and Safety of Degludec versus Glargine in Type 2 Diabetes. N Engl J Med. 2017;377(8):723-32.
168. Karnell JL, Rieder SA, Ettinger R, Kolbeck R. Targeting the CD40-CD40L pathway in autoimmune diseases: Humoral immunity and beyond. Adv Drug Deliv Rev. 2019;141:92-103.
169. Daub S, Lutgens E, Münzel T, Daiber A. CD40/CD40L and Related Signaling Pathways in Cardiovascular Health and Disease-The Pros and Cons for Cardioprotection. Int J Mol Sci. 2020;21(22).
170. Strohm L, Ubbens H, Münzel T, Daiber A, Daub S. Role of CD40(L)-TRAF signaling in inflammation and resolution-a double-edged sword. Front Pharmacol. 2022;13:995061.
171. Michel NA, Zirlik A, Wolf D. CD40L and Its Receptors in Atherothrombosis-An Update. Front Cardiovasc Med. 2017;4:40.
172. de la Morena MT. Clinical Phenotypes of Hyper-IgM Syndromes. J Allergy Clin Immunol Pract. 2016;4(6):1023-36.
173. Foy TM, Aruffo A, Bajorath J, Buhlmann JE, Noelle RJ. Immune regulation by CD40 and its ligand GP39. Annu Rev Immunol. 1996;14:591-617.
174. Bosmans LA, Bosch L, Kusters PJH, Lutgens E, Seijkens TTP. The CD40-CD40L Dyad as Immunotherapeutic Target in Cardiovascular Disease. J Cardiovasc Transl Res. 2021;14(1):13-22.
175. Zirlik A, Maier C, Gerdes N, MacFarlane L, Soosairajah J, Bavendiek U, et al. CD40 ligand mediates inflammation independently of CD40 by interaction with Mac-1. Circulation. 2007;115(12):1571-80.
176. Léveillé C, Bouillon M, Guo W, Bolduc J, Sharif-Askari E, El-Fakhry Y, et al. CD40 ligand binds to alpha5beta1 integrin and triggers cell signaling. J Biol Chem. 2007;282(8):5143-51.
177. Loubaki L, Semlali A, Boisvert M, Jacques E, Plante S, Aoudjit F, et al. Crosstalk between T cells and bronchial fibroblasts obtained from asthmatic subjects involves CD40L/alpha 5 beta 1 interaction. Mol Immunol. 2010;47(11-12):2112-8.
178. Bian ZM, Field MG, Elner SG, Kahlenberg JM, Elner VM. Distinct CD40L receptors mediate inflammasome activation and secretion of IL-1β and MCP-1 in cultured human retinal pigment epithelial cells. Exp Eye Res. 2018;170:29-39.
179. André P, Prasad KS, Denis CV, He M, Papalia JM, Hynes RO, et al. CD40L stabilizes arterial thrombi by a beta3 integrin--dependent mechanism. Nat Med. 2002;8(3):247-52.
180. Popa M, Tahir S, Elrod J, Kim SH, Leuschner F, Kessler T, et al. Role of CD40 and ADAMTS13 in von Willebrand factor-mediated endothelial cell-platelet-monocyte interaction. Proc Natl Acad Sci U S A. 2018;115(24):E5556-e65.
181. Banchereau J, Dubois B, Fayette J, Burdin N, Brière F, Miossec P, et al. Functional CD40 antigen on B cells, dendritic cells and fibroblasts. Adv Exp Med Biol. 1995;378:79-83.
182. Schönbeck U, Libby P. CD40 signaling and plaque instability. Circ Res. 2001;89(12):1092-103.

183. Bishop GA, Hostager BS. Molecular mechanisms of CD40 signaling. Arch Immunol Ther Exp (Warsz). 2001;49(2):129-37.
184. Bradley JR, Pober JS. Tumor necrosis factor receptor-associated factors (TRAFs). Oncogene. 2001;20(44):6482-91.
185. Wicovsky A, Henkler F, Salzmann S, Scheurich P, Kneitz C, Wajant H. Tumor necrosis factor receptor-associated factor-1 enhances proinflammatory TNF receptor-2 signaling and modifies TNFR1-TNFR2 cooperation. Oncogene. 2009;28(15):1769-81.
186. Arron JR, Pewzner-Jung Y, Walsh MC, Kobayashi T, Choi Y. Regulation of the subcellular localization of tumor necrosis factor receptor-associated factor (TRAF)2 by TRAF1 reveals mechanisms of TRAF2 signaling. J Exp Med. 2002;196(7):923-34.
187. Schwenzer R, Siemienski K, Liptay S, Schubert G, Peters N, Scheurich P, et al. The human tumor necrosis factor (TNF) receptor-associated factor 1 gene (TRAF1) is up-regulated by cytokines of the TNF ligand family and modulates TNF-induced activation of NF-kappaB and c-Jun N-terminal kinase. J Biol Chem. 1999;274(27):19368-74.
188. Edilova MI, Abdul-Sater AA, Watts TH. TRAF1 Signaling in Human Health and Disease. Front Immunol. 2018;9:2969.
189. Tsitsikov EN, Laouini D, Dunn IF, Sannikova TY, Davidson L, Alt FW, et al. TRAF1 is a negative regulator of TNF signaling. enhanced TNF signaling in TRAF1-deficient mice. Immunity. 2001;15(4):647-57.
190. Missiou A, Köstlin N, Varo N, Rudolf P, Aichele P, Ernst S, et al. Tumor necrosis factor receptor-associated factor 1 (TRAF1) deficiency attenuates atherosclerosis in mice by impairing monocyte recruitment to the vessel wall. Circulation. 2010;121(18):2033-44.
191. Park YC, Burkitt V, Villa AR, Tong L, Wu H. Structural basis for self-association and receptor recognition of human TRAF2. Nature. 1999;398(6727):533-8.
192. Lalani AI, Zhu S, Gokhale S, Jin J, Xie P. TRAF molecules in inflammation and inflammatory diseases. Curr Pharmacol Rep. 2018;4(1):64-90.
193. Lin WJ, Su YW, Lu YC, Hao Z, Chio, II, Chen NJ, et al. Crucial role for TNF receptor-associated factor 2 (TRAF2) in regulating NFκB2 signaling that contributes to autoimmunity. Proc Natl Acad Sci U S A. 2011;108(45):18354-9.
194. Yeh WC, Shahinian A, Speiser D, Kraunus J, Billia F, Wakeham A, et al. Early lethality, functional NF-kappaB activation, and increased sensitivity to TNF-induced cell death in TRAF2-deficient mice. Immunity. 1997;7(5):715-25.
195. Divakaran VG, Evans S, Topkara VK, Diwan A, Burchfield J, Gao F, et al. Tumor necrosis factor receptor-associated factor 2 signaling provokes adverse cardiac remodeling in the adult mammalian heart. Circ Heart Fail. 2013;6(3):535-43.
196. Huang Y, Wu D, Zhang X, Jiang M, Hu C, Lin J, et al. Cardiac-specific Traf2 overexpression enhances cardiac hypertrophy through activating AKT/GSK3β signaling. Gene. 2014;536(2):225-31.
197. Devergne O, Hatzivassiliou E, Izumi KM, Kaye KM, Kleijnen MF, Kieff E, et al. Association of TRAF1, TRAF2, and TRAF3 with an Epstein-Barr virus LMP1 domain important for B-lymphocyte transformation: role in NF-kappaB activation. Mol Cell Biol. 1996;16(12):7098-108.
198. Xu Y, Cheng G, Baltimore D. Targeted disruption of TRAF3 leads to postnatal lethality and defective T-dependent immune responses. Immunity. 1996;5(5):407-15.
199. Jiang X, Deng KQ, Luo Y, Jiang DS, Gao L, Zhang XF, et al. Tumor necrosis factor receptor-associated factor 3 is a positive regulator of pathological cardiac hypertrophy. Hypertension. 2015;66(2):356-67.

200. Urbich C, Mallat Z, Tedgui A, Clauss M, Zeiher AM, Dimmeler S. Upregulation of TRAF-3 by shear stress blocks CD40-mediated endothelial activation. J Clin Invest. 2001;108(10):1451-8.
201. Gissler MC, Stachon P, Wolf D, Marchini T. The Role of Tumor Necrosis Factor Associated Factors (TRAFs) in Vascular Inflammation and Atherosclerosis. Front Cardiovasc Med. 2022;9:826630.
202. Pullen SS, Miller HG, Everdeen DS, Dang TT, Crute JJ, Kehry MR. CD40-tumor necrosis factor receptor-associated factor (TRAF) interactions: regulation of CD40 signaling through multiple TRAF binding sites and TRAF hetero-oligomerization. Biochemistry. 1998;37(34):11836-45.
203. Leo E, Welsh K, Matsuzawa S, Zapata JM, Kitada S, Mitchell RS, et al. Differential requirements for tumor necrosis factor receptor-associated factor family proteins in CD40-mediated induction of NF-kappaB and Jun N-terminal kinase activation. J Biol Chem. 1999;274(32):22414-22.
204. Xu W, Zhang L, Ma S, Zhang Y, Cai Z, Zhang K, et al. TRAF5 protects against myocardial ischemia reperfusion injury via AKT signaling. Eur J Pharmacol. 2020;878:173092.
205. Zirlik A, Bavendiek U, Libby P, MacFarlane L, Gerdes N, Jagielska J, et al. TRAF-1, -2, -3, -5, and -6 are induced in atherosclerotic plaques and differentially mediate proinflammatory functions of CD40L in endothelial cells. Arterioscler Thromb Vasc Biol. 2007;27(5):1101-7.
206. Gissler MC, Anto-Michel N, Pennig J, Scherrer P, Li X, Marchini T, et al. Genetic Deficiency of TRAF5 Promotes Adipose Tissue Inflammation and Aggravates Diet-Induced Obesity in Mice. Arterioscler Thromb Vasc Biol. 2021;41(10):2563-74.
207. Bian Z, Dai J, Hiroyasu N, Guan H, Yuan Y, Gan L, et al. Disruption of tumor necrosis factor receptor associated factor 5 exacerbates pressure overload cardiac hypertrophy and fibrosis. J Cell Biochem. 2014;115(2):349-58.
208. Donners MM, Beckers L, Lievens D, Munnix I, Heemskerk J, Janssen BJ, et al. The CD40-TRAF6 axis is the key regulator of the CD40/CD40L system in neointima formation and arterial remodeling. Blood. 2008;111(9):4596-604.
209. Lutgens E, Lievens D, Beckers L, Wijnands E, Soehnlein O, Zernecke A, et al. Deficient CD40-TRAF6 signaling in leukocytes prevents atherosclerosis by skewing the immune response toward an antiinflammatory profile. J Exp Med. 2010;207(2):391-404.
210. Cao Z, Xiong J, Takeuchi M, Kurama T, Goeddel DV. TRAF6 is a signal transducer for interleukin-1. Nature. 1996;383(6599):443-6.
211. Baud V, Liu ZG, Bennett B, Suzuki N, Xia Y, Karin M. Signaling by proinflammatory cytokines: oligomerization of TRAF2 and TRAF6 is sufficient for JNK and IKK activation and target gene induction via an amino-terminal effector domain. Genes Dev. 1999;13(10):1297-308.
212. Akiyama T, Maeda S, Yamane S, Ogino K, Kasai M, Kajiura F, et al. Dependence of self-tolerance on TRAF6-directed development of thymic stroma. Science. 2005;308(5719):248-51.
213. Polykratis A, van Loo G, Xanthoulea S, Hellmich M, Pasparakis M. Conditional targeting of tumor necrosis factor receptor-associated factor 6 reveals opposing functions of Toll-like receptor signaling in endothelial and myeloid cells in a mouse model of atherosclerosis. Circulation. 2012;126(14):1739-51.
214. Ji YX, Zhang P, Zhang XJ, Zhao YC, Deng KQ, Jiang X, et al. The ubiquitin E3 ligase TRAF6 exacerbates pathological cardiac hypertrophy via TAK1-dependent signalling. Nat Commun. 2016;7:11267.
215. Renshaw BR, Fanslow WC, 3rd, Armitage RJ, Campbell KA, Liggitt D, Wright B, et al. Humoral immune responses in CD40 ligand-deficient mice. J Exp Med. 1994;180(5):1889-900.

216. Hausding M, Jurk K, Daub S, Kröller-Schön S, Stein J, Schwenk M, et al. CD40L contributes to angiotensin II-induced pro-thrombotic state, vascular inflammation, oxidative stress and endothelial dysfunction. Basic Res Cardiol. 2013;108(6):386.
217. Steven S, Dib M, Hausding M, Kashani F, Oelze M, Kröller-Schön S, et al. CD40L controls obesity-associated vascular inflammation, oxidative stress, and endothelial dysfunction in high fat diet-treated and db/db mice. Cardiovasc Res. 2018;114(2):312-23.
218. Prasad KS, Andre P, He M, Bao M, Manganello J, Phillips DR. Soluble CD40 ligand induces beta3 integrin tyrosine phosphorylation and triggers platelet activation by outside-in signaling. Proc Natl Acad Sci U S A. 2003;100(21):12367-71.
219. Boumpas DT, Furie R, Manzi S, Illei GG, Wallace DJ, Balow JE, et al. A short course of BG9588 (anti-CD40 ligand antibody) improves serologic activity and decreases hematuria in patients with proliferative lupus glomerulonephritis. Arthritis Rheum. 2003;48(3):719-27.
220. Kawai T, Andrews D, Colvin RB, Sachs DH, Cosimi AB. Thromboembolic complications after treatment with monoclonal antibody against CD40 ligand. Nat Med. 2000;6(2):114.
221. Shock A, Burkly L, Wakefield I, Peters C, Garber E, Ferrant J, et al. CDP7657, an anti-CD40L antibody lacking an Fc domain, inhibits CD40L-dependent immune responses without thrombotic complications: an in vivo study. Arthritis Res Ther. 2015;17(1):234.
222. Tocoian A, Buchan P, Kirby H, Soranson J, Zamacona M, Walley R, et al. First-in-human trial of the safety, pharmacokinetics and immunogenicity of a PEGylated anti-CD40L antibody fragment (CDP7657) in healthy individuals and patients with systemic lupus erythematosus. Lupus. 2015;24(10):1045-56.
223. Chamberlain C, Colman PJ, Ranger AM, Burkly LC, Johnston GI, Otoul C, et al. Repeated administration of dapirolizumab pegol in a randomised phase I study is well tolerated and accompanied by improvements in several composite measures of systemic lupus erythematosus disease activity and changes in whole blood transcriptomic profiles. Ann Rheum Dis. 2017;76(11):1837-44.
224. Fadul CE, Mao-Draayer Y, Ryan KA, Noelle RJ, Wishart HA, Channon JY, et al. Safety and Immune Effects of Blocking CD40 Ligand in Multiple Sclerosis. Neurol Neuroimmunol Neuroinflamm. 2021;8(6).
225. Kawabe T, Naka T, Yoshida K, Tanaka T, Fujiwara H, Suematsu S, et al. The immune responses in CD40-deficient mice: impaired immunoglobulin class switching and germinal center formation. Immunity. 1994;1(3):167-78.
226. Chatzigeorgiou A, Seijkens T, Zarzycka B, Engel D, Poggi M, van den Berg S, et al. Blocking CD40-TRAF6 signaling is a therapeutic target in obesity-associated insulin resistance. Proc Natl Acad Sci U S A. 2014;111(7):2686-91.
227. Goldwater R, Keirns J, Blahunka P, First R, Sawamoto T, Zhang W, et al. A phase 1, randomized ascending single-dose study of antagonist anti-human CD40 ASKP1240 in healthy subjects. Am J Transplant. 2013;13(4):1040-6.
228. Vincenti F, Klintmalm G, Yang H, Ram Peddi V, Blahunka P, Conkle A, et al. A randomized, phase 1b study of the pharmacokinetics, pharmacodynamics, safety, and tolerability of bleselumab, a fully human, anti-CD40 monoclonal antibody, in kidney transplantation. Am J Transplant. 2020;20(1):172-80.
229. Anil Kumar MS, Papp K, Tainaka R, Valluri U, Wang X, Zhu T, et al. Randomized, controlled study of bleselumab (ASKP1240) pharmacokinetics and safety in patients with moderate-to-severe plaque psoriasis. Biopharm Drug Dispos. 2018;39(5):245-55.
230. Albach FN, Wagner F, Hüser A, Igel J, Joseph D, Hilbert J, et al. Safety, pharmacokinetics and pharmacodynamics of single rising doses of BI 655064, an antagonistic anti-CD40 antibody

in healthy subjects: a potential novel treatment for autoimmune diseases. Eur J Clin Pharmacol. 2018;74(2):161-9.
231. Visvanathan S, Daniluk S, Ptaszyński R, Müller-Ladner U, Ramanujam M, Rosenstock B, et al. Effects of BI 655064, an antagonistic anti-CD40 antibody, on clinical and biomarker variables in patients with active rheumatoid arthritis: a randomised, double-blind, placebo-controlled, phase IIa study. Ann Rheum Dis. 2019;78(6):754-60.
232. Kasran A, Boon L, Wortel CH, Hogezand RA, Schreiber S, Goldin E, et al. Safety and tolerability of antagonist anti-human CD40 Mab ch5D12 in patients with moderate to severe Crohn's disease. Aliment Pharmacol Ther. 2005;22(2):111-22.
233. Perper SJ, Westmoreland SV, Karman J, Twomey R, Seagal J, Wang R, et al. Treatment with a CD40 Antagonist Antibody Reverses Severe Proteinuria and Loss of Saliva Production and Restores Glomerular Morphology in Murine Systemic Lupus Erythematosus. J Immunol. 2019;203(1):58-75.
234. Duivenvoorden R, Senders ML, van Leent MMT, Pérez-Medina C, Nahrendorf M, Fayad ZA, et al. Nanoimmunotherapy to treat ischaemic heart disease. Nat Rev Cardiol. 2019;16(1):21-32.
235. Van De Vyver AJ, Weinzierl T, Eigenmann MJ, Frances N, Herter S, Buser RB, et al. Predicting Tumor Killing and T-Cell Activation by T-Cell Bispecific Antibodies as a Function of Target Expression: Combining In Vitro Experiments with Systems Modeling. Mol Cancer Ther. 2021;20(2):357-66.
236. Gissler MC, Scherrer P, Anto-Michel N, Pennig J, Hoppe N, Füner L, et al. Deficiency of Endothelial CD40 Induces a Stable Plaque Phenotype and Limits Inflammatory Cell Recruitment to Atherosclerotic Lesions in Mice. Thromb Haemost. 2021;121(11):1530-40.
237. Lacy M, Bürger C, Shami A, Ahmadsei M, Winkels H, Nitz K, et al. Cell-specific and divergent roles of the CD40L-CD40 axis in atherosclerotic vascular disease. Nat Commun. 2021;12(1):3754.
238. Bosmans LA, van Tiel CM, Aarts S, Willemsen L, Baardman J, van Os BW, et al. Myeloid CD40 deficiency reduces atherosclerosis by impairing macrophages' transition into a pro-inflammatory state. Cardiovasc Res. 2023;119(5):1146-60.
239. Reiche ME, Poels K, Bosmans LA, Vos WG, Van Tiel CM, Gijbels MJJ, et al. Adipocytes control hematopoiesis and inflammation through CD40 signaling. Haematologica. 2023;108(7):1873-85.
240. Zarzycka B, Seijkens T, Nabuurs SB, Ritschel T, Grommes J, Soehnlein O, et al. Discovery of small molecule CD40-TRAF6 inhibitors. J Chem Inf Model. 2015;55(2):294-307.
241. Seijkens TTP, van Tiel CM, Kusters PJH, Atzler D, Soehnlein O, Zarzycka B, et al. Targeting CD40-Induced TRAF6 Signaling in Macrophages Reduces Atherosclerosis. J Am Coll Cardiol. 2018;71(5):527-42.
242. Lameijer M, Binderup T, van Leent MMT, Senders ML, Fay F, Malkus J, et al. Efficacy and safety assessment of a TRAF6-targeted nanoimmunotherapy in atherosclerotic mice and non-human primates. Nat Biomed Eng. 2018;2(5):279-92.
243. Bishop RT, Marino S, Carrasco G, Li B, Allen RJ, Sparatore A, et al. Combined administration of a small-molecule inhibitor of TRAF6 and Docetaxel reduces breast cancer skeletal metastasis and osteolysis. Cancer Lett. 2020;488:27-39.
244. Marino S, Hannemann N, Bishop RT, Zeng F, Carrasco G, Meurisse S, et al. Anti-inflammatory, but not osteoprotective, effect of the TRAF6/CD40 inhibitor 6877002 in rodent models of local and systemic osteolysis. Biochem Pharmacol. 2022;195:114869.

245. Aarts S, Seijkens TTP, Kusters PJH, van der Pol SMA, Zarzycka B, Heijnen P, et al. Inhibition of CD40-TRAF6 interactions by the small molecule inhibitor 6877002 reduces neuroinflammation. J Neuroinflammation. 2017;14(1):105.
246. Bosch L, de Haan J, Seijkens T, van Tiel C, Brans M, Pasterkamp G, et al. Small molecule-mediated inhibition of CD40-TRAF6 reduces adverse cardiac remodelling in pressure overload induced heart failure. Int J Cardiol. 2019;279:141-4.
247. Coleman DL. Obese and diabetes: two mutant genes causing diabetes-obesity syndromes in mice. Diabetologia. 1978;14(3):141-8.
248. Hummel KP, Dickie MM, Coleman DL. Diabetes, a new mutation in the mouse. Science. 1966;153(3740):1127-8.
249. Eguchi J, Wang X, Yu S, Kershaw EE, Chiu PC, Dushay J, et al. Transcriptional control of adipose lipid handling by IRF4. Cell Metab. 2011;13(3):249-59.
250. Alzet. Osmotic Pumps Mechanism of Operation https://www.alzet.com/products/alzet_pumps/how-does-it-work/ (accessed on 7 January 2024).
251. Theeuwes F, Yum SI. Principles of the design and operation of generic osmotic pumps for the delivery of semisolid or liquid drug formulations. Ann Biomed Eng. 1976;4(4):343-53.
252. Daugherty A, Rateri D, Hong L, Balakrishnan A. Measuring blood pressure in mice using volume pressure recording, a tail-cuff method. J Vis Exp. 2009(27).
253. Feng M, Whitesall S, Zhang Y, Beibel M, D'Alecy L, DiPetrillo K. Validation of volume-pressure recording tail-cuff blood pressure measurements. Am J Hypertens. 2008;21(12):1288-91.
254. Grune J, Blumrich A, Brix S, Jeuthe S, Drescher C, Grune T, et al. Evaluation of a commercial multi-dimensional echocardiography technique for ventricular volumetry in small animals. Cardiovasc Ultrasound. 2018;16(1):10.
255. Bhan A, Sirker A, Zhang J, Protti A, Catibog N, Driver W, et al. High-frequency speckle tracking echocardiography in the assessment of left ventricular function and remodeling after murine myocardial infarction. Am J Physiol Heart Circ Physiol. 2014;306(9):H1371-83.
256. Daiber A, August M, Baldus S, Wendt M, Oelze M, Sydow K, et al. Measurement of NAD(P)H oxidase-derived superoxide with the luminol analogue L-012. Free Radic Biol Med. 2004;36(1):101-11.
257. Wenzel P, Knorr M, Kossmann S, Stratmann J, Hausding M, Schuhmacher S, et al. Lysozyme M-positive monocytes mediate angiotensin II-induced arterial hypertension and vascular dysfunction. Circulation. 2011;124(12):1370-81.
258. Kröller-Schön S, Steven S, Kossmann S, Scholz A, Daub S, Oelze M, et al. Molecular mechanisms of the crosstalk between mitochondria and NADPH oxidase through reactive oxygen species-studies in white blood cells and in animal models. Antioxid Redox Signal. 2014;20(2):247-66.
259. Kalinovic S, Oelze M, Kröller-Schön S, Steven S, Vujacic-Mirski K, Kvandová M, et al. Comparison of Mitochondrial Superoxide Detection Ex Vivo/In Vivo by mitoSOX HPLC Method with Classical Assays in Three Different Animal Models of Oxidative Stress. Antioxidants (Basel). 2019;8(11).
260. Zhao H, Joseph J, Fales HM, Sokoloski EA, Levine RL, Vasquez-Vivar J, et al. Detection and characterization of the product of hydroethidine and intracellular superoxide by HPLC and limitations of fluorescence. Proc Natl Acad Sci U S A. 2005;102(16):5727-32.
261. Zhao H, Kalivendi S, Zhang H, Joseph J, Nithipatikom K, Vásquez-Vivar J, et al. Superoxide reacts with hydroethidine but forms a fluorescent product that is distinctly

different from ethidium: potential implications in intracellular fluorescence detection of superoxide. Free Radic Biol Med. 2003;34(11):1359-68.
262. Kumar R, Gullapalli RR. High Throughput Screening Assessment of Reactive Oxygen Species (ROS) Generation using Dihydroethidium (DHE) Fluorescence Dye. J Vis Exp. 2024(203).
263. Skatchkov MP, Sperling D, Hink U, Mülsch A, Harrison DG, Sindermann I, et al. Validation of lucigenin as a chemiluminescent probe to monitor vascular superoxide as well as basal vascular nitric oxide production. Biochem Biophys Res Commun. 1999;254(2):319-24.
264. Li Y, Zhu H, Kuppusamy P, Roubaud V, Zweier JL, Trush MA. Validation of lucigenin (bis-N-methylacridinium) as a chemilumigenic probe for detecting superoxide anion radical production by enzymatic and cellular systems. J Biol Chem. 1998;273(4):2015-23.
265. Ludmer PL, Selwyn AP, Shook TL, Wayne RR, Mudge GH, Alexander RW, et al. Paradoxical vasoconstriction induced by acetylcholine in atherosclerotic coronary arteries. N Engl J Med. 1986;315(17):1046-51.
266. del Campo L, Ferrer M. Wire Myography to Study Vascular Tone and Vascular Structure of Isolated Mouse Arteries. Methods Mol Biol. 2015;1339:255-76.
267. Münzel T, Daiber A, Mülsch A. Explaining the phenomenon of nitrate tolerance. Circ Res. 2005;97(7):618-28.
268. Münzel T, Giaid A, Kurz S, Stewart DJ, Harrison DG. Evidence for a role of endothelin 1 and protein kinase C in nitroglycerin tolerance. Proc Natl Acad Sci U S A. 1995;92(11):5244-8.
269. Münzel T, Kurz S, Rajagopalan S, Thoenes M, Berrington WR, Thompson JA, et al. Hydralazine prevents nitroglycerin tolerance by inhibiting activation of a membrane-bound NADH oxidase. A new action for an old drug. J Clin Invest. 1996;98(6):1465-70.
270. Jespersen B, Tykocki NR, Watts SW, Cobbett PJ. Measurement of Smooth Muscle Function in the Isolated Tissue Bath-applications to Pharmacology Research. JoVE. 2015(95):e52324.
271. Kossmann S, Schwenk M, Hausding M, Karbach SH, Schmidgen MI, Brandt M, et al. Angiotensin II-induced vascular dysfunction depends on interferon-γ-driven immune cell recruitment and mutual activation of monocytes and NK-cells. Arterioscler Thromb Vasc Biol. 2013;33(6):1313-9.
272. Picot J, Guerin CL, Le Van Kim C, Boulanger CM. Flow cytometry: retrospective, fundamentals and recent instrumentation. Cytotechnology. 2012;64(2):109-30.
273. Truett GE, Heeger P, Mynatt RL, Truett AA, Walker JA, Warman ML. Preparation of PCR-quality mouse genomic DNA with hot sodium hydroxide and tris (HotSHOT). Biotechniques. 2000;29(1):52, 4.
274. Münzel T, Daiber A, Steven S, Tran LP, Ullmann E, Kossmann S, et al. Effects of noise on vascular function, oxidative stress, and inflammation: mechanistic insight from studies in mice. Eur Heart J. 2017;38(37):2838-49.
275. Kröller-Schön S, Daiber A, Steven S, Oelze M, Frenis K, Kalinovic S, et al. Crucial role for Nox2 and sleep deprivation in aircraft noise-induced vascular and cerebral oxidative stress, inflammation, and gene regulation. Eur Heart J. 2018;39(38):3528-39.
276. Strohm L, Daiber A, Ubbens H, Krishnankutty R, Oelze M, Kuntic M, et al. Role of inflammatory signaling pathways involving the CD40–CD40L–TRAF cascade in diabetes and hypertension—insights from animal and human studies. Basic Research in Cardiology. 2024.
277. Bradford MM. A rapid and sensitive method for the quantitation of microgram quantities of protein utilizing the principle of protein-dye binding. Anal Biochem. 1976;72:248-54.
278. Laemmli UK. Cleavage of structural proteins during the assembly of the head of bacteriophage T4. Nature. 1970;227(5259):680-5.

279. Gallagher SR. One-dimensional SDS gel electrophoresis of proteins. Curr Protoc Cell Biol. 2007;Chapter 6:Unit 6.1.
280. Towbin H, Staehelin T, Gordon J. Electrophoretic transfer of proteins from polyacrylamide gels to nitrocellulose sheets: procedure and some applications. Proc Natl Acad Sci U S A. 1979;76(9):4350-4.
281. Stochaj WR, Berkelman T, Laird N. Staining membrane-bound proteins with ponceau s. CSH Protoc. 2006;2006(5).
282. Assarsson E, Lundberg M, Holmquist G, Björkesten J, Thorsen SB, Ekman D, et al. Homogenous 96-plex PEA immunoassay exhibiting high sensitivity, specificity, and excellent scalability. PLoS One. 2014;9(4):e95192.
283. Lundberg M, Eriksson A, Tran B, Assarsson E, Fredriksson S. Homogeneous antibody-based proximity extension assays provide sensitive and specific detection of low-abundant proteins in human blood. Nucleic Acids Res. 2011;39(15):e102.
284. Herzog J, Schmidt FP, Hahad O, Mahmoudpour SH, Mangold AK, Garcia Andreo P, et al. Acute exposure to nocturnal train noise induces endothelial dysfunction and pro-thromboinflammatory changes of the plasma proteome in healthy subjects. Basic Res Cardiol. 2019;114(6):46.
285. Rocha VZ, Libby P. Obesity, inflammation, and atherosclerosis. Nat Rev Cardiol. 2009;6(6):399-409.
286. Chatzigeorgiou A, Phieler J, Gebler J, Bornstein SR, Chavakis T. CD40L stimulates the crosstalk between adipocytes and inflammatory cells. Horm Metab Res. 2013;45(10):741-7.
287. Poggi M, Engel D, Christ A, Beckers L, Wijnands E, Boon L, et al. CD40L deficiency ameliorates adipose tissue inflammation and metabolic manifestations of obesity in mice. Arterioscler Thromb Vasc Biol. 2011;31(10):2251-60.
288. Reiche ME, den Toom M, Willemsen L, van Os B, Gijbels MJJ, Gerdes N, et al. Deficiency of T cell CD40L has minor beneficial effects on obesity-induced metabolic dysfunction. BMJ Open Diabetes Res Care. 2019;7(1):e000829.
289. Guo CA, Kogan S, Amano SU, Wang M, Dagdeviren S, Friedline RH, et al. CD40 deficiency in mice exacerbates obesity-induced adipose tissue inflammation, hepatic steatosis, and insulin resistance. Am J Physiol Endocrinol Metab. 2013;304(9):E951-63.
290. Yi Z, Stunz LL, Bishop GA. CD40-mediated maintenance of immune homeostasis in the adipose tissue microenvironment. Diabetes. 2014;63(8):2751-60.
291. Aarts S, Reiche ME, den Toom M, Beckers L, Gijbels MJJ, Gerdes N, et al. Macrophage CD40 plays a minor role in obesity-induced metabolic dysfunction. PLoS One. 2018;13(8):e0202150.
292. Mehta PK, Griendling KK. Angiotensin II cell signaling: physiological and pathological effects in the cardiovascular system. Am J Physiol Cell Physiol. 2007;292(1):C82-97.
293. Srahna M, Remacle JE, Annamalai K, Pype S, Huylebroeck D, Boogaerts MA, et al. NF-kappaB is involved in the regulation of CD154 (CD40 ligand) expression in primary human T cells. Clin Exp Immunol. 2001;125(2):229-36.
294. Souza HP, Frediani D, Cobra AL, Moretti AI, Jurado MC, Fernandes TR, et al. Angiotensin II modulates CD40 expression in vascular smooth muscle cells. Clin Sci (Lond). 2009;116(5):423-31.
295. Maurizi G, Della Guardia L, Maurizi A, Poloni A. Adipocytes properties and crosstalk with immune system in obesity-related inflammation. J Cell Physiol. 2018;233(1):88-97.
296. Deng T, Lyon CJ, Minze LJ, Lin J, Zou J, Liu JZ, et al. Class II major histocompatibility complex plays an essential role in obesity-induced adipose inflammation. Cell Metab. 2013;17(3):411-22.

297. van den Berg SM, Seijkens TT, Kusters PJ, Zarzycka B, Beckers L, den Toom M, et al. Blocking CD40-TRAF6 interactions by small-molecule inhibitor 6860766 ameliorates the complications of diet-induced obesity in mice. Int J Obes (Lond). 2015;39(5):782-90.
298. Kiper C, Grimes B, Van Zant G, Satin J. Mouse strain determines cardiac growth potential. PLoS One. 2013;8(8):e70512.
299. Wang Z, Zhou Z, Guo P, Wang M, Sun H, Tai Y, et al. DBA/1 mice display equivalent cardiac function to C57BL/6J mice. Exp Physiol. 2021;106(4):868-81.
300. Karbach SH, Schönfelder T, Brandão I, Wilms E, Hörmann N, Jäckel S, et al. Gut Microbiota Promote Angiotensin II-Induced Arterial Hypertension and Vascular Dysfunction. J Am Heart Assoc. 2016;5(9).
301. Kanneganti T-D, Dixit VD. Immunological complications of obesity. Nature Immunology. 2012;13(8):707-12.
302. Winer S, Winer DA. The adaptive immune system as a fundamental regulator of adipose tissue inflammation and insulin resistance. Immunol Cell Biol. 2012;90(8):755-62.
303. Guldiken S, Demir M, Arikan E, Turgut B, Azcan S, Gerenli M, et al. The levels of circulating markers of atherosclerosis and inflammation in subjects with different degrees of body mass index: Soluble CD40 ligand and high-sensitivity C-reactive protein. Thromb Res. 2007;119(1):79-84.
304. Poggi M, Jager J, Paulmyer-Lacroix O, Peiretti F, Gremeaux T, Verdier M, et al. The inflammatory receptor CD40 is expressed on human adipocytes: contribution to crosstalk between lymphocytes and adipocytes. Diabetologia. 2009;52(6):1152-63.
305. Missiou A, Wolf D, Platzer I, Ernst S, Walter C, Rudolf P, et al. CD40L induces inflammation and adipogenesis in adipose cells--a potential link between metabolic and cardiovascular disease. Thromb Haemost. 2010;103(4):788-96.
306. Baena-Fustegueras JA, Pardina E, Balada E, Ferrer R, Catalán R, Rivero J, et al. Soluble CD40 Ligand in Morbidly Obese Patients: Effect of Body Mass Index on Recovery to Normal Levels After Gastric Bypass Surgery. JAMA Surgery. 2013;148(2):151-6.
307. Landmesser U, Cai H, Dikalov S, McCann L, Hwang J, Jo H, et al. Role of p47(phox) in vascular oxidative stress and hypertension caused by angiotensin II. Hypertension. 2002;40(4):511-5.
308. Fukai T, Siegfried MR, Ushio-Fukai M, Griendling KK, Harrison DG. Modulation of Extracellular Superoxide Dismutase Expression by Angiotensin II and Hypertension. Circulation Research. 1999;85(1):23-8.
309. Bergholm R, Leirisalo-Repo M, Vehkavaara S, Mäkimattila S, Taskinen MR, Yki-Järvinen H. Impaired responsiveness to NO in newly diagnosed patients with rheumatoid arthritis. Arterioscler Thromb Vasc Biol. 2002;22(10):1637-41.
310. Mehta NN, Azfar RS, Shin DB, Neimann AL, Troxel AB, Gelfand JM. Patients with severe psoriasis are at increased risk of cardiovascular mortality: cohort study using the General Practice Research Database. Eur Heart J. 2010;31(8):1000-6.
311. Henein MY, Vancheri S, Longo G, Vancheri F. The Role of Inflammation in Cardiovascular Disease. Int J Mol Sci. 2022;23(21).
312. Ridker PM, Cannon CP, Morrow D, Rifai N, Rose LM, McCabe CH, et al. C-reactive protein levels and outcomes after statin therapy. N Engl J Med. 2005;352(1):20-8.
313. Daiber A, Steven S, Euler G, Schulz R. Vascular and Cardiac Oxidative Stress and Inflammation as Targets for Cardioprotection. Curr Pharm Des. 2021;27(18):2112-30.
314. Heusch G, Andreadou I, Bell R, Bertero E, Botker HE, Davidson SM, et al. Health position paper and redox perspectives on reactive oxygen species as signals and targets of cardioprotection. Redox Biol. 2023;67:102894.

315. Griendling KK, FitzGerald GA. Oxidative stress and cardiovascular injury: Part I: basic mechanisms and in vivo monitoring of ROS. Circulation. 2003;108(16):1912-6.
316. Schöttker B, Brenner H, Jansen EH, Gardiner J, Peasey A, Kubínová R, et al. Evidence for the free radical/oxidative stress theory of ageing from the CHANCES consortium: a meta-analysis of individual participant data. BMC Med. 2015;13:300.
317. Jang IK, Lee ZH, Kim YJ, Kim SH, Kwon BS. Human 4-1BB (CD137) signals are mediated by TRAF2 and activate nuclear factor-kappa B. Biochem Biophys Res Commun. 1998;242(3):613-20.
318. Kawamata S, Hori T, Imura A, Takaori-Kondo A, Uchiyama T. Activation of OX40 signal transduction pathways leads to tumor necrosis factor receptor-associated factor (TRAF) 2- and TRAF5-mediated NF-kappaB activation. J Biol Chem. 1998;273(10):5808-14.
319. Ma BY, Mikolajczak SA, Danesh A, Hosiawa KA, Cameron CM, Takaori-Kondo A, et al. The expression and the regulatory role of OX40 and 4-1BB heterodimer in activated human T cells. Blood. 2005;106(6):2002-10.
320. Futagawa T, Akiba H, Kodama T, Takeda K, Hosoda Y, Yagita H, et al. Expression and function of 4-1BB and 4-1BB ligand on murine dendritic cells. Int Immunol. 2002;14(3):275-86.
321. Akiba H, Nakano H, Nishinaka S, Shindo M, Kobata T, Atsuta M, et al. CD27, a member of the tumor necrosis factor receptor superfamily, activates NF-kappaB and stress-activated protein kinase/c-Jun N-terminal kinase via TRAF2, TRAF5, and NF-kappaB-inducing kinase. J Biol Chem. 1998;273(21):13353-8.
322. Borghi A, Verstrepen L, Beyaert R. TRAF2 multitasking in TNF receptor-induced signaling to NF-κB, MAP kinases and cell death. Biochem Pharmacol. 2016;116:1-10.
323. Pan G, Bauer JH, Haridas V, Wang S, Liu D, Yu G, et al. Identification and functional characterization of DR6, a novel death domain-containing TNF receptor. FEBS Lett. 1998;431(3):351-6.
324. Bei JJ, Liu C, Peng S, Liu CH, Zhao WB, Qu XL, et al. Staphylococcal SSL5-induced platelet microparticles provoke proinflammatory responses via the CD40/TRAF6/NFκB signalling pathway in monocytes. Thromb Haemost. 2016;115(3):632-45.
325. Vos S, Aaron R, Weng M, Daw J, Rodriguez-Rivera E, Subauste CS. CD40 Upregulation in the Retina of Patients With Diabetic Retinopathy: Association With TRAF2/TRAF6 Upregulation and Inflammatory Molecule Expression. Invest Ophthalmol Vis Sci. 2023;64(7):17.
326. Kornbluth RS. An expanding role for CD40L and other tumor necrosis factor superfamily ligands in HIV infection. J Hematother Stem Cell Res. 2002;11(5):787-801.
327. de Ramon L, Ripoll E, Merino A, Lúcia M, Aran JM, Pérez-Rentero S, et al. CD154-CD40 T-cell co-stimulation pathway is a key mechanism in kidney ischemia-reperfusion injury. Kidney Int. 2015;88(3):538-49.
328. Liu D, Xu H, Shih C, Wan Z, Ma X, Ma W, et al. T-B-cell entanglement and ICOSL-driven feed-forward regulation of germinal centre reaction. Nature. 2015;517(7533):214-8.
329. Zuñiga E, Rabinovich GA, Iglesias MM, Gruppi A. Regulated expression of galectin-1 during B-cell activation and implications for T-cell apoptosis. J Leukoc Biol. 2001;70(1):73-9.
330. Espinoza DA, Le Coz C, Cruz Cabrera E, Romberg N, Bar-Or A, Li R. Distinct stage-specific transcriptional states of B cells derived from human tonsillar tissue. JCI Insight. 2023;8(7).
331. Mathur RK, Awasthi A, Wadhone P, Ramanamurthy B, Saha B. Reciprocal CD40 signals through p38MAPK and ERK-1/2 induce counteracting immune responses. Nat Med. 2004;10(5):540-4.
332. Almansa R, Heredia-Rodríguez M, Gomez-Sanchez E, Andaluz-Ojeda D, Iglesias V, Rico L, et al. Transcriptomic correlates of organ failure extent in sepsis. J Infect. 2015;70(5):445-56.

333. Nicolson GL. Mitochondrial Dysfunction and Chronic Disease: Treatment With Natural Supplements. Integr Med (Encinitas). 2014;13(4):35-43.
334. Madamanchi NR, Runge MS. Mitochondrial dysfunction in atherosclerosis. Circ Res. 2007;100(4):460-73.
335. Chong ZZ, Wang S, Shang YC, Maiese K. Targeting cardiovascular disease with novel SIRT1 pathways. Future Cardiol. 2012;8(1):89-100.
336. Grootaert MOJ, Bennett MR. Sirtuins in atherosclerosis: guardians of healthspan and therapeutic targets. Nat Rev Cardiol. 2022;19(10):668-83.
337. Döring Y, Libby P, Soehnlein O. Neutrophil Extracellular Traps Participate in Cardiovascular Diseases: Recent Experimental and Clinical Insights. Circ Res. 2020;126(9):1228-41.
338. Zeglinski MR, Granville DJ. Granzymes in cardiovascular injury and disease. Cell Signal. 2020;76:109804.
339. Lin M, Yuan W, Su Z, Lin C, Huang T, Chen Y, et al. Yes-associated protein mediates angiotensin II-induced vascular smooth muscle cell phenotypic modulation and hypertensive vascular remodelling. Cell Prolif. 2018;51(6):e12517.
340. Wen T, Liu J, He X, Dong K, Hu G, Yu L, et al. Transcription factor TEAD1 is essential for vascular development by promoting vascular smooth muscle differentiation. Cell Death Differ. 2019;26(12):2790-806.
341. Oka SI, Sabry AD, Cawley KM, Warren JS. Multiple Levels of PGC-1α Dysregulation in Heart Failure. Front Cardiovasc Med. 2020;7:2.
342. Sihag S, Cresci S, Li AY, Sucharov CC, Lehman JJ. PGC-1alpha and ERRalpha target gene downregulation is a signature of the failing human heart. J Mol Cell Cardiol. 2009;46(2):201-12.
343. Craige SM, Kröller-Schön S, Li C, Kant S, Cai S, Chen K, et al. PGC-1α dictates endothelial function through regulation of eNOS expression. Sci Rep. 2016;6:38210.
344. Kadlec AO, Chabowski DS, Ait-Aissa K, Gutterman DD. Role of PGC-1α in Vascular Regulation: Implications for Atherosclerosis. Arterioscler Thromb Vasc Biol. 2016;36(8):1467-74.
345. Morris BJ. Insulin receptor gene in hypertension. Clin Exp Hypertens. 1997;19(5-6):551-65.
346. Stankiewicz AM, Goscik J, Swiergiel AH, Majewska A, Wieczorek M, Juszczak GR, et al. Social stress increases expression of hemoglobin genes in mouse prefrontal cortex. BMC Neurosci. 2014;15:130.
347. Ostovaneh MR, Ambale-Venkatesh B, Fuji T, Bakhshi H, Shah R, Murthy VL, et al. Association of Liver Fibrosis With Cardiovascular Diseases in the General Population: The Multi-Ethnic Study of Atherosclerosis (MESA). Circ Cardiovasc Imaging. 2018;11(3):e007241.
348. Mak S, Sun H, Acevedo F, Shimmin LC, Zhao L, Teng BB, et al. Differential expression of genes in the calcium-signaling pathway underlies lesion development in the LDb mouse model of atherosclerosis. Atherosclerosis. 2010;213(1):40-51.
349. Jia G, Hill MA, Sowers JR. Diabetic Cardiomyopathy: An Update of Mechanisms Contributing to This Clinical Entity. Circ Res. 2018;122(4):624-38.
350. Zahran MH, Hussein AM, Barakat N, Awadalla A, Khater S, Harraz A, et al. Sildenafil activates antioxidant and antiapoptotic genes and inhibits proinflammatory cytokine genes in a rat model of renal ischemia/reperfusion injury. Int Urol Nephrol. 2015;47(11):1907-15.
351. Rafiq A, Aashaq S, Jan I, Beigh MA. SIX1 transcription factor: A review of cellular functions and regulatory dynamics. Int J Biol Macromol. 2021;193(Pt B):1151-64.

352. Christou MA, Christou PA, Kyriakopoulos C, Christou GA, Tigas S. Effects of Hypoglycemia on Cardiovascular Function in Patients with Diabetes. Int J Mol Sci. 2023;24(11).
353. Bharath LP, Nikolajczyk BS. The intersection of metformin and inflammation. Am J Physiol Cell Physiol. 2021;320(5):C873-c9.
354. Goel S, Singh R, Singh V, Singh H, Kumari P, Chopra H, et al. Metformin: Activation of 5' AMP-activated protein kinase and its emerging potential beyond anti-hyperglycemic action. Front Genet. 2022;13:1022739.
355. Sun Q, Li J, Gao F. New insights into insulin: The anti-inflammatory effect and its clinical relevance. World J Diabetes. 2014;5(2):89-96.
356. Schultz TI, Raucci FJ, Jr., Salloum FN. Cardiovascular Disease in Duchenne Muscular Dystrophy: Overview and Insight Into Novel Therapeutic Targets. JACC Basic Transl Sci. 2022;7(6):608-25.
357. Li D, Zhang C, Li J, Che J, Yang X, Xian Y, et al. Long non-coding RNA MALAT1 promotes cardiac remodeling in hypertensive rats by inhibiting the transcription of MyoD. Aging (Albany NY). 2019;11(20):8792-809.
358. Sahoo S, Meijles DN, Al Ghouleh I, Tandon M, Cifuentes-Pagano E, Sembrat J, et al. MEF2C-MYOCD and Leiomodin1 Suppression by miRNA-214 Promotes Smooth Muscle Cell Phenotype Switching in Pulmonary Arterial Hypertension. PLoS One. 2016;11(5):e0153780.
359. Potthoff MJ, Olson EN. MEF2: a central regulator of diverse developmental programs. Development. 2007;134(23):4131-40.
360. Kleinert H, Wallerath T, Euchenhofer C, Ihrig-Biedert I, Li H, Förstermann U. Estrogens increase transcription of the human endothelial NO synthase gene: analysis of the transcription factors involved. Hypertension. 1998;31(2):582-8.
361. Hsu SP, Lee WS. Effects of female sex hormones on the development of atherosclerosis. Chin J Physiol. 2020;63(6):256-62.
362. Boardman HM, Hartley L, Eisinga A, Main C, Roqué i Figuls M, Bonfill Cosp X, et al. Hormone therapy for preventing cardiovascular disease in post-menopausal women. Cochrane Database Syst Rev. 2015;2015(3):Cd002229.
363. Marjoribanks J, Farquhar C, Roberts H, Lethaby A, Lee J. Long-term hormone therapy for perimenopausal and postmenopausal women. Cochrane Database Syst Rev. 2017;1(1):Cd004143.
364. Li C, Li N, Zhang Z, Song Y, Li J, Wang Z, et al. The specific mitochondrial unfolded protein response in fast- and slow-twitch muscles of high-fat diet-induced insulin-resistant rats. Front Endocrinol (Lausanne). 2023;14:1127524.
365. Kim T, He L, Johnson MS, Li Y, Zeng L, Ding Y, et al. Carnitine Palmitoyltransferase 1b Deficiency Protects Mice from Diet-Induced Insulin Resistance. J Diabetes Metab. 2014;5(4):361.
366. Katsogiannos P, Kamble PG, Boersma GJ, Karlsson FA, Lundkvist P, Sundbom M, et al. Early Changes in Adipose Tissue Morphology, Gene Expression, and Metabolism After RYGB in Patients With Obesity and T2D. J Clin Endocrinol Metab. 2019;104(7):2601-13.
367. Sun Y, Fan W, Xue R, Dong B, Liang Z, Chen C, et al. Transcribed Ultraconserved Regions, Uc.323, Ameliorates Cardiac Hypertrophy by Regulating the Transcription of CPT1b (Carnitine Palmitoyl transferase 1b). Hypertension. 2020;75(1):79-90.
368. de Winther MPJ, Lutgens E. The Link between Hematopoiesis and Atherosclerosis. N Engl J Med. 2019;380(19):1869-71.
369. Peikert A, Kaier K, Merz J, Manhart L, Schäfer I, Hilgendorf I, et al. Residual inflammatory risk in coronary heart disease: incidence of elevated high-sensitive CRP in a real-world cohort. Clinical Research in Cardiology. 2020;109(3):315-23.

370. Conen D, Ridker PM. Clinical Significance of High-Sensitivity C-Reactive Protein in Cardiovascular Disease. Biomarkers in Medicine. 2007;1(2):229-41.
371. Klarin D, Zhu QM, Emdin CA, Chaffin M, Horner S, McMillan BJ, et al. Genetic analysis in UK Biobank links insulin resistance and transendothelial migration pathways to coronary artery disease. Nature Genetics. 2017;49(9):1392-7.
372. Howson JMM, Zhao W, Barnes DR, Ho W-K, Young R, Paul DS, et al. Fifteen new risk loci for coronary artery disease highlight arterial-wall-specific mechanisms. Nature Genetics. 2017;49(7):1113-9.
373. Karbach S, Wenzel P, Waisman A, Munzel T, Daiber A. eNOS Uncoupling in Cardiovascular Diseases - the Role of Oxidative Stress and Inflammation. Current Pharmaceutical Design. 2014;20(22):3579-94.
374. Kaptoge S, Seshasai SRK, Gao P, Freitag DF, Butterworth AS, Borglykke A, et al. Inflammatory cytokines and risk of coronary heart disease: new prospective study and updated meta-analysis. European Heart Journal. 2014;35(9):578-89.
375. Ridker PM. A Test in Context: High-Sensitivity C-Reactive Protein. Journal of the American College of Cardiology. 2016;67(6):712-23.
376. Kaptoge S, Di Angelantonio E, Lowe G, Pepys MB, Thompson SG, Collins R, et al. C-reactive protein concentration and risk of coronary heart disease, stroke, and mortality: an individual participant meta-analysis. Lancet. 2010;375(9709):132-40.
377. Barron E, Lara J, White M, Mathers JC. Blood-borne biomarkers of mortality risk: systematic review of cohort studies. PLoS One. 2015;10(6):e0127550.

List of Publications

1. **Strohm L**, Daiber A, Ubbens H, Krishnankutty R, Oelze M, Kuntic M, Hahad O, Klein V, Hoefer IE, von Kriegsheim A, Kleinert H, Atzler D, Lurz P, Weber C, Wild PS, Münzel T, Knosalla C, Lutgens E, Daub S. Role of inflammatory signaling pathways involving the CD40-CD40L-TRAF cascade in diabetes and hypertension-insights from animal and human studies. Basic Res Cardiol. 2024 Mar 30. doi: 10.1007/s00395-024-01045-1. Epub ahead of print. PMID: 38554187.

2. Chai YL, **Strohm L**, Zhu Y, Chia RSL, Chong JR, Suresh DD, Zhou LH, Too HP, Hilal S, Radivoyevitch T, Koo EH, Chen CP, Poplawski GHD. Extracellular Vesicle-Enriched miRNA-Biomarkers Show Improved Utility for Detecting Alzheimer's Disease Dementia and Medial Temporal Atrophy. J Alzheimers Dis. 2024;99(4):1317-1331. doi: 10.3233/JAD-230572. PMID: 38788066; PMCID: PMC11191453.

3. Keppeler K, Pesi A, Lange S, Helmstädter J, **Strohm L**, Ubbens H, Kuntić M, Kuntić I, Mihaliková D, Vujačić-Mirski K, Rosenberger A, Küster L, Frank C, Oelze M, Finger S, Zakrzewska A, Verdu E, Wild J, Karbach S, Wenzel P, Wild P, Leistner D, Münzel T, Daiber A, Schuppan D, Steven S. Vascular dysfunction and arterial hypertension in experimental celiac disease are mediated by gut-derived inflammation and oxidative stress. Redox Biol. 2024 Apr;70:103071. doi: 10.1016/j.redox.2024.103071. Epub 2024 Feb 8. PMID: 38354629; PMCID: PMC10876911.

4. Kvandová M, Rajlic S, Stamm P, Schmal I, Mihaliková D, Kuntic M, Bayo Jimenez MT, Hahad O, Kollárová M, Ubbens H, **Strohm L**, Frenis K, Duerr GD, Foretz M, Viollet B, Ruan Y, Jiang S, Tang Q, Kleinert H, Rapp S, Gericke A, Schulz E, Oelze M, Keaney JF Jr, Daiber A, Kröller-Schön S, Jansen T, Münzel T. Mitigation of aircraft noise-induced vascular dysfunction and oxidative stress by exercise, fasting, and pharmacological α1AMPK activation: molecular proof of a protective key role of endothelial α1AMPK against environmental noise exposure. Eur J Prev Cardiol. 2023 Oct 26;30(15):1554-1568. doi: 10.1093/eurjpc/zwad075 . PMID: 37185661

5. Kuntic M, Kuntic I, Krishnankutty R, Gericke A, Oelze M, Junglas T, Bayo Jimenez MT, Stamm P, Nandudu M, Hahad O, Keppeler K, Daub S, Vujacic-Mirski K, Rajlic S, **Strohm L**, Ubbens H, Tang Q, Jiang S, Ruan Y, Macleod KG, Steven S, Berkemeier T, Pöschl U, Lelieveld J, Kleinert H, von Kriegsheim A, Daiber A, Münzel T. Co-exposure to urban particulate matter and aircraft noise adversely impacts the cerebro-pulmonary-cardiovascular axis in mice. Redox Biol. 2023 Feb;59:102580. doi:

10.1016/j.redox.2022.102580 . Epub 2022 Dec 18. PMID: 36566737 ; PMCID: PMC9804249.

6. **Strohm L**, Ubbens H, Münzel T, Daiber A, Daub S. Role of CD40(L)-TRAF signaling in inflammation and resolution-a double-edged sword. Front Pharmacol. 2022 Oct 4;13:995061. doi: 10.3389/fphar.2022.995061 . PMID: 36267276 ; PMCID: PMC9577411.

7. Frenis K, Kalinovic S, Ernst BP, Kvandova M, Al Zuabi A, Kuntic M, Oelze M, Stamm P, Bayo Jimenez MT, Kij A, Keppeler K, Klein V, **Strohm L**, Ubbens H, Daub S, Hahad O, Kröller-Schön S, Schmeisser MJ, Chlopicki S, Eckrich J, Strieth S, Daiber A, Steven S, Münzel T. Long-Term Effects of Aircraft Noise Exposure on Vascular Oxidative Stress, Endothelial Function and Blood Pressure: No Evidence for Adaptation or Tolerance Development. Front Mol Biosci. 2022 Jan 31;8:814921. doi: 10.3389/fmolb.2021.814921 . PMID: 35174211 ; PMCID: PMC8841864.

List of External Communication

2024

1. **Oral presentation** (Istanbul, Turkey)
   Annual Meeting of the Society for Free Radical Research – Europe (SFRR-E) *05.06. – 07.06.2024*
   Travel grant
   SFRR-E Young Investigator Award

2. **Oral presentation** (Mannheim, Germany)
   Annual Meeting German Cardiac Society (DGK) *03.04. – 06.04.2024*

2023

3. **Poster presentation** (Düsseldorf, Germany)
   GBM Meeting Redox Biology – Compartementalized Redox Biology *04.09.2023*

4. **Poster presentation** (Singapore)
   Annual Meeting of the Asian Pacific Society of Cardiology (APSC) *13.07. – 15.07.2023*

5. **Oral presentation** (Mainz, Germany)
   Science Day Mainz Research School of Translational Medicine (TransMed) *06.09. – 07.09.2023*

6. **Oral presentation** (Vienna, Austria)
   Annual Meeting of the Society for Free Radical Research – Europe (SFRR-E) *06.06 – 09.06.2023*

7. **Poster presentation** (Mannheim, Germany)
   Annual Meeting German Cardiac Society (DGK) *12.04 – 15.04.2023*

8. **Poster presentation** (Humlebak, Denmark)
   Annual Meeting from the Scandinavian Society for Atherosclerosis Research (SSAR) *22.03. – 25.03.2023*

2022

9. **Oral presentation** (Mainz, Germany)

Science Day Mainz Research School of Translational Medicine (TransMed) *14.09.2022*

Best Presentation Award

10. **Oral and poster presentation** (Spetses, Greece)
FEBS advanced lecture course – Redox Alterations and Cellular Responses: Form Signaling to Interventions *19.09. – 25.09.2022*

Travel grant

Curriculum Vitae

XX

Related Publication

Basic Research in Cardiology
https://doi.org/10.1007/s00395-024-01045-1

ORIGINAL CONTRIBUTION

Role of inflammatory signaling pathways involving the CD40–CD40L–TRAF cascade in diabetes and hypertension—insights from animal and human studies

Lea Strohm[1] · Andreas Daiber[1,2,16] · Henning Ubbens[1] · Roopesh Krishnankutty[3] · Matthias Oelze[1] · Marin Kuntic[1] · Omar Hahad[1,2] · Veronique Klein[1] · Imo E. Hoefer[4] · Alex von Kriegsheim[3] · Hartmut Kleinert[5] · Dorothee Atzler[6,7,8] · Philipp Lurz[1,2] · Christian Weber[6,7,9,10] · Philipp S. Wild[11,17,18,19] · Thomas Münzel[1,2] · Christoph Knosalla[12,13,14] · Esther Lutgens[6,7,15] · Steffen Daub[1]

Received: 28 November 2023 / Revised: 9 February 2024 / Accepted: 2 March 2024

Abstract
CD40L–CD40–TRAF signaling plays a role in atherosclerosis progression and affects the pathogenesis of coronary heart disease (CHD). We tested the hypothesis that CD40L–CD40–TRAF signaling is a potential therapeutic target in hyperlipidemia, diabetes, and hypertension. In mouse models of hyperlipidemia plus diabetes (db/db mice) or hypertension (1 mg/kg/d angiotensin-II for 7 days), TRAF6 inhibitor treatment (2.5 mg/kg/d for 7 or 14 days) normalized markers of oxidative stress and inflammation. As diabetes and hypertension are important comorbidities aggravating CHD, we explored whether the CD40L–CD40–TRAF signaling cascade and their associated inflammatory pathways are expressed in CHD patients suffering from comorbidities. Therefore, we analyzed vascular bypass material (aorta or internal mammary artery) and plasma from patients with CHD with diabetes and/or hypertension. Our Olink targeted plasma proteomic analysis using the IMMUNO-ONCOLOGY panel revealed a pattern of step-wise increase for 13/92 markers of low-grade inflammation with significant changes. CD40L or CD40 significantly correlated with 38 or 56 other inflammatory targets. In addition, specific gene clusters that correlate with the comorbidities were identified in isolated aortic mRNA of CHD patients through RNA-sequencing. These signaling clusters comprised CD40L–CD40–TRAF, immune system, hemostasis, muscle contraction, metabolism of lipids, developmental biology, and apoptosis. Finally, immunological analysis revealed key markers correlated with comorbidities in CHD patients, such as CD40L, NOX2, CD68, and 3-nitrotyrosine. These data indicate that comorbidities increase inflammatory pathways in CHD, and targeting these pathways will be beneficial in reducing cardiovascular events in CHD patients with comorbidities.

Keywords Coronary heart disease · Comorbidities · Diabetes · Hypertension · Inflammation · CD40L–CD40–TRAF6 axis · Oxidative stress

Abbreviations

3NT	3-Nitrotyrosine
4HNE	4-Hydroxynonenal
ACS	Acute coronary syndrome
AngPT1	Angiopoetin 1
ATII	Angiotensin-II
CAIX	Carbonic anhydrase
CCL	C–C-chemokine ligand
CD	Cluster of differentiation
CD40L	CD40 Ligand
CHD	Coronary heart disease
CLPP	Caseinolytic mitochondrial matrix peptidase
CPT1B	Carnitine palmitoyltransferase 1B
CVD	Cardiovascular disease
CXCL	C–X–C chemokine ligand
DR6	Death receptor 6
DMD	Dystrophin
eNOS	Endothelial-nitric-oxide-synthase
ET-1	Endothelin-1
FASLG	Fas ligand
Gal	Galactin
GZMA	Granzyme A
HDL	High-density lipoprotein
HT	Hypertension

Lea Strohm and Andreas Daiber have contributed equally.

Extended author information available on the last page of the article

Published online: 30 March 2024

HMGB1	High mobility group box 1
HO-1	Heme oxygenase 1
ICOSLG	Inducible T cell co-stimulatory ligand
IL6	Interleukin 6
IMA	Internal mammary artery
IPA	Ingenuity pathway analysis
KLRD1	Killer cell lectin-like receptor subfamily D, member 1
Lag3	Lymphocyte-activation gene 3
MDA	Malondialdehyde
MCP	Monocyte chemoattractant peptide
MI	Myocardial infarction
MMP	Matrix metalloproteinase
MYOD1	Myogenic differentiation 1
NADPH	Nicotinamide adenine dinucleotide phosphate
NCR1	Natural cytotoxicity triggering receptor 1
NF-κB	Nuclear factor kappa light chain enhancer of activated B cells
NLRP3	NLR family pyrin domain containing 3
NOX2	NADPH oxidase 2
p47phox	Neutrophil cytosol factor 1
PAR1	Protease-activated receptor 1
PGF	Placental growth factor
pMARCKS	P-myristoylated-glycation-end-products
RAGE	Receptor for advanced glycosylation end products
ROS	Reactive oxygen species
SIX1	Sine oculis homeobox homolog 1
T2DM	Type 2 diabetes mellitus
TEAD	TEA domain transcription factor
TGFB1	Transforming growth factor beta 1
TIE2	Angiopoietin receptor-2
TNF	Tumor necrosis factor
TNFRSF	TNF receptor superfamily
TRAF	TNF receptor-associated factor
TSP-1	Thrombospondin-1
TXNIP	Thioredoxin-interacting protein
VCAM-1	Vascular cell adhesion molecule-1

Introduction

Cardiovascular diseases (CVD), notably ischemic heart disease and heart failure, are the leading causes of disease burden and the primary causes of death worldwide [12]. CVD patients often have comorbidities, including type 2 diabetes mellitus (T2DM), obesity, and hypertension, which increase the prevalence of CVD and mitigate the benefits of effective cardiovascular interventions [9]. In a large-scale population study containing 55,099,280 patients, a strong association of hypertension with myocardial infarction (MI) with an odds ratio of 3.11 (95% CI 3.05–3.17) was shown. Also, T2DM increases the risk of MI with an odds ratio of 1.89 (95% CI 1.86–1.91) [16]. These comorbidities result in increased myocardial oxidative stress, mainly from increased activity of nicotinamide adenine dinucleotide phosphate (NADPH) oxidases, uncoupled endothelial nitric oxide synthase (eNOS), mitochondria, as well as downregulation of antioxidant defense systems [2]. Moreover, hypertension [18, 43] and T2DM [4, 46] trigger inflammation, an independent cardiovascular risk factor [22, 45]. Inflammation and oxidative stress are known to enhance each other in a cross-talk fashion [11, 44] and prevention of excessive reactive oxygen species is a hallmark of most cardioprotective therapies [21].

The CD40L–CD40 co-stimulatory dyad is an important driver of cardiovascular disease. Inhibition of CD40 or its ligand CD40L reduces the extent of atherosclerosis and induces plaque stability in hyperlipidemic mice by reducing major inflammatory pathways. Likewise, genetic deletion of CD40L prevents cardiovascular oxidative stress and inflammation as well as endothelial dysfunction in hypertensive and diabetic/obese mice [19, 38]. Targeting downstream CD40 signaling molecules has been proven beneficial and safe to treat CVD [10, 25, 27]. Treatment with a small molecule inhibitor that targets CD40-TRAF6 signaling can reduce atherosclerosis without causing immune suppression [37]. Incorporation of this small molecule inhibitor into high-density lipoprotein (HDL) nanoparticles allowed targeted delivery in macrophages, induced plaque stabilization, and was proven safe in non-human primates [25].

The present study investigated whether targeting CD40-TRAF6 signaling is a potential therapeutic target in diabetic and hypertensive mice. We also provide evidence that the CD40L–CD40–TRAF6 cascade is involved in the network of low-grade inflammation in coronary heart disease (CHD) patients with comorbidities such as hypertension and diabetes. Whether targeting the CD40L–CD40–TRAF6 axis can ameliorate comorbidity-associated aggravation of CVD in humans remains to be established.

Materials and methods

Animals and treatment

Animal treatment was under the Guide for the Care and Use of Laboratory Animals as adopted and promulgated by the US National Institutes of Health and was approved by the Ethics Commission according to the German Law on the Protection of Animals (Landesuntersuchungsamt Rheinland-Pfalz, Koblenz, Germany; No.: G19-1–068 and extension from March 2022 for hypertensive (ATII) mice; No.: 23 177–07/G 11–1-020 and extension from June 2016 for diabetic (db/db) mice).

Male db/db mice (BKS.Cg-Dock7^{m} + / + Lepr^{db}/J) and respective control mice (BKS.CgTemoin) at the age of 12 weeks from Charles River (Sulzfeld, Germany) were treated for two weeks with a TRAF6 inhibitor (compound 6877002, Tocris, Bristol, UK) at a dose of 10 µmol/kg/d (2.5 mg/kg/d) in 25% DMSO by osmotic minipumps (Alzet, model 1002). Here we use as terminology for the diabetic animals "db/db" and for the control mice the term "WT". The pumps were implanted *s.c.* under ketamine/xylazine anesthesia (1 ml/kg of a ready-to-use solution containing 80 mg/ml ketamine and 12 mg/ml xylazine, Sigma-Aldrich) [38]. The mice were sacrificed after the treatment by exsanguination under isoflurane anesthesia, and the blood, kidney, and heart were collected for analysis. In total, 18 mice per group were used.

In another study, male B6 mice (C57BL/6) from Charles River (Sulzfeld Germany) at the age of 9–10 weeks were treated with either angiotensin II (ATII) at a dose of 1 mg/kg/d in 0,9% NaCl as described previously [19], TRAF6 inhibitor (compound 6877002, Tocris, Bristol, UK) at a dose of 2,5 mg/kg/d in 25% DMSO or both of it by osmotic minipumps (Alzet model 1007D). TRAF6 inhibitor and ATII are administered in two separate pumps because of the different solubility of the two drugs. The pumps were implanted *s.c.* under ketamine/xylazine anesthesia (120 mg/kg; 16 mg/kg body weight; injected fluid volume 0.1–0.2 ml). The mice were killed under ketamine/xylazine anesthesia by opening the thorax and rapid exsanguination by heart puncture. In total, six mice per group were used.

Human samples

All human studies were following the Declaration of Helsinki. Human aortic, internal mammary artery (IMA), and plasma samples were provided from the DZHK Heart Bank at the "Deutsches Herzzentrum der Charité" in Berlin under ethical permission Numbers EA4/035/18 and EA4/032/23. They are fully characterized regarding clinical chemistry parameters (e.g., blood cholesterol, triglycerides, glucose, and creatinine) and clinical functional, lifestyle and physiological parameters (e.g., blood pressure, heart rate, smoking status, and body mass index) and disease state (e.g., multi-vessel disease, acute coronary syndrome). For patient characteristics, see Table 1. Patients eligible for elective coronary artery bypass graft (CABG) were enrolled in the study after giving informed consent to their samples being stored in the biobank. With two exceptions, all patients had multivessel disease with the two exceptions being concomitant surgical aortic valve replacement and coronary arterial dissection, respectively. As far as available, there was no significant difference in the prevalence of chronic coronary syndrome, acute coronary syndrome, non-ST-segment elevation myocardial infarction, and angina pectoris among the different patient groups.

Protein and gene expression analysis, proteomics, RNA sequencing, and bioinformatical analysis

These methods are described in full detail in the online supplemental data file. For RNA sequencing data, canonical pathway analyses to envisage the biochemical processes that are changed by the two comorbidities arterial hypertension and diabetes in CHD patients were performed with IPA as shown in Suppl. Figs. S7 and S8.

Statistical analysis

Immunoblotting, Olink, and qRT-PCR Data are shown as mean with ± SD. The normality test One-way ANOVA (with Tukey's correction for multiple comparisons) was used. If the normality test failed, the Kruskal–Wallis test (with Dunn's correction for multiple comparisons) was performed. Outliers were identified and removed with the ROUT (Q = 1%) method. *P* values > 0.05 were considered statistically significant. $^{*}p \leq 0.05$, $^{**}p \leq 0.01$, $^{***}p \leq 0.001$ and **** $p \leq 0.0001$. For statistical analysis, GraphPad Prism 9.4.1 was utilized.

Results

TRAF6 inhibition in diabetic (db/db) mice reduces expression of inflammatory, apoptotic, and oxidative stress markers

Db/db mice were used to model T2DM and obesity. The mice were treated with TRAF6 inhibitor compound 6877002 (referring to inhibition of the "CD40-TRAF6" signaling pathway) to attenuate their inflammatory phenotype, as described before [38]. Significantly reduced endothelial function (Fig. 1A) and significantly increased blood glucose levels (Fig. 1B) were observed in db/db mice compared to WT animals without significant improvement by TRAF6 inhibitor treatment. The overall ROS production in aortic tissue was measured by DHE staining, which showed a significant increase in diabetic mice and suppressed ROS formation by TRAF6 inhibition (Fig. 1C, E). Superoxide anion levels were measured in cardiac tissue by HPLC analysis. In diabetic mice, TRAF6 inhibition resulted in somewhat reduced superoxide anion levels (Fig. 1D, F). Cardiac protein expression of inflammatory, apoptotic, and oxidative stress markers was measured by immunoblotting and significantly increased in db/db mice compared to WT control mice for most of the markers. Renal protein expression of eNOS, pMARCKS, HO-1, and ET-1 (Fig. 1G–J) was

Table 1 Patient characteristics

	CHD ($n=20$)	CHD + HT ($n=49$)	CHD + HT + T2DM ($n=25$)	p value
General parameters				
Age [y] (SD)	64 (10)	58 (6)	60 (5)	0.001
Sex (male)	70% (14/20)	84% (41/49)	72% (18/25)	0.34
Current Smoker	40% (8/20)	45% (21/47)	38% (9/24)	0.891
Ex-smoker	20% (4/20)	17% (8/47)	29% (7/24)	0.489
Physiological parameters				
Height [cm] (SD)	173 (8)	176 (8)	171 (9)	0.104
BMI [kg/m^2] (SD)	25 (4)	28 (3)	31 (4)	< 0.001
SBP [mmHg] (SD)	125 (15)	136 (26)	143 (17)	0.02
DBP [mmHg] (SD)	70 (7)	75 (13)	75 (10)	0.155
Heart rate [bpm] (SD)	73 (13)	68 (11)	74 (11)	0.107
CHD				
Multivessel disease	100% (20/20)	96% (47/49)	100% (25/25)	0.391
LMCA affected	40% (8/20)	31% (15/49)	36% (9/25)	0.735
Comorbidities				
HT	0% (0/20)	100% (49/49)	100% (25/25)	
T2DM	0% (0/20)	0% (0/49)	100% (25/25)	
Laboratory parameters				
Cholesterol [mg/dl]	190 (9/20)	158 (28/49)	173 (15/25)	0.284
Creatinine [mg/dl]	0.91 (20/20)	0.99 (49/49)	1.09 (25/25)	0.038
CRP [mg/dl]	1.32(18/20)	1.4 (38/49)	0.48 (22/25)	0.269
Glucose [mg/dl]	113 (20/20)	111 (49/49)	246 (25/25)	< 0.001
HDL [mg/dl]	40 (9/20)	36 (28/49)	36 (15/25)	0.784
LDL cholesterol [mg/dl]	124 (9/20)	95 (28/49)	103 (15/25)	0.247
Triglycerides [mg/dl]	169 (9/20))	143 (28/49)	209 (14/25)	0.082
Medication				
ASS	65% (13/20)	51% (25/49)	76% (19/25)	0.104
ACEi/ARB	50% (10/20)	88% (43/49)	80% (20/25)	0.003
BB	65% (13/20)	84% (41/49)	76% (19/25)	0.234
Nitrates	15% (3/20)	20% (10/49)	28% (7/25)	0.558
CCB	0% (0/20)	14% (7/49)	36% (9/25)	0.005
MRA	20% (4/20)	29% (14/49)	16% (4/25)	0.444
Statin	75% (15/20)	78% (38/49)	84% (21/25)	0.733
Sulfonylureas	0% (0/20)	0% (0/49)	12% (3/25)	0.014
Thiazide/distal loop	10% (2/20)	14% (7/49)	24% (6/25)	0.399
Loop diuretic	15% (3/20)	22% (11/49)	16% (4/25)	0.695
RA insulin	0% (0/20)	0% (0/49)	60% (15/25)	< 0.001
LA insulin	0% (0/20)	0% (0/49)	48% (12/25)	< 0.001
Metformin	0% (0/20)	0% (0/49)	36% (9/25)	< 0.001
SGLT2i	0% (0/22)	0% (0/49)	4% (1/25)	0.248
DPP4i	0% (0/20)	0% (0/49)	12% (3/25)	0.014
GLP1i	0% (0/20)	0% (0/49)	8% (2/25)	0.06

BMI body mass index, *SBP* systolic blood pressure, *DBP* diastolic blood pressure, *CHD* coronary heart disease, *LMCA* left main coronary artery, *HT* arterial hypertension, *T2DM* type 2 diabetes, *LDL* low density lipoprotein, *ASS* acetylsalicylic acid, *ACEi* angiotensin-converting enzyme inhibitor, *ARB* angiotensin receptor blocker, *BB* beta blockers, *CCB* calcium channel blocker, *MRA* mineralocorticoid receptor antagonist, *RA Insulin* rapid-acting insulin, *LA insulin* long-acting insulin, *SGLT2i* sodium-glucose cotransporter-2 inhibitors, *DPP4i* dipeptidyl peptidase-4 inhibitors, *GLP1* glucagon-like peptide-1 antagonist

significantly decreased in db/db mice after TRAF6 inhibitor treatment. Serum and renal levels of oxidative stress markers like 3NT and 4HNE were somewhat reduced after TRAF6 inhibition (Fig. 1K–N). In db/db mice, cardiac protein levels of NOX2, eNOS, p47phox, CD40L, and RAGE (Fig. 2A–D, G) were significantly decreased after TRAF6 inhibition. The protein expression of inflammatory and apoptotic markers like Tsp1, Par1, VCAM-1, and caspase3 (Fig. 2E, F, H, I) were not significantly decreased in db/db mice treated with TRAF6 inhibitor, although a trend was noticed for VCAM-1 ($p = 0.0612$). TRAF6 inhibitor treatment in WT mice did not significantly affect the expression levels of the utilized marker proteins.

TRAF6 inhibition in hypertensive mice decreases expression of inflammatory and oxidative stress markers

Arterial hypertension in WT mice was induced by angiotensin-II (ATII) application, leading to an increase in systolic blood pressure of 122 to 148 mmHg. TRAF6 inhibition in hypertensive animals significantly decreased the systolic blood pressure from 148 to 132 mmHg (Fig. 3A). Endothelial function was significantly impaired in hypertensive animals, which was prevented by trend by TRAF6 inhibitor treatment ($p = 0.129$) (Fig. 3B). Aortic ROS production in hypertensive animals was increased, which was normalized by TRAF6 inhibition (Fig. 3C, D). Cardiac RAGE, TXNIP, renal RAGE, and VCAM-1 expression significantly decreased in hypertensive animals after TRAF6 inhibitor treatment (Fig. 3E–G, I). Renal HO-1 expression was reduced in these animals by trend ($p = 0.066$) (Fig. 3H). Also, TRAF6 inhibition decreased the expression of the inflammatory marker 3NT by trend ($p = 0.081$), whereas IL6 was not changed significantly (Fig. 3K, L). Levels of MDA-positive proteins were reduced significantly (Fig. 3J).

CHD patients with either hypertension or hypertension and diabetes show increased expression of oxidative stress and inflammatory markers in plasma and vascular bypass tissue

To explore whether the CD40L–CD40 pathway, as well as associated pathways, were upregulated in patients with CHD suffering from comorbidities, we performed plasma proteomic analysis of CHD patients with either hypertension (HT) or hypertension and diabetes (HT + T2DM) using the Olink IMMUNO-ONCOLOGY panel. A total of 23/92 markers showed significant changes compatible with a worse phenotype in the presence of comorbidities. Some members of the TNF(R)SF family, including CD27 and DR6 (TNFRSF21), followed a step-wise increasing pattern, although the increase in hypertension did not reach significance in contrast to patients with HT + T2DM. Also, other markers of inflammation, including TNFα, IL12, CCL4, and CCL3, followed a similar pattern. Immune cell markers, including CD83, CD5, CD244, ICOSLG, and KLRD1, were increased in patients suffering from comorbidities, as were TIE2 and Gal1 (Fig. 4A–M). In summary, a total of 13/92 markers showed significant changes and a pattern of step-wise increase with each additional comorbidity. The online supplemental data display other markers that are at least elevated by minor trend with one comorbidity without a clear pattern of step-wise increase (Suppl. Figs. S1, S2).

Cluster analysis of the proteins differentially expressed in the plasma revealed that T2DM elicited the most significant changes. Overall, we identified three clusters (Fig. 5A). Cluster one contains proteins downregulated by T2DM, cluster two proteins induced by HT and T2DM, whereas cluster three encompasses proteins upregulated by T2DM. Cluster three contains numerous cytokines linked to TNF, interleukins, and immune-cell surface markers. Network analysis of the proteins differentially expressed when comparing the comorbidities revealed that T2DM dysregulated the plasma proteome most significantly (Figs. 5B–D). Analysis of proteins regulated by T2DM revealed a closely connected network. When comparing CHD to CHD + HT + T2DM, we detected four subnetworks containing either growth factors (TGFB1, PGF, PDGFB, etc.), chemokines (CCL2, CCL3, etc.) or cell surface proteins (TNF receptors, PDCD1, CD5, etc.). Intriguingly, all three networks were linked by TNF, suggesting a potential central role for this cytokine/adipokine in the observed expression change linked to T2DM. In order to demonstrate the involvement of CD40L and CD40 in this low-grade inflammatory cluster, linear regression analysis identified a significant correlation of CD40L or CD40 with 38 or 56 other inflammatory targets (see Suppl. Tables S1 and S2). Those correlated targets that are central in the cluster analysis are highlighted in suppl. Figs. S3 and S4. Targets that were not included in the TNF-centered cluster depicted in Fig. 5 mostly showed weak linear correlation without reaching significance (e.g. TRAIL, TWEAK, IL33, DCN, PTN, MIC-A/B or ARG1).

Further dot blot analysis with the patient's plasma was performed. The protein expression of NOX2 increased by trend in CHD patients with comorbidities ($p = 0.0787$ (NOX2)), whereas CD40L only showed a similar pattern (Suppl. Fig. S5). CD68 protein expression was significantly increased in CHD patients with HT + T2DM, whereas 3NT levels were significantly decreased in CHD patients with HT compared to CHD patients with HT + T2DM.

These data reveal that patients with CHD suffering from HT or HT + T2DM display elevated levels of markers of low-grade inflammation, also linked to the CD40L–CD40 co-stimulatory dyad.

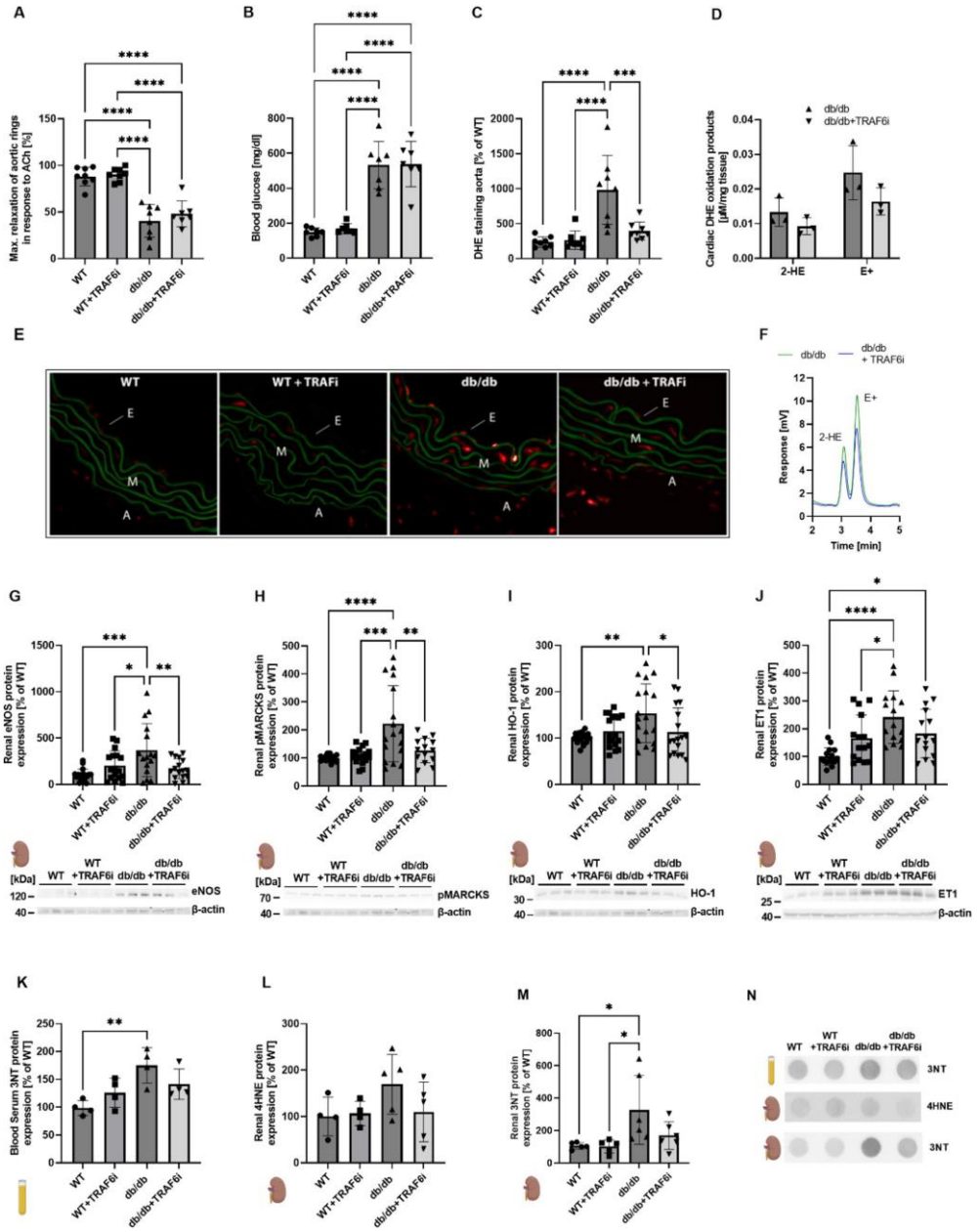
A
Max. relaxation of aortic rings in response to ACh [%]
B
Blood glucose [mg/dl]
C
DHE staining aorta [% of WT]
D
Cardiac DHE oxidation products [µM/mg tissue]
db/db
db/db+TRAF6i
2-HE
E+
E
WT
WT + TRAFi
db/db
db/db + TRAFi
M
A
F
db/db
db/db + TRAF6i
Response [mV]
Time [min]
G
Renal eNOS protein expression [% of WT]
H
Renal pMARCKS protein expression [% of WT]
I
Renal HO-1 protein expression [% of WT]
J
Renal ET1 protein expression [% of WT]
WT
WT+TRAF6i
db/db
db/db+TRAF6i
[kDa]
+TRAF6i
eNOS
pMARCKS
HO-1
ET1
β-actin
K
Blood Serum 3NT protein expression [% of WT]
L
Renal 4HNE protein expression [% of WT]
M
Renal 3NT protein expression [% of WT]
N
3NT
4HNE
3NT

◂**Fig. 1** TRAF6 inhibition in diabetic (db/db) mice leads to decreased renal and sera protein expression of representative markers for inflammation and oxidative stress. Endothelial function was measured by isometric tension studies (data reproduced from published work [38]) (**A**), and glucose levels were determined in whole blood samples without previous fasting (**B**). Aortic ROS levels were analyzed in cryo-sections by DHE staining (**C**). Representative pictures are shown in (**E**). Superoxide anion levels (2-hydroxyethidium, 2-HE) and unspecific ROS formation (ethidium, E+) in cardiac tissue were measured via HPLC analysis, and corresponding representative chromatograms are shown (**D**, **F**). Renal protein expression of eNOS (**G**), pMARCKS (**H**), HO-1 (**I**), and ET-1 (**J**) was determined by immunoblotting. The densitometric quantifications are shown together with the original representative blots below. In addition, Dot Blot analysis was performed to determine the serum content of 3NT-positive proteins (**K**) and the renal levels of 4HNE- (L) and 3NT-positive proteins (**M**). Representative original blots that belong to the quantification of (**K**, **M**) are shown in (**N**). Data are mean ± SD of $n = 7$–8 (**A**–**C**), $n = 3$ (**D**), $n = 18$ (**G**–**I**), $n = 15$ (**J**), $n = 4$ (**K**, **L**), and $n = 5$ (**M**) animals per group. *$p \le 0.05$, **$p \le 0.01$, ***$p \le 0.001$ and ****$p \le 0.0001$. *WT* wild type (BKS.CgTemoin mice), *TRAF6i* TRAF6 inhibitor, *ACh* acetylcholine, *DHE* dihydroethidium, *2-HE* 2-hydroxy-ethidium, *E+* ethidium, *E* endothel, *M* media, *A* adventitia, *ROS* reactive oxygen species, *eNOS* endothelial nitric oxide synthase, *pMARCKS* myristolated alanine-rich C kinase substrate, *HO-1* heme oxygenase 1, *ET-1* endothelin1, *3NT* 3-nitrotyrosine, *4HNE* 4-hydroxynonenal

Hypertension or hypertension and diabetes show marked changes in mRNA expression levels of multiple genes

Aortic tissue samples from CHD, CHD + HT, or CHD + HT + T2DM patients were analyzed for total mRNA expression using the RNA-Seq method and analyzed with CLC genomics workbench (see Suppl. Fig. S6 for the Volcano plots). We found 2074 different expressed genes (DEG, $p < 0.05$) for the comparison of CHD + HT vs. CHD, 1695 DEGs for CHD + HT + T2DM vs. CHD, and 2928 DEGs for CHD + HT + T2DM vs. CHD + HT (see suppl. Tables S3, S4, S5). These DEGs were used for the pathway analyses using the Ingenuity Pathway Analysis (IPA, Qiagen). The regulated DEGs can also be assigned to certain signaling clusters such as CD40L–CD40–TRAF, immune system, hemostasis, muscle contraction, metabolism of lipids, developmental biology, and apoptosis (Suppl. Table S6).

The graphical summary of the IPA analysis is shown in Suppl. Fig. S7A–C. As expected, most pathways indicated as activated in CHD + HT vs. CHD patients (Suppl. Fig. S7A) are important for inflammatory reactions (e.g., the response of myeloid cells and phagocytes, activation of T lymphocytes and mononuclear leukocytes). Interestingly, one of the central pathways indicated to be activated is centered around CD40L. In the disease complexes of the patients, T2DM centrally changed the regulated pathways (Suppl. Fig. S7B). The function and contractility of different muscles are indicated to be inhibited. Also, the comparison CHD + HT + T2DM versus CHD + HT (Suppl. Fig. S7C) showed mainly inhibition of pathways, and also muscle activity is indicated to be regulated negatively.

Analyses of the top 5 regulated canonical pathways showed markedly enhanced mitochondrial dysfunction, oxidative phosphorylation, sirtuin pathways activation, neutrophil extracellular trap dependent signaling, and granzyme A activity in the CHD + HT patients compared to the CHD patients control (Suppl. Fig. S8A). Comparison of the CHD + HT + T2DM group with the CHD control group showed enhanced granulocyte diapedesis, reduced calcium pathway activity, reduced dilated cardiomyopathy, enhanced hepatic fibrosis, and reduced effects of sildenafil (Suppl. Fig. S8B). Finally, the comparison of the CHD + HT + T2DM group with the CHD + HT group showed a marked reduction of oxidative phosphorylation, mitochondrial dysfunction, sirtuin signaling, estrogen receptor activity, and calcium-dependent regulations (Suppl. Fig. S8C).

The IPA analysis of the top 5 upstream regulators showed enhanced activities of the factors TEAD (transcription factor), PPARGC1A (transcriptional coactivator), CD40 (receptor of CD40L), INSR (insulin receptor), and Hbb-b1 (hemoglobin, beta adult major chain) in the CHD + HT compared to the CHD group (Suppl. Fig. S9A). Compared to the CHD control group, the CHD + HT + T2DM group showed enhanced effects of SIX1 (transcription factor) and reduced activities of DMD (human dystrophin gene), MYOD1 (transcription factor), MEF2C (transcription factor), and beta-estradiol (sex hormone; Suppl. Fig. S9B). Finally, the CHD + HT + T2DM group reduced TEAD and DMD activities, whereas enhanced SIX1, CLPP (mitochondrial protease component), and CPT1B (carnitine palmitoyltransferase 1B) activities were observed compared to the CHD + HT group (Suppl. Fig. S9C).

Discussion

This study establishes that inflammatory signaling via the CD40L–CD40–TRAF6 axis plays a crucial role in diabetic (db/db) and hypertensive (ATII) mice. We also demonstrate that TRAF6 inhibition has beneficial effects in these animal models. In addition, we show that some markers (like CD40L, NOX2, and 3NT) identified in the mouse models showed a pattern of step-wise upregulation in CHD patients by the presence of comorbidities such as hypertension or hypertension + diabetes. CD40L and CD40 were also significantly correlated with an appreciable number of targets of a low-grade inflammatory cluster in hypertensive/diabetic patients.

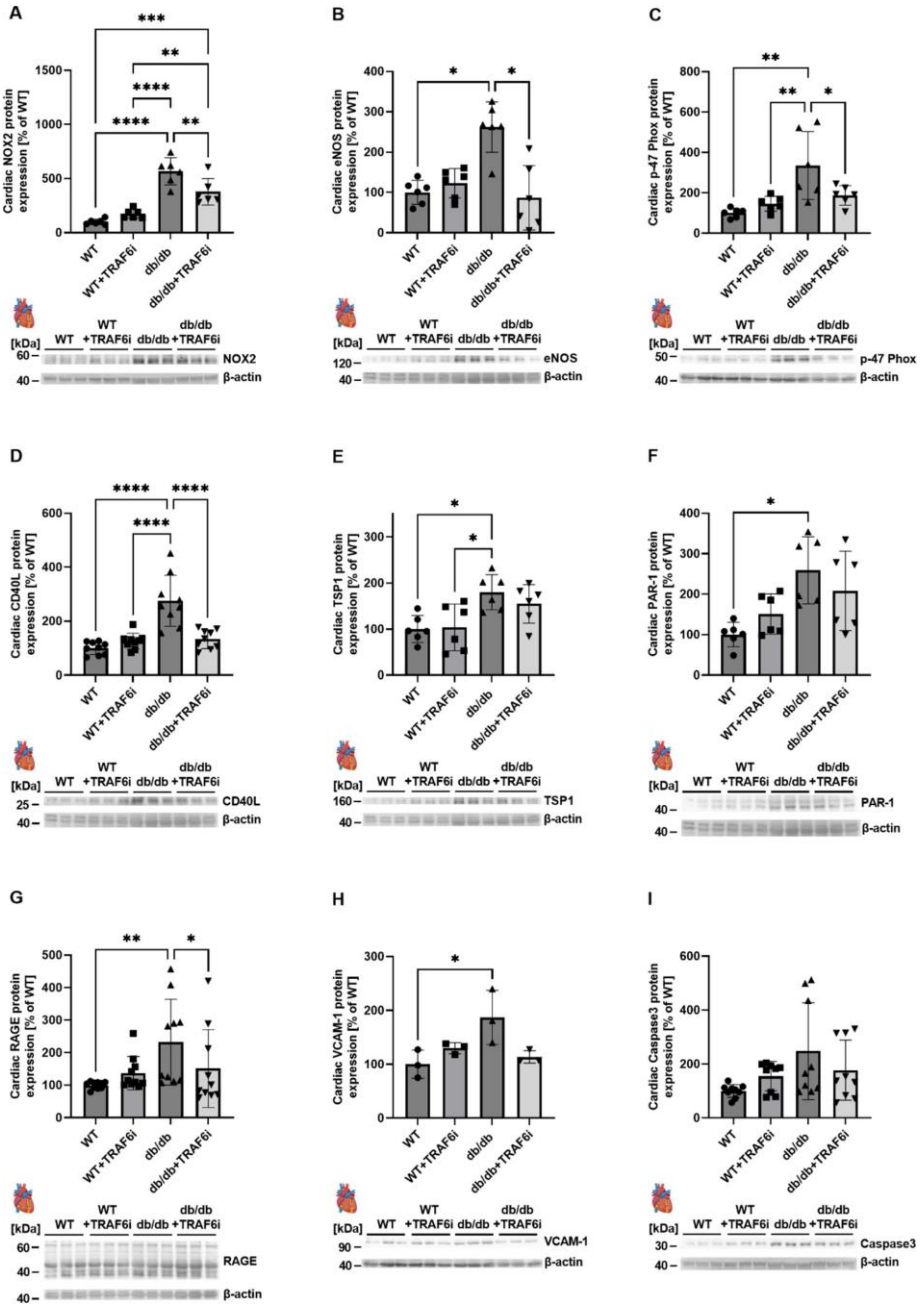
A
Cardiac NOX2 protein expression [% of WT]
WT
WT+TRAF6i
db/db
db/db+TRAF6i
[kDa]
NOX2
β-actin
B
Cardiac eNOS protein expression [% of WT]
eNOS
β-actin
C
Cardiac p-47 Phox protein expression [% of WT]
p-47 Phox
β-actin
D
Cardiac CD40L protein expression [% of WT]
CD40L
β-actin
E
Cardiac TSP1 protein expression [% of WT]
TSP1
β-actin
F
Cardiac PAR-1 protein expression [% of WT]
PAR-1
β-actin
G
Cardiac RAGE protein expression [% of WT]
RAGE
β-actin
H
Cardiac VCAM-1 protein expression [% of WT]
VCAM-1
β-actin
I
Cardiac Caspase3 protein expression [% of WT]
Caspase3
β-actin

◂**Fig. 2** TRAF6 inhibition in diabetic (db/db) mice leads to decreased cardiac protein expression of representative markers for inflammation, apoptosis, and oxidative stress. Cardiac protein expression of NOX2 (**A**), eNOS (**B**), p47phox (**C**), CD40L (**D**), TSP1 (**E**), PAR-1 (**F**), RAGE (**G**), VCAM-1 (**H**) and Caspase3 (**I**) was determined by immunoblotting. Below the densitometric quantification, original representative blots are shown. Untreated control mice (BKS.CgTemoin) and TRAF6 inhibitor-treated mice were used as controls. Data are mean ± SD of $n = 6$ (**A**–**C**), $n = 9$ (D), $n = 6$ (**E**, **F**), $n = 10$ (G), $n = 3$ (H), and $n = 9$ (**I**) animals per group. $^{*}p \leq 0.05$, $^{**}p \leq 0.01$, $^{***}p \leq 0.001$ and $^{****}p \leq 0.0001$. *WT* wild type (BKS.CgTemoin mice), *TRAF6i* tumor necrosis factor receptor-associated factor 6 inhibitor, *TSP1* thrombospondin-1, *eNOS* endothelial nitric oxide synthase, p47phox (NCF1) neutrophil cytosol factor 1, *NOX2* NADPH oxidase 2, *PAR-1* protease activated receptor 1, *RAGE* receptor for advanced glycosylation end products, *VCAM-1* vascular cell adhesion molecule 1

Animal data

A previous study showed that TRAF6 inhibition (often also termed "CD40-TRAF6" inhibition) by compound 6877002 suppressed the expression of TNFα, CCL2, and different interleukins in activated macrophages and diminished the expression of TNFα, CD40, and CD40L by trend in isolated B cells [37]. We showed that TRAF6 inhibition in diabetic mice (db/db), at least by trend, normalizes the upregulation of proteins centered around platelet activation (e.g., CD40L, TSP1, PAR1). Previously, we established that TRAF6 inhibition partially prevented endothelial dysfunction, weight gain, increase in HbA1c values, oxidative burst of whole blood leukocytes, cardiac RAGE signaling, vascular ROS formation, and impaired catalase/glutathione peroxidase 1 expression in db/db mice [38]. It is already known that the release of soluble CD40L and mainly CD40L–CD40 mediated signaling of platelets, endothelial cells, and monocytes strongly affects CHD [1, 13, 39]. Indeed, one way of expressing CD40 and mobilizing CD40 on the membrane in endothelial cells is induced via PAR-1, which could represent another link between thrombosis and inflammation [30]. Besides sCD40L, TSP-1 could be a potential biomarker in diagnosing acute coronary syndrome (ACS) [15]. We conclude from this data that inhibition of the CD40–TRAF6 signaling cascade in diabetic mice is suitable for suppressing thrombosis and the progression of CD40L–CD40-mediated inflammation.

Inhibition of TRAF6 also decreased the expression of proteins that are involved in reactive oxygen species formation (e.g., p47phox, NOX2), inflammatory signaling (e.g., VCAM-1, RAGE), and cell death (e.g., caspase-3) in diabetic animals. NADPH oxidase (NOX2) activation is associated with superoxide production, activation of NF-κB signaling, and release of pro-thrombotic molecules (e.g., sCD40L). Also, high CD40 surface protein levels affect the activation of NOX2 [32] [28]. In addition, RAGE could be activated via advanced glycation end products (AGE) to enhance the expression of adhesion and inflammatory molecules, including CD40 expression and mobilization to the surface of monocytes, which results in increased T cell activation and TNFα and interferon-γ levels [40]. With our present data, we could show that these processes are suppressed by TRAF6 inhibition in diabetic mice. Also, upregulated eNOS, reflecting compensatory upregulation of the uncoupled enzyme, was normalized by inhibition of the CD40–TRAF6 pathway in the heart and kidney. Furthermore, renal phosphorylation of MARCKS, reflecting p47phox-mediated NOX2 activation, and antioxidant response (e.g., HO-1) and vasoconstrictor expression (e.g., ET-1) was suppressed by TRAF6 inhibition in db/db mice. Also, aortic ROS formation was increased in diabetic mice, leading to endothelial dysfunction, all of which was improved, at least by trend, by TRAF6 inhibitor treatment. In contrast, the severely increased blood glucose levels in db/db mice were not decreased by TRAF6 inhibition.

Previous data indicate that ATII-mediated arterial hypertension is related to increased CD40L expression, most likely mediated by monocytes [43] and endothelial cells [19, 24]. Accordingly, we here observed a similar trend for the protective effects of TRAF6 inhibition in hypertensive mice as documented in diabetic mice. Indeed, in hypertensive mice with TRAF6 inhibitor treatment, cardiac RAGE and TXNIP expression were significantly reduced. TXNIP is a key component of high-mobility group box 1 protein (HMGB1) and NLR family pyrin domain containing 3 protein (NLRP3) activation, leading to inflammation. In addition, renal RAGE, HO-1, and VCAM-1 showed a similar trend in hypertensive mice. Oxidative stress markers such as 3NT, MDA, and 4HNE were upregulated in the blood or kidney of diabetic or hypertensive mice and normalized by CD40-TRAF6 inhibition. Of note, these biochemical changes were also mirrored by functional changes—TRAF6 inhibition partially normalized increased systolic blood pressure, endothelial dysfunction, and aortic ROS formation in hypertensive mice. Moreover, some of the mentioned biochemical markers (like CD40L, NOX2, and 3NT) identified in the mouse models were also step-wise upregulated in CHD patients by the presence of comorbidities such as hypertension or hypertension + diabetes.

Human protein data

Increased cardiovascular risk is observed in patients suffering from systemic inflammatory diseases [6, 31]. Therefore, CVDs were classified as an inflammatory-related entity [3]. This correlation was also demonstrated in patients with ACS in which C-reactive protein (CRP) levels positively correlated with adverse clinical outcomes [33]. In the CANTOS trial, pharmacological agents like Canakinumab, an IL-1β antagonist, are employed in

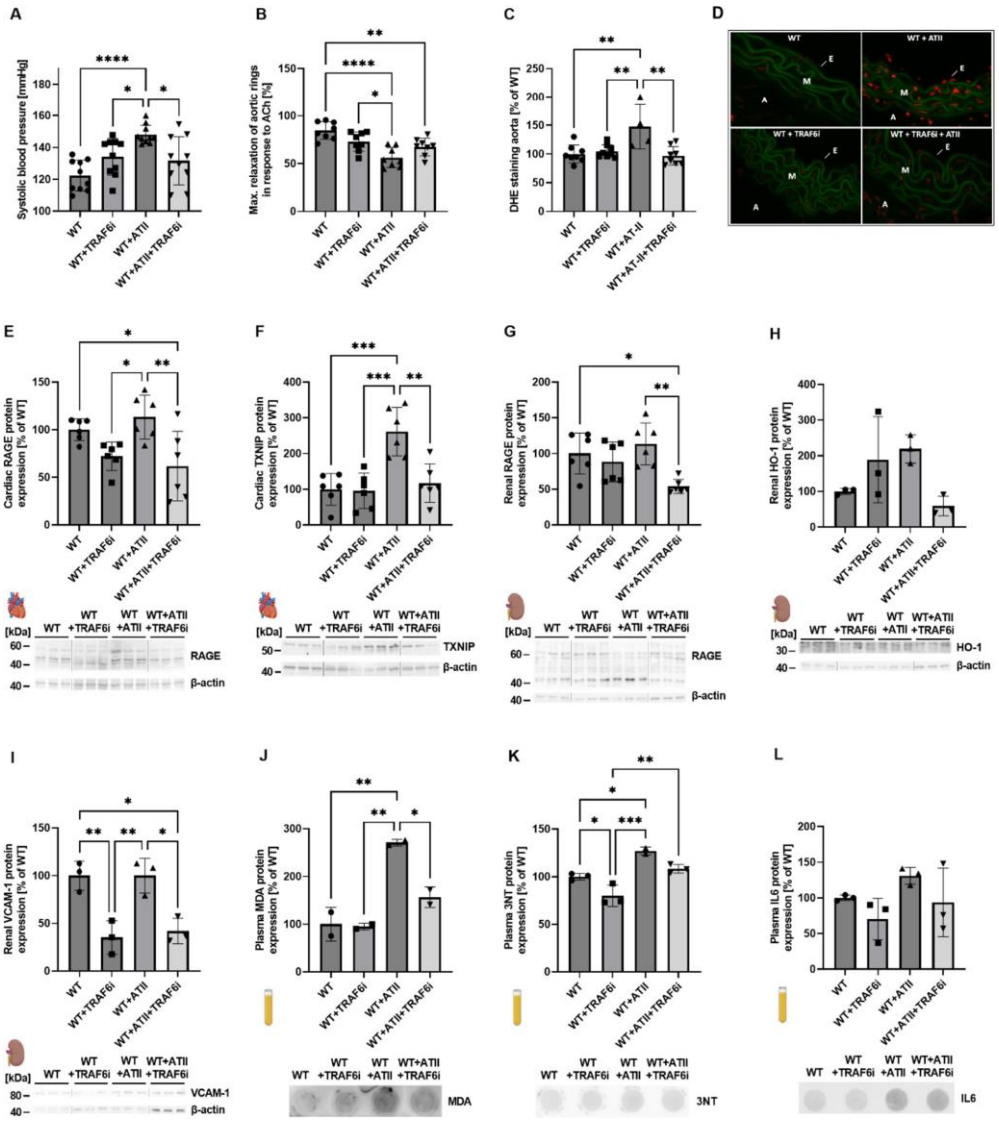

patients with high cardiovascular risk as anti-inflammatory therapy to improve their outcomes [34]. Besides inflammation, oxidative stress represents a hallmark of most CVDs, characterized by a mismatch between ROS formation and degradation [17, 20], e.g., as shown by a positive correlation between glutathione peroxidase-1 and outcomes in patients with CVD [8] as well as markers of oxidative stress and cardiovascular mortality [36].

In our proteomic analysis of CHD patients' plasma, we identified some step-wise increased targets in association with the number of their comorbidities (CHD < CHD + HT < CHD + HT + T2DM). Cluster analysis identified TNFα as a central player. Detailed extended discussion of all

◂**Fig. 3** Pharmacological TRAF6 inhibition in hypertensive mice induced by angiotensin-II leads to decreased cardiac, renal, and plasma protein expression of representative markers for inflammation and oxidative stress. Systolic blood pressure was measured non-invasively by tail-cuff recordings (**A**). Isometric tension studies were performed to analyze the endothelial function (**B**). Aortic ROS levels were analyzed with DHE stainings (**C**), and representative pictures are shown in (**D**). Cardiac protein expression of RAGE (**E**) and TXNIP (**F**), as well as renal protein expression of RAGE (**G**), HO-1 (**H**), and VCAM-1 (**I**), was determined by immunoblotting. Representative blots are shown together with the densitometric quantification below. In addition, the protein expression of MDA (**J**), 3NT (**K**), and IL6 (**L**) was determined in plasma by dot blot analysis. Representative original dot blots are shown below the densiometric quantification. Data are mean ± SD of $n = 10$ (**A**), $n = 8$ (**B**), $n = 4$–8 (**C**), $n = 6$ (**E**–**G**), $n = 3$ (**H**, **I**), and $n = 3$ (**J**–**L**) animals per group. $*p \leq 0.05$, $**p \leq 0.01$ *and* $***p \leq 0.001$. WT wild type (C57BL/6 J), *TRAF6i* TRAF6 inhibitor, *ACh* acetylcholine, *DHE* dihydroethidium, *E* endothel, *M* media, *A* adventitia, *ROS* reactive oxygen species, *RAGE* receptor for advanced glycosylation endproducts, *TXNIP* thioredoxin interacting protein, *HO-1* heme oxygenase, *VCAM-1* vascular cell adhesion protein, *MDA* malondialdehyde, *3NT* 3-nitrotyrosine, *IL6* interleukin 6

regulated targets and the cluster data are provided in the online Supplemental Data file. Taken together, the central position of TNFα in the plasma protein cluster analysis provides evidence for an involvement of the CD40(L)-TRAF6 pathway in patients with HT and T2DM as comorbidities, which is further supported by the substantial correlations of CD40L and CD40 with a majority of other targets of the low-grade inflammatory cluster (Suppl. Tables S1 and S2, Figs. S3 and S4). Previous work showed that silencing of CD40 or TNF receptor (TNFR)-associated factor 6 (TRAF6) gene largely abrogated phosphorylation and nuclear translocation of NF-κB (p65), and hence TNFα expression [5]. Blockade of CD40 and CD40L interactions with neutralizing antibodies significantly reduced monocyte release of inflammatory mediators and migration by CCL2 (MCP-1). Another study reported upregulation of CD40, TRAF2, and TRAF6 in patients with diabetic retinopathy, where CD40 was associated with the expression of pro-inflammatory molecules such as intercellular adhesion molecule 1 (CD54), CCL2, and TNFα [42]. Several other factors identified in the cluster analysis of patients with HT and T2DM were previously reported for pathways associated with CD40L and other tumor necrosis factor superfamily ligands in HIV infection [23]. It is also well established that TNFα cooperates with CD40L, RANK, and IL1β to regulate TRAF6/NF-κB signaling [29], which is also supported by the observation that TRAF6 inhibition by compound 6877002 prevents CD40L-dependent activation (nuclear translocation) of NF-κB [7].

Human RNA sequencing data

In accordance with our proteomic data, we found in CHD patients with comorbidities (CHD < CHD + HT + T2DM) increased aortic gene expression of NK cell-specific markers (e.g., CD244, KLRD1, NCR1), apoptotic markers (e.g., Gal1, TNFRSF21), cytokines/chemokines (e.g., TNF, CCL3, CCL4, IL12, IL8), T cell activation-associated markers (e.g., TNFRSF4, TNFRSF9, CD5, ICOSLG, CD70), and pro-angiogenic markers (e.g., AngPT1, TIE2).

The comparison of our proteomic data with our RNA-seq data (see Suppl. Table S8) showed only a small overlap in the regulated genes and differences in the regulation direction. In the RNA-seq analysis of the CHD + HT vs. CHD group, only CD8 and CD5 were upregulated, and CCL13 (MCP4) and CA9 (CAIX) were downregulated. There were no significant changes in the mRNA expression of the other genes. The comparative analysis of the proteomic data with the RNA-seq data of the comparison CHD + HT + T2DM vs. CHD shows more genes regulated on the mRNA expression level. However, in this comparison, several genes are downregulated on the mRNA level, which has been found to be upregulated on the protein level in the plasma. In this group 4 genes (PGF, AngPT1, CXCL8, NCR1) showed enhanced mRNA expression, whereas 5 genes (CA9, GAL, CXCL11, TNFRSF21, LAG3) showed reduced mRNA expression. However, as protein expression in the plasma (whole body) and mRNA expression in aorta samples are supposed only to show a minor overlap, our data are not surprising. Detailed extended discussion of IPA analysis of RNA-seq data is provided in the online Supplemental Data file, including suppl. Figs. S7,S8,S9.

The proteomic and transcriptomic data of human samples are further supported in this study by protein expression analysis. In patients' plasma, we could observe the same trend of upregulation for proteins involved in reactive oxygen formation/oxidative stress (e.g., NOX-2, 3NT) and inflammation (e.g., CD40L, CD68), like in the proteomic analysis before (Suppl. Fig. S5).

Limitations of the study

The chosen mouse model for diabetes (db/db) develops a quite severe vascular phenotype, as reported previously [38]. However, even a short-term TRAF6 inhibition partially reversed vascular complications such as impaired endothelial function, vascular ROS formation, and increased HbA1c and RAGE signaling [38]. Our mouse model of induced arterial hypertension via ATII treatment reflects only one possible pathway underlying the development of hypertension. In addition, the model of hypertension with one week of ATII infusion does not fully reflect hypertension-triggered end-organ damage by remodeling and accumulating oxidative modifications (e.g., in the kidney and heart). Accordingly, the impact of TRAF6 inhibition on end-organ damage could not be tested to a full extent here. However, we have previously shown that CD40L

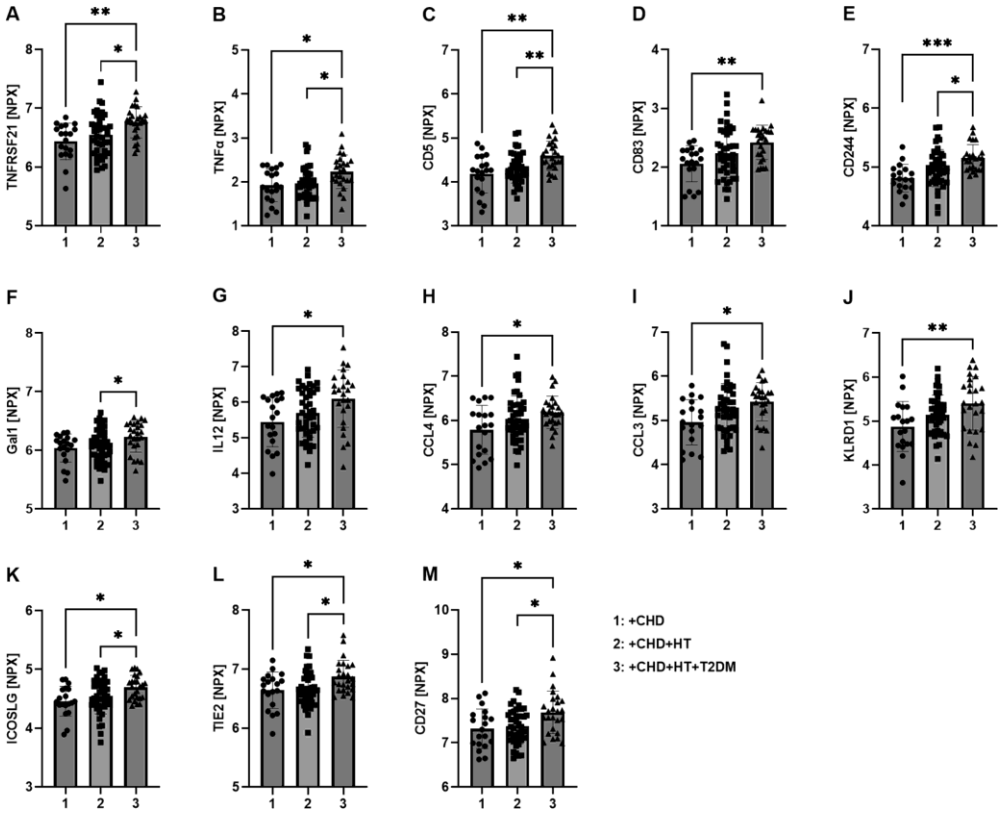

Fig. 4 Selected markers of low-grade inflammation show a pattern of step-wise increase in plasma from CHD patients with either hypertension or hypertension and diabetes. Olink analysis in plasma from CHD patients with either no comorbidity (1) hypertension (2) or hypertension and diabetes (3) was performed, and the following step-wise increased targets (at least by trend) were identified: TNFRSF21 (**A**), TNFα (**B**), CD5 (**C**), CD83 (**D**), CD244 (**E**), Gal1 (**F**), IL12 (**G**), CCL4 (**H**), CCL3 (**I**), KLRD1 (**J**), ICOSLG (**K**), TIE2 (**L**), and CD27 (**M**). Data are mean ± SD CHD n = 19, CHD + HT $n = 42$, and CHD + HT + T2DM = 25 patients per group. *$p \le 0.05$, **$p \le 0.01$ and ***$p \le 0.001$. Outliers were identified and removed with the ROUT ($Q = 1\%$) method. *CHD* coronary heart disease, *HT* hypertension, *T2DM* type 2 diabetes mellitus, *TNFRSF* tumor necrosis factor receptor superfamily, *TNF* tumor necrosis factor, *Gal1* galectin1, *CCL* C–C motif chemokine ligand, *KLRD* killer cell lectin-like receptor D, *ICOSLG* inducible T cell co-stimulatory ligand, TIE2 angiopoietin 1 receptor

deficiency prevents all major complications induced by ATII treatment [19]. Hypertension development is multifactorial in humans, with the renin–angiotensin–aldosterone system playing a substantial role. Nevertheless, we think this model is suitable for our studies, especially in the context of the CD40L–CD40–TRAF signaling. We could show in the past that the ATII model is primarily driven by the immigration of (CD40L expressing) inflammatory cells. The negative influence of ATII-induced arterial hypertension on vascular function and severe blood pressure increase is well documented and has been intensively investigated, particularly in our research group [19, 43] and by others [14, 26]. Although the ATII-based hypertension mouse or rat model causes severe hypertension and drastic elevation of oxidative stress and inflammation, it is frequently used to study the pathophysiology of arterial hypertension in a short time window of 1–2 weeks. The beneficial action of all classical antihypertensive drugs, such as AT1-receptor blockers and angiotensin-converting enzyme inhibitors, supports the relevance of these models for human hypertension.

Concerning the Olink proteomic data, the variability within individuals arises from several factors aside from

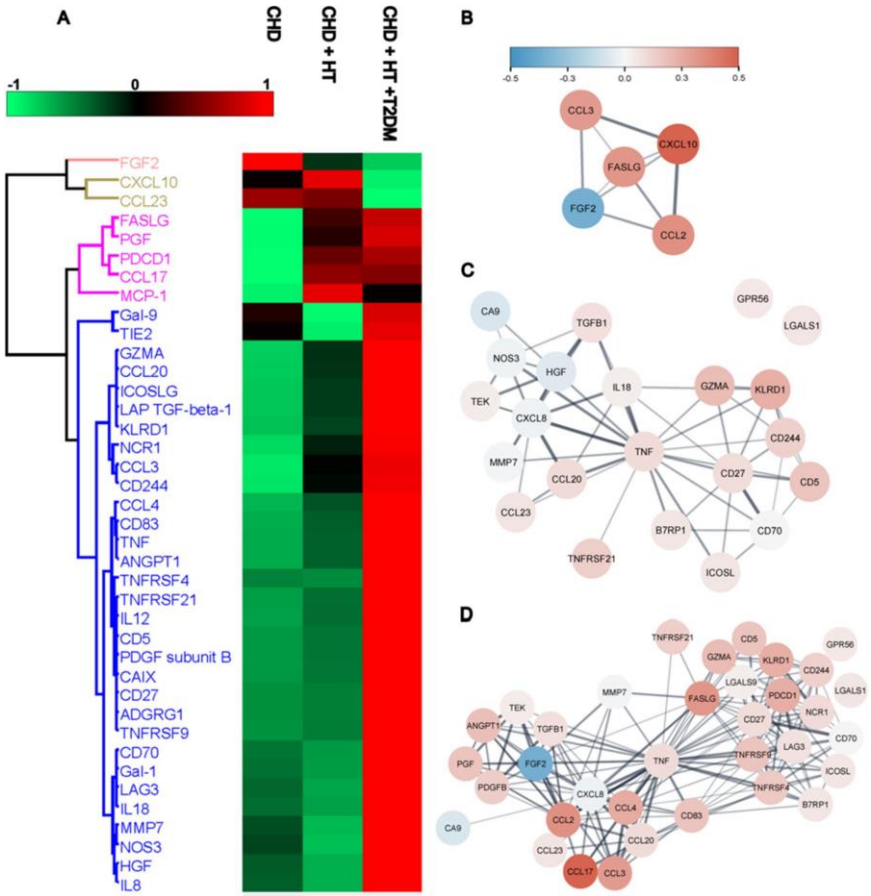

Fig. 5 Markers of inflammation are increased in plasma from CHD patients with either hypertension or hypertension and diabetes. Olink analysis in plasma from CHD patients with either hypertension or hypertension and diabetes was performed, and the dataset was filtered for differentially expressed proteins. Median values were determined for each group and Z-normalised. **A** Euclidean Clustering of median expression. **B–D** Protein network of differentially expressed proteins with B comparing CHD to CHD + HT, C comparing CHD + HT to CHD + HT + T2DM, and D comparing CHD to CHD + HT + T2DM. *FGF* fibroblast growth factor, *CXCL* C-X-X motif chemokine ligand, *CCL* C–C motif chemokine ligand, *FASLG* Fas ligand, *PGF* placental growth factor, *PDCD* programmed cell death ligand, *MCP* monocyte chemoattractant protein, *Gal* galectin, *TIE2* angiopoietin receptor-2, *GZMA* granzyme A, *ICOSLG* inducible T cell co-stimulatory ligand, *LAP TGF* latency-associated peptide transforming growth factor, *KLRD* killer cell lectin-like receptor D, *NCR* natural cytotoxicity triggering receptor, *CD* cluster of differentiation, *TNF* tumor necrosis factor, *ANGPT1* angiopoietin-1, *TNFRSF* tumor necrosis factor receptor superfamily, *IL* interleukin, *PDGF* platelet derived growth factor, *CAIX* carbonic anhydrase, *ADGRG1* adhesion G-protein-coupled receptor, *LAG* lymphocyte activation gene, *MMP* matrix metalloproteinase, *NOS* nitric oxide synthase, *HGF* hepatocyte growth factor. Data are mean ± SD CHD $n = 21$, CHD + HT $n = 42$, and CHD + HT + T2DM = 25 patients per group

the differentiating morbidities/comorbidities. Circadian rhythms, environmental stressors, age, diet, and known or unknown factors can regulate the plasma proteome. The cohort size was too small to account for these confounding factors. They can be overcome by increasing the sample number. We quantified the plasma proteome of 88 individuals with a range of comorbidities. The number of patients in the individual cohorts is likely limiting; we also cannot rule out unexpected confounding factors. In addition, we

monitored a small number of proteins in a targeted fashion, limiting the breadth of analysis.

Compared to RNA-Seq data obtained with inbred animals, there is a greater heterogeneity in the transcriptomes of tissue samples obtained from human beings. These heterogeneities are likely related to differences in the DNA sequences of the different participants and, therefore, genetically related differences in the transcriptional activity. This fact results in lower p-levels in gene expression compared to healthy and diseased participants. This higher variance may result in undetected disease-related transcriptomic changes. To circumvent the limitations of the RNA-Seq method, larger numbers of healthy/ill tissues are needed. However, the obtainment of healthy aorta samples is quite problematic. The analysis of our RNA-Seq data showed relatively high heterogeneity in the mRNA expression in samples of the participants of one group. However, for example, the IPA analyses of the CHD + HT vs. CHD comparison resulted in detecting the CD40L–CD40 pathway as a major regulator

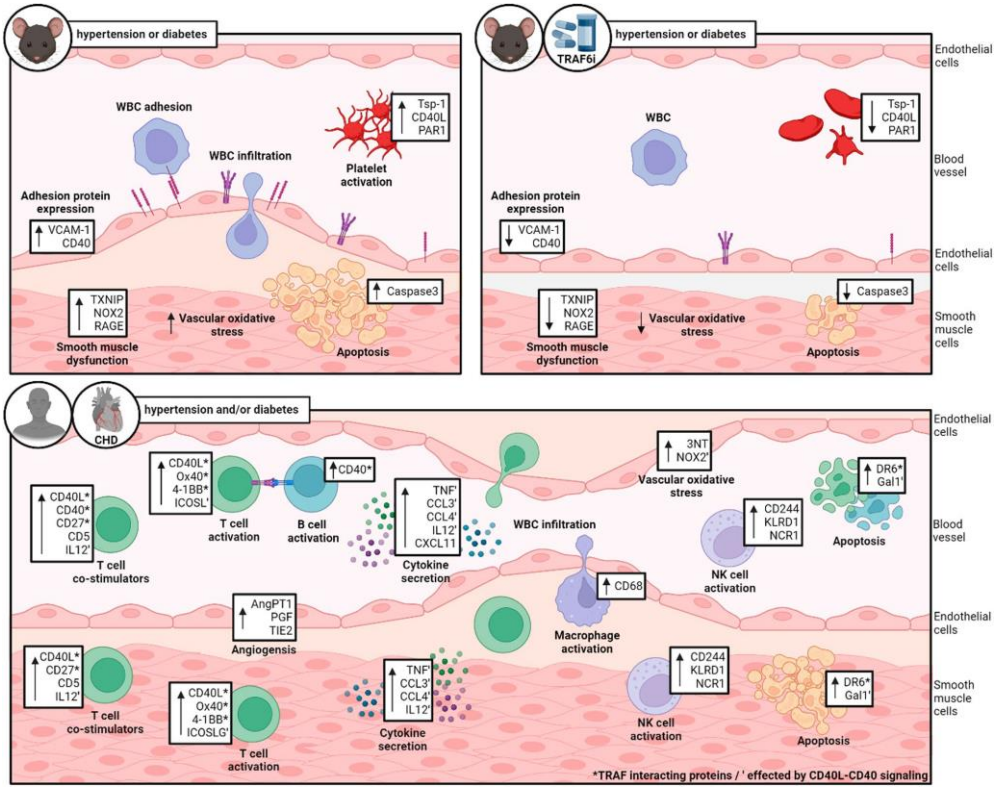

Fig. 6 Central scheme. Upper left panel: the central pathomechanisms associated with CD40(L)–TRAF signaling in hypertensive or diabetic mice. Upper right panel: protective effects of TRAF6i treatment in hypertensive or diabetic mice. Lower panel: markers associated with CD40(L)–TRAF signaling observed in CHD patients with no comorbidity or hypertension or hypertension + diabetes. It must be stressed that an appreciable part of the targets mentioned here were only changed by trend. *WBC* white blood cell, *Tsp-1* thrombospondin-1, *CD* cluster of differentiation, *CD40L* CD40 ligand, *PAR1* protease-activated receptor 1, *VCAM-1* vascular cell adhesion molecule-1, *TXNIP* thioredoxin-interacting protein, *NOX2* NADPH oxidase 2, *RAGE* receptor for advanced-glycation-end-products, *TNF* tumor necrosis factor, *TRAF6i* TNF receptor associated factor-6 inhibitor, *CHD* coronary heart disease, *IL12* interleukin-12, *TNFRSF4 (or ox40 or CD134)* TNF receptor superfamily member-4, *TNFRSF9 (or 4-1BB or CD137)* TNF receptor superfamily member-9, *ICOSL* inducible costimulator ligand, *AngPT1* angiopoietin-1, *PGF* placental growth factor, *TIE2* angiopoietin receptor-2, *CCL3/CCL4* C–C motif chemokine ligand-3/-4, *CXCL11* C-X-C motif chemokine ligand-11, *3NT* 3-nitrotyrosine, *KLRD1* killer cell lectin like receptor D-1, *NCR1* natural cytotoxicity triggering receptor-1, *DR6* death receptor-6, *Gal1* galactin-1, *NK* natural killer cell. Created with BioRender.com

of the gene expression changes, which fits quite well with our animal data.

Another limitation of our RNA-Seq studies is the usage of whole aorta specimens. As in this specimen, different cells (endothelial cells, smooth muscle cells, fibroblasts, immune cells, etc.) are included; the specific gene expression cannot be related to a specific cell type. In addition, infections may change the number of immune cells in the specimen and disturb the data.

As all participants in the study were treated with several drugs (partially overlapping between the different groups), the effects of the drugs on gene expression may also mask disease-related transcriptional changes.

Finally, since samples were used from a biobank, the included patients had no follow-up since this was not foreseen. Also, the sample size in two of the patient groups was quite low ($n = 21$ for CHD and $n = 25$ for HT + Dia), making the human study an exploratory pilot study. Also, the lack of the CHD patient group with only diabetes as a comorbidity represents a major limitation of the human part of the study.

Conclusion and clinical impact

Recent large clinical trials demonstrated that anti-inflammatory therapy can reduce cardiovascular risk by broad suppression of inflammatory pathways, as shown by the COLCOT study [41], or by highly specific targeting of the inflammatory cascade, e.g., as shown by the CANTOS study [34, 35]. Our present study could link CD40L–CD40-mediated signaling and platelet activation, the activation of different leukocytes, oxidative stress, inflammation, and angiogenesis, thereby generating new hypotheses. The major pathomechanisms in hypertensive or diabetic mice are associated with CD40(L)–TRAF signaling. Also, in patients with CHD, some key mediators of this pathway were found (summarized in Fig. 6). We conclude that CD40L–CD40 signaling is important in mediating cardiovascular complications in mouse models of obesity, dyslipidemia, hyperglycemia, and arterial hypertension. In addition, the proteomic and genomic analysis in plasma and vascular bypass tissue of CHD patients without comorbidities or with the comorbidities hypertension and/or hypertension + diabetes identified some key mediators of CD40(L)–TRAF signaling, centered around TNFα. However, the present data cannot clarify whether the stepwise increase in levels of low-grade inflammation markers is mediated directly by the comorbidities hypertension and/or diabetes or by the more severe CHD/events driven by these comorbidities; however, the disease state characteristics did not change significantly by the comorbidities.

In conclusion, hypertension and lipid metabolic disorders are important risk factors and leading causes of atherothrombotic vascular diseases like MI and cerebral ischemia. A targeted CD40-TRAF6 inhibitor treatment could provide a novel therapeutic strategy for these diseases, which circumvents the potential risks of a general blockade of CD40L or CD40-like thromboembolic events and solid immune suppression. It remains to be established if a long-term CD40-TRAF6 inhibitor treatment also provides some risks, like the blockade of CD40L or CD40. Finally, human studies are needed to test the beneficial effects of TRAF6 inhibition in hypertension and diabetes.

Supplementary Information The online version contains supplementary material available at https://doi.org/10.1007/s00395-024-01045-1.

Acknowledgements We are indebted to Alexandra Rosenberger, Nicole Glas, and Angelica Karpi for expert technical assistance and Antje Müller for help with patient data collection. This article contains results that are part of the doctoral thesis of Lea Strohm.

Funding Open Access funding enabled and organized by Projekt DEAL. SD was supported by a vascular biology research grant on "CD40L and inflammation in hypertension" of the Else-Kröner-Fresenius Foundation (2019_A110) and a research stipend from the foundation Heart of Mainz. LS and HU hold PhD stipends of the TransMed PhD Program financed by the Else-Kröner-Fresenius Foundation (2019_A110). CK, EL, and AD were supported by shared expertise grants of the DZHK (German Center for Cardiovascular Research), Partner Site Berlin, Partner Site Munich Heart Alliance, and Partner Site Rhine-Main, Mainz, Germany. A translational research grant from the DZHK supported DA, EL, and CW. CW, CK, PW, and TM are PIs, and AD, MK, OH are (Young) Scientists of the DZHK (German Center for Cardiovascular Research), Partner Site Munich, Berlin, and Rhine-Main, Mainz, Germany. CW is a van der Laar-Professor of Atherosclerosis. The collaboration of the authors was supported by the European COST Action EU-CARDIOPROTECTION (CA16225) and COST Innovation Grant 16225 "IMproving Preclinical Assessment of Cardioprotective Therapies (IMPACT)".

Data availability All data are available in the manuscript or the supplementary materials.

Declarations

Conflict of interest All authors declare no conflict of interest for this contribution.

References

1. Andre P, Prasad KS, Denis CV, He M, Papalia JM, Hynes RO, Phillips DR, Wagner DD (2002) CD40L stabilizes arterial thrombi by a beta3 integrin–dependent mechanism. Nat Med 8:247–252. https://doi.org/10.1038/nm0302-247
2. Andreadou I, Daiber A, Baxter GF, Brizzi MF, Di Lisa F, Kaludercic N, Lazou A, Varga ZV, Zuurbier CJ, Schulz R, Ferdinandy P (2021) Influence of cardiometabolic comorbidities on myocardial function, infarction, and cardioprotection: role of cardiac redox signaling. Free Radic Biol Med 166:33–52. https://doi.org/10.1016/j.freeradbiomed.2021.02.012
3. Bartekova M, Barancik M, Ferenczyova K, Dhalla NS (2018) Beneficial Effects of N-acetylcysteine and N-mercaptopropionylglycine on Ischemia Reperfusion Injury in the Heart. Curr Med Chem 25:355–366. https://doi.org/10.2174/0929867324666170608111917
4. Basta G, Schmidt AM, De Caterina R (2004) Advanced glycation end products and vascular inflammation: implications for accelerated atherosclerosis in diabetes. Cardiovasc Res 63:582–592. https://doi.org/10.1016/j.cardiores.2004.05.001
5. Bei JJ, Liu C, Peng S, Liu CH, Zhao WB, Qu XL, Chen Q, Zhou Z, Yu ZP, Peter K, Hu HY (2016) Staphylococcal SSL5-induced platelet microparticles provoke proinflammatory responses via the CD40/TRAF6/NFkappaB signalling pathway in monocytes. Thromb Haemost 115:632–645. https://doi.org/10.1160/TH15-04-0322
6. Bergholm R, Leirisalo-Repo M, Vehkavaara S, Makimattila S, Taskinen MR, Yki-Jarvinen H (2002) Impaired responsiveness to NO in newly diagnosed patients with rheumatoid arthritis. Arterioscler Thromb Vasc Biol 22:1637–1641
7. Bishop RT, Marino S, Carrasco G, Li B, Allen RJ, Sparatore A, Ottewell PD, Mollat P, Sims AH, Capulli M, Wang N, Idris AI (2020) Combined administration of a small-molecule inhibitor of TRAF6 and Docetaxel reduces breast cancer skeletal metastasis and osteolysis. Cancer Lett 488:27–39. https://doi.org/10.1016/j.canlet.2020.05.021
8. Blankenberg S, Rupprecht HJ, Bickel C, Torzewski M, Hafner G, Tiret L, Smieja M, Cambien F, Meyer J, Lackner KJ, AtheroGene I (2003) Glutathione peroxidase 1 activity and cardiovascular events in patients with coronary artery disease. N Engl J Med 349:1605–1613. https://doi.org/10.1056/NEJMoa030535
9. Bozkurt B, Aguilar D, Deswal A, Dunbar SB, Francis GS, Horwich T, Jessup M, Kosiborod M, Pritchett AM, Ramasubbu K, Rosendorff C, Yancy C, American Heart Association Heart F, Transplantation Committee of the Council on Clinical C, Council on Cardiovascular S, Anesthesia, Council on C, Stroke N, Council on H, Council on Q, Outcomes R (2016) Contributory Risk and Management of Comorbidities of Hypertension, Obesity, Diabetes Mellitus, Hyperlipidemia, and Metabolic Syndrome in Chronic Heart Failure: A Scientific Statement From the American Heart Association. Circulation 134:e535–e578. https://doi.org/10.1161/CIR.0000000000000450
10. Chatzigeorgiou A, Seijkens T, Zarzycka B, Engel D, Poggi M, van den Berg S, van den Berg S, Soehnlein O, Winkels H, Beckers L, Lievens D, Driessen A, Kusters P, Biessen E, Garcia-Martin R, Klotzsche-von Ameln A, Gijbels M, Noelle R, Boon L, Hackeng T, Schulte KM, Xu A, Vriend G, Nabuurs S, Chung KJ, Willems van Dijk K, Rensen PC, Gerdes N, de Winther M, Block NL, Schally AV, Weber C, Bornstein SR, Nicolaes G, Chavakis T, Lutgens E (2014) Blocking CD40-TRAF6 signaling is a therapeutic target in obesity-associated insulin resistance. Proc Natl Acad Sci U S A 111:2686–2691. https://doi.org/10.1073/pnas.1400419111
11. Daiber A, Steven S, Vujacic-Mirski K, Kalinovic S, Oelze M, Di Lisa F, Munzel T (2020) Regulation of vascular function and inflammation via cross talk of reactive oxygen and nitrogen species from mitochondria or NADPH oxidase-implications for diabetes progression. Int J Mol Sci. https://doi.org/10.3390/ijms21103405
12. Diseases GBD, Injuries C (2020) Global burden of 369 diseases and injuries in 204 countries and territories, 1990–2019: a systematic analysis for the Global Burden of Disease Study 2019. Lancet 396:1204–1222. https://doi.org/10.1016/S0140-6736(20)30925-9
13. Ferroni P, Guadagni F (2008) Soluble CD40L and its role in essential hypertension: diagnostic and therapeutic implications. Cardiovasc Hematol Disord: Drug Targets 8:194–202. https://doi.org/10.2174/187152908785849125
14. Fukai T, Siegfried MR, Ushio-Fukai M, Griendling KK, Harrison DG (1999) Modulation of extracellular superoxide dismutase expression by angiotensin II and hypertension. Circ Res 85:23–28. https://doi.org/10.1161/01.res.85.1.23
15. Garrido VT, Sonzogni L, Mtatiro SN, Costa FF, Conran N, Thein SL (2017) Association of plasma CD40L with acute chest syndrome in sickle cell anemia. Cytokine 97:104–107. https://doi.org/10.1016/j.cyto.2017.05.017
16. Ghoneim S, Dhorepatil A, Shah AR, Ram G, Ahmad S, Kim C, Asaad I (2020) Non-alcoholic steatohepatitis and the risk of myocardial infarction: a population-based national study. World J Hepatol 12:378–388. https://doi.org/10.4254/wjh.v12.i7.378
17. Griendling KK, FitzGerald GA (2003) Oxidative stress and cardiovascular injury: Part I: basic mechanisms and in vivo monitoring of ROS. Circulation 108:1912–1916
18. Guzik TJ, Hoch NE, Brown KA, McCann LA, Rahman A, Dikalov S, Goronzy J, Weyand C, Harrison DG (2007) Role of the T cell in the genesis of angiotensin II induced hypertension and vascular dysfunction. J Exp Med 204:2449–2460. https://doi.org/10.1084/jem.20070657
19. Hausding M, Jurk K, Daub S, Kroller-Schon S, Stein J, Schwenk M, Oelze M, Mikhed Y, Kerahrodi JG, Kossmann S, Jansen T, Schulz E, Wenzel P, Reske-Kunz AB, Becker C, Munzel T, Grabbe S, Daiber A (2013) CD40L contributes to angiotensin II-induced pro-thrombotic state, vascular inflammation, oxidative stress and endothelial dysfunction. Basic Res Cardiol 108:386. https://doi.org/10.1007/s00395-013-0386-5
20. Heitzer T, Schlinzig T, Krohn K, Meinertz T, Munzel T (2001) Endothelial dysfunction, oxidative stress, and risk of cardiovascular events in patients with coronary artery disease. Circulation 104:2673–2678. https://doi.org/10.1161/hc4601.099485
21. Heusch G, Andreadou I, Bell R, Bertero E, Botker HE, Davidson SM, Downey J, Eaton P, Ferdinandy P, Gersh BJ, Giacca M, Hausenloy DJ, Ibanez B, Krieg T, Maack C, Schulz R, Sellke F, Shah AM, Thiele H, Yellon DM, Di Lisa F (2023) Health position paper and redox perspectives on reactive oxygen species as signals and targets of cardioprotection. Redox Biol 67:102894. https://doi.org/10.1016/j.redox.2023.102894
22. Kaptoge S, Seshasai SR, Gao P, Freitag DF, Butterworth AS, Borglykke A, Di Angelantonio E, Gudnason V, Rumley A, Lowe GD, Jorgensen T, Danesh J (2014) Inflammatory cytokines and risk of coronary heart disease: new prospective study and updated meta-analysis. Eur Heart J 35:578–589. https://doi.org/10.1093/eurheartj/eht367
23. Kornbluth RS (2002) An expanding role for CD40L and other tumor necrosis factor superfamily ligands in HIV infection. J Hematother Stem Cell Res 11:787–801. https://doi.org/10.1089/152581602760404595
24. Kröller-Schön S, Steven S, Kossmann S, Scholz A, Daub S, Oelze M, Xia N, Hausding M, Mikhed Y, Zinssius E, Mader M, Stamm P, Treiber N, Scharffetter-Kochanek K, Li H, Schulz E, Wenzel P, Münzel T, Daiber A (2014) Molecular mechanisms of the crosstalk between mitochondria and NADPH oxidase through reactive oxygen species-studies in white blood cells and

in animal models. Antioxid Redox Signal 20:247–266. https://doi.org/10.1089/ars.2012.4953
25. Lameijer M, Binderup T, van Leent MMT, Senders ML, Fay F, Malkus J, Sanchez-Gaytan BL, Teunissen AJP, Karakatsanis N, Robson P, Zhou X, Ye Y, Wojtkiewicz G, Tang J, Seijkens TTP, Kroon J, Stroes ESG, Kjaer A, Ochando J, Reiner T, Perez-Medina C, Calcagno C, Fisher EA, Zhang B, Temel RE, Swirski FK, Nahrendorf M, Fayad ZA, Lutgens E, Mulder WJM, Duivenvoorden R (2018) Efficacy and safety assessment of a TRAF6-targeted nanoimmunotherapy in atherosclerotic mice and non-human primates. Nat Biomed Eng 2:279–292. https://doi.org/10.1038/s41551-018-0221-2
26. Landmesser U, Cai H, Dikalov S, McCann L, Hwang J, Jo H, Holland SM, Harrison DG (2002) Role of p47(phox) in vascular oxidative stress and hypertension caused by angiotensin II. Hypertension 40:511–515. https://doi.org/10.1161/01.HYP.0000032100.23772.98
27. Lutgens E, Lievens D, Beckers L, Wijnands E, Soehnlein O, Zernecke A, Seijkens T, Engel D, Cleutjens J, Keller AM, Naik SH, Boon L, Oufella HA, Mallat Z, Ahonen CL, Noelle RJ, de Winther MP, Daemen MJ, Biessen EA, Weber C (2010) Deficient CD40-TRAF6 signaling in leukocytes prevents atherosclerosis by skewing the immune response toward an antiinflammatory profile. J Exp Med 207:391–404. https://doi.org/10.1084/jem.20091293
28. Malada-Edelstein YF, Hadad N, Levy R (2017) Regulatory role of cytosolic phospholipase A(2) alpha in the induction of CD40 in microglia. J Neuroinflammation 14:33. https://doi.org/10.1186/s12974-017-0811-z
29. Marino S, Hannemann N, Bishop RT, Zeng F, Carrasco G, Meurisse S, Li B, Sophocleous A, Sparatore A, Baeuerle T, Vukicevic S, Auberval M, Mollat P, Bozec A, Idris AI (2022) Anti-inflammatory, but not osteoprotective, effect of the TRAF6/CD40 inhibitor 6877002 in rodent models of local and systemic osteolysis. Biochem Pharmacol 195:114869. https://doi.org/10.1016/j.bcp.2021.114869
30. Martinez de Lizarrondo S, Roncal C, Calvayrac O, Rodriguez C, Varo N, Purroy A, Lorente L, Rodriguez JA, Doeuvre L, Hervas-Stubbs S, Angles-Cano E, Paramo JA, Martinez-Gonzalez J, Orbe J (2012) Synergistic effect of thrombin and CD40 ligand on endothelial matrix metalloproteinase-10 expression and microparticle generation in vitro and in vivo. Arterioscler Thromb Vasc Biol 32:1477–1487. https://doi.org/10.1161/ATVBAHA.112.248773
31. Mehta NN, Azfar RS, Shin DB, Neimann AL, Troxel AB, Gelfand JM (2010) Patients with severe psoriasis are at increased risk of cardiovascular mortality: cohort study using the General Practice Research Database. Eur Heart J 31:1000–1006. https://doi.org/10.1093/eurheartj/ehp567
32. Pastori D, Esposito A, Carnevale R, Bartimoccia S, Novo M, Fantauzzi A, Di Campli F, Pignatelli P, Violi F, Mezzaroma I (2015) HIV-1 induces in vivo platelet activation by enhancing platelet NOX2 activity. J Infect 70:651–658. https://doi.org/10.1016/j.jinf.2015.01.005
33. Ridker PM, Cannon CP, Morrow D, Rifai N, Rose LM, McCabe CH, Pfeffer MA, Braunwald E, Pravastatin or Atorvastatin E, Infection Therapy-Thrombolysis in Myocardial Infarction I (2005) C-reactive protein levels and outcomes after statin therapy. N Engl J Med 352:20–28. https://doi.org/10.1056/NEJMoa042378
34. Ridker PM, Everett BM, Thuren T, MacFadyen JG, Chang WH, Ballantyne C, Fonseca F, Nicolau J, Koenig W, Anker SD, Kastelein JJP, Cornel JH, Pais P, Pella D, Genest J, Cifkova R, Lorenzatti A, Forster T, Kobalava Z, Vida-Simiti L, Flather M, Shimokawa H, Ogawa H, Dellborg M, Rossi PRF, Troquay RPT, Libby P, Glynn RJ, Group CT (2017) Antiinflammatory therapy with canakinumab for atherosclerotic disease. N Engl J Med 377:1119–1131. https://doi.org/10.1056/NEJMoa1707914
35. Ridker PM, MacFadyen JG, Everett BM, Libby P, Thuren T, Glynn RJ, Group CT (2018) Relationship of C-reactive protein reduction to cardiovascular event reduction following treatment with canakinumab: a secondary analysis from the CANTOS randomised controlled trial. Lancet 391:319–328. https://doi.org/10.1016/S0140-6736(17)32814-3
36. Schottker B, Brenner H, Jansen EH, Gardiner J, Peasey A, Kubinova R, Pajak A, Topor-Madry R, Tamosiunas A, Saum KU, Holleczek B, Pikhart H, Bobak M (2015) Evidence for the free radical/oxidative stress theory of ageing from the CHANCES consortium: a meta-analysis of individual participant data. BMC Med 13:300. https://doi.org/10.1186/s12916-015-0537-7
37. Seijkens TTP, van Tiel CM, Kusters PJH, Atzler D, Soehnlein O, Zarzycka B, Aarts S, Lameijer M, Gijbels MJ, Beckers L, den Toom M, Slutter B, Kuiper J, Duchene J, Aslani M, Megens RTA, van't Veer C, Kooij G, Schrijver R, Hoeksema MA, Boon L, Fay F, Tang J, Baxter S, Jongejan A, Moerland PD, Vriend G, Bleijlevens B, Fisher EA, Duivenvoorden R, Gerdes N, de Winther MPJ, Nicolaes GA, Mulder WJM, Weber C, Lutgens E (2018) Targeting CD40-induced TRAF6 signaling in macrophages reduces atherosclerosis. J Am Coll Cardiol 71:527–542. https://doi.org/10.1016/j.jacc.2017.11.055
38. Steven S, Dib M, Hausding M, Kashani F, Oelze M, Kroller-Schon S, Hanf A, Daub S, Roohani S, Gramlich Y, Lutgens E, Schulz E, Becker C, Lackner KJ, Kleinert H, Knosalla C, Niesler B, Wild PS, Munzel T, Daiber A (2018) CD40L controls obesity-associated vascular inflammation, oxidative stress, and endothelial dysfunction in high fat diet-treated and db/db mice. Cardiovasc Res 114:312–323. https://doi.org/10.1093/cvr/cvx197
39. Stokes KY, Calahan L, Hamric CM, Russell JM, Granger DN (2009) CD40/CD40L contributes to hypercholesterolemia-induced microvascular inflammation. Am J Physiol Heart Circul Physiol 296:H689-697. https://doi.org/10.1152/ajpheart.00962.2008
40. Takahashi HK, Mori S, Wake H, Liu K, Yoshino T, Ohashi K, Tanaka N, Shikata K, Makino H, Nishibori M (2009) Advanced glycation end products subspecies-selectively induce adhesion molecule expression and cytokine production in human peripheral blood mononuclear cells. J Pharmacol Exp Ther 330:89–98. https://doi.org/10.1124/jpet.109.150581
41. Tardif JC, Kouz S, Waters DD, Bertrand OF, Diaz R, Maggioni AP, Pinto FJ, Ibrahim R, Gamra H, Kiwan GS, Berry C, López-Sendón J, Ostadal P, Koenig W, Angoulvant D, Grégoire JC, Lavoie MA, Dubé MP, Rhainds D, Provencher M, Blondeau L, Orfanos A, L'Allier PL, Guertin MC, Roubille F (2019) Efficacy and safety of low-dose colchicine after myocardial infarction. N Engl J Med 381:2497–2505. https://doi.org/10.1056/NEJMoa1912388
42. Vos S, Aaron R, Weng M, Daw J, Rodriguez-Rivera E, Subauste CS (2023) CD40 upregulation in the retina of patients with diabetic retinopathy: association with TRAF2/TRAF6 upregulation and inflammatory molecule expression. Invest Ophthalmol Vis Sci 64:17. https://doi.org/10.1167/iovs.64.7.17
43. Wenzel P, Knorr M, Kossmann S, Stratmann J, Hausding M, Schuhmacher S, Karbach SH, Schwenk M, Yogev N, Schulz E, Oelze M, Grabbe S, Jonuleit H, Becker C, Daiber A, Waisman

A, Munzel T (2011) Lysozyme M-positive monocytes mediate angiotensin II-induced arterial hypertension and vascular dysfunction. Circulation 124:1370–1381. https://doi.org/10.1161/CIRCULATIONAHA.111.034470

44. Wenzel P, Kossmann S, Munzel T, Daiber A (2017) Redox regulation of cardiovascular inflammation—immunomodulatory function of mitochondrial and nox-derived reactive oxygen and nitrogen species. Free Radic Biol Med 109:48–60. https://doi.org/10.1016/j.freeradbiomed.2017.01.027

45. Willerson JT, Ridker PM (2004) Inflammation as a cardiovascular risk factor. Circulation 109:II2-10. https://doi.org/10.1161/01.CIR.0000129535.04194.38

46. Zhang L, Zalewski A, Liu Y, Mazurek T, Cowan S, Martin JL, Hofmann SM, Vlassara H, Shi Y (2003) Diabetes-induced oxidative stress and low-grade inflammation in porcine coronary arteries. Circulation 108:472–478. https://doi.org/10.1161/01.CIR.0000080378.96063.23

Authors and Affiliations

Lea Strohm[1] · Andreas Daiber[1,2,16] · Henning Ubbens[1] · Roopesh Krishnankutty[3] · Matthias Oelze[1] · Marin Kuntic[1] · Omar Hahad[1,2] · Veronique Klein[1] · Imo E. Hoefer[4] · Alex von Kriegsheim[3] · Hartmut Kleinert[5] · Dorothee Atzler[6,7,8] · Philipp Lurz[1,2] · Christian Weber[6,7,9,10] · Philipp S. Wild[11,17,18,19] · Thomas Münzel[1,2] · Christoph Knosalla[12,13,14] · Esther Lutgens[6,7,15] · Steffen Daub[1]

✉ Andreas Daiber
daiber@uni-mainz.de

1 Department of Cardiology, Cardiology I, University Medical Center of the Johannes Gutenberg-University, Mainz, Germany

2 German Center for Cardiovascular Research (DZHK), Partnersite Rhine-Main, Mainz, Germany

3 Institute of Genetics and Cancer, University of Edinburgh, Edinburgh, UK

4 Central Diagnostic Laboratory, UMC Utrecht, Utrecht, The Netherlands

5 Department of Pharmacology, University Medical Center of the Johannes Gutenberg-University, Mainz, Germany

6 Institute for Cardiovascular Prevention (IPEK), Ludwig-Maximilians Universität, Munich, Germany

7 German Center for Cardiovascular Research (DZHK), Partner Site Munich Heart Alliance, Munich, Germany

8 Walther Straub Institute of Pharmacology and Toxicology, LMU Munich, Munich, Germany

9 Munich Cluster for Systems Neurology (SyNergy), Munich, Germany

10 Department of Biochemistry, Cardiovascular Research Institute Maastricht (CARIM), Maastricht University, Maastricht, The Netherlands

11 Preventive Cardiology and Preventive Medicine, Department of Cardiology, University Medical Mainz, Johannes Gutenberg-University Mainz, Mainz, Germany

12 Department of Cardiothoracic and Vascular Surgery, Deutsches Herzzentrum der Charité, Berlin, Germany

13 Charité-Universitätsmedizin Berlin, Corporate Member of Freie Universität Berlin and Humboldt-Universität zu Berlin, Berlin, Germany

14 German Center for Cardiovascular Research (DZHK), Partner Site Berlin, Berlin, Germany

15 Department Cardiovascular Medicine and Immunology, Mayo Clinic, Rochester, MN, USA

16 Universitätsmedizin der Johannes Gutenberg-Universität Zentrum für Kardiologie 1, Labor für Molekulare Kardiologie, Geb. 605, Raum 3.262, Langenbeckstr. 1, 55131 Mainz, Germany

17 Clinical Epidemiology and Systems Medicine, Center for Thrombosis and Hemostasis, University Medical Center Mainz, Johannes Gutenberg University Mainz, Mainz, Germany

18 German Center for Cardiovascular Research (DZHK), Partnersite Rhine-Main, University Medical Center Mainz, Johannes Gutenberg University Mainz, Mainz, Germany

19 Systems Medicine, Institute of Molecular Biology (IMB), Mainz, Germany

Danksagung

XX

Eidesstattliche Erklärung

Hiermit versichere ich gemäß §12, Abs. 2 der Promotionsverordnung vom 27.03.2018, dass ich die als Dissertation vorgelegte Arbeit selbst angefertigt und alle benutzten Hilfsmittel in der Arbeit angegeben habe. Weiterhin habe oder hatte ich die als Dissertation vorgelegte Arbeit nicht als Prüfungsarbeit für eine staatliche oder andere wissenschaftliche Prüfung eingereicht. Ich hatte weder die als Dissertation vorgelegte Arbeit noch Teile davon bei einer anderen Fakultät bzw. einem anderen Fachbereich als Dissertation eingereicht.

Mainz, August 2024 _____(Lea Sophie Strohm)